12-2012

Integration of process parameter control and digital image correlation methods in an investigation of the variability of marine polymer matrix composite material properties

Keith Andrew Berube

INTEGRATION OF PROCESS PARAMETER CONTROL AND DIGITAL IMAGE CORRELATION METHODS IN AN INVESTIGATION OF THE VARIABILITY OF MARINE POLYMER MATRIX COMPOSITE MATERIAL PROPERTIES

By

Keith Andrew Berube

B.S. University of Maine, 1997

M.S. University of Maine, 1999

A Dissertation

Submitted in Partial Fulfillment of the

Requirements for the Degree of

Doctor of Philosophy

(in Mechanical Engineering)

The Graduate School

The University of Maine

December, 2012

Advisory Committee:

Roberto A. Lopez-Anido, Professor of Civil and Environmental Engineering, Advisor

Vincent Caccese, Professor of Mechanical Engineering

Senthil Vel, Professor of Mechanical Engineering

Andrew Goupee, Research Assistant Professor, Advanced Structures and Composites Center

Paul Hess, Program Manager, Office of Naval Research, External Graduate Faculty

DISSERTATION ACCEPTANCE STATEMENT

On behalf of the Graduate Committee for Keith A. Berube I affirm that this manuscript is the final and accepted dissertation. Signatures of all committee members are on file with the Graduate School at the University of Maine, 42 Stodder Hall, Orono, Maine.

Dr. Roberto Lopez-Anido, Professor of Civil and Environmental Engineering Date

LIBRARY RIGHTS STATEMENT

In presenting this dissertation in partial fulfillment of the requirements for an advanced degree at The University of Maine, I agree that the Library shall make it freely available for inspection. I further agree that permission for "fair use" copying of this dissertation for scholarly purposes may be granted by the Librarian. It is understood that any copying or publication of this dissertation for financial gain shall not be allowed without my written permission.

Signature:

Date:

INTEGRATION OF PROCESS PARAMETER CONTROL AND DIGITAL IMAGE CORRELATION METHODS IN AN INVESTIGATION OF THE VARIABILITY OF MARINE POLYMER MATRIX COMPOSITE MATERIAL PROPERTIES

By Keith Andrew Berube

Dissertation Advisor: Dr. Roberto A. Lopez-Anido

An Abstract of the Dissertation Presented
in Partial Fulfillment of the Requirements for the
Degree of Doctor of Philosophy
(in Mechanical Engineering)
December, 2012

The very nature of continuous fiber composite materials, with their heterogeneous structure of layered and interwoven fibers bound together by a polymer resin matrix, lead to an inevitable variability in mechanical properties. This is especially true if the fabrication process is not well controlled. Unlike fabricating components with metals, where the properties of the material are known beforehand, the final properties of the composite material are determined during the process of fabricating the composite part. The research described herein was undertaken to better enable the use of polymer matrix composites in the marine construction industry by developing a knowledge base on the inter-relationships between process parameters and system material properties.

Professionals from the marine composite fabrication industry were consulted to obtain insight into the process parameters of concern for today's composite materials and manufacturing methods. The survey of industrial marine designers and fabricators was intended to identify potential sources of variability and to characterize processing issues. A set of composite constituent materials, vinyl-ester resin and woven roving fiber reinforcement, and a single processing method, vacuum assisted resin transfer molding (VARTM), were selected for further

investigation based on this industry survey. In addition to the survey, a thorough literature review was conducted to identify current research areas for VARTM processing of composite laminates.

A manufacturing round-robin study was conducted amongst marine composite fabricators to establish the extent of material property variability. The methodology employed for the experimental material characterization included the use of three-dimensional digital image correlation (DIC) methods to measure the full-field strain in the test specimens. The DIC method was chosen over conventional foil strain gage techniques since it can better capture, and account for, the large strain gradients that are present in composite specimens fabricated with woven roving fabrics typically found in marine grade composites. The statistical analysis of the test results was performed to characterize the variability in material properties in accordance with the guidelines set forth in Composite Materials Handbook-17, which is the composite industry's standard for testing and analysis of laminated composite materials. A methodology was developed based on these guidelines and employed throughout the different studies conducted.

A laboratory study of resin, fiber and manufacturing effects was designed to capture the relationship between the processing parameters and the final material properties of the composite laminates. The parameters and test methods used in this study were selected based on the results of the industry survey and the round-robin study.

This integrated research will contribute to advance scientific understanding on the inter-relationships between process parameters and mechanical property variability of marine composite materials. The broad impact of the research is to enable the development of rational composites fabrication methods and reliable engineering design procedures.

DEDICATION

In memory of

my father Raynald G. Berube

and my friend Devereux R. Eaton.

ACKNOWLEDGEMENTS

I would like to thank my advisor Roberto Lopez-Anido for taking me onto this project and his guidance throughout the process, but more so for his immense patience every time I got sidetracked with other interesting endeavors at the Lab that prolonged my status as a student.

I sincerely appreciate the funding provided by the Office of Naval Research (ONR) under grant number N00014-04-1-0358, without which this research would not have been possible. I would like to thank Dr. Paul Hess and Dr. Roshdy Barsoum of ONR who both provided program oversight during different phases of the project.

I would like to thank Mr. Brian Jones and Mr. Paul A. Coffin of the Naval Sea Warfare Center - Carderock Division (NSWC-CD) for their input and guidance during the experimental phase of the project. I would like to thank Dr. Timothy Pepper, Mr. Michael Stevens and their colleagues at Ashland Chemical for their input on resin chemistries during the laboratory study. I would like to thank the anonymous manufacturers and suppliers that responded to the industry survey and also provided test materials during the Round-Robin study.

I would like to thank Dr. Larry Thompson for bringing this opportunity to my attention and for the encouragement while I was deciding whether or not to take on this challenge. I would like to thank Matthew Dura, Katherine Beaumont, and Fadi El-Chiti for their assistance in bringing me up to speed with the digital image correlation system; a tool I hated at first, but have since grown to wonder how I could ever do without. I would like to thank the numerous undergraduate students that worked with me on this research; unfortunately, they are too numerous to mention here.

I would like to thank all of the staff, friends, and colleagues at the Advanced Structures and Composites Center for their assistance with my research, especially all of the staff in the front office, who everyone knows are really the people running the place.

I would like to thank the faculty and staff in the Department of Mechanical Engineering for their support and use of laboratory facilities at Crosby Lab and the Advanced Manufacturing Center during various phases of my research. I want to thank Drs. Mick Petersen and Senthil Vel for their support during their tenure as graduate advisors in the Department of Mechanical Engineering.

I want to thank Dr. Vincent Caccese from the Department of Mechanical Engineering for getting me hooked on experimental work, and Dr. George Krueger from the Department of Physics for fueling my appreciation for attention to detail.

Lastly, and most important of all, I would like to thank my Mom for always offering unconditional support and delighting in my determination to seek a doctoral degree, all the while asking when I would FINALLY be done with school.

TABLE OF CONTENTS

LIST OF TABLES

LIST OF FIGURES

CHAPTER 1

EXECUTIVE SUMMARY

1.1 Introduction

Despite advances in the Vacuum-Assisted Resin Transfer Molding (VARTM) manufacturing process, questions remain regarding the consistency of material properties in large, fiber-reinforced polymer (FRP) composite parts. The marine industry is an area where the VARTM process is used extensively. The common method of implementing the VARTM process in the marine industry involves one-sided hard tooling and a pliable vacuum bag. This process is favored since it is a relatively inexpensive method to fabricate large parts using room-temperature cure resin systems. However, the very nature of the process, using vacuum pressure to consolidate the fiber-preform and then using that same pressure differential as the means to draw the resin into the part, can lead to many process variations. In addition, the size, shape, and thickness of the part, will determine the flow media configuration, inlet hose spacing, and resin catalyzing recipe formulation that a fabricator will use depending on their prior experience with similar parts and the particular resin system. With a large number of process variables controlled by the fabricator, the question remains as to the effect of these process variations on the quality and consistency of the structural properties of the resulting parts.

This research was undertaken with the intent to determine some of the manufacturing effects on variability in material properties of marine grade composite laminates. “Marine grade” referring to the heavy tow fabrics that are normally employed when fabricating large parts with thick laminates in the marine industry. The heavy fabrics facilitate a more rapid build up of laminate thickness during the lay-up process

and tend to be more resilient in the types of environments that the final parts will be exposed to during their lifetime in the marine environment.

This work is part of a larger project sponsored by the Office of Naval Research to investigate the causes of variability in material properties of E-glass/vinyl-ester marine grade composites. The sources of variability being investigated in the larger project include those due to manufacturing, post processing, and testing of composites. While this portion of the research is focused on variability due to manufacturing, the results from the prior phases on post-curing [1] and test method variability [2] were implemented in this portion of the study.

1.2 Experimental and Analytical Procedures

This portion of the research, which was focused on manufacturing variability, was broken up into two distinct phases; A *Round-Robin Study* and a *Laboratory Study*. The Round-Robin Study was intended to investigate the variability in material properties encountered when different manufacturers fabricate identical composite parts with identical base materials, while the Laboratory Study investigated the effects of various manufacturing variables during the fabrication of composite laminates under controlled conditions.

A single fiber reinforcement and resin system were used throughout this entire study. A single fiber/resin system eliminates variations due to fiber architectures that may overshadow variations due to manufacturing and testing. The fiber reinforcement used was a Saint Gobain Vetrotex 324 woven roving with a weight per unit area of 814 g/m^2 (24 oz/yd^2). It is a plain weave fabric with a tow spacing of 5.1 mm (5 tows per inch) in the warp direction, and 6.4 mm (4 tows per inch) in the fill direction. The polymer resin

used was Ashland Derakane 8084, which is an elastomer-modified epoxy vinyl-ester resin. This system was selected since both the fabric and resin display the level of properties that would typically be implemented in marine construction using a VARTM process. All the panels fabricated for this study were post-cured on-site at 82ºC (180ºF) for a period of 4 hours, which had been shown to be sufficient in an earlier phase of the study [1].

All of the material coupon testing was conducted at the Advanced Structures and Composites Center, at the University of Maine in Orono, Maine using servo-hydraulic load frames equipped with side-loading hydraulic grips, and located in an environmentally controlled test lab in an environment of 23 ± 2°C and 50 ± 5% relative humidity.

A three-dimensional digital image correlation (3-D DIC) system was implemented throughout this research. The DIC method provides full-field strain and position data over the entire visible imaging area of the test specimen. It has been used for determining material properties in many studies [3-7] and has shown that it is a useful method for measuring properties at multiple scales [6] and under conditions that preclude more conventional techniques [7]. This is especially advantageous when testing heavy woven fabric composites where conventional foil strain gage size and placement can influence test results due to strain variations on the specimen [8]. The variations are a result of the strain gradients present on the surface of the specimen due to the size of the fiber tows and the alternating nature of the woven warp and fill tow orientations. As a non-contact technique, it allows for simplified experimental test setup and provides reduced specimen preparation time and reduced time between tests. Additionally, the

image acquisition process permits test review and post-processing long after the time of testing which enables additional analysis to be conducted on the same test specimens at a later date in time. The non-contact nature of the method is also advantageous for displacement measurements in space-limited test configurations.

The statistical analysis methods outlined in the Composite Materials Handbook (MIL-HDBK-17F-1) for single point data were used to analyze the material property test results in this research [9]. Specifically, the STAT17F Excel workbook, which executes most of the statistical methods outlined in Section 8 of MIL-HDBK-17F-1, was used to generate the results. While STAT17F computes the statistics for different population distributions, the latest update of MIL-HDBK-17-1 states that a normal distribution is the preferred distribution to assign when computing material properties. Therefore, only the results for a normal distribution were used when comparing material property data. After verifying the normality of the dataset distributions using the Anderson-Darling method, the mean and coefficient of variation (CV) were computed for each material property investigated. As a means of determining if the results from each material property dataset were statistically discernible for the different consolidation parameters investigated, the k-sample Anderson-Darling (ADK) method was employed. If the calculated ADK value for the dataset is less than the critical ADK value, then one can conclude with a 2.5 percent risk of being in error, that the groups were drawn from the same population.

1.3 Dissertation Format

The format of the Dissertation is such that each of the chapters are self contained units, where each chapter has either been published in a peer reviewed journal, a

conference proceedings, or is somewhere in the process of publication (submission or under revision). The organization of the chapters is as follows:

- Chapters 1-3 Investigations Related to the Round-Robin Study
- Chapters 4-6 Three Phases of the Laboratory Study
- Chapters 7-8 Digital Image Correlation Implementations

1.4 Round-Robin Study

The Round-Robin Study was intended to investigate the variability in material properties encountered when different manufacturers fabricate identical composite parts with identical base materials. The work conducted during the Round-Robin study resulted in three papers: The first on the overall results of the Round-Robin [10]; the second on the effect of styrene content on material properties [11]; and the third one on the ability of the DIC system to reduce variability during testing [12].

1.4.1 Round-Robin Study Results (Chapter 2)

The objective of the Round-Robin study was to determine the extent of variability in material properties that could be encountered when different manufacturers were used to fabricate identical composite parts. The manufacturers were instructed to use a specific fabric, resin and fiber lay-up when fabricating the laminates. The five manufacturers that participated in this study either had US naval, or commercial marine, composite fabrication experience. The manufacturers were instructed to fabricate a given number of flat panels for structural and coupon testing using the typical VARTM process. Standardized material property tests were conducted on coupon specimens from each of panels for constituent volume (ASTM D2584), tension (ASTM D3039), compression (ASTM D6641), in-plane shear (ASTM D4255), and flexure (ASTM D7264).

A methodology to quantify the variability of mechanical properties of marine grade composites fabricated by the VARTM process was developed during the study. A procedure for statistical representations of strength and elastic properties, as recommended in MIL-HDBK-17F-1, was implemented as a means to compare the different datasets.

The recommended normalization procedure employed to account for variations in fiber volume fraction for the tension and compression results seemed to work for tension, but had a lesser effect on the compression results when faced with a significant volume fraction difference for one of the individual manufacturer's datasets. This resulted in statistically significant differences in some of the strength and elastic properties for individual panels.

The combined manufacturer dataset results indicated that compression exhibited the most variability in both strength and modulus, while the flexural strength and tensile modulus had the least amount of variability. The variability in compression properties are attributed to the inherent imperfections due to the waviness of the woven fabric reinforcement. Further research would need to be conducted to determine ways to minimize this effect during manufacturing.

1.4.2 Effect of Styrene Content (Chapter 3)

During the Round-Robin study it was decided that in addition to the five sets of panels produced by outside manufacturers, two sets of panels would be fabricated in-house and tested alongside the other manufacturers. This lead to a side study on the effect of Styrene content on material properties

E-glass/vinyl-ester composite laminate panels were fabricated using two different resin formulations to investigate the effects of styrene content on material properties. The first resin formulation was "as received" containing 40wt% styrene, and the second formulation was diluted with an additional 5wt% styrene monomer, for a total of 45wt% styrene. The increase of styrene content reduced the wet-out time of the fiber preforms by 22-29% on average compared to the infusions with the base resin formulation, which was one of the objectives of diluting the resin; however, it also reduced the resin gel time by 6-15%.

As in the Round-Robin Study, material test coupons were cut from each of the four panels, two from each resin formulation. Material testing was comprised of ASTM test standards for constituent volume content, tension, compression, in-plane shear, and four-point flexure with 1/4-point loading.

The increase in styrene content reduced the mean value for the majority of the strength and modulus properties for the tension, compression and shear tests. The tensile results produced statistically discernible decreases of 14% for strength in the *y*-direction and 1.8% for modulus in the *x*-direction for the increased styrene formulation. The compression strength in the y-direction also proved to be statistically significant with a 5% decrease for the elevated styrene content resin formulation. The shear properties in the *x* and *y*-directions did not produce any statistically significant results.

The flexural tests produced the only results that indicated an increase in properties for the specimens with the increased styrene formulation. The mean modulus in the x-direction increased by 4% with increased styrene content and was shown to be statistically significant.

Based on the material property variations with increased styrene content for the Derakane 8084 resin observed in this study, it would be prudent to thoroughly investigate the effects of further dilutions prior to implementing such a formulation during an infusion.

1.4.3 Full-field Strain Measurements for Determining Flexural Properties (Chapter 4)

A 3-D DIC strain measurement system was implemented in an experimental program for characterizing the flexural properties of polymer matrix composites (PMC) with woven-roving reinforcement with the intent of reducing the variability of the results. One camera was used in a 2-D mode, to monitor mid-span deflection and in-plane strains, and the other two were used as a pair, in 3-D mode, to record full-field strains on the top surface of the specimen.

The strains measured by the DIC system were compared with the strain level computed by the beam equations in the ASTM flexural standard. The mean ASTM strain value was 15.7% larger than the mean DIC strain value, while the CV was a 1.5 percentage points higher for the ASTM value. The assumption of beam theory in the ASTM standard, which does not account for shear deflections, coupled with the strain gradients present on the woven roving composites is the reason for the difference.

In addition to reducing the variability of the results, the DIC system's post processing capabilities allowed each test to be reviewed as a means to inspect the formation of the strain field and to observe the nature of the progressive failure of the flexural test specimens.

1.5 Laboratory Study

The VARTM process has been investigated in several studies over the past 15 years [13-18]. The parameters that have been shown to have the greatest effect on composite mechanical properties include fiber preform consolidation, resin chemistry and curing, fiber sizing, interphase formation, and post-cure. Some of these effects were investigated during three separate phases of the laboratory study.

- Effect of Fiber Preform Consolidation (Chapter 5) [19]
- Effect of Resin Catalyzing Recipe and Ambient Temperature (Chapter 6) [20]
- Effect of Fiber Preform Conditioning (Chapter 7) [21]

The parameters from each phase that produced the least amount of variability in test results were then carried through to the next phase to minimize variability due to those manufacturing variables.

An infusion pressure control system was implemented during the fabrication of the composite panels in this portion of the research. This allowed for precise control of infusion pressure used during the infusion process, and monitoring of infusion pressure, resin temperature and ambient conditions through a data acquisition system.

To reduce variability due to fabricating different sized panels, a common panel size was fabricated during all three phases of the Laboratory Study. The FRP panel dimensions were 610 mm x 965 mm (24 x 38 in.) and consisted of ten layers of fabric reinforcement in a warps-parallel configuration, for a nominal thickness of 6.4 mm (0.25 in.). It is worth noting that the panel size allowed for a complete second set of specimens to be obtained from the panel if there were problems during specimen preparation or

testing of the original set. This reduced the variability that may occur during manufacturing by eliminating the need to re-fabricate panels.

Cracks in the form of delaminations and disbonds are the most common defects found in composite structures [22]. As a result, Mode-I fracture tests were implemented during the laboratory study. The Mode-I fracture toughness properties computed in this study were the visual onset fracture toughness, the nonlinear onset fracture toughness, and the propagation fracture toughness.

1.5.1 Effect of Fiber Preform Consolidation (Chapter 5)

The objective of the study was to determine how preform consolidation routines commonly used during laminate fabrication affect the Mode-I fracture toughness of marine grade polymer composites.

The range of infusion pressures and consolidation times were chosen based on discussions with industry fabricators and personnel from the Naval Surface Warfare Center - Carderock Division (NSWC-CD), and were intended to encompass the range of pressures and times encountered when fabricating marine composite laminates of varying degrees of complexity. The fabrication matrix that includes the range of consolidation variables used during this phase of the study is presented in Table 1.1.

Table 1.1. Panel Fabrication Matrix.

Consolidation Pressure (gage)	**Panel Replicates for each Consolidation Time Period**		
bar (in-Hg)	***1 hour***	***2 hours***	***5 hours***
0.847 *(25.0)*	3	3	3
0.914 *(27.0)*	3	3	3
0.982 *(29.0)*	3	3	3

Standardized material property tests were conducted for Mode-I fracture, constituent volume fraction, and Barcol hardness on specimens from each of the three replicate laminates fabricated for each condition. The Mode-I fracture test was selected for this study since it was the material property of primary interest, and the constituent volume fraction test was selected since it is a good indicator of the effects of the consolidation of the preform. In addition, Barcol hardness measurements were made on resin samples prior to, and after, post-curing of the specimens as a means to verify the consistency of the post-cure process on the resin in the specimens.

The results indicated that longer consolidation times produced statistically discernible variations in the mean fiber volume fraction of the panels fabricated at the two lower consolidation pressures. Likewise, the variation in consolidation pressure produced discernible effects on the mean fiber volume fraction of the panels fabricated with the shortest consolidation time, but not on the panels fabricated with the two longer consolidation times.

There was no correlation found between the global fiber volume fraction of the panels and the three fracture properties (visual onset, nonlinear onset, and propagation) computed in this study. This is similar to what other studies have found where fracture toughness was sensitive to the localized fiber volume fraction in the region of the crack tip and not to the global volume fraction of the specimen [23].

Barcol hardness of the resin from all of the datasets equilibrated to a similar magnitude after post-curing; therefore it is safe to conclude that the material state of the resin should not have played a role in the variation of the fracture toughness properties, and no correlation between the two was observed.

For the Mode-I fracture results, grouping the datasets by consolidation time produced more statistically discernible results than grouping by consolidation pressure. The general trend at the lower consolidation pressures was that shorter consolidation times produced the maximum onset fracture toughness values but minimum propagation toughness values, while longer consolidation times produced the minimum onset fracture toughness values but maximum propagation fracture toughness properties. Further study is recommended to investigate the inverse trend between the onset and propagation fracture toughness properties.

1.5.2 Effect of Resin Catalyzing Recipe and Ambient Temperature (Chapter 6)

The objective of this portion of the laboratory study was to investigate composite material property variations due to variations of resin catalyzing recipe at ambient temperatures commonly encountered when infusing polymer composites for the marine industry.

Laminates were fabricated under three ambient temperature conditions, 15.6, 21.1, and 26.7ºC (60, 70, and 80ºF), and using three different gel times (1.0, 2.5 and 6.0 hours). The range of ambient temperatures and gel times were chosen based on discussions with industry fabricators and personnel from NSWC-CD. These ranges were intended to encompass the range of temperatures and gel times commonly encountered when fabricating marine composite laminates of varying degrees of complexity. Standardized material property tests were conducted for compression, Mode-I fracture, fiber volume fraction, and Barcol hardness on specimens from each of the three replicate laminates fabricated for each condition.

The Barcol hardness results showed a variation in mean hardness of 7.2% from maximum to minimum value, which is almost three times larger than the values obtained during the preform consolidation phase of the study where a single resin recipe was used. This could indicate that some variation due to catalyzing recipe was present even after post curing of the specimens. The compression tests produced statistically discernible strength results for a couple of the dataset comparisons, but no consistent trends in the data were identified.

The Mode-I results produced overall trends in the visual onset fracture property, with respect to gel time and ambient temperature, that were shown to be statistically discernible differences. The ambient temperature dataset groupings produced an overall trend where higher ambient temperatures resulted in larger visual onset fracture toughness values; however, the trend was not consistent across all gel times. Additionally, there were statistically discernible differences for both the NL onset and propagation fracture toughness properties that could not be directly correlated with the parameters in the study.

While there were not many direct correlations identified between the measured material properties and the parameters investigated in this part of the study, there were several statistically discernible differences in the measured properties. These differences could not be discarded as random, since they were generally consistent among the three replicate panels fabricated for each combination of ambient temperature and gel time. Further study is required to identify the source of these differences.

1.5.3 Effect of Fiber Preform Conditioning (Chapter 7)

Woven roving E-glass fabric was conditioned at two different environments prior to fabricating e-glass/vinyl-ester composite laminates to investigate possible mechanical property variations due to fabric sizing degradation. The first environment was a control at 21°C (70°F) and 50% relative humidity and the second was at 32°C (90°F) and 80% relative humidity. The elevated temperature and humidity conditioning was meant to simulate what could occur to the fabric during the lay-up of a large part where the fabric could be exposed to the ambient environment for an extended period of time prior to infusion.

Standardized testing for fiber volume fraction, compression, Mode-I fracture, and Barcol hardness were performed on test specimens from each of the three replicate composite panels fabricated for both of the environmental conditions.

Barcol hardness exhibited the most variability both within and between the conditioning datasets; however, this is typical for this type of test on thermoset polymers. Fiber volume fraction magnitudes and spatial distributions were consistent with the prior phases of this research.

The magnitudes of the mean values and CV for the compression and Mode-I property tests were consistent with the prior phases of this research and indicated no statistical variation between fabric conditioning datasets.

The results of the testing indicate that the elevated temperature and humidity conditioning had negligible effect on the material properties investigated in this study. Since research by other investigators has shown a degradation of sizings due to environmental conditioning, longer durations of conditioning should be investigated in the future.

1.6 Digital Image Correlation Implementations

The 3-D DIC system proved to be an invaluable tool during its implementation throughout the different phases of the study. Aside from its intended use to measure strains and/or deflections during a given test, the added ability to completely visualize what is occurring to the specimen during a test and review this information at a later date provided insight for further study. Two such studies are included here:

- Variability in Flexural Response of FRP Composites (Chapter 8)
- Simultaneous Measurement of Flexural and Shear Moduli (Chapter 9)

1.6.1 Variability in Flexural Response of FRP Composites (Chapter 8)

A flexure study was conducted intended to investigate the variability in flexural strength, flexural modulus, stress distribution, failure type, and failure location due to selection of load-head size.

The test panels consisted of 40 layers of fabric reinforcement with the warp direction alternating (from 0 to 90 degrees) from layer to layer, for a nominal thickness of 25.4 mm (1.0 in.). The test specimens were cut from the panels to a nominal dimension of 38.1 mm (1.5 in.) wide by 610 mm (24 in.) long, using a wet saw with a diamond coated blade. A 4-point flexural test configuration, with quarter-point loading, was used for this investigation with a specimen span-to-thickness ratio of 22-to-1 used for all tests. A 3-D DIC system was used to record the mid-span deflection and the full-field strain distribution during each test.

Six different load-head configurations were investigated during this study. Specifically, 12.7 mm (0.5 in.), 25.4 mm (1.0 in.), and 50.8 mm (2.0 in.) diameter load-heads, with and without tabbing material, were investigated.

The majority of the specimens failed in compression of the top surface followed by a delamination, with the remaining specimens failing in compression either near the center of the beam, or at the load-head.

A load-head size of 50.8 mm (2.0 in.), without tabbing material, resulted in the highest mean and lowest CV for the flexural strength, for the six test configurations investigated. The tabbing material helped reduce the surface damage to the specimens, but showed less benefit at reducing failures near the load-heads for the larger diameter load-heads.

The DIC system was successful at recording the mid-span deflections and photographically documenting the tests. The system also gave a detailed visualization of, and quantified, the stress distribution through the thickness of the specimen.

1.6.2 Simultaneous Measurement of Flexural and Shear Moduli (Chapter 9)

A 3-D DIC system was implemented with an analytical optimization routine to measure the flexural (E) and shear moduli (G) during flexure testing of FRP composite laminate beams. The 3-D DIC system recorded the deflected shape at the neutral axis of composite beams during four-point flexural testing at span-to-thickness ratios of 8, 12, 16, and 24-to-1. A MatLab optimization routine was used to curve-fit the first order shear deformation theory (FSDT) analytical equations, over the half-span of the beam, to the experimental deflection and slope data from the neutral axis of the beam.

The majority of the span-to-thickness ratios investigated produced reasonable results for G for 50% of the specimens in the dataset. The slope-optimization produced less variability and more realistic results for E and G when compared to the deflection-optimization for the range of span-to-thickness ratios investigated in this study. The

slope-optimization is thought to be more sensitive at discerning the magnitude of *G* due to the sharp discontinuity in the FSDT analytical slope equation at the load points.

The asymmetry of the deflected shape of the neutral axis about the mid-span of the beam is thought to be the main reason for the variability in the results and the inability of the optimization routine to detect shear deflections in approximately 50% of the datasets analyzed.

1.7 Conclusions

The level of variation in material properties that was observed in the round-robin study was not observed for the same properties in the laboratory studies or in the study with added styrene content, which was conducted in-house and parallel to the round-robin study. The lack of significant variation of basic properties in the lab studies would indicate that quality control plays a greater role in property variation than the range of parameters that was investigated when measuring basic properties (compression, tension, shear, and flexure). The other conclusion is that the variation in properties in the round-robin study could be due to factors that were not captured in the laboratory studies. The most obvious of which would be a difference in resin or fiber properties due to lot variations, which was not investigated in the laboratory study.

Aside from the general quality control issues, a general observation was that lower resin viscosities simplified the infusions through a reduced infusion time and produced less special variation in properties. The reduced viscosity produced a faster and more thorough wet-out of the fiber preform, thereby reducing gradients in fiber volume fraction. Elevation of the ambient temperature, or the mold temperature, is the best way to accomplish this since resin dilution can result in a reduction of material properties.

The applicability of some of the laboratory study findings to other fiber/resin systems is difficult to determine. The results of the consolidation research study should transfer to other fiber systems, while the resin/temperature and preform conditioning studies results could be highly specific to the type of resin and/or fiber sizing. Further investigation would need to be conducted to determine these interactions.

The implementation of the DIC system with composite materials testing not only provides a method of determining bulk material properties (strength and modulus) and reducing property variability, but also a means of verifying analytical models for composite mechanics research. This is a research area that the author will continue to investigate for the foreseeable future.

The run-arrest response during Mode-I testing of woven roving composites makes it difficult to properly measure fracture toughness. Ways to reduce this effect should be investigated further if repeatable fracture properties are to be obtained for this material system. In addition to the issues with run-arrest behavior of Mode-I fracture test specimens, the current version of the ASTM Mode-I fracture test standard is not conducive to producing repeatable results for the onset fracture toughness properties. Determining the onset toughness via visual means is simply unreliable, while the nonlinear method as outlined in the standard does not provide any real guidance that would lead to a repeatable procedure from one investigator to the next. At the time of this writing, the Mode-I standard is currently undergoing revision by the ASTM D30 composites committee, and the author hopes to offer suggestions that will provide a better defined analysis procedure for the nonlinear onset fracture property. The suggestions will be based on work that was conducted during a different phase of the ONR project [24],

and was the method employed to compute the nonlinear onset fracture toughness during all phases of the research presented in this dissertation.

1.8 Recommendations

The following recommendations are based on the findings of the research conducted during this study:

- More so than the other properties investigated, compression properties are reduced due to fiber waviness in woven roving composites. Further research would need to be conducted to determine ways to minimize this effect during VARTM manufacturing with woven rovings.
- A thorough investigation should be conducted prior to the addition of diluents to a base resin, since this research showed that additions as small as 5wt% styrene monomer can reduce laminate properties by as much as 14%.
- The Mode-I fracture toughness issues outlined in the conclusions need to be addressed if the Mode-I property is to be measured consistently.
- Further study is recommended to investigate the inverse trend between the Mode-I onset fracture and propagation fracture toughness properties and its relation to fiber preform consolidation time and pressure.
- Further study is required to identify the source of the variation in material properties outlined in the resin catalyzing recipe study (Chapter 6). A well structured design of experiment (DOE) study is recommended. This would at least be a start at identifying which resin catalyzing variables play the greatest role in material property variation.

- Research by other investigators has shown a degradation of fiber sizing due to environmental conditioning; therefore, a more thorough study including longer durations of environmental conditioning of fiber preforms should be investigated in the future.
- The ability to consistently measure flexural and shear moduli simultaneously during a flexure test would prove to be a useful test procedure. Further investigations are recommended to resolve the shortcomings encountered in the current study.
- A 3-D DIC system is an invaluable tool that should be implemented into any research or industrial testing program at either the material coupon or structural testing levels of composite materials. This is especially true for marine grade composites where large surface strain gradients are present due to the woven pattern of the heavy fiber tows (i.e. large unit-cell). The insights it provides are innumerable and the benefits of such a tool can not be stressed enough.

1.9 References

1.1 Cain J J, Post N L, Lesko J J, Case S W, Lin Y, Riffle J S, and Hess P E (2006) Post-Curing Effects on Marine VARTM FRP Composite Material Properties for Test and Implementation. Journal of Engineering Materials and Technology, Transactions of the ASME, 128:34-40.

1.2 El-Chiti F (2005) Experimental Variability of E-Glass Reinforced Vinyl Ester Composites Fabricated by VARTM/SCRIMP. MS Thesis in Mechanical Engineering, University of Maine, Orono, ME.

1.3 Lopez-Anido R, El-Chiti F W, Muszynski L, Dagher H J, Thompson L, and Hess P E (2004) Composite Material Testing Using a 3-D Digital Image Correlation System. Proceedings of the ACMA Composites 2004 Convention and Trade Show, Tampa, FL, October 6-8, 2004, American Composites Manufacturers Association, Arlington, VA.

1.4 El-Chiti F, Lopez-Anido R A, Dagher H J, Thompson L, Muszynski L, and Hess P E (2005) Experimental Approach for Characterizing VARTM Composites Using a 3-D Digital Image Correlation System. Proceedings of the SEM XII Int. Congress and Exposition on Experimental and Applied Mechanics, Portland, OR, June 7-9, 2005, Society for Experimental Mechanics, Bethel, CT, 8p.

1.5 Berube K A and Lopez-Anido R (2008) Full-field Strain Measurements for Determining Mechanical Properties of Marine Composite Laminates. Experimental Mechanics Applied to Damage: Detection, Analysis and Mitigation, SEM XI International Congress Exposition on Experimental and Applied Mechanics, Orlando, FL, June 2-5, 2008, Society for Experimental Mechanics, Bethel, CT, 8p.

1.6 Nicoletto G, Marin T, Anzelotti G, and Roncella R (2011) Application of High Magnification Digital Image Correlation Technique to Micromechanical Strain Analysis. Strain 47:E66-E73.

1.7 Khennouf D, Dulieu-Barton J M, Chambers A R, Lennard F J, and Eastop D D (2010) Assessing the Feasibility of Monitoring Strain in Historical Tapestries Using Digital Image Correlation. Strain, 46:19-32.

1.8 Masters J (1996) Strain Gage Selection Criteria for Textile Composite Materials. NASA Contractor Report 198286, National Aeronautics and Space Administration, Langley Research Center, VA.

1.9 MIL-HDBK-17F-1 (2002) Composite Materials Handbook Volume 1 - Polymer Matrix Composites Guidelines for Characterization of Structural Materials, ASTM International, West Conshohocken, PA, p. 8.1-110.

1.10 Berube K A and Lopez-Anido R A (2010) Variability in the Material Properties of Polymer Matrix Composites for Marine Structures. Journal of ASTM International 7(4):18p.

1.11 Berube K A and Lopez-Anido R A (2012) Effect of Styrene Monomer on the Material Properties of Marine Grade Polymer Matrix Composite Materials Fabricated with a VARTM Process, Tech Note to be submitted.

1.12 Berube K A and Lopez-Anido R A (2008) Full-Field Strain Measurements for Determining Mechanical Properties of Marine Composite Laminates. SEM XI International Congress Exposition on Experimental and Applied Mechanics, Orlando, FL, June 2-5, 2008, Society for Experimental Mechanics, Bethel, CT, 8p

1.13 Han K, Jiang S, Zhang C, and Wang B (2000) Flow Modeling and Simulation of SCRIMP for Composites Manufacturing. Composites: Part A, 31:79-86.

1.14 Hammami A and Gebart B R (2000) Analysis of Vacuum Infusion Molding Process. Polymer Composites, 21(1):28-40.

1.15 Hammami A (2001) Effect of Reinforcement Structure on Compaction Behavior in the Vacuum Infusion Process. Polymer Composites, 22(3):337-348.

1.16 Stadtfeld H C, Erninger M, Bickerton S, and Advani S G (2002) An Experimental Method to Continuously Measure Permeability of Fiber Preforms as a Function of Fiber Volume Fraction. Journal of Reinforced Plastics and Composites, 21:879-899.

1.17 Modi D, Johnson M, Long A, Rudd C (2009) Analysis of Pressure Profile and Flow Progression in the Vacuum Infusion Process. Composites Science and Technology, 69:1458-1464.

1.18 Yenilmez B and Sozer E M (2009) Variation of Part Thickness and Compaction Pressure in Vacuum Infusion Process. Composites Science and Technology, 69:1710-1719.

1.19 Berube K A and Lopez-Anido R A (2011) Effect of Preform Consolidation on the Fracture Toughness of Marine Grade Polymer Matrix Composite Materials Fabricated With a VARTM Process. Journal of Advanced Materials 43(1):30-48.

1.20 Berube K A and Lopez-Anido R A (2012) Effect of Resin Cure Recipe and Ambient Processing Temperature on the Material Properties of Marine Grade Polymer Matrix Composite Materials. Submitted to Materials Performance and Characterization.

1.21 Berube K A and Lopez-Anido R A (2012) Effect of Woven Roving Environmental Conditioning on the Material Properties of Marine Grade Polymer Matrix Composite Materials Fabricated with a VARTM Process. Tech Note to be submitted.

1.22 Bolotin V V (2001) Mechanics of Delaminations in Laminate Composite Structures. Mechanics of Composite Materials, 37:367-380.

1.23 Compston P and Jar P-Y B (1998) Comparison of Interlaminar Fracture Toughness in Unidirectional and Woven Roving Marine Composites. Applied Composite Materials, 5(3):189-206.

1.24 Blake S P, Berube K A, and Lopez-Anido R A (2011) Interlaminar Fracture Toughness of Woven E-Glass Fabric Composites. Journal of Composite Materials, 46(13):1583-1592.

CHAPTER 2

VARIABILITY IN THE MATERIAL PROPERTIES OF POLYMER MATRIX COMPOSITES FOR MARINE STRUCTURES

2.1 Abstract

The test results from a composite material round-robin manufacturing study are presented. The objective of the study was to investigate material property variability when different manufacturers were used to fabricate identical composite parts. The study was part of an ongoing Office of Naval Research project to determine the causes of material property variability of E-glass/vinyl-ester structural composites fabricated with a VARTM process. The manufacturers that participated in the study consisted of five industrial composite fabricators that either had experience with US Naval fabrication projects, or possessed commercial marine fabrication experience. The materials specified for the study were a 24oz woven-roving E-glass fabric and a rubber-toughened vinyl-ester resin system. The tests performed included constituent volume, tension, compression, in-plane shear, and flexure. The material coupon tests were performed on 5.1 mm (0.20 in.) thick cross-ply laminates in a warps-parallel lay-up. A 3-D digital image correlation system was used to measure strain during testing to reduce the variability often experienced when using conventional foil strain gauges on heavy woven fabrics. The results of the testing indicated that compression properties had the most variability in both strength and modulus, which was attributed to the waviness of the fabric, while the flexural strength and tensile modulus had the least amount of variability.

2.2 Introduction

Despite advances in the vacuum assisted resin transfer molding (VARTM) manufacturing process, questions remain regarding the consistency of material properties in large, fiber-reinforced polymer composite parts. The marine industry is an area where the VARTM process is used extensively. The common method of implementing the VARTM process in the fabrication of composites parts in the marine industry involves one-sided hard tooling and a vacuum bag. The very nature of the this process, using vacuum pressure to consolidate the fiber-preform and then using that same pressure differential as the means to draw the resin into the part, can lead to many process variations. In addition, the size, shape, and thickness of the part, will determine the flow media configuration, inlet hose spacing, and resin catalyzing recipe formulation that a fabricator will use depending on their prior experience with similar parts. With a large number of process variables controlled by the fabricator, the question remains as to the effect of these process variations on the quality and consistency of the structural properties of the resulting parts. A round robin study was undertaken in an attempt to investigate this variability.

The objective of the round robin study was to determine the extent of variability in material properties that could be encountered when different manufacturers were used to fabricate identical composite parts. The manufacturers were instructed to use a specific fabric, resin and fiber lay-up when fabricating the laminates. The five manufacturers that participated in this study either had US naval, or commercial marine, composite fabrication experience. Each manufacturer was assigned a letter-code, A through E, in order to track the test specimens during all phases of the testing. Aside from the primary

author, no one involved in any phase of the testing was aware of which letter-code corresponded to which manufacturer.

The round robin study is part of a larger project sponsored by the Office of Naval Research to investigate the causes of variability in material properties of E-glass/vinyl-ester marine grade composites. The sources of variability being investigated in the larger project include those due to manufacturing, post processing, and testing of composites. A prior phase of the study investigated the variability due to the use of specific test standards on composites fabricated with heavy woven e-glass fabrics [1]. Specifically, two different ASTM test standards were compared for each of the following material properties: tension, compression, and shear. The results of that study were used to determine the test methods used for the round robin study. In addition, flexure and constituent volume tests were performed during the round robin.

2.3 Composite Material Evaluated

A marine grade fiber-reinforced polymer (FRP) composite reinforced with woven roving was tested in this study. The FRP panels consisted of E-glass/vinyl-ester and were fabricated using a VARTM process. The fiber reinforcement used was a Saint Gobain Vetrotex 324 woven roving with a weight per unit area of 814 g/m^2 (24 oz/yd^2). The tow spacing is 5.1 mm (5 tows per inch) in the warp direction, and 6.4 mm (4 tows per inch) in the fill direction. This results in 55% of the fiber orientated in the warp direction and 45% in the fill direction. The polymer resin used was Ashland Derakane 8084, which is an elastomer-modified epoxy vinyl-ester resin.

The manufacturers were instructed to fabricate a given number of flat panels for structural testing using a common VARTM process that consisted of one-sided hard

tooling and a pliable vacuum bag. The panel dimensions were 1.22 m x 1.22 m (4 ft x 4 ft) with nominal thicknesses of 12.7 mm (0.5 in.) and 25.4 mm (1.0 in.). In addition, they were instructed to fabricate a 1.22 m x 1.22 m "witness panel" during each infusion process of the structural panels, with a minimum of two witness panels required. The purpose of the witness panels was to provide a thin laminate for material coupon testing that was fabricated with the same materials and infusion variables as the structural panels and should therefore be representative of the properties of the thicker structural panels. The witness panels consisted of eight layers of fabric reinforcement with the warps parallel, for a nominal thickness of 5.1 mm (0.20 in.). The lay-up notation is $[08]_f$, where the orientation indicates the warp direction of the fabric. Additional specifications that were requested of the manufacturer included:

- No fabric overlaps within the panel
- The panels should NOT be post-cured.
- Provide promoter, accelerator and additive types and quantities used, unless deemed proprietary.
- Manufacturers were provided with a device to monitor and log ambient temperature and %RH. Manufacturers were asked to place the device in proximity to the panel infusion location.

Shortly after arrival at the test lab, the 1.22 m x 1.22 m witness panels were post-cured in a large oven at 82ºC (180ºF) for 4 hours. This temperature and duration had been shown to be appropriate for this material system at this thickness in an earlier phase of the study [2].

2.4 Experimental Methods

The material property tests conducted during the round robin study included constituent volume fraction, tension, compression, in-plane shear, and flexure. The specific tests performed were the ASTM standards as listed below.

- Constituent Volume - ASTM D2584 [3]
- Tension - ASTM D3039 [4]
- Compression - ASTM D6641 [5]
- Shear - ASTM D4255 [6]
- Flexure - ASTM D7264 [7]

Eight specimens were cut from the two witness panels from each of the five manufacturers for each test type and fiber orientation, where the warp and fill orientations of the fabric correspond to the x and y-directions of the panels, respectively. This resulted in a total of 80 specimens for each combination of test type and fiber orientation. Specimens in the x and y-orientations were used for the tension, compression, and shear tests, while specimens in the x-direction were used for the flexural tests. Eight specimens were also cut from each panel for constituent volume testing. The position of the specimens in the panel was distributed at eight locations to capture spatial variability of properties due to location in the panel, as shown in Figure 2.1. CNC water-jet machining was used to cut all of the specimens. In addition to expediting the specimen cutting operation, the CNC water-jet method reduces the variability in specimen dimensions. As an example, the coefficient of variation (CV) for specimen width of all the compression specimens was within 0.40%.

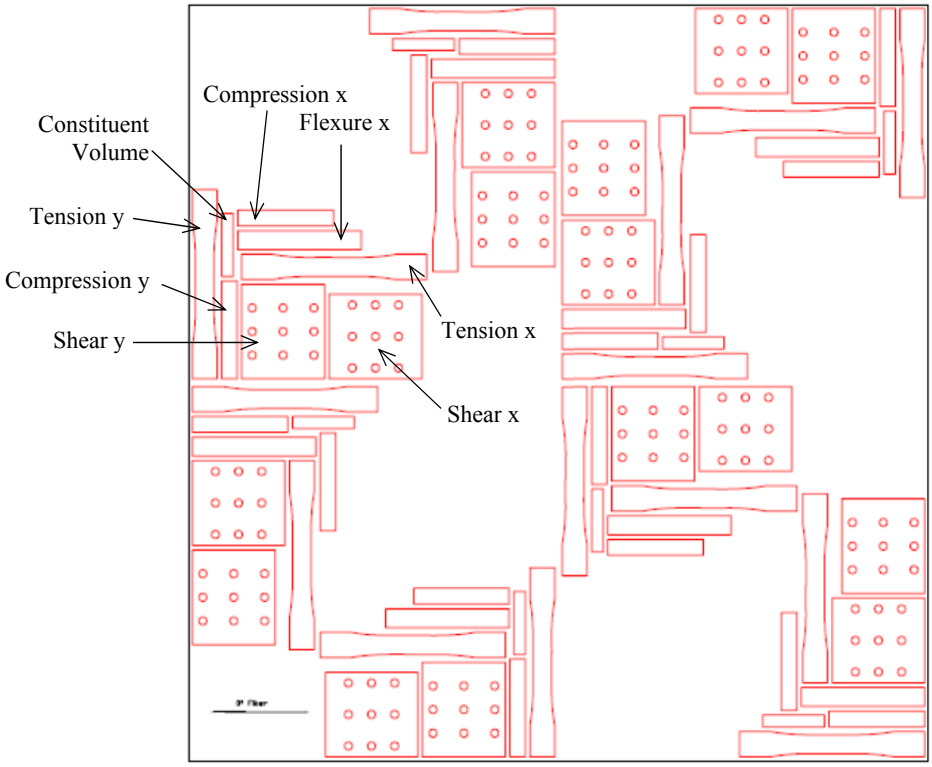

Figure 2.1. Specimen distribution across the panel.

A 3-D Digital Image Correlation (DIC) system was used to record the full-field strains on the test specimens during testing. The DIC system provides an advantage over conventional strain gages as it allows a larger area of the specimen to be monitored during testing. This is especially advantageous when testing heavy woven fabrics where strain gage size and placement can influence test results due to strain variations on the specimen [8-10]. The variations are a result of the strain gradients present on the surface of the specimen due to the size of the fiber tows and the alternating nature of the woven warp and fill tow orientations.

Prior to testing, all specimens were conditioned at 23 ± 2°C (73.4 ± 3.6°F) and 50 ± 10% relative humidity for a minimum of 48 hours, as recommended in the ASTM standards. Since the objective of the study was to determine the extent of material

property variability encountered when different manufacturers were used to fabricate identical laminates, and not to produce material design allowables, all of the testing was conducted on specimens in a room-temperature dry condition. The production of material design allowables would have required different batches of material to be fabricated and then exposed to various environmental conditions to account for the exposure that the laminates could encounter during their operational lifetime. For marine composites, these conditions include temperature, moisture, and ultra-violet light exposure. While these conditions have been shown to significantly reduce the material properties of similar marine laminate materials [11-13], such an investigation was considered to be beyond the scope of this study.

All specimens were examined prior to testing for visible defects due to manufacturing or specimen preparation. In addition to inspecting the exterior of the specimens for excessive fiber waviness or large thickness variations, the inspection included backlighting of the specimens, which would reveal macroscopic inclusions and voids produced during manufacturing, and delaminations produced during specimen preparation. Any of the above defects could adversely affect the material properties [1, 14-16]; however, none were observed in any of the specimens. The dimensions of all specimens were measured and recorded as outlined in the respective standards. All of the specimen thickness variations were within acceptable limits as outlined by their respective standards. The specimens were then prepared for the DIC measurement system by applying a speckled grayscale pattern of paint to the area of the specimen that would be observed during testing. A typical speckle pattern that was applied to a specimen is

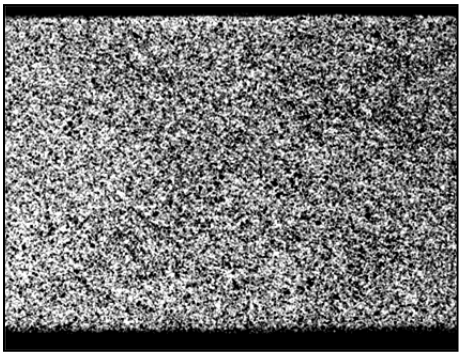

Figure 2.2. Typical speckle pattern on the face of a specimen.

presented in Figure 2.2. This pattern allows the DIC system to track each point of the specimen in the gage area during testing.

All of the tests were conducted at the AEWC Advanced Structures and Composites Center, at the University of Maine in Orono, Maine. The tension, compression, shear, and flexure tests were performed on a 100 kN (22.5 kip) Instron load frame equipped with side-loading hydraulic grips, and located in an environmentally controlled test lab at an environment of 23 ± 2°C and 50 ± 5% relative humidity.

2.4.1 Constituent Volume Test

ASTM test standard D2584 was used to determine the constituent volume fraction of the witness panel specimens. The specimen size used for the test was 19.0 mm x 76.2 mm (0.75 in. x 3.0 in.). The specimens were placed in a crucible in a muffle furnace at a temperature of 565ºC for a period of 2.5 hours, which prior experience with this material system had shown to be sufficient for complete resin removal. [1]

2.4.2 Tension Test

The results of the prior test evaluation phase of the project indicated that a larger tensile specimen was required to properly capture the representative width of the 24 oz

woven roving fabric [1]. In addition, a dog-bone shaped specimen was favored over a tabbed rectangular specimen. An optimized dog-bone specimen, as shown in Figure 2.3, was used for the tensile tests [17]. Aside from the larger dog-bone shaped specimen, ASTM tensile test standard D3039 was used as a guideline for performing the tests.

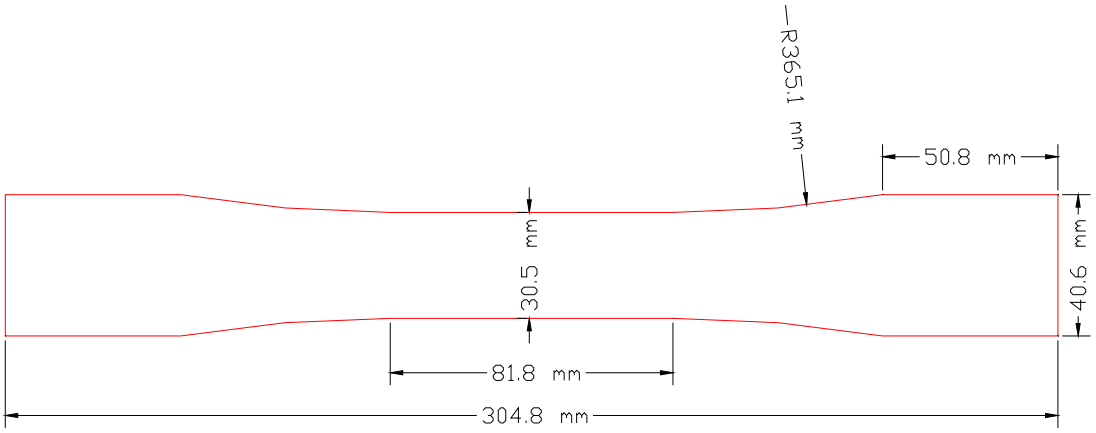

Figure 2.3. Optimized dog-boned tensile test specimen.

A gripping force of 43.4 kN (9.75 kip) was applied to the grip area of the specimen during testing. The specimens were tested in displacement control at a crosshead rate of 0.30 mm/sec (0.012 in/sec) resulting in an average test time of approximately 3 minutes. Load and crosshead displacement data were recorded at a sampling rate of 10 Hz on the Instron control computer and at 1 Hz on the DIC system. The 1 Hz sampling rate was chosen such that it reduced post-processing time on the DIC system without compromising the resolution and accuracy of the results, as indicated by the agreement within 0.50% between the DIC and Instron data acquisition systems.

2.4.3 Compression Test

The test evaluation study indicated that ASTM test standard D6641 was the preferred method for compression testing of marine grade composites [1]. The test

specimen size was 25.4 mm x 152.4 mm (1.0 in. x 6.0 in.). The length of 152.4 mm is slightly longer than normal and was chosen to allow more area of the specimen to be observed by the DIC system. This length was shown to allow the specimens to fail in compression and still avoid buckling failures. A jig was fabricated and used to mount the specimens into the compression test fixture, which helped minimize variations due to specimen alignment in the fixture. The specimens were tested in displacement control at a crosshead rate of 0.01 mm/sec (0.0004 in/sec). This resulted in an average test time of approximately 5 minutes. A self-leveling compression platen was used on the stationary crosshead to account for any misalignment during loading. Load and crosshead displacement data were recorded at a sampling rate of 10 Hz on the Instron control computer and at 1 Hz on the DIC system. The sampling rate was chosen to reduce post-processing time on the DIC system without compromising the resolution and accuracy of the results.

2.4.4 Shear Test

The test evaluation study indicated that Procedure B, Three-Rail Shear, of ASTM test standard D4255 was the preferred method for in-plane shear testing of marine grade composites [1]. The specimen size was 136.5 mm x 152.4 mm (5.38 in. x 6.0 in.).The specimens were tested in displacement control at a crosshead rate of 0.015 mm/sec (0.0006 in/sec), resulting in an average test time of approximately 7.5 minutes. Since this test method does not produce a catastrophic failure of the specimen, the tests were allowed to progress until the load reached approximately 85 kN. This ensured that the load-displacement curve was fully developed and would permit the use of an offset method to obtain the failure strength. Load and crosshead displacement data were

recorded at a sampling rate of 10 Hz on the Instron control computer and at 0.67 Hz on the DIC system. As before, the DIC sampling rate was chosen such that it reduced post-processing time without compromising the resolution and accuracy of the results.

2.4.5 Flexure Test

The ASTM standard D7264 was used to conduct the flexural tests. The specimen size was 25.4 mm x 203 mm (1.0 in. x 8.0 in.) and was tested in 4-point flexure with a ¼-point load configuration at a span-to-thickness ratio of 32. The specimens were tested in displacement control at a cross head rate of 5.1 mm/min (0.20 in/min), resulting in an average test time of approximately 4.5 minutes. The DIC system was used to record both the strain on the top surface of the flexure specimen and the mid-span deflection of the specimen [18]. Load and crosshead displacement data were recorded at a sampling rate of 10 Hz on the Instron control computer and at 0.67 Hz on the DIC system.

2.5 Analysis of Results

The intent of the study was to determine the extent of the variability in mechanical properties when different manufacturers were used. The analysis procedure that was implemented ignored dataset pooling and population distribution issues for the sake of maintaining consistency in the comparison of all the datasets. The dataset pooling and population distribution discrepancies were treated as a level of variability and are presented in the results. If the intent of the study had been to produce material design allowables based on the pooling of all the datasets from all the manufacturers, then a more strict reliability based approach would have been implemented.

2.5.1 Analysis Procedure

The statistical analysis methods outlined in the Composite Materials Handbook (MIL-HDBK-17F-1) for single point data were used to analyze the material property test results for each test type [19]. Specifically, the STAT17F Excel workbook, which executes most of the statistical methods outlined in Section 8 of MIL-HDBK-17F-1, was used to generate the results. While STAT17F computes the statistics for different population distributions, the latest update of MIL-HDBK-17-1 states that a normal distribution is the preferred distribution to assign when computing material properties. Therefore, only the results for a normal distribution are presented and used for comparing the material property results.

Two sets of analysis were conducted in order to investigate different aspects of variability. The first analysis was intended to look at the variability in material properties between the individual manufacturer's two witness panels, while the second analysis was intended to investigate the variability in material properties among all of the manufacturers. An outline of the analysis procedure that was used on each mechanical property is as follows:

- Individual Manufacturer Analysis:
    1. Calculate the mean and coefficient of variation for each property of the individual manufacturer's dataset. (IM-dataset)
    2. Check for outliers in each property IM-dataset using the Maximum Normed Residual (MNR). The MNR is a screening procedure for identifying an outlier in a set of data. A value is declared to be an outlier if it has an absolute deviation from the sample mean which, when compared to the sample standard deviation, is too large to be due to chance.

3. Check if the mechanical property data from the two panels from the same manufacturer can be pooled using the k-sample Anderson-Darling (ADK) goodness-of-fit method. The ADK test is a statistical procedure that tests the hypothesis that the populations from which two or more groups of data were sampled are identical. If the calculated ADK value for the dataset is less than a set critical value then one can conclude, with a five percent risk of being in error, that the groups were drawn from the same population.
4. Check for outliers in each pooled property IM-dataset using the MNR.
5. Check how well the pooled property IM-dataset fits a Normal Distribution by calculating the Observed Significance Level (OSL) using Anderson-Darling. If the OSL > 0.05, then the dataset fits a Normal Distribution.
6. Calculate the B-Basis value based on a Normal Distribution for the pooled property IM-dataset. The B-Basis value is the calculated value at which there is a 95% confidence that 90% of the data values from the population are greater than this value.
7. Calculate the %-of-mean. The %-of mean is the ratio of B-basis value to the Mean.

- Combined Manufacturer Analysis:
    1. Check if the mechanical property data for all five manufacturers can be pooled using the k-sample Anderson-Darling goodness-of-fit method.
    2. Check for outliers in each pooled property combined manufacturer's dataset (CM-dataset) using the Maximum Normed Residual.

3. Check how well the pooled property CM-dataset fits a Normal Distribution by calculating the Observed Significance Level (OSL) using Anderson-Darling.
4. Calculate the B-Basis value based on a Normal Distribution for the pooled property CM-dataset.
5. Calculate the CM-%-of-mean. The CM-%-of-mean is the ratio of the B-basis to the Mean.

It is worth noting that the general practice is to use the mean value for modulus, and not the B-basis, when producing material design allowables. The B-basis was employed here simply to quantify a measure of variability and to establish a correlation between strength and elastic properties.

As recommended in MIL-HDBK-17F-1 for warps-parallel laminates, the strength and modulus results for the tension and compression tests were normalized with respect to panel thickness. Each result was multiplied by the ratio of a specimen thickness to a nominal thickness. This procedure has been shown to account for variations in fiber volume fraction, due to thickness variations, for fiber dominated material properties when the same fiber reinforcement with the same areal weight has been used for fabrication of the test laminates. The thickness used as the nominal thickness was 4.8 mm (0.190 in.), which was approximately the mean thickness of all the specimens used in the study.

All of the property data in the results that follow were plotted using one of three different scales: 0 to 6, 0 to 60, or 0 to 600. In some cases the axes were then truncated to display a total range of 3, 30, or 300, without changing the scale, for the purpose of clarity. The selection of scale was an attempt to make a qualitative comparison of the variability of the different material properties.

2.5.2 Constituent Volume Results

The mean and CV results for the constituent volume tests for the pooled IM-datasets are presented in Table 2.1 and Figure 2.4. The dataset distribution showing the test data for each panel is shown in Figure 2.5. The mean values ranged from a low of 50.4%, for panel D2, to a high of 56.6% for panel A2. Panels A1 and A2 had the largest variability and as the distribution of Figure 2.5 indicates, there was no overlap of the A1 and A2 datasets. This discrepancy was verified by retest and panel thickness measurements.

Table 2.1. Fiber volume fraction test results.

		Individual Panel		Combined Panels	
Mfg.	Panel	mean	CV	mean	CV
ID	*#*	*%*	*%*	*%*	*%*
A	**1**	50.7	2.3	53.6	6.1
	2	56.6	1.9		
B	**1**	53.4	1.7	53.4	1.5
	2	53.4	1.4		
C	**1**	52.0	3.1	52.4	2.7
	2	52.8	2.1		
D	**1**	52.4	2.2	51.4	3.7
	2	50.4	4.0		
E	**1**	54.3	3.5	54.4	2.9
	2	54.4	2.2		

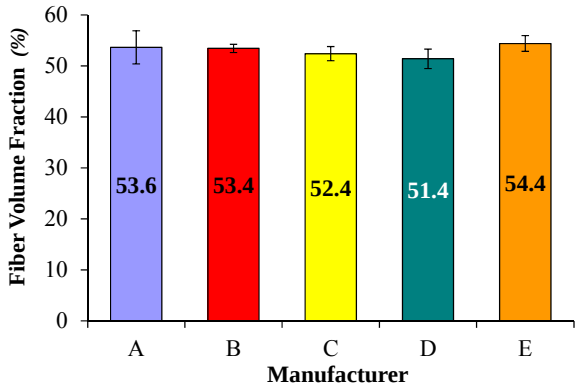

Figure 2.4. Fiber volume fraction results for each IM-Dataset.

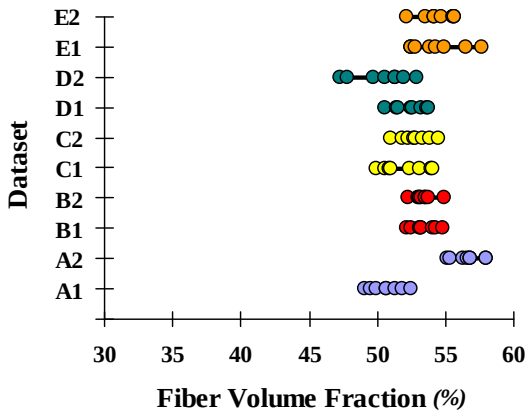

Figure 2.5. Test data for the constituent volume tests.

2.5.3 Tension Results

A stress-strain plot for a typical tension test is presented in Figure 2.6a. While the stress-strain curves typically exhibited a bilinear response, there was not a well defined transition point, or "knee", in the curves. Instead, there was a gradual transition region. The stress-strain curve is presented in Figure 2.6b with the bilinear regions extended showing that the transition region occurs between 4500 to 10,000 micro-strain, which was typical for the tensile test specimens in the study. The tensile secant modulus was calculated in the strain range of 1000 to 3000 micro-strain as recommended in ASTM D3039. The tensile failure strains are presented in Table 2.2. All specimens failed in either the gage area or in the transition region, which have been shown in prior studies to be acceptable failures modes for this specimen configuration [1, 17]. Typical failures are presented in Figure 2.7.

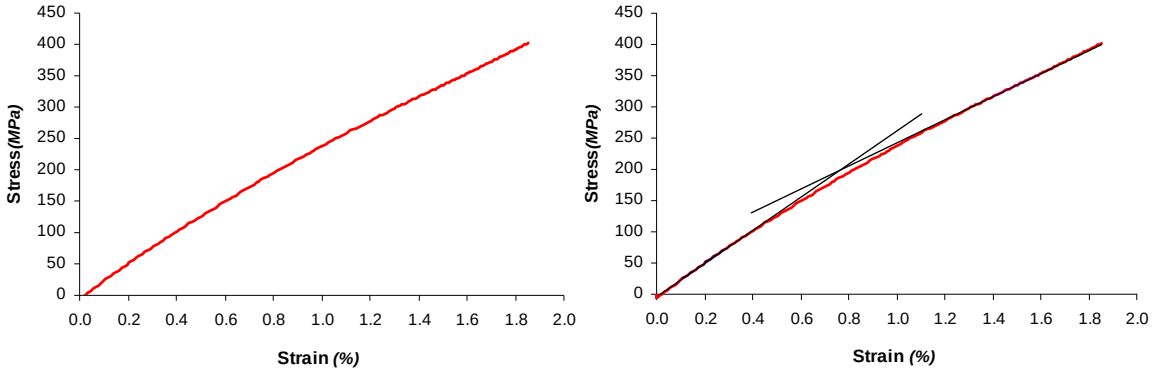

a) b)

Figure 2.6. Stress-strain curve; a) for a typical tension specimen, b) showing bilinear transition region.

Table 2.2. Tensile failure strain results.

Dataset	mean	CV
ID	*%*	*%*
Ax	1.71	10.0
Ay	1.67	6.0
Bx	1.97	4.3
By	2.01	5.2
Cx	2.15	3.3
Cy	2.02	3.7
Dx	1.94	7.8
Dy	2.10	3.1
Ex	1.95	12.1
Ey	2.01	9.6

Figure 2.7. Typical tension specimen failures in the gage area (top) and the transition region (bottom).

The tensile strength and modulus data were normalized as specified in MIL-HDBK-17F-1 using the nominal thickness of 4.8 mm (0.190 in.). The dataset distributions showing the test data for each manufacturer's two panels are presented in Figures 2.8 and 2.9 for the tensile strength and tensile modulus, respectively. The material property data for the x and y-directions are presented side by side in Figures 2.8 and 2.9 for comparison purposes. The strength data was plotted with an x-axis scale of 0-600 MPa, while the modulus data was plotted with a 0-60 GPa scale. The axes were then truncated for clarity without changing the relative scales.

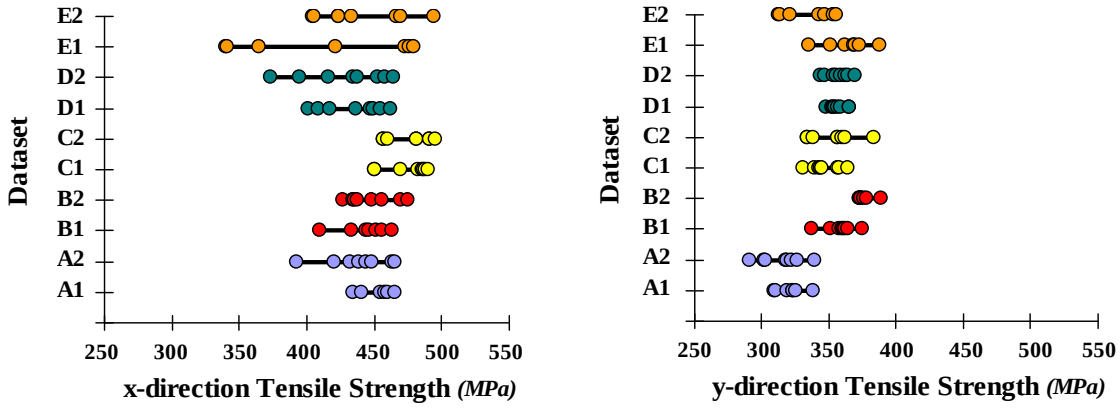

Figure 2.8. Test data for the normalized tensile strength in the x and y-directions.

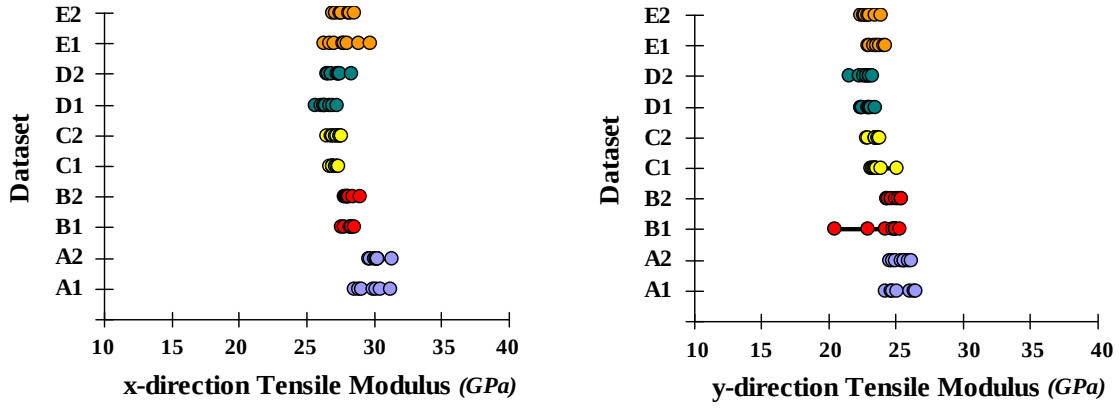

Figure 2.9. Test data for the normalized tensile modulus in the x and y-directions.

The tensile failure strains were of comparable magnitude (1.94 to 2.15%) for IM-datasets B through E; however, the magnitude was considerably lower for IM-datasets Ax and Ay (1.67 and 1.71%). In addition, the CV ranged from 3.1 to 12.1% for IM-datasets Dy and Ex, respectively.

The IM-dataset results for the tensile strength and modulus in the x and y-directions are plotted in Figure 2.10. For the purpose of comparing general variability, the data is presented in a concise format, with both the strength and modulus data included on the same plot. A dual axis was used for the plots, where the strength data is plotted using the left y-axis and the modulus is plotted using the right y-axis. The plotted results include the Mean, B-Basis, and error bars (±1 standard deviation) for each IM-dataset and property.

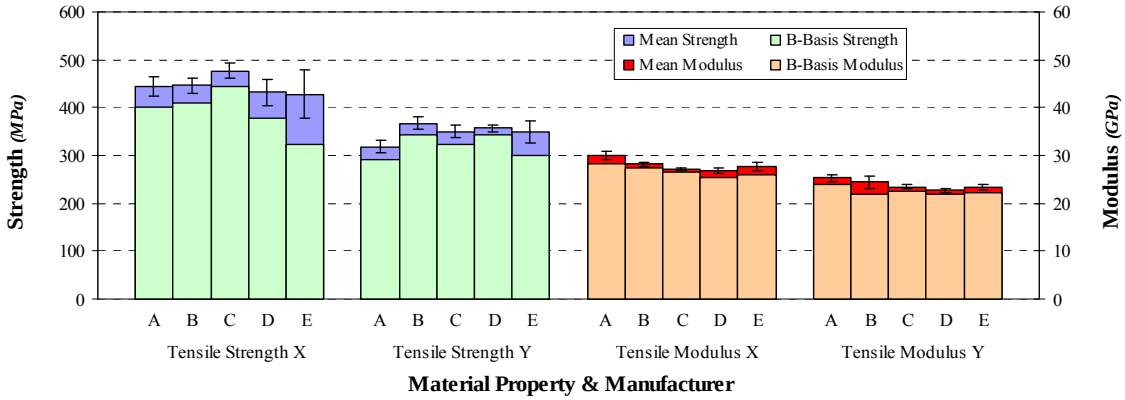

Figure 2.10. Tensile strength and modulus in the x and y-directions for the IM-Datasets.

The mean strength in the x-direction for the IM-datasets ranged from 428 to 476 MPa, with the CV ranging from 3.4 to 11.7%. The B-basis values ranged from 324 to 444 MPa, with a %-of-mean range of 75.8 to 93.2%. The minimum B-basis value occurred for IM-dataset E, while IM-dataset C had the largest B-basis for strength in the x-

direction. The CM-dataset analysis resulted in a B-basis tensile strength in the x-direction of 394 MPa and a CM-%-of-mean of 88.4%.

The mean strength in the y-direction for the IM-datasets ranged from 318 to 367 MPa, with a CV range of 2.0 to 6.5%. The B-basis values ranged from 291 to 342 MPa, with a %-of-mean range of 86.3 to 95.9%. In the y-direction, IM-dataset B had the largest B-basis value and IM-dataset A had the smallest value. The CM-dataset analysis resulted in a B-basis tensile strength in the y-direction of 315 MPa and CM-%-of-mean of 90.2%.

The mean tensile modulus in the x-direction for the IM-datasets ranged from 26.8 to 30.0 GPa, with the CV ranging from 1.1 to 3.2%. The B-basis tensile modulus values ranged from 25.5 to 28.4 GPa, with a %-of-mean range of 93.3 to 97.7%. The minimum B-basis value for tensile modulus occurred for IM-dataset D and minimum %-of-mean for the x-direction tensile modulus occurred for IM-dataset E, while IM-dataset A had the largest B-basis and IM-dataset C had the largest %-of-mean. The CM-dataset analysis resulted in a B-basis tensile modulus in the x-direction of 25.9 GPa and a CM-%-of-mean of 92.8%.

The mean tensile modulus in the y-direction for the IM-datasets ranged from 22.7 to 25.3 GPa, with the CV ranging from 2.0 to 5.0%. The B-basis values ranged from 21.8 to 23.9 GPa, with a %-of-mean range of 89.8 to 95.9%. The minimum B-basis value occurred for IM-dataset D and the minimum %-of-mean for IM-dataset B, while IM-dataset A had the largest B-basis and IM-dataset D the largest %-of-mean. The CM-dataset analysis resulted in a B-basis tensile modulus in the y-direction of 22.0 GPa and CM-%-of-mean of 92.3%.

2.5.4 Compression Results

A stress-strain plot for a typical compression test specimen is presented in Figure 2.11a. All specimens failed in an acceptable manner, as outlined in the standard, and typical failures are presented in Figure 2.11b. The compressive failure strains are presented in Table 2.3. The compressive secant modulus was calculated in the strain range of 1000 to 3000 micro-strain as recommended in ASTM D6641. The compression strength and modulus data were normalized using a common thickness as specified in MIL-HDBK-17F-1 for fiber-dominated material properties. The dataset distributions from each manufacturer's panels are presented in Figures 2.12 and 2.13 for the compression strength and modulus, respectively. The property data for the x and y-directions are presented side by side for comparison purposes. The strength data was plotted with an x-axis scale of 0-600 MPa, while the modulus data was plotted with a 0-60 GPa scale. The axes were then truncated for clarity without changing the relative scales.

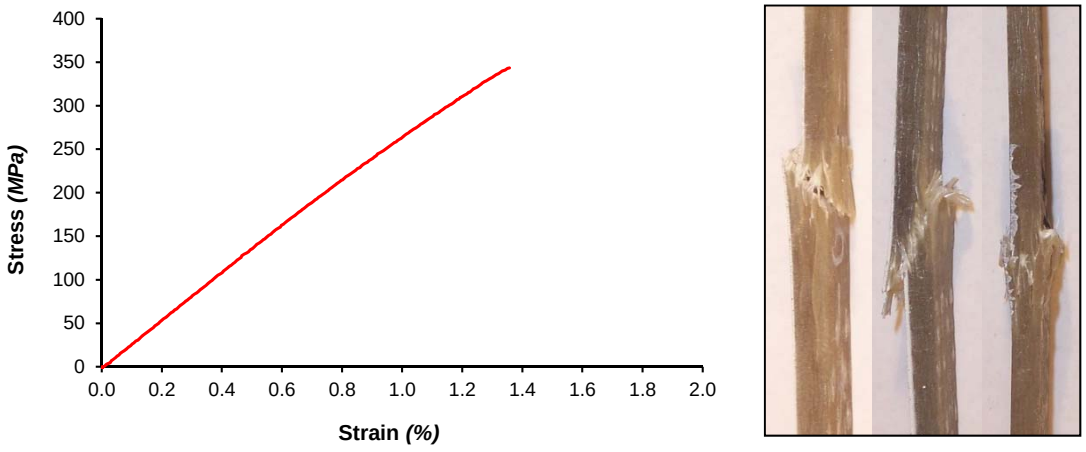

a) b)

Figure 2.11. Typical compression specimen: a) stress-strain curve and b) failure modes.

Table 2.3. Compressive failure strain results.

Dataset	mean	CV
ID	*%*	*%*
Ax	1.68	10.0
Ay	1.76	14.7
Bx	1.45	9.9
By	1.49	11.4
Cx	1.56	13.1
Cy	1.60	12.4
Dx	1.64	12.1
Dy	1.50	10.8
Ex	1.47	16.6
Ey	1.75	11.0

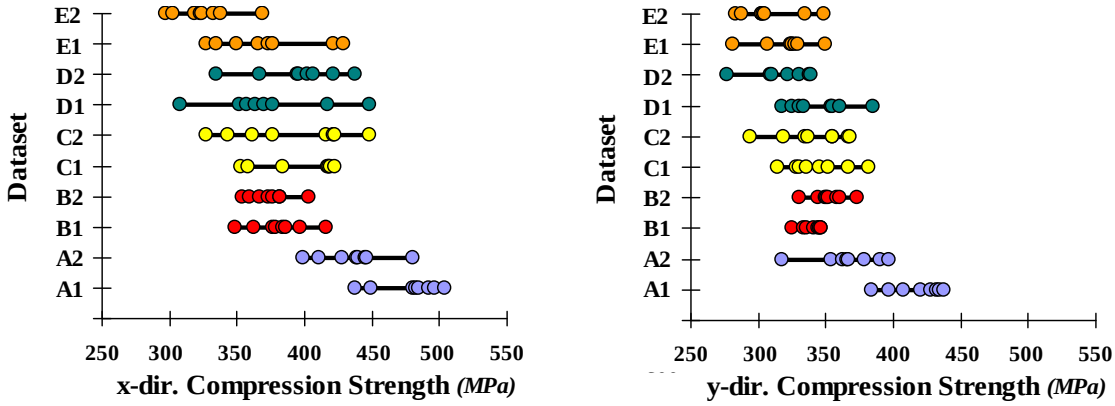

Figure 2.12. Test data for the normalized compression strength in the x and y-directions.

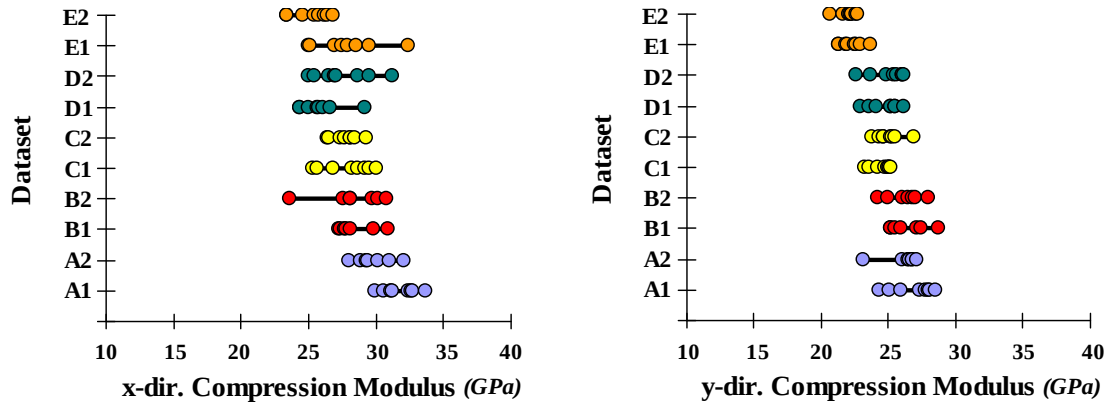

Figure 2.13. Test data for the normalized compression modulus in the x and y-directions.

The compressive failure strains ranged from 1.47% for IM-dataset Ex to 1.76% for IM-dataset Ay. In addition, the CV ranged from 9.9% to 16.6% for IM-datasets Bx and Ex, respectively. The mean value of 1.72% compressive failure strain for IM-dataset A is comparable to the 1.69% mean tensile failure strain for the same dataset. In contrast, the mean compressive failure strains were on-average 22.5% lower than the tensile failure strains for the remaining IM-datasets.

The IM-dataset results for the compressive strength and modulus in the x and y-directions are plotted in Figure 2.14. The mean compressive strength in the x-direction for the IM-datasets ranged from 349 to 457 MPa, with the CV ranging from 4.7 to 10.9%. The B-basis values ranged from 271 to 393 MPa, with a %-of-mean range of 77.8 to 90.4%. The minimum B-basis value for compressive strength in the x-direction occurred for dataset E and the maximum value for dataset A. The maximum %-of-mean occurred for dataset B and the minimum for dataset E. The CM-dataset analysis resulted in a B-basis compressive strength of 317 MPa and a CM-%-of-mean of 80.8%.

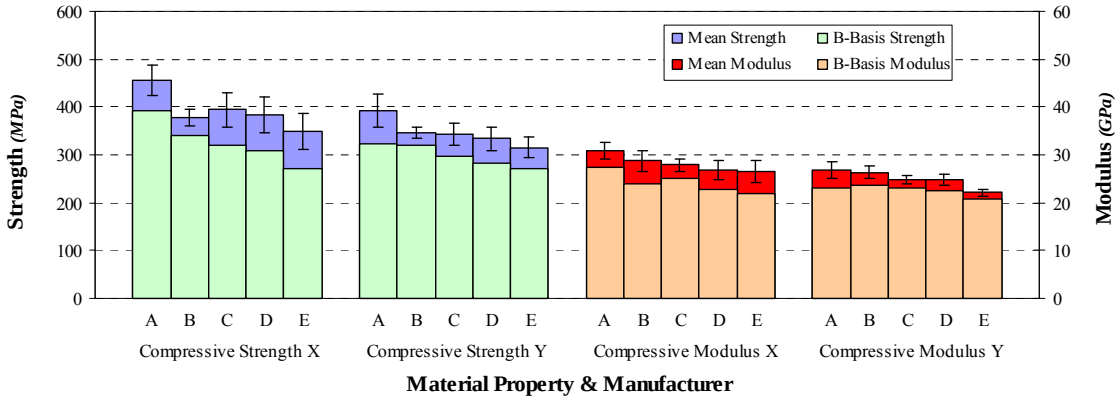

Figure 2.14. Compressive strength and modulus in the x and y-directions for the IM-Datasets.

The mean compressive strength in the y-direction for the IM-datasets ranged from 315 to 392 MPa, with the CV ranging from 3.5 to 8.7%. The B-basis values ranged from 271 to 323 MPa, with a %-of-mean range of 82.3 to 92.9%. The minimum B-basis value for compressive modulus in the y-direction occurred for IM-dataset E and the maximum value for IM-dataset A. The maximum %-of-mean occurred for IM-dataset B and the minimum for IM-dataset A. The CM-dataset analysis resulted in a B-basis compressive strength of 291 MPa and a CM-%-of-mean of 84.3%.

The mean compressive modulus in the x-direction for the IM-datasets ranged from 26.5 to 30.9 GPa, with the CV ranging from 5.0 to 8.7%. The B-basis values ranged from 21.9 to 27.5 GPa, with a %-of-mean range of 82.3 to 89.9%. The minimum B-basis value for compressive modulus in the x-direction occurred for IM-dataset E and the maximum value for IM-dataset A. The maximum %-of-mean occurred for IM-dataset C and the minimum for IM-dataset E. The CM-dataset analysis resulted in a B-basis compressive modulus of 24.2 GPa and a CM-%-of-mean of 86.3%.

The mean compressive modulus in the y-direction for the IM-datasets ranged from 22.1 to 26.8 GPa, with the CV ranging from 3.2 to 6.5%. The B-basis values ranged from 20.7 to 23.6 GPa, with a %-of-mean range of 86.8 to 93.5%. The minimum B-basis value for compressive modulus in the y-direction occurred for IM-dataset E and the maximum value from IM-dataset B. The maximum %-of-mean occurred for IM-dataset E and the minimum for IM-dataset A. The CM-dataset analysis resulted in a B-basis compressive modulus of 21.8 GPa and a CM-%-of-mean of 87.4%.

2.5.5 Shear Results

A stress-strain plot for a typical shear test specimen is presented in Figure 2.15. As seen in the figure, the three-rail test method does not result in a catastrophic failure of the test specimen. Therefore, an offset method was used to determine the shear strength. The method employed in this study used the strain range of 2000 to 6000 micro-strain to construct a line parallel to the linear portion of the stress-strain curve and offset along the strain axis by 0.2%. The intercept of this offset line with the load curve was taken as the failure strength and failure strain. The shear failure strains are presented in Table 2.4. The dataset distributions from each manufacturer's individual panel are presented in Figures 2.16 and 2.17 for the shear strength and modulus, respectively. The strength data was plotted with an x-axis scale of 0-60 MPa, while the modulus data was plotted with a 0-6 GPa scale. The axes were then truncated for clarity without changing the relative scales. Both pair of property datasets for manufacturers A and B show less overlap than the other manufacturer's datasets.

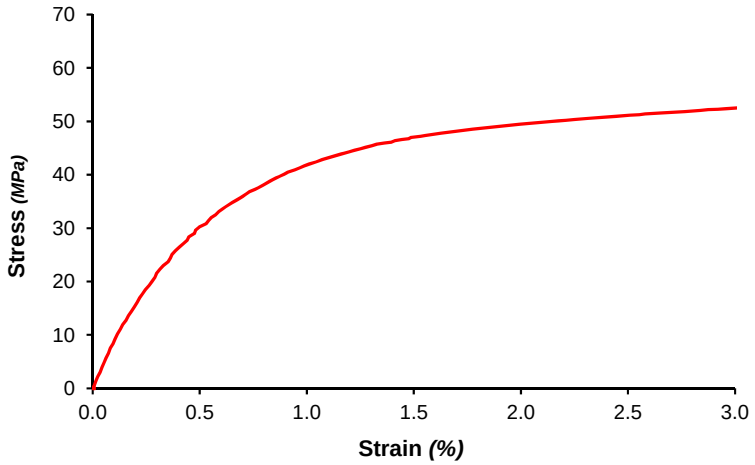

Figure 2.15. Stress-strain curve for a typical shear test specimen.

Table 2.4. Shear failure strain results.

Dataset	mean	CV
ID	*%*	*%*
Ax	1.23	2.4
Ay	1.20	1.2
Bx	1.23	2.8
By	1.20	2.0
Cx	1.22	2.9
Cy	1.23	1.6
Dx	1.22	2.9
Dy	1.24	1.7
Ex	1.23	1.3
Ey	1.23	1.8

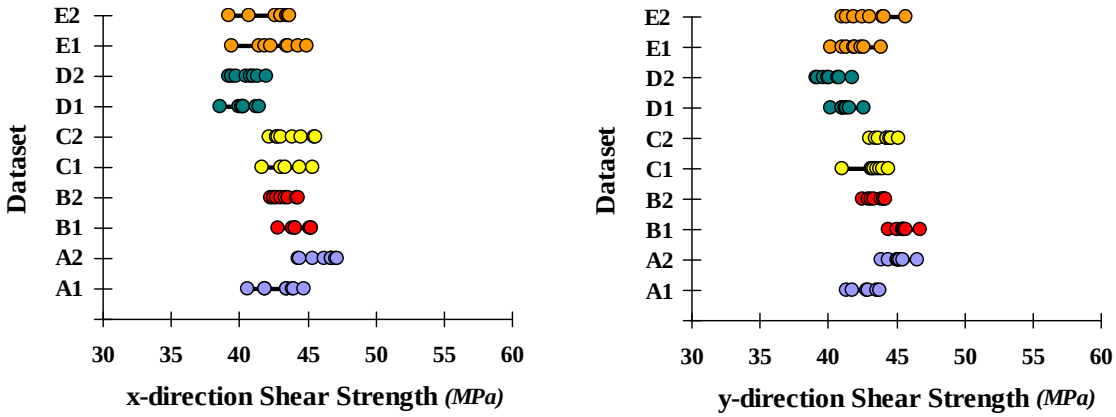

Figure 2.16. Test data for the shear strength in the x and y-directions.

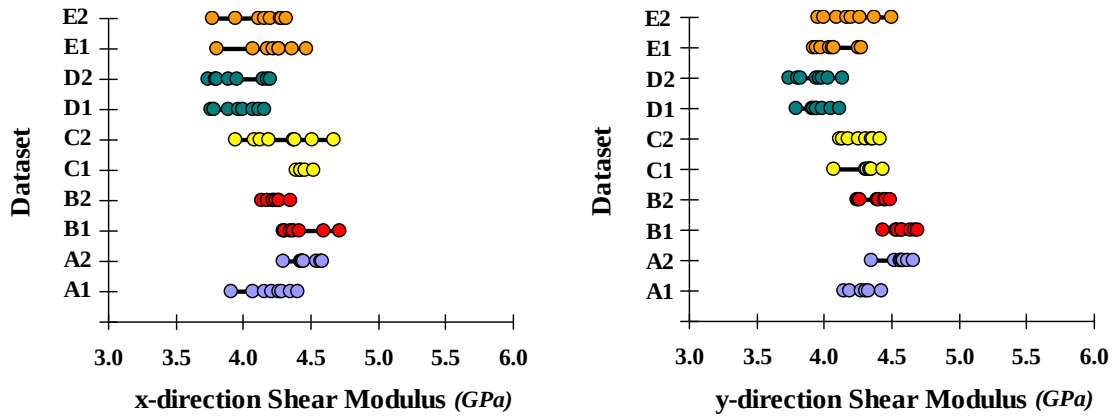

Figure 2.17. Test data for the shear modulus in the x and y-directions.

The shear failure strains ranged from 1.20 to 1.24% for all of the IM-datasets, with the CV ranging from 1.2 to 2.9%. The shear strength and modulus results in the x and y-directions for the IM-datasets are plotted in Figure 2.18. The mean shear strength in the x-direction for the IM-datasets ranged from 40.4 to 44.5 MPa, with the CV ranging from 2.2 to 4.5%. The B-basis values ranged from 38.5 to 41.8 MPa, with a %-of-mean range of 90.9 to 95.4%. The minimum B-basis value for shear strength in the x-direction occurred for IM-dataset D and the maximum value for IM-dataset B. The minimum %-of-mean occurred for IM-dataset A and the maximum for IM-dataset D. The CM-dataset analysis resulted in a B-basis shear strength in the x-direction of 39.8 MPa and a CM-%-of-mean of 92.6%.

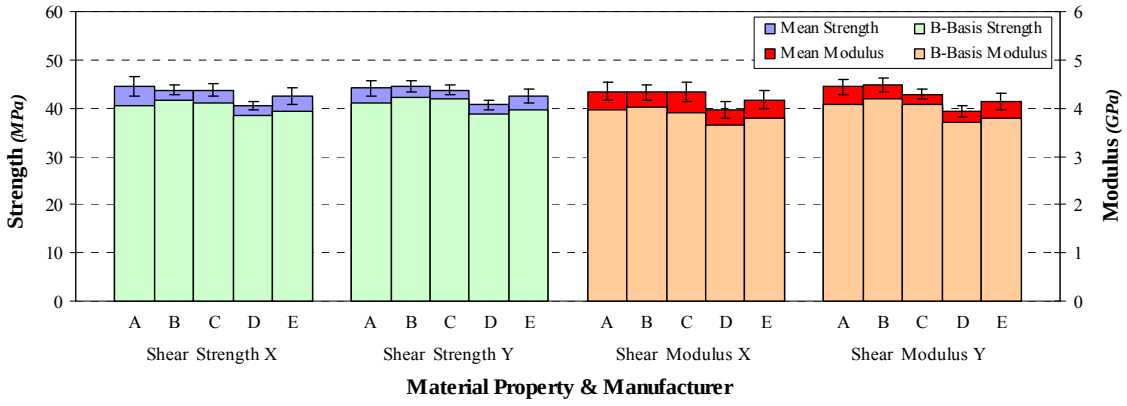

Figure 2.18. Shear strength and modulus in the x and y-directions for the IM-Datasets.

The mean shear strength in the y-direction for the IM-datasets ranged from 40.7 to 44.5 MPa, with the CV ranging from 2.1 to 3.4%. The B-basis values ranged from 38.8 to 42.1 MPa, with a %-of-mean range of 92.9 to 95.7%. The minimum B-basis value for shear modulus in the y-direction occurred for IM-dataset D and the maximum B-basis value for IM-dataset B. The minimum %-of-mean occurred for IM-dataset A and the

maximum for IM-dataset C. The CM-dataset analysis resulted in a B-basis shear strength in the y-direction of 40.2 MPa and a CM-%-of-mean of 93.4%.

The mean shear modulus in the x-direction for the IM-datasets ranged from 3.97 to 4.35 GPa, with the CV ranging from 3.5 to 4.7%. The B-basis values ranged from 3.63 to 4.01 GPa, with a %-of-mean range of 89.9 to 92.7%. The minimum B-basis value for shear modulus in the x-direction occurred for IM-dataset D and the maximum value for IM-dataset B. The minimum %-of-mean occurred for IM-dataset C and the maximum for IM-dataset B. The CM-dataset analysis resulted in a B-basis shear modulus in the x-direction of 3.86 GPa and a CM-%-of-mean of 91.4%.

The mean shear modulus in the y-direction for the IM-datasets ranged from 3.94 to 4.48 GPa, with the CV ranging from 2.5 to 4.1%. The B-basis values ranged from 3.72 to 4.19 GPa, with a %-of-mean range of 91.8 to 94.9%. The minimum B-basis value for shear modulus in the y-direction occurred for IM-dataset D and the maximum value for IM-dataset B. The minimum %-of-mean occurred for IM-dataset E and the maximum for IM-dataset C. The CM-dataset analysis resulted in a B-basis shear modulus in the y-direction of 3.87 GPa and a CM-%-of-mean of 91.1%.

2.5.6 Flexure Results

The flexural tests were conducted on specimens in the x-direction only; therefore, the specimen orientation will not be referred to when discussing the flexural results. A stress-strain plot for a typical flexural test specimen is presented in Figure 2.19a. As seen in the plot there was typically some progressive failure occurring prior to final failure. The typical specimen failure mode, as shown if Figure 2.19b, was a combination of compressive failure on the top surface of the specimen followed by either a tensile failure

of the bottom surface, or a delamination. All specimen failures occurred between the load-heads. The flexural secant modulus was calculated in the strain range of 1000 to 3000 micro-strain as recommended in ASTM D7264. The flexural failure strains are presented in Table 2.5. The dataset distributions from each manufacturer's individual panel are presented in Figure 2.20 for the flexure strength and modulus. The strength data was plotted with an x-axis scale of 0-600 MPa, while the modulus data was plotted with a 0-60 GPa scale. The axes were then truncated for clarity without changing the relative scales. All the dataset pairs with the exception of the strength results for dataset B show significant overlap.

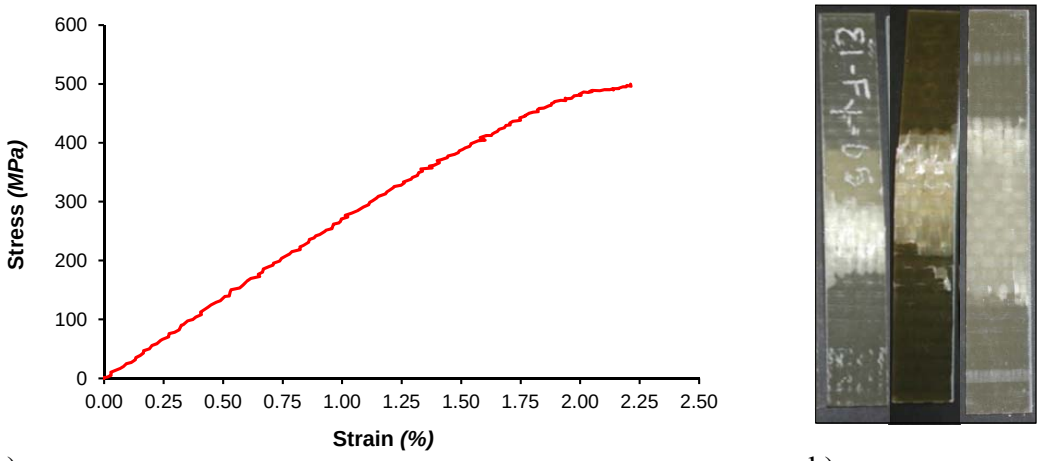

a) b)

Figure 2.19. Typical flexural test specimen: a) stress-strain curve and b) failure modes.

Table 2.5. Flexural failure strain results.

Dataset ID	mean %	CV %
Ax	2.07	5.3
Bx	2.10	5.2
Cx	2.05	16.6
Dx	2.13	9.1
Ex	2.13	17.2

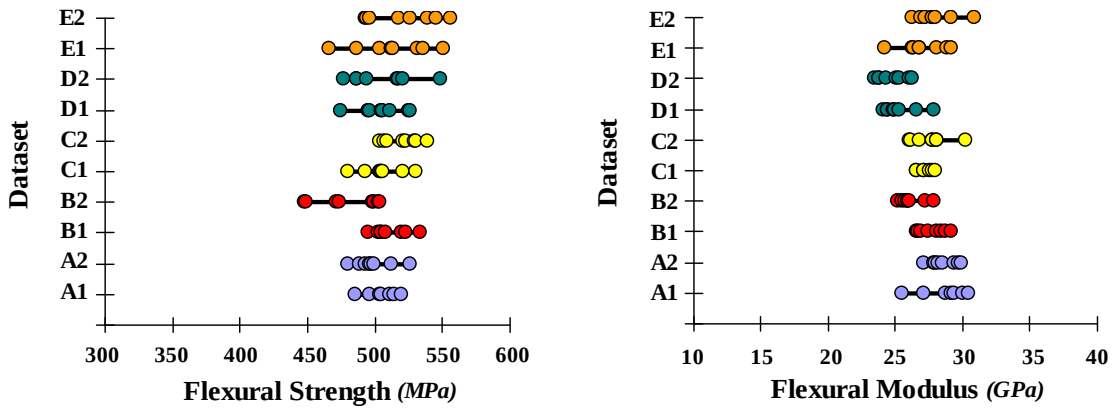

Figure 2.20. Test data for the flexural strength and modulus in the x-direction.

The flexural failure strains were similar for all of the IM-datasets and ranged from 2.05 to 2.13%, with the CV ranging from 5.2 to 17.2%. The flexural failure strains were comparable to the tensile failure strains (~2%) for all but IM-dataset A. The flexural strains at failure, which were measured on the compression face of the flexural test specimens, were significantly higher than the compressive failure strains measured during the compression tests.

The IM-dataset results for the flexural strength and modulus are plotted in Figure 2.21. The mean flexural strength for the pooled data ranged from 496 to 517 MPa, with the CV ranging from 2.6 to 5.0%. The B-basis values ranged from 447 to 481 MPa, with a %-of-mean range of 89.9 to 94.7%. The minimum B-basis value for flexural strength occurred for IM-dataset B and the maximum value for IM-dataset C. The maximum %-of-mean occurred for IM-dataset A and the minimum for IM-dataset E. The CM-dataset analysis resulted in a B-basis flexural strength of 473 MPa and a CM-%-of-mean of 93.5%.

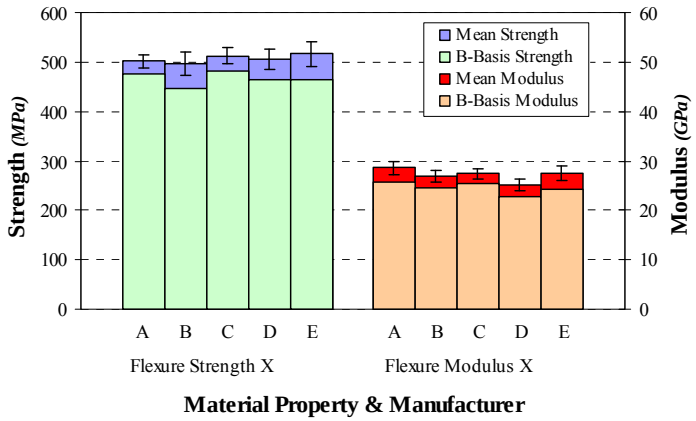

Figure 2.21. Flexural strength and modulus in the x-direction for the IM-Datasets.

The mean flexural modulus for the IM-datasets ranged from 25.0 to 28.6 GPa, with the CV ranging from 3.8 to 5.6%. The B-basis values ranged from 22.6 to 25.8 GPa, with a %-of-mean range of 88.6 to 92.2%. The minimum B-basis value for flexural modulus occurred for IM-dataset D and the maximum value for IM-dataset A. The minimum %-of-mean occurred for IM-dataset E and the maximum for IM-dataset C. The CM-dataset analysis resulted in a B-basis flexural modulus of 24.3 GPa and a CM-%-of-mean of 89.8%.

2.5.7 Proposed Approach to Quantify Variability

The B-basis and %-of-mean were used as the method to quantify the variability in results of each material property test for each IM-dataset. A summary of the %-of-mean results for all the tests performed are presented in Table 2.6. The table includes the maximum and minimum %-of-mean for the IM-datasets (IM max and IM min) for each test-type and orientation, for both strength and modulus. In addition, the %-of-mean for the CM-datasets (CM) and coefficient of variation for the CM-datasets (CM CV) are included. The CM-%-of-mean could be interpreted as the knockdown to produce a design

Table 2.6. Round-robin %-of-mean results.

Property		%-of-mean Strength				%-of-mean Modulus			
		IM min	IM max	CM	CM CV	IM min	IM max	CM	CM CV
ASTM D3039 [a]	Tension-x	75.8	93.2	88.4	7.4	93.3	97.7	92.8	4.6
	Tension-y	86.3	95.9	90.2	6.2	89.8	95.9	92.3	4.9
ASTM D6641	Compression-x	77.8	90.4	80.8	12.3	82.3	89.9	86.3	8.8
	Compression-y	82.3	92.9	84.3	10.1	86.8	93.5	87.4	8.1
ASTM D4255	Shear-x	90.9	95.4	92.6	4.7	89.9	92.7	91.4	5.5
	Shear-y	92.9	95.7	93.4	4.2	91.8	94.9	91.1	5.7
ASTM D7264	Flexure-x	89.9	94.7	93.5	4.2	88.6	92.2	89.8	6.5

[a] Guidelines of the standard were used with a modified dog-bone specimen.

value when combining all of the datasets within a test type and fiber orientation. The CM-%-of-mean and CM CV were used as the means to quantify the variability between the different test types. The CM-%-of-mean strength ranged from 80.8 to 93.5% and the CM-%-of-mean modulus ranged from 86.3 to 92.8%. The flexural strength had the highest CM-%-of-mean and compressive strength in the x-direction had the lowest CM-%-of-mean. The tensile modulus in the x-direction had the highest CM-%-of-mean and compressive modulus in the x-direction had the lowest CM-%-of-mean.

The results of the ADK test for pooling and the test for Normal distribution for the property data from the two panels for each dataset are presented in Table 2.7. A "1" indicates that the datasets failed the ADK pooling criteria, which means they are not statistically from the same population. A "2" indicates that the datasets did not meet the OSL criteria for a Normal distribution. As seen in the table, dataset A and B had several property datasets fail the ADK test for pooling. The large discrepancy in fiber volume fraction for dataset A's two panels (50.9% vs. 56.4%) is likely the cause of the pooling failures for the shear properties. The discrepancies in the compression results are not as clear, since the normalization performed on the compression data should have accounted for the volume fraction differences. It is the Author's opinion that the likely cause of the

Table 2.7. ADK pooling and normal distribution results for each IM-Dataset.

Test Type	Property	IM-Dataset & Fiber Orientation									
		A		B		C		D		E	
		x	*y*	*x*	*y*	*x*	*y*	*x*	*y*	*x*	*y*
Tension	Strength				1	2					1
	Modulus				2		2	1			
Compression	Strength	1	1		1	2				1	
	Modulus	1							2	1	
Shear	Strength	1	1		1				1		
	Modulus	1	1	1, 2	1		2				
Flexure	Strength			1, 2							
	Modulus			1							

NOTE: Dataset Failure Types: 1 - ADK Pooling Failure 2 - Normal Distribution Failure

discrepancies in the compression results was caused by the waviness of the woven fabric, since other studies have shown that the degree of waviness directly affects the compressive strength and failure modes [15, 20-21]. The property results for dataset C had no issues with pooling, but had four instances of failing to meet the Normal distribution criteria.

It is important to note that a comprehensive reliability analysis intended to produce actual design values was not undertaken in this study. In order to produce actual design values, the results of the ADK goodness-of-fit tests would have had to be taken into account and the data would have had to been analyzed differently. In some cases the Stat-17 worksheet indicted that an ANOVA should have been used when analyzing the CM-datasets.

2.6 Conclusions

A methodology to quantify variability of mechanical properties of marine grade composites fabricated by the VARTM process was developed. Material coupon-level tests for tension, compression, in-plane shear, and flexure were selected to characterize

variability of strength and elastic properties for five different manufacturers. Experimental techniques based on non-contact digital image correlation were adopted for strain measurement to account for strain variations due to the relatively heavy fiber reinforcement tows of marine grade composites.

A procedure for statistical representations of strength and elastic properties, as recommended in MIL-HDBK-17F-1, were implemented as a means to compare the different datasets. The recommended normalization procedure employed to account for variations in fiber volume fraction for the tension and compression results seemed to work for tension but had a lesser effect on the compression results when faced with a significant volume fraction difference for one of the individual manufacturer's datasets. This led to statistically significant differences in some of the strength and elastic properties for individual panels.

The combined manufacturer dataset results indicated that compression had the most variability in both strength and modulus, while the flexural strength and tensile modulus had the least amount of variability.

Tensile failure strains had relatively high strain to failure with a low CV (3 to 12%). On the other hand, compressive failure strains were noticeably lower with a higher CV (10 to 16%). Compressive failure strains, which are related to local instability, are affected by the inherent imperfections due to the waviness of the woven fabric reinforcement. It is this "inherent imperfection" of a woven fabric composite that would result in the large variability in the compression strength and stiffness properties observed in this study. Further research would need to be conducted to determine ways to minimize this effect during manufacturing.

An additional observation was that the flexural strains to failure, which occurred on the compression face, are significantly higher than the failure strains of the compression specimens. This increase in strain to failure is partially attributed to the partial restraint provided by the flexure specimen. Additionally, since a linear strain distribution may be assumed through-the-thickness of the flexure specimen, only the outer layer is subjected to the maximum strain. Therefore, the higher strains measured at failure on the compression face of the flexure specimen, when compared with the compression specimen, could be attributed to size-effects.

2.7 References

2.1 El-Chiti F (2005) Experimental Variability of E-Glass Reinforced Vinyl Ester Composites Fabricated by VARTM/SCRIMP. MS Thesis in Mechanical Engineering, University of Maine, Orono, ME.

2.2 Cain J J, Post N L, Lesko J J, Case S W, Lin Y, Riffle J S, and Hess P E (2006) Post-Curing Effects on Marine VARTM FRP Composite Material Properties for Test and Implementation. Journal of Engineering Materials and Technology, Transactions of the ASME, 128:34-40.

2.3 ASTM Standard D2584 (2002) Standard Test Method for Ignition Loss of Cured Reinforced Resins. ASTM International, West Conshohocken, PA, www.astm.org.

2.4 ASTM Standard D3039 (2007) Standard Test Method for Tensile Properties of Polymer Matrix Composite Materials. ASTM International, West Conshohocken, PA, www.astm.org.

2.5 ASTM Standard D6641 (2009) Standard Test Method for Determining the Compressive Properties of Polymer Matrix Composite Laminates Using a Combined Loading Compression (CLC) Test Fixture. ASTM International, West Conshohocken, PA, www.astm.org.

2.6 ASTM Standard D4255 (2001) Standard Test Method for In-Plane Shear Properties of Polymer Matrix Composite Materials by the Rail Shear Method. ASTM International, West Conshohocken, PA, www.astm.org.

2.7 ASTM Standard D7264 (2007) Standard Test Method for Flexural Properties of Polymer Matrix Composite Materials. ASTM International, West Conshohocken, PA, www.astm.org.

2.8 Masters J (1996) Strain Gage Selection Criteria for Textile Composite Materials. NASA Contractor Report 198286, National Aeronautics and Space Administration, Langley Research Center, VA.

2.9 Lopez-Anido R A, El-Chiti F W, Muszynski L, Dagher H J, Thompson L, and Hess P E (2004) Composite Material Testing Using a 3-D Digital Image Correlation System. Proceedings of the ACMA Composites 2004 Convention and Trade Show, Tampa, FL, October 6-8, 2004, American Composites Manufacturers Association, Arlington, VA.

2.10 El-Chiti F, Lopez-Anido R A, Dagher H J, Thompson L, Muszynski L, and Hess P E (2005) Experimental Approach for Characterizing VARTM Composites Using a 3-D Digital Image Correlation System. Proceedings of the SEM XII Int. Congress and Exposition on Experimental and Applied Mechanics, Portland, OR, June 7-9, 2005, Society for Experimental Mechanics, Bethel, CT, 8p.

2.11 Hammami A and Al-Ghuilani N (2004) Durability and Environmental Degradation of Glass-Vinylester Composites. Polymer Composites, 25(6):609-616.

2.12 Karbhari V M and Zhang S (2003) E-Glass/Vinyl Ester Composites in Aqueous Environments - I: Experimental Results. Applied Composite Materials 10:19-48.

2.13 Puccini G (1993) Environmental Aspects, In Composite Materials in Maritime Structures: Vol. 1, Shenoi R A (Editor), Cambridge University Press, Cambridge, UK.

2.14 Tarnopol'skii Y M and Kulakov V L (2001) Tests Methods for Composites, Mechanics of Composite Materials, 37(5/6):431-448.

2.15 Lee J and Soutis C A (2007) Study on the Compressive Strength of Thick Carbon Fi-Bre/Epoxy Laminates. Composites Science and Technology, 67(10):2015-2026.

2.16 Lavoie J A, Soutis C, and Morton J (2000) Apparent Strength Scaling in Continuous Fiber Composite Laminates. Composites Science and Technology, 60(2):283-299.

2.17 Walls J and Thompson L (2005) Parametric Shape Optimization of Tensile Coupons for Marine Grade Glass Fiber Reinforced Plastics. Report# ATS-RELY/2-2005-02, Applied Thermal Sciences, Orono, ME.

2.18 Berube K A and Lopez-Anido R A (2008) Full-Field Strain Measurements for Determining Mechanical Properties of Marine Composite Laminates. Experimental Mechanics Applied to Damage: Detection, Analysis and Mitigation, SEM XI International Congress Exposition on Experimental and Applied Mechanics, Orlando, FL, June 2-5, 2008, Society for Experimental Mechanics, Bethel, CT, 8p.

2.19 MIL-HDBK-17F-1 (2002) Composite Materials Handbook Volume 1 - Polymer Matrix Composites Guidelines for Characterization of Structural Materials, ASTM International, West Conshohocken, PA, p. 8.1-110.

2.20 Yang B, Kozeya V, Adanurb S, and Kumara S (2000) Bending, Compression, and Shear Behavior of Woven Glass Fiber-Epoxy Composites. Composites Part B 31:715-721.

2.21 Kim J, Shioya M, Kobayashi H, Junichi Kaneko J, and Kido M (2004) Mechanical Properties of Woven Laminates and Felt Composites Using Carbon Fibers. Part 1: In-Plane Properties. Composites Science and Technology 64:2221-2229.

CHAPTER 3

THE EFFECT OF STYRENE CONTENT ON THE MATERIAL PROPERTIES OF MARINE GRADE POLYMER COMPOSITES

3.1 Abstract

One of the variables that affect the vacuum assisted resin transfer molding process is the viscosity of the resin systems used during fabrication. Vinyl-ester resin is a thermosetting polymer widely used because of its low cost and good combination of toughness and chemical resistance. A common diluent for vinyl-ester resin is styrene monomer, with most commercial vinyl-esters consisting of 30 to 60% styrene by weight. This study investigated the effects of adding an additional 5wt% to a commercially available vinyl-ester resin, as might be done in practice to improve the viscosity and wet-out during the infusion process. Composite laminate panels were fabricated using the base resin system and the increased styrene formulation. Standardized material coupon tests were conducted for fiber volume fraction, tension, compression, in-plane shear, and flexure on specimens from each of the composite laminates. Results indicate that the increased styrene content produced statistically discernible reductions in tensile and compressive strength and an increase in flexural modulus, with a negligible effect on in-plane shear properties. Based on these findings it would be advisable to thoroughly investigate further dilutions of this resin system prior to its implementation.

3.2 Introduction

The marine industry is an area where the vacuum assisted resin transfer molding (VARTM) process is used extensively when fabricating composite parts. The common

method of implementing the VARTM process in the marine industry involves one-sided hard tooling with a pliable vacuum bag as the opposite surface. The pliable bag enables the use of vacuum pressure to both consolidate the fiber-preform and infuse the resin throughout the part. The placement of flow media and the locations of the resin inlet and vacuum lines are crucial to the proper wetting of the fiber preform; however, this is governed to a large degree by the viscosity of the resin system that is being used.

Many resin systems are too viscous in their basic form to be used during vacuum infusion. As the vacuum infusion process has become increasingly popular, manufacturers have overcome the viscosity issue by incorporating diluents into the base resin system. Vinyl-ester resin is a thermosetting polymer widely used because of its low cost and good combination of toughness and chemical resistance [1]. A commonly used diluent for vinyl-ester resin is styrene monomer. Most commercial vinyl-ester resins contain 30 to 60% styrene by weight [2]. Styrene serves as a diluent to reduce the room temperature viscosity of the resin and enabling processing by methods such as VARTM, and enhances linear chain extension in the resin allowing for room temperature curing. Room temperature curing is crucial to the marine industry where post-curing of parts can be both cost-prohibitive and sometimes impossible due to the shear size of the parts.

Styrene monomer in vinyl-ester resin also facilitates a higher degree of vinyl-ester polymerization [2, 3]. During the cure of vinyl-ester resin, vinyl-ester molecules cross-link, while styrene serves as a means to link the adjacent vinyl-ester chains [2, 4]. The overall extent of resin conversion of the vinyl-ester double bonds has been found to increase with increasing styrene concentration, without an increased conversion of the styrene double bonds [2, 5, 6]. The development of the polymer network significantly

affects the physical, chemical and mechanical properties of the polymer, ultimately affecting the properties of the composite. [2]

The increase in processability does appear to come at a cost however, as some studies have shown a decrease in polymerization rate [2, 4, 7] and a decrease in material properties at higher levels of styrene content. The increased concentration of diluent styrene monomer reduces the polymerization rate due to the lower crosslink density and the plasticizing effect of the diluent. The decrease in polymerization rate increases the gel time and lowers the peak exotherm [8], which can affect the final properties [9].

Increasing the styrene content has been shown in several studies to decrease the glass transition temperature (T_g) [5, 7, 10]. In addition to the decrease in T_g, Rodriguez [10] found that an increase in styrene resulted in an increase in damping and a decrease in compression strength and modulus of neat resin specimens of Derakane 411-350 and Derakane 411-350 Momentum. In that study compression modulus decreased by an average of 4% for each 10% increase in styrene while strength dropped by an average of 2% over the same range. Rosario [11] and Shan [12] both found that fracture toughness of neat resin specimens decreased with increasing styrene content. Sultania [8] found that styrene contents of 35-45% in vinyl-ester resins enhanced tensile, flexural and impact properties, but properties decreased with styrene percentages over 45%. He attributed it to increased flexibility caused by the uncrosslinked styrene monomer present in the laminates. Agarwal [13] found that increasing the styrene content decreased the tensile modulus of FRP specimens. Styrene has been shown to dominate the swelling of the sizing layer on the fiber [14], which may contribute to some of the variations in

mechanical properties with increasing styrene content. In addition to the mechanical property issues, low residual styrene content is important for health considerations [15].

With all of the complexities of the interactions between the fiber, resin, diluents and catalyzing recipes incorporated during the infusion process, the formulation of a vinyl-ester resin is a trade-off between its viscosity and the properties of the composite material when cured. With a large number of the variations controlled by the fabricator, questions remain as to the effect of these variations on the consistency of the structural properties of the composite laminates. The objective of this study was to determine if small amounts of additional styrene added to the base resin to reduce viscosity and improve fiber wet-out would affect the material properties of the final laminate. This study is part of a larger program sponsored by the Office of Naval Research intended to investigate the causes of variability in material properties of composite laminates fabricated using the VARTM process. The sources of variability being investigated in the larger project include those due to manufacturing [16, 17, 18], post processing [19], and testing of composites [20].

3.3 Panel Fabrication

A marine grade fiber-reinforced polymer (FRP) composite reinforced with woven roving was tested in this study. The FRP panels consisted of E-glass/vinyl-ester and were fabricated using a VARTM process. The fiber reinforcement used was Saint Gobain Vetrotex 324 woven roving with a weight per unit area of 814 g/m^2 (24 oz/yd^2). The tow spacing is 5.1 mm (5 tows per inch) in the warp direction, and 6.4 mm (4 tows per inch) in the fill direction resulting in 55% of the fiber orientated in the warp direction.

The polymer resin used was Ashland Derakane 8084, which is an elastomer-modified epoxy vinyl-ester resin. Two different resin formulations were used in this study. The first batch, designated as resin **V**, consisted of the 8084 resin as received, which has 40wt% styrene [21]. The second batch, designated as resin **S**, was diluted with an additional 5.0wt% styrene monomer (Nova Chemicals), for a final weight content of 45% styrene. The target gel-time was one hour and both resin batches were promoted with identical catalyzing recipes as follows:

- 2.00 wt% Trigonox 239A (AkzoNobel)
- 0.30 wt% Cobalt 6% Napthenate (Puritan Products)
- 0.20 wt% N,N-Dimethylaniline (Puritan Products)
- 0.05 wt% 2,4-Pentanedione (J.T. Baker)

Two panels were fabricated for each of the two resin formulations and were designated as **V1**, **V2**, **S1**, and **S2**. The panel dimensions were 1.22 m x 1.22 m (4 ft x 4 ft) with nominal thicknesses of 5.1 mm (0.20 in.). The panels consisted of eight layers of the woven roving reinforcement in a warps-parallel orientation designated by the notation $[0_8]_f$, where the orientation indicates the warp direction of the fabric. After an 18 hour room temperature cure, the panels were removed from the infusion table and were post-cured at 82ºC (180ºF) for a period of 4 hours. This temperature and duration had been shown to be appropriate for this material system at this thickness in an earlier phase of the study [19].

3.4 Experimental Methods

The material property tests conducted during the study included constituent volume fraction, tension, compression, in-plane shear, and flexure. These tests had been

selected to run in conjunction with another phase of the larger study [16] and they were conducted per the following ASTM test standards.

- Constituent Content - ASTM D3171 [22]
- Tension - ASTM D3039 [23]
- Compression - ASTM D6641 [24]
- Shear - ASTM D4255 [25]
- Flexure - ASTM D7264 [26]

Eight specimens were cut from each of the four panels for each test type and fiber orientation, where the warp and fill orientations of the fabric correspond to the *x* and *y*-directions of the panels, respectively. This resulted in a total of 32 specimens for each combination of test type and fiber orientation. Tests were performed in the *x* and *y*-orientations for the tension, compression, and shear tests, while specimens in the *x*-direction only were performed for the flexural tests. Eight specimens were also cut from each panel for constituent volume testing. The position of all specimens in the panel was distributed at eight locations to capture spatial variability of properties due to location in the panel, as shown in Figure 3.1. Computer numeric controlled (CNC) water-jet abrasive machining was used to cut all of the specimens.

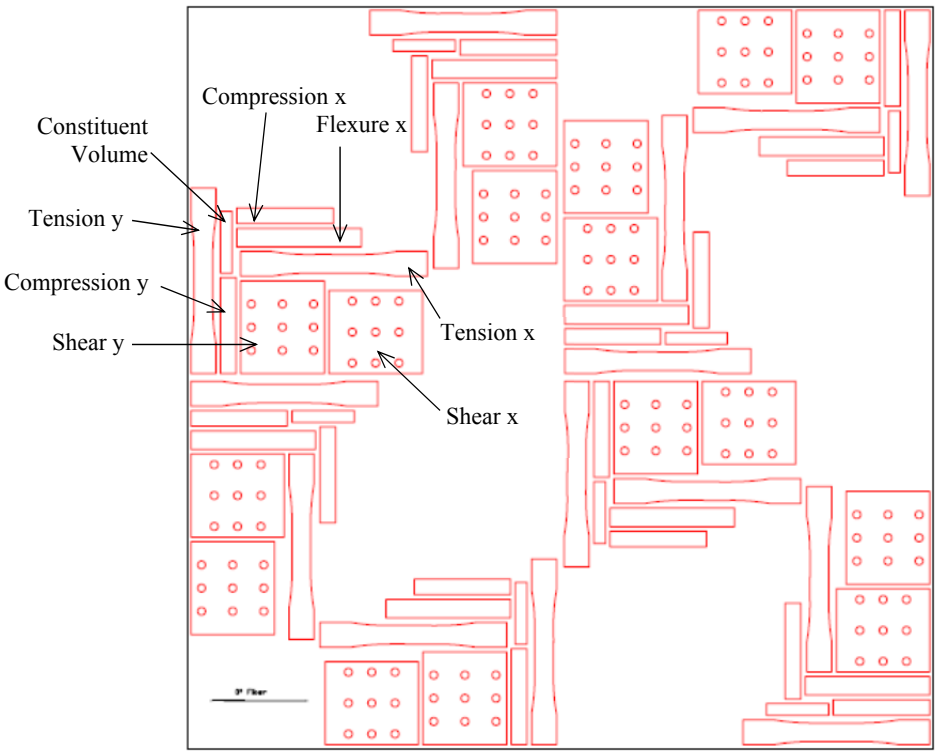

Figure 3.1. Specimen locations in the composite panels.

A three-dimensional digital image correlation (DIC) system was used to record full-field strains during testing. The DIC system provides an advantage over resistive foil gages as it allows a larger area of the specimen to be monitored during testing. This is advantageous when testing heavy woven fabrics where strain gage size and placement can influence test results due to strain variations on the specimen [27, 28].

All specimens were examined prior to testing for visible defects due to manufacturing or specimen preparation. In addition to the visual inspection of the exterior of the specimens for excessive fiber waviness and other macroscopic defects, the inspection included backlighting of the specimens. This reveals macroscopic inclusions, voids, and delaminations produced during manufacturing and specimen preparation. There were no objectionable defects observed in any of the specimens.

The specimens were prepared for the DIC measurement system by applying a speckled pattern of paint to produce a 50% grayscale pattern in the area of the specimen that would be observed during testing. A typical speckle pattern that was applied to the specimens is presented in Figure 3.2.

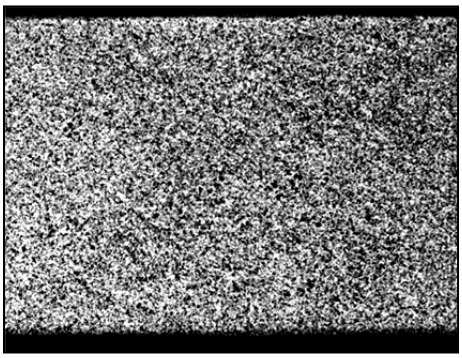

Figure 3.2. Typical speckle pattern for DIC measurements.

Prior to testing, all specimens were conditioned at 23 ± 2°C (73.4 ± 3.6°F) and 50 ± 10% relative humidity for a minimum of 48 hours. The tension, compression, shear, and flexure tests were performed on a 100 kN (22.5 kip) Instron load frame equipped with side-loading hydraulic grips, and located in an environmentally controlled test lab at an environment of 23 ± 2°C and 50 ± 5% relative humidity. All of the tests were conducted at the Advanced Structures and Composites Center, at the University of Maine in Orono, Maine.

3.4.1 Constituent Volume Test

ASTM test standard D2584 was used to determine the constituent volume fraction of the specimens. The specimen size was 19.0 mm x 76.2 mm (0.75 in. x 3.0 in.). The specimens were placed in a crucible in a muffle furnace at a temperature of 565ºC for a period of 2.5 hours, which had shown to be sufficient for complete resin removal with this material system. [16]

3.4.2 Tension Test

The results of the prior phase of the project indicated that a larger tensile specimen was required to properly capture the representative width of the 24 oz woven roving fabric [20]. In addition, a dog-bone shaped specimen was favored over a tabbed rectangular specimen. An optimized dog-bone specimen was used for the tensile tests [29] as shown in Figure 3.3. Other than the dog-bone shaped specimen, ASTM D3039 was used as a guideline for performing the tests.

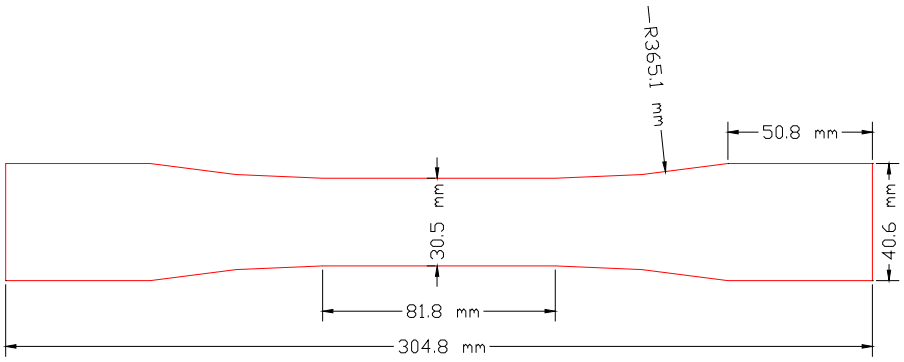

Figure 3.3. Optimized tensile dog-bone specimen.

The specimens were tested in displacement control at a crosshead rate of 0.30 mm/sec (0.012 in/sec) resulting in an average test time of approximately three minutes. Load and crosshead displacement data were recorded at a sampling rate of 10 Hz on the Instron control computer and at 1 Hz on the DIC system. The 1 Hz sampling rate on the DIC system had been shown to be sufficient for this test configuration [16].

3.4.3 Compression Test

ASTM test standard D6641 was used as a guideline for conducting the compression tests. The test specimen size was 25.4 mm x 152.4 mm (1.0 in. x 6.0 in.). The length of 152.4 mm is slightly longer than what the standard calls for and was

selected since it allows more area of the specimen to be observed by the DIC system. The specimens were tested in displacement control at a crosshead rate of 0.01 mm/sec (0.0004 in/sec). This resulted in an average test time of approximately five minutes. A self-leveling compression platen was used on the stationary crosshead to account for any misalignment during loading. Load and crosshead displacement data were recorded at a sampling rate of 10 Hz on the Instron control computer and at 1 Hz on the DIC system. The sampling rate was chosen to reduce post-processing time on the DIC system without compromising the resolution and accuracy of the results.

3.4.4 Shear Test

ASTM test standard D4255 was shown to be the preferred method for in-plane shear testing of woven roving composites [20]. The specimen size was 136.5 mm x 152.4 mm (5.38 in. x 6.0 in.). The specimens were tested in displacement control at a crosshead rate of 0.015 mm/sec (0.0006 in/sec), resulting in an average test time of approximately 7.5 minutes. Since this test method does not produce a catastrophic failure of the specimen, the tests were allowed to progress until the load reached approximately 85 kN. This ensured that the load-displacement curve was fully developed and would permit the use of an offset method to obtain the failure strength. Load and crosshead displacement data were recorded at a sampling rate of 10 Hz on the Instron control computer and at 0.67 Hz on the DIC system. As before, the DIC sampling rate was chosen such that it reduced post-processing time without compromising the resolution and accuracy of the results.

3.4.5 Flexure Test

ASTM standard D7264 was used to conduct the flexural tests. The specimen size was 25.4 mm x 203 mm (1.0 in. x 8.0 in.). The specimens were tested in 4-point flexure with a ¼-point load configuration at a span-to-thickness ratio of 32. The specimens were tested in displacement control at a cross head rate of 5.1 mm/min (0.20 in/min), resulting in an average test time of approximately 4.5 minutes. The DIC system was used to record both the strain on the top surface of the specimen and the mid-span deflection of the specimen [30]. Load and crosshead displacement data were recorded at a sampling rate of 10 Hz on the Instron control computer and at 0.67 Hz on the DIC system.

3.5 Results

3.5.1 Analysis Procedures

The data from each of the two replicate panels were grouped and treated as a single dataset for the statistical analysis. After verifying normality of the dataset distributions using the Anderson-Darling method, the mean and coefficient of variation (CV) were computed for each of the material properties investigated. The k-sample Anderson-Darling (ADK) method was used to determine if the results of each dataset were statistically different for the two resin formulations [31]. The ADK method is the method recommended in the Composite Materials Handbook (MIL-17) to screen for pooling of datasets and was implemented throughout the different phases of the larger study [16-18]. If the computed ADK value for the dataset is less than the critical ADK value, then one can conclude (with 97.5% confidence) that the datasets are from the same population. The ratio of the computed value to critical value was calculated as a means to

determine the level to which the datasets were statistically different. This ADK ratio is tabulated and presented for each dataset comparison in the results that follow.

The Maximum Normed Residual (MNR) method was used to identify outliers [31]. While the method did identify a couple of outliers in the data, they were not removed from the dataset, since no specimen or testing anomaly could be identified.

As recommended in MIL-HDBK-17F-1 for warps-parallel laminates, the strength and modulus results for the tension and compression tests were normalized with respect to panel thickness. Each result was multiplied by the ratio of the test specimen thickness to a nominal thickness. This procedure accounts for variations in fiber volume fraction, due to thickness variations, for fiber dominated material properties for a given fiber reinforcement and areal weight. The thickness used as the nominal thickness was 4.8 mm (0.190 in.), which was approximately the mean thickness of all the specimens used in the study.

All of the property data in the results that follow were plotted using one of three different scales: 0 to 5.5, 0 to 55, or 0 to 550. The selection of scale was an attempt to allow a qualitative comparison of the variability in the different material properties.

Panel Fabrication Results

The panel fabrication results matrix is presented in Table 3.1. As seen in the table, the additional styrene reduced the wet-out time of the panel infusions by 22-29% on average compared to the base resin panel infusions, which was one of the objectives of diluting the resin; however, it also reduced the resin gel time by 6-15%. The differences in gel time are not significant, but they are contrary to prior studies where increased styrene content decreased the reaction rate thereby increasing the gel time [2, 4, 7].

Table 3.1. Panel fabrication results.

Resin Formulation	Panel ID	Wet-out Time min	Gel Time min
8084 (**V**)	V1	48	63
	V2	50	61
8084 +5% Styrene (**S**)	S1	35	58
	S2	38	53

3.5.2 Constituent Volume Results

The fiber volume fraction (FVF) results are presented in the plot in Figure 3.4 with the statistical results in Table 3.2. Dataset **S** produced a mean FVF that was approximately one percentage-point greater than dataset **V**. The less viscous resin of dataset **S** would have been expected to wet-out the tows better than resin **V**, but the longer time between wet-out and gelation, as seen in Table 3.1 would also have improved the FVF. As indicated by the ADK ratios less than 1.0 in Table 3.2, there was no statistically discernible difference between the two panels within the datasets or between datasets **S** and **V**.

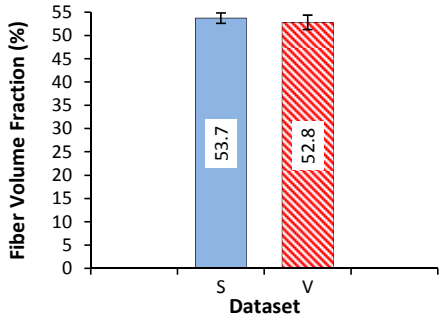

Figure 3.4. Fiber volume fraction results.

Table 3.2. Fiber volume fraction statistics.

Dataset Id	mean %	CV %	ADK Ratio
S	53.7	2.1	0.33
V	52.8	2.9	0.18
Total	53.2	2.6	0.67

Note: ADK ratios < 1 indicate no statistically discernible difference between datasets

3.5.3 Tension Results

The tensile stress-strain curves exhibited a bilinear response, which is common with woven roving composites, but there was not a well defined transition point in the curves; instead, there was a gradual transition region. This is similar to what had been observed in the larger study with the specimens fabricated by other manufacturers using the identical material system [16]. The tensile secant modulus was calculated in the strain range of 1000 to 3000 micro-strain as recommended in ASTM D3039. All specimens failed in either the gage area or in the transition region, which have been shown to be acceptable failure modes for this specimen configuration [16, 20].

The normalized tensile strength and modulus results for the *x* and *y*-orientations are presented in the plot in Figure 3.5. A dual axis was used for the plots, where the strength data is plotted using the left *y*-axis and the modulus is plotted using the right *y*-axis. The strength data was plotted with a *y*-axis scale of 0-550 MPa, while the modulus data was plotted with a 0-55 GPa scale. The plotted results include the Mean value with error bars (±1 standard deviation) for each resin dataset and tensile property. The statistical results are presented in Table 3.3.

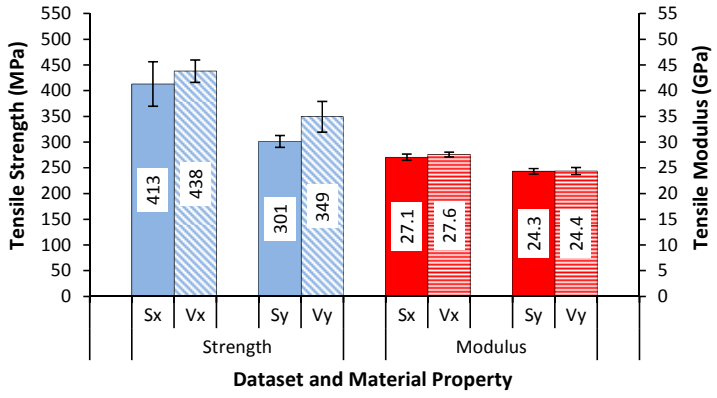

Figure 3.5. Tension test results.

Table 3.3. Tension test statistics.

	x-direction						y-direction					
	Strength			Modulus			Strength			Modulus		
Dataset	mean	CV	ADK	mean	CV	ADK	mean	CV	ADK	mean	CV	ADK
Id	*MPa*	*%*	Ratio	*GPa*	*%*	Ratio	*MPa*	*%*	Ratio	*GPa*	*%*	Ratio
S	413	10	0.31	27.1	2.3	0.13	301	3.9	0.11	24.3	2.2	0.13
V	438	5.0	0.57	27.6	1.7	0.18	349	8.5	***2.22***	24.4	2.9	0.13
Total	425	8.5	0.83	27.3	2.2	***1.11***	325	10	***3.79***	24.4	2.5	0.22

Note: ADK ratios < 1 indicate no statistically discernible difference between datasets

There was a decrease in the mean values of all tensile properties for the **S** datasets compared to the **V** Datasets. The strength was reduced by 6% and 14% in the *x* and *y*-orientations respectively, while the modulus saw reductions of 2% and 0.4% in the *x* and *y*-orientations, respectively. The ADK ratios in Table 3.3 indicate that there were statistical differences between the resin formulations in only two of the properties; modulus in the *x*-direction (*x*-modulus) and strength in the *y*-direction (*y*-strength). The difference in mean *y*-strength was substantial at 48 MPa, but the difference in *x*-modulus was only 0.5 GPa. Reductions in tensile properties with increasing styrene monomer content have been recorded in other studies [8], but it occurred at styrene weight percentages exceeding 45%.

3.5.4 Compression Results

All specimens failed in an acceptable manner, as outlined in the standard. The compressive secant modulus was calculated in the strain range of 1000 to 3000 micro-strain as recommended in ASTM D6641. The normalized compressive strength and modulus results for the *x* and *y*-directions are presented in the plot in Figure 3.6. As with the previous property results a dual axis was used for the strength and modulus data in the plots. The strength data was plotted with a *y*-axis scale of 0-550 MPa, while the modulus data was plotted with a 0-55 GPa scale. The plotted results include the mean value with

error bars (±1 standard deviation) for each resin formulation and compressive property. The statistical results are presented in Table 3.4.

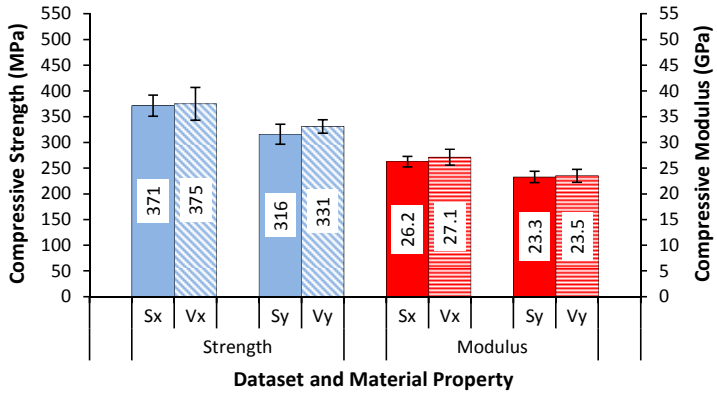

Figure 3.6. Compression test results.

Table 3.4. Compression test statistics.

	x-direction						y-direction					
	Strength			Modulus			Strength			Modulus		
Dataset	**mean**	**CV**	**ADK**	**mean**	**CV**	**ADK**	**mean**	**CV**	**ADK**	**mean**	**CV**	**ADK**
Id	*MPa*	*%*	**Ratio**	*GPa*	*%*	**Ratio**	*MPa*	*%*	**Ratio**	*GPa*	*%*	**Ratio**
S	371	5.5	0.55	26.2	3.8	0.22	316	6.2	0.18	23.3	4.8	0.25
V	375	8.5	0.13	27.1	5.7	0.10	331	4.0	0.35	23.5	5.3	0.40
Total	373	7.1	0.24	26.7	5.1	0.71	324	5.6	***1.11***	23.0	5.0	0.23

Note: ADK ratios < 1 indicate no statistically discernible difference between datasets

As with the tension results, there was a decrease in the mean values of all compressive properties for the **S** datasets compared to the **V** datasets, but at smaller magnitudes for the strength properties when compared to tension. The strength was reduced by 1% and 5% in the *x* and *y*-directions, respectively, while the modulus saw reductions of 3% and 0.9% in the *x* and *y*-directions, respectively. The ADK ratios in Table 3.4 however, indicate that the only property that produced statistical differences between resin formulations was the *y*-strength with a difference in means of 15 MPa, The 5% reduction in y-strength with a 5% increase in styrene is larger than what was found for Derakane 411-350 where strength was reduced by 2% for a 10% increase in styrene

monomer [10]. The fact that the x-strength saw smaller reductions could indicate that there are other factors contributing to the differences in *y*-strength, such as the differences in the weave structure between the warp and fill directions in a fabric which have been shown to affect compression properties [32, 33].

3.5.5 Shear Results

The three-rail test method does not result in a catastrophic failure of the test specimen; therefore, an offset method was used to determine the shear strength as recommended in ASTM D4255. The method employed in this study used the strain range of 2000 to 6000 micro-strain to construct the 0.2% offset line. The intercept of this offset line with the load curve was taken as the offset failure strength.

The shear strength and modulus results for the *x* and *y*-directions are presented in the plot in Figure 3.7. As with the previous property results a dual axis was used for the strength and modulus data in the plots. The strength data was plotted with an *x*-axis scale of 0-55 MPa, while the modulus data was plotted with a 0.0-5.5 GPa scale. The plotted results include the mean value with error bars (±1 standard deviation) for each resin formulation and shear property. The statistical results are presented in Table 3.5.

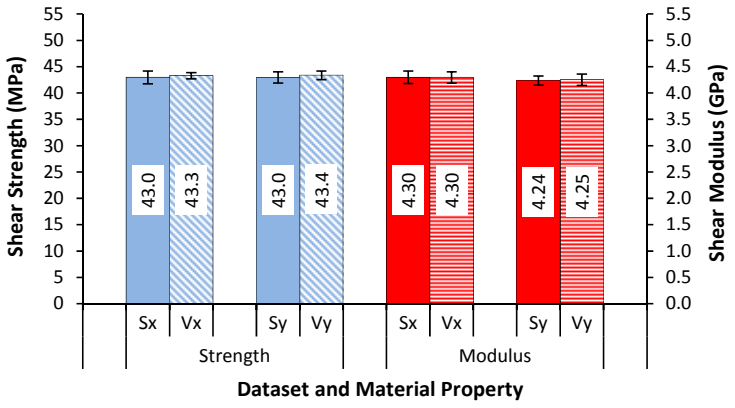

Figure 3.7. Shear test results.

Table 3.5. Shear test statistics.

	x-direction						y-direction					
	Strength			Modulus			Strength			Modulus		
Dataset	mean	CV	ADK	mean	CV	ADK	mean	CV	ADK	mean	CV	ADK
Id	*MPa*	*%*	Ratio	*GPa*	*%*	Ratio	*MPa*	*%*	Ratio	*GPa*	*%*	Ratio
S	43.0	2.8	***1.48***	4.30	2.8	***1.81***	43.0	2.4	0.67	4.24	2.0	0.26
V	43.3	1.4	0.44	4.30	2.5	0.40	43.4	1.9	0.14	4.25	2.6	0.16
Total	43.1	2.2	0.46	4.30	2.6	0.15	43.2	2.2	0.64	4.24	2.3	0.21

Note: ADK ratios < 1 indicate no statistically discernible difference between datasets

There was a negligible decrease in the mean values of the shear properties for the **S** datasets compared to the **V** Datasets. The mean of the x and y-strength results was reduced by 1%, while the mean moduli decreased by less than 1%. In addition the CV for all of the properties was below 3%. The ADK ratios in Table 3.5 indicate that there were no statistical differences between the resin formulations for any of the shear properties. There were however, statistical differences within the **S** dataset for both *x*-strength and *x*-modulus. Results of this nature are not unexpected considering the very small CV for the datasets, and are similar to what was experienced in the larger study with the shear property results [16].

3.5.6 Flexure Results

The flexural tests were conducted on specimens in the *x*-direction only. The stress strain response of the test specimens typically displayed some progressive failure occurring prior to final failure. All specimens failed between the load-heads. The typical specimen failure mode was a combination of compressive failure on the top surface of the specimen followed by either a tensile failure of the bottom surface, or a delamination in the specimen between the load-heads.

The flexural secant modulus was calculated in the strain range of 1000 to 3000 micro-strain as recommended in ASTM D7264. The flexural strength and modulus

results for the *x*-orientations are presented in the plot in Figure 3.8. As with the previous property results a dual axis was used for the strength and modulus data in the plots. The strength data was plotted with an x-axis scale of 0-550 MPa, while the modulus data was plotted with a 0-55 GPa scale. The plotted results include the mean value with error bars (±1 standard deviation) for each resin formulation and flexural property. The statistical results are presented in Table 3.6.

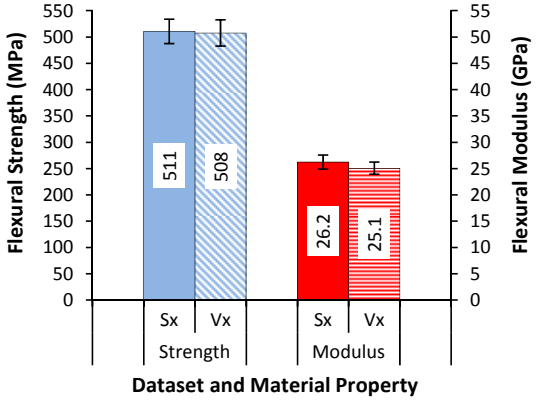

Figure 3.8. Flexure test results.

Table 3.6. Flexure test statistics.

	x-direction					
	Strength			Modulus		
Dataset	mean	CV	ADK	mean	CV	ADK
Id	*MPa*	*%*	Ratio	*GPa*	*%*	Ratio
S	511	4.5	0.60	26.2	5.1	0.22
V	508	4.9	0.19	25.1	4.6	0.29
Total	509	4.7	0.10	25.7	5.3	***1.10***

Note: ADK ratios < 1 indicate no statistically discernible difference between datasets

Unlike the other material properties investigated in this study, dataset **S** produced larger mean values than dataset **V** for both x-strength and x-modulus. The mean x-strength increased by 0.6% and the mean x-modulus increased by 4% for dataset **S**. The ADK ratios in Table 3.6 indicate that the increase in modulus was statistically significant.

An increase in flexural properties with increasing styrene content up to 45 wt% styrene content is consistent with what was found by Sultania [8].

The flexural modulus, which was based on measurements of strain on the compression face of the flexure specimen, was identical to the compressive modulus for dataset **S**, while it decreased by 7.4% for dataset **V** compared to the compression modulus.

3.6 Conclusions

E-glass/vinyl-ester composite laminate panels were fabricated using two different resin formulations to investigate the effects of styrene content on material properties. The first resin formulation was "as received" containing 40wt% styrene, and the second formulation was diluted with an additional 5wt% styrene monomer, for a total of 45wt% styrene. The increase of styrene content reduced the wet-out time of the fiber preforms by 22-29% on average compared to the infusions with the base resin formulation, which was one of the objectives of diluting the resin; however, it also reduced the resin gel time by 6-15%. The differences in gel time are not significant, but they are contrary to prior studies where increased styrene content resulted in increased gel times [2, 4, 7].

Material test coupons were cut from each of the four panels, two from each resin formulation. Material testing was comprised of ASTM test standards for constituent volume content, tension, compression, in-plane shear, and four-point flexure with 1/4-point loading.

The increase in styrene content produced a mean fiber volume fraction that was approximately one percentage-point greater than the base resin system. While the less viscous resin formulation would be expected to wet-out the fiber tows more thoroughly, it

could also be attributed to the longer time between wet-out and gelation which would also improve the wet-out of the fiber preform.

The increase in styrene content reduced the mean value for the majority of the strength and modulus properties for the tension, compression and shear tests. The tensile strength property experienced the greatest decrease at 6% and 14% for the *x* and *y* warp fiber directions, respectively; however, only the decrease in *y*-strength proved to statistically significant. While the difference in tensile *x*-modulus was also statistically significant, it decreased by a mere 1.8% with the 5wt% increase in styrene. The compression strength in the y-direction also proved to be statistically significant with a 5% decrease for the elevated styrene content resin formulation, but the difference could possibly be attributed to variations in weave structure as has been found in other studies [16]. The shear properties in the *x* and *y*-directions decreased with increasing styrene content, but at magnitudes of less than 1%, of which none proved to be statistically significant.

The flexural tests produced the only results that indicated an increase in properties for the specimens with the increased styrene formulation. The mean strength in the x-direction increased by a mere 0.6% for the increased styrene formulation specimens and proved not to be statistically significant; however the mean modulus in the x-direction increased by 4% with increased styrene content and was shown to be statistically significant.

Based on the finding of prior studies [1-15] and the material property variations due to an increase in styrene content for the Derakane 8084 resin observed in this study; specifically, reductions of 14% and 5% in the tensile and compressive strengths in the y-

direction, respectively, and a 4% increase in flexural modulus, it would be prudent to thoroughly investigate the effects of further dilutions prior to implementing such a formulation during an infusion.

3.7 References

3.1 Abdelwahab M, Agag T, Akelah A, Takeichi T (2012) Synthesis and Characterization of Styrene Modified Vinylester Resin-Clay Nanocomposites. Polymer Engineering and Science, 52(1):125-132.

3.2 Dua S, McCukkough R L, Palmese G R (1999) Copolymerization Kinetics of Styrene/Vinyl- Ester Systems: Low Temperature Reactions. Polymer Composites 20(3):379-391.

3.3 Yang H and Lee J (2001) A Kinetic Model for Free-Radical Crosslinking Co-Polymerization of Styrene/Vinylester Resin. Polymer Composites 22(5):668-679.

3.4 Cardona F, Rogers D, Davey S, Van Erp G (2007) Investigation of the Effect of Styrene Content on the Ultimate Curing of Vinylester Resins by TGA-FTIR. Journal of Composite Materials, 41(2):137-152.

3.5 Brill R P and Palmese G R (2000) An Investigation of Vinyl-Ester/Styrene Bulk Copolymerization Cure Kinetics Using Fourier Transform Infrared Spectroscopy. Journal of Applied Polymer Science 76:1572-1582.

3.6 Scott T F, Cook W D, Forsythe J S (2008) Effect of the Degree of Cure on the Viscoelastic Properties of Vinyl Ester Resins. European Polymer Journal 44:3200-3212.

3.7 Scott T F, Cook W D, Forsythe J S (2003) Photo-DSC Cure Kinetics of Vinyl Ester Resins II: Influence of Diluent Concentration. Polymer 44:671-680.

3.8 Sultania M, Yadaw S B, Rai J S P, Srivastava D (2010) Laminates Based on Vinyl Ester Resin and Glass Fabric: A Study on the Thermal, Mechanical and Morphological Characteristics. Materials Science and Engineering A 527:4560-4570.

3.9 Li P, Yu Y, Yang X (2008) Effects of Initiators on the Cure Kinetics and Mechanical Properties of Vinyl Ester Resins. Journal of Applied Polymer Science 109(4):2539-2545.

3.10 Rodriguez E, Larranaga M, Mondragon I, Vazquez A (2006) Relationship Between the Network Morphology and Properties of Commercial Vinyl Ester Resins. Journal of Applied Polymer Science 100:3895-3903.

3.11 Rosario A C, Burts-Cooper E, Riffle J S (2007) Copolymerization Behavior and Properties of Dimethacrylate-Styrene Networks. Polymer 48:1203-1211.

3.12 Shan L, Robertson C G, Verghese K N E, Burts E, Riffle J S, Ward T C, Reifsnider K L (2001) Influence of Vinyl Ester/Styrene Network Structure on

Thermal and Mechanical Behavior. Journal of Applied Polymer Science 80:917-927.

3.13 Agarwal N, Singh A, Varma I K, Choudhary V (2008) Effect of Structure on Mechanical Properties of Vinyl Ester Resins and Their Glass Fiber-Reinforced Composites. Journal of Applied Polymer Science, 108:1942-1948.

3.14 Larson B K, Drzal L T, and Van Antwerp J (1995) Swelling and Dissolution Rates of Glass Fiber Sizings in Matrix Resin Via Micro-Dielectrometry. Polymer Composites 16(5):415-420.

3.15 Crawford S and Lungu C T (2011) Influence of Temperature on Styrene Emission from a Vinyl Ester Resin Thermoset Composite Material, Science of the Total Environment 409:3403-3408.

3.16 Berube K A and Lopez-Anido R A (2010) Variability in the Material Properties of Polymer Matrix Composites for Marine Structures. Journal of ASTM International 7(4):18p.

3.17 Berube K A and Lopez-Anido R A (2011) Effect of Preform Consolidation on the Fracture Toughness of Marine Grade Polymer Matrix Composite Materials Fabricated With a VARTM Process. Journal of Advanced Materials 43(1):30-48

3.18 Berube K A and Lopez-Anido R A (2012) Effect of Resin Cure Recipe and Ambient Processing Temperature on the Material Properties of Marine Grade Polymer Matrix Composite Materials. Submitted for Publication to Materials Performance and Characterization.

3.19 Cain J J, Post N L, Lesko J J, Case S W, Lin Y, Riffle J S, and Hess P E (2006) Post-Curing Effects on Marine VARTM FRP Composite Material Properties for Test and Implementation. Journal of Engineering Materials and Technology, Transactions of the ASME, 128:34-40.

3.20 El-Chiti F (2005) Experimental Variability of E-Glass Reinforced Vinyl Ester Composites Fabricated by VARTM/SCRIMP. MS Thesis in Mechanical Engineering, University of Maine, Orono, ME.

3.21 Ashland Chemical (2011) Technical Datasheet, Document 1820 V3 F2, Revised: 2011-8-30, 4p.

3.22 ASTM Standard D3171 (2006) Standard Test Methods for Constituent Content of Composite Materials. ASTM International, West Conshohocken, PA, www.astm.org.

3.23 ASTM Standard D3039 (2007) Standard Test Method for Tensile Properties of Polymer Matrix Composite Materials. ASTM International, West Conshohocken, PA, www.astm.org.

3.24 ASTM Standard D6641 (2009) Standard Test Method for Determining the Compressive Properties of Polymer Matrix Composite Laminates Using a Combined Loading Compression (CLC) Test Fixture. ASTM International, West Conshohocken, PA, www.astm.org.

3.25 ASTM Standard D4255 (2001) Standard Test Method for In-Plane Shear Properties of Polymer Matrix Composite Materials by the Rail Shear Method. ASTM International, West Conshohocken, PA, www.astm.org.

3.26 ASTM Standard D7264 (2007) Standard Test Method for Flexural Properties of Polymer Matrix Composite Materials. ASTM International, West Conshohocken, PA, www.astm.org.

3.27 Masters J (1996) Strain Gage Selection Criteria for Textile Composite Materials. NASA Contractor Report 198286, National Aeronautics and Space Administration, Langley Research Center, VA.

3.28 El-Chiti F, Lopez-Anido R A, Dagher H J, Thompson L, Muszynski L, and Hess P E (2005) Experimental Approach for Characterizing VARTM Composites Using a 3-D Digital Image Correlation System. Proceedings of the SEM XII Int. Congress and Exposition on Experimental and Applied Mechanics, Portland, OR, June 7-9, 2005, Society for Experimental Mechanics, Bethel, CT, 8p.

3.29 Walls J and Thompson L (2005) Parametric Shape Optimization of Tensile Coupons for Marine Grade Glass Fiber Reinforced Plastics. Report# ATS-RELY/2-2005-02, Applied Thermal Sciences, Orono, ME.

3.30 Berube K A and Lopez-Anido R A (2008) Full-Field Strain Measurements for DeterminIng Mechanical Properties of Marine Composite Laminates. Experimental Mechanics Applied to Damage: Detection, Analysis and Mitigation, SEM XI International Congress Exposition on Experimental and Applied Mechanics, Orlando, FL, June 2-5, 2008, Society for Experimental Mechanics, Bethel, CT, 8p.

3.31 MIL-HDBK-17F-1 (2002) Composite Materials Handbook Volume 1 - Polymer Matrix Composites Guidelines for Characterization of Structural Materials, ASTM International, West Conshohocken, PA, p8.1-110.

3.32 Yang B, Kozeya V, Adanurb S, and Kumara S (2000) Bending, Compression, and Shear Behavior of Woven Glass Fiber-Epoxy Composites. Composites Part B 31:715-721.

3.33 Kim J, Shioya M, Kobayashi H, Junichi Kaneko J, and Kido M (2004) Mechanical Properties of Woven Laminates and Felt Composites Using Carbon Fibers. Part 1: In-Plane Properties. Composites Science and Technology 64:2221-2229.

CHAPTER 4

FULL-FIELD STRAIN MEASUREMENTS FOR DETERMINING MATERIAL PROPERTIES OF MARINE COMPOSITE LAMINATES

4.1 Abstract

Determining the mechanical properties of marine grade composites using conventional strain gages can pose an insurmountable problem when dealing with heavy woven fabrics. The variability in the recorded strain values can vary significantly depending on the tow spacing and whether the gage is placed on a "warp" or "fill" tow orientation. The work presented in this paper demonstrates the use of a 3-D Digital Image Correlation (DIC) system for determining the mechanical properties of 24oz woven-roving, eglass/vinyl-ester composite laminates. The DIC system permits individual test review, after post-processing of the data, which allows the examiner to visually observe the strain field formation and distribution throughout the gage area of the test specimen for the duration of the test. While the tests conducted over the course of the entire study included standardized tension, compression, shear, and flexural tests of composite material coupons, and flexural tests on structural components, only the use of the DIC system for the flexural tests are presented here. The tests were part of a manufacturing round robin study designed to investigate the variability in mechanical properties due to the use of multiple manufacturers for fabricating identical parts. The work was part of an Office of Naval Research project to determine the variability in mechanical properties of marine grade composites fabricated using a VARTM process.

4.2 Introduction

A 3-D Digital Image Correlation (DIC) strain measurement system was implemented in an experimental program for characterizing the flexural properties of polymer matrix composites (PMC) with woven-roving reinforcement. The 3-D DIC system has the capability of measuring non-contact full-field strains and displacements of specimens under stress. The test setup used to conduct the experimental study using the 3-D DIC system is presented including specimen preparation. The parameters of the system used to measure strain and the technique of strain measurement by the DIC system is explained. In addition, the precision and accuracy of the system is discussed and referenced to a study comparing conventional measuring techniques to DIC system strain measurement.

4.3 Background

Conventional measurements used in composite material testing are bonded strain gages, extensometers, and linear variable differential transducers (LVDTs). Strain gages are surface bonded resistance gages. The conventional instrumentation provides one measurement at a time, either strain or displacement. Typical problems accompany the use of conventional measurement devices. Strain gages have problems due to proper bonding of the strain gage and avoiding de-bonding during the loading of the specimen. Alignment of the strain gage with the fibers is also a source of difficulty when using strain gages on composite materials. In addition, the transverse sensitivity of the strain gage material has to be accommodated. The use of an extensometer usually requires the removal of the device from the specimen prior to specimen failure to avoid damage to the instrument. As for the LVDT, it only provides displacement information. All of the

conventional measurements require surface contact with the specimen and provide single point information.

A three-dimensional digital image correlation (DIC) photogrammetry system is capable of non-contact full-field measurements of strains and displacements. The DIC technology was developed in the 1980's and was used to measure deformation and strains under various loading regimes [1,2]. In addition, the technology has been applied to determine strains in solid wood, individual wood fibers and papers [3,4], resin films [5], fiber reinforced Polymer Composites [6-8] and Concrete [9].

A more recent work on fracture mechanics has been done using the DIC system. The system was used to track the crack propagation length and the crack opening displacement between a wood plastic composite and a fiber reinforced polymer [10]. In addition, the DIC system was used to characterize the creep properties of wood plastic composites [11].

The digital image correlation system determines the displacement and deformation of selected points of the mesh on the surface of the specimen under testing. The displacement and deformation of the points are determined by comparing successive images taken during the loading of the specimens and correlated to the original state of the specimen prior to loading. Two cameras are used to cross correlate the distances and obtain out of plane displacements. The mesh on the surface of the specimen is recognized by the system as a variable gray intensity pattern. Once each mesh is correlated with its neighboring mesh, in-plane strain values are obtained based on triangular or rectangular networks of points [7]. The out of plane displacement is accurately measured when two cameras are utilized. The two cameras, once in position in front of the specimen and

calibrated, can provide stereoscopic information of the specimen surface. The DIC technology used for this study was the ARAMIS system provided by GOM, MbH, and has been successfully applied to a wide range of experimental studies [12,13].

4.4 Composite Materials Evaluated

A marine grade polymer matrix composite (PMC) reinforced with woven roving was tested in this study. The PMC panels consisted of E-glass/vinyl-ester and were fabricated using a Vacuum Assisted Resin Transfer Molding (VARTM) process. The fiber reinforcement used was a Saint Gobain Vetrotex 324 woven roving with a weight per unit area of 814 g/m^2 (24 oz/yd^2). The tow spacing is 5.1 mm (5 tows per inch) in the warp direction, and 6.4 mm (4 tows per inch) in the fill direction. This results in 55% of the fiber orientated in the warp direction and 45% in the fill direction. The polymer resin used was an Ashland Derakane 8084, which is an elastomer-modified epoxy vinyl-ester resin.

Each of the five participating manufacturers provided two panels for the material coupon testing portion of the study. The panel dimensions were 1.22 m x 1.22 m (4 ft x 4 ft) and consisted of 8 layers of fabric reinforcement with the warps parallel, for a nominal thickness of 5.1 mm (0.20 in.). The lay-up notation is $[0]_{4sf}$, where the warp direction corresponds to the principal material direction-1, and the fill direction to the principal material direction-2 as presented in Figure 4.1.

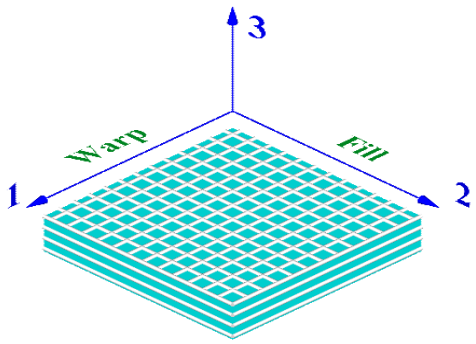

Figure 4.1. Laminate coordinate reference system.

4.5 Composite Specimen Preparation

Eight specimens were cut from each of the ten panels using a water-jet cutter. The nominal specimen dimensions were 1 inch wide by 8 inches long by 0.2 inches thick. The only preparation required for the DIC strain measurement was the application of a speckle pattern to the surfaces that will be monitored during the test. The specimen surface was first cleaned with a degreaser to remove any residue remaining from the manufacturing of the panels. The pattern was then created by applying a thin layer of white paint followed by a speckle pattern of black paint. The only requirement of the pattern is that it be approximately a 50% grayscale pattern with the black speckles of 3 to 5 pixels in size when observed through the DIC cameras. This type of speckle pattern allows the DIC system to establish a unique finite mesh pattern of gray intensity which is used to identify and locate each mesh element relative to its neighboring elements.

4.6 Experimental Test Setup

A 4-point flexural test configuration, with quarter-point loading, was used for this investigation, as shown in Figure 4.2. As recommended in ASTM D7264 [14] a span-to-thickness ratio of 32 was used for all tests. The testing was performed on an Instron 100

kN (22.5 kip) load frame, in the environmentally controlled Mechanical Test Lab at the Advanced Engineered Wood Composites (AEWC) Center, at the University of Maine. The rate of crosshead loading was constant at 0.20 in/min. This rate was calculated based on the rate equation given in the ASTM standard to obtain the recommended rate of straining in the outer surface of the test specimen.

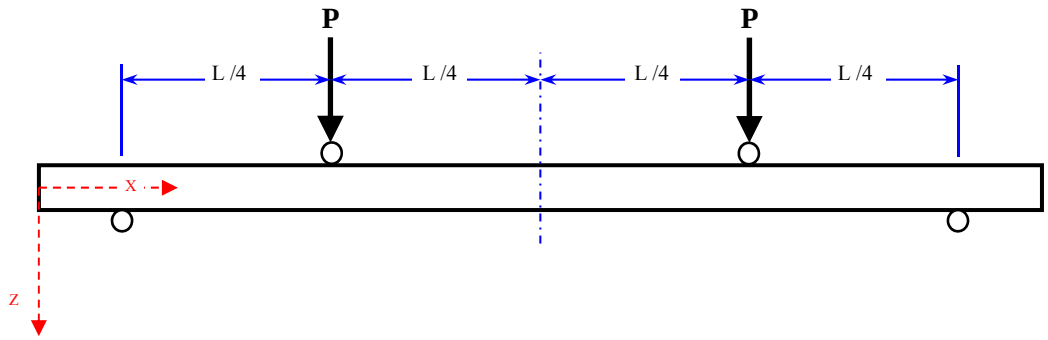

Figure 4.2. Four-point flexure with ¼-point loading configuration.

The Digital Image Correlation (DIC) system was used to record both the mid-span deflection and the full-field strain distribution during each test. A total of three cameras were used during the testing. One camera was used in a 2-D mode, to monitor mid-span deflection and in-plane strains, and the other two were used as a pair, in 3-D mode, to record full-field strains on the top surface of the specimen. Schematics of the viewing areas are shown in Figure 4.3. Photos taken by the DIC system cameras during a typical test are shown in Figure 4.4.

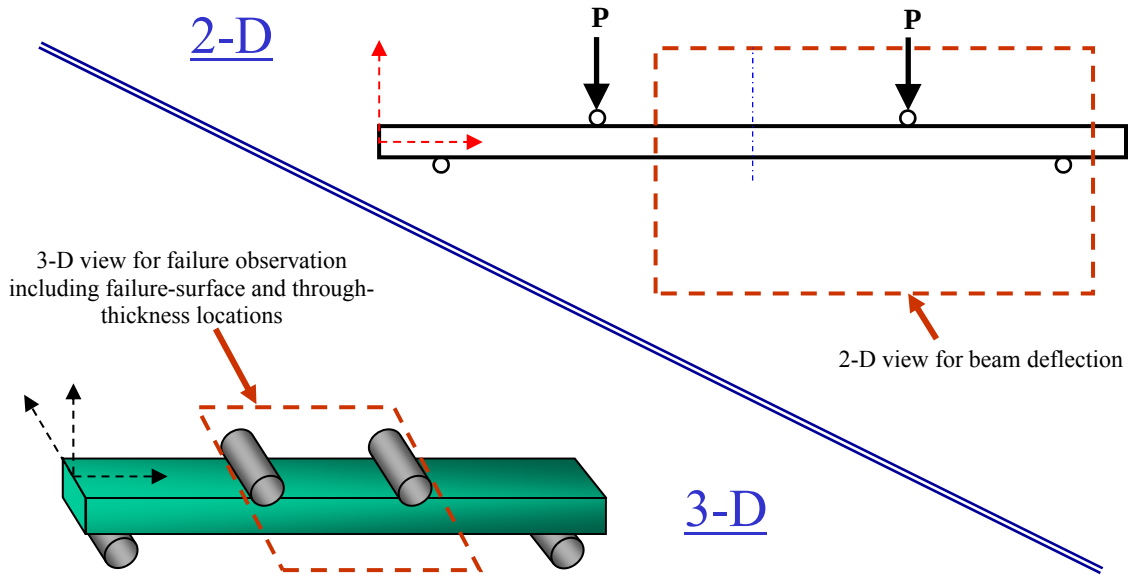

Figure 4.3. Schematic of the 2-D and 3-D camera observation areas during flexural testing.

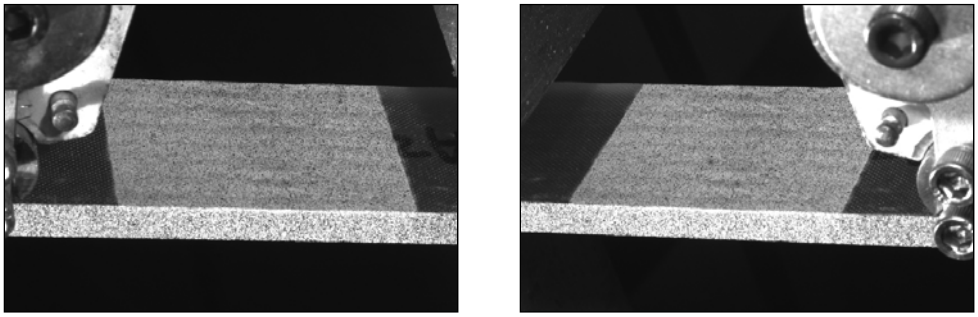

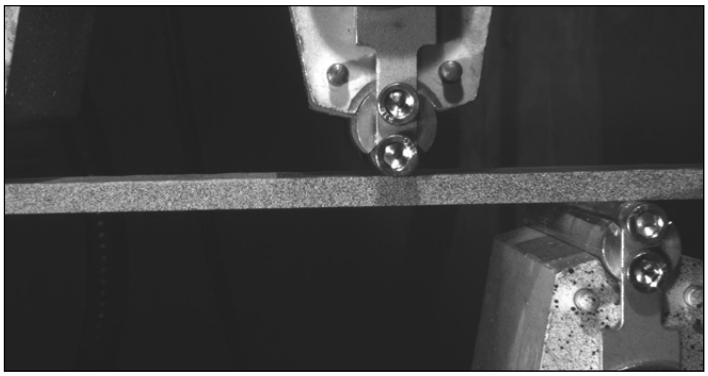

Figure 4.4. Images from the DIC cameras showing the specimen field of view, a) 3-D left camera, b) 3-D right camera, and c) 2-D camera.

The DIC system was calibrated prior to testing. Once the cameras were calibrated, the system was able to recognize the speckle pattern and track the motions and strains on the surfaces relative to its original state at the start of the test. Uniform lighting was used to illuminate the specimen surface and minimize shadows from the fixturing.

During the test, the system was capturing pictures at a frequency of 1 hertz. The selection of this sampling rate for the image acquisition was determined such that approximately 200 photos were taken per test. This sampling was more than sufficient to obtain the desired increment in strain during each load step without increased computation time. The computation time was the time needed, after the test was concluded, for the system to correlate the left and right photos for each sampling period and yield the full-field strain of the specimen surfaces relative to the original state of the specimen just prior to loading. The typical computation time was 5 minutes.

4.7 Full-Field Strain Recognition

As previously mentioned, the DIC system recognized a mesh on the surface of the specimen. Since the specimen was prepared with a speckle pattern of black and white, each pixel in the mesh is defined by its gray intensity. The system recognizes a set of pixels, defined as a pixel neighborhood, in a square region. Each square pixel neighborhood is defined as a facet. The facet size can be set by the user in reference to the number of pixels that define the edge of the square. The facet size used in the study was 15 pixels. In addition, the distance between two facets is defined as the facet step, similarly, defined by the number of pixels. For this study, the facet step was taken to be 13 pixels.

4.7.1 Strain Computation

During the test process, the DIC system snapped images at a frequency set by the operator. For every snap, the DIC system captured a pair of images, one from the left camera and one from the right camera, which represented a stage of loading. Once the test was completed, the images were stored on an external hard drive. The strain computation of the specimen starts with the system recognizing a single facet on all of the images. Once the facets were recognized, the DIC system compared each image to the reference image which was usually the image taken at the start of the test. The comparison was done by taking each facet from the image and comparing it to the same facet in the reference image and calculating the strains of each facet by measuring the relative change in position of its 8 neighboring facets, for a computation base of 3. The strains computed represented the deformation of each facet in the x-direction, ε_x, in the y-direction, ε_y, and in-plane shear, γ_{xy}. In addition, the displacement vectors were calculated to determine the amount of displacement each facet has moved. The system had the capability of transforming the computed strains to any orthogonal coordinate system. This transformation accounted for any misalignment of the cameras parallel (or perpendicular) to the line of loading on the specimen. Compared to strain gages, the DIC transformation enabled the operator to reduce errors produced by bonding the strain gage at an angle with the line of loading on the specimen.

Once the strain was computed, full-field strains were generated for each stage during the loading of the specimen. For the flexural study presented here, an area of the full-field strain was selected on the top surface of the specimen in the gage section and the mean strain from each stage was exported to build the stress-strain curve and obtain the elastic properties of the material.

4.7.2 DIC Parameters

The facet size, facet step, and computation base were controlled by the operator. Each of these parameters affects the computation results and computation time differently. These issues were discussed in detail in the prior study on marine composites [1], so will not be discussed further except to say that the parameters were selected such that the system noise was minimized.

4.7.3 Accuracy and Precision

A study was conducted comparing conventional strain measuring tools to the DIC system [15]. The conventional strain measuring tools in the study were a resistive foil strain gage and a linear extensometer. The study concluded that the DIC system produced lower variation than, or as low as, the conventional strain measuring tools when testing a tensile specimen. The DIC system resulted in measuring the elastic modulus and Poisson's ratio to within 2% of the expected values.

4.8 Discussion of Results

The results for the flexural strength and modulus for all the datasets in the study are given in the plots of Figure 4.5. The values plotted are the mean strengths and modulus for the eight specimens from each dataset, with the coefficients of variation indicated by the error bars. The strength values ranged from 69.7-ksi for dataset B2 to 75.6-ksi for dataset E2. The modulus values showed more variability ranging from 3.59 Msi for dataset D2 to 4.14 Msi for dataset A2.

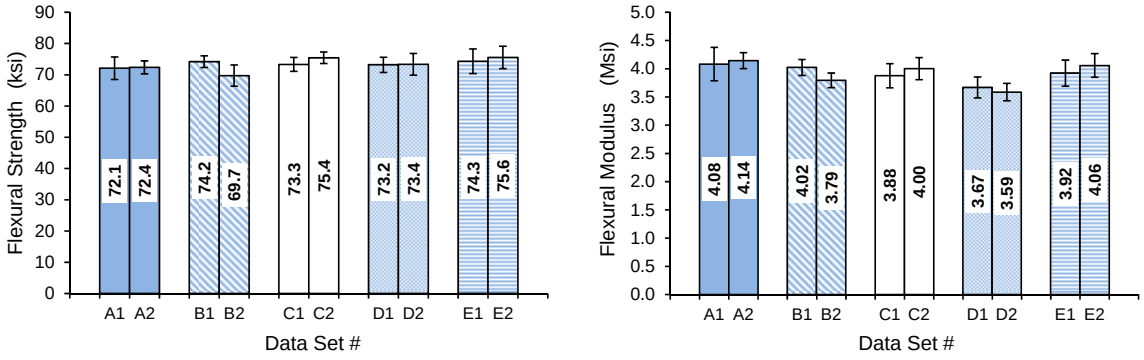

Figure 4.5. Flexural strength and modulus results for each dataset.

As an example of the variability within a dataset, the load-deflection and stress-strain results are plotted in Figure 4.6 for a typical set of material coupon test specimens. The variability that is evident in the load deflection curves is a result of the slight differences in specimen width and thickness. This variability is nearly eliminated in the stress strain curves, as evidenced by the tighter clustering of the curves, because the specimen dimensions are incorporated into the flexural stress calculations.

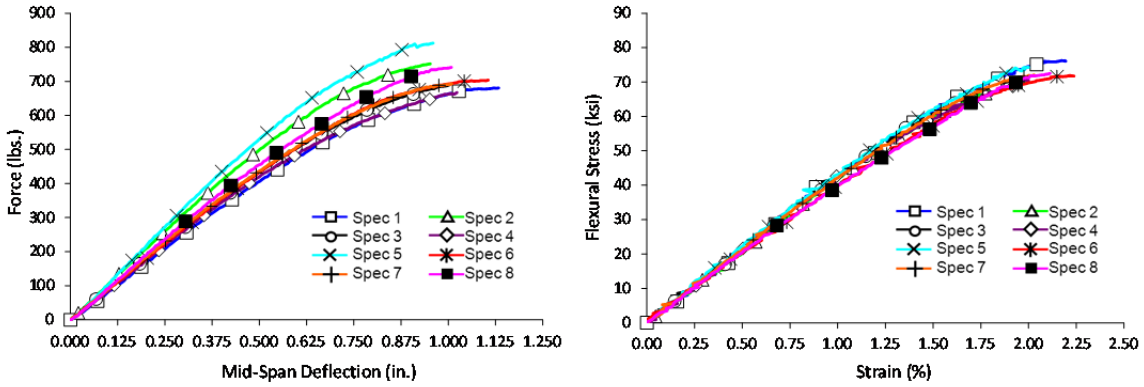

Figure 4.6. Typical force-deflection and stress-strain plots for a set of test specimens.

A comparison of the measured strain results, obtained using the DIC system, with the calculated strain value, obtained using the equation from Section 13.5 of ASTM D7264 are presented in the plot of Figure 4.7 and in Table 4.1. Included in the table is the

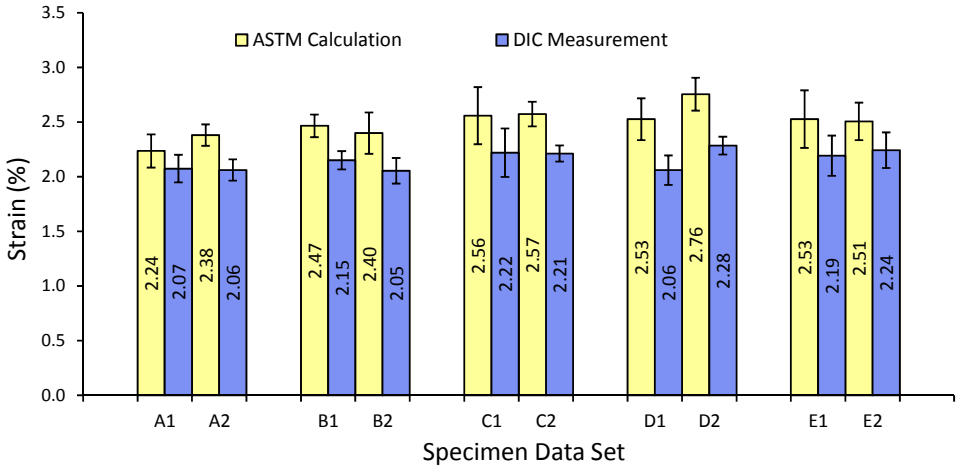

Figure 4.7. Measured (DIC) and calculated (ASTM) strains for each material coupon dataset.

Table 4.1. Strain results for the material coupon flexure tests.

Dataset	**3-D DIC Strain**	**ASTM Strain**	**Δ Strain**
ID	*%*	*%*	*%*
A1	2.07	2.24	-7.8
A2	2.06	2.38	-15.5
B1	2.15	2.47	-14.7
B2	2.05	2.40	-16.8
C1	2.22	2.56	-15.2
C2	2.21	2.57	-16.4
D1	2.06	2.53	-22.7
D2	2.28	2.76	-20.6
E1	2.19	2.53	-15.2
E2	2.24	2.51	-11.7
Mean	2.16	2.49	-15.7
CV	4.0	5.5	

calculated error indicating the percent difference between the two strain values. The error bars in the plot are ±1 standard deviation.

As indicated in Table 4.1 the range of DIC strains ranged from 2.05 to 2.28%, while the strain range for the ASTM calculated value was 2.24 to 2.76%. The ASTM value was larger then the DIC value for all datasets. The mean calculated ASTM strain value was 15.7% larger than the mean measured DIC value (2.49% compared to 2.16%),

while the Coefficient of Variation (CV) was a 1.5 percentage points higher for the ASTM value.

The majority of the specimens failed in compression along the top surface, usually followed by a delamination. The remainder of the specimens failed in compression either near the center of the beam, or near one of the load-heads. Approximately 90% of the failures were preceded by localized failures without any measurable decrease in the applied load, which then led to a progressive failure with an observable drop in load. The remaining specimens failed in a more catastrophic nature without a preceding load drop.

After post processing of the DIC data, it was possible to observe localized strain "hot spots" in the speckled region of the specimen. In some instances it was also possible to observe localized resin crazing and progressive tow failure in the non-speckled region of the upper surface of the flexure specimens. The ultimate failure normally occurred at one of these observable hot-spots, or progressive failure locations on the top surface of the flexure specimen.

The development of the strain field is shown in Figure 4.8 for a typical flexural test specimen. As shown in the series of pictures, the top of the beam goes into compression while the bottom of the beam experiences a tensile strain equal in magnitude to the compressive side.

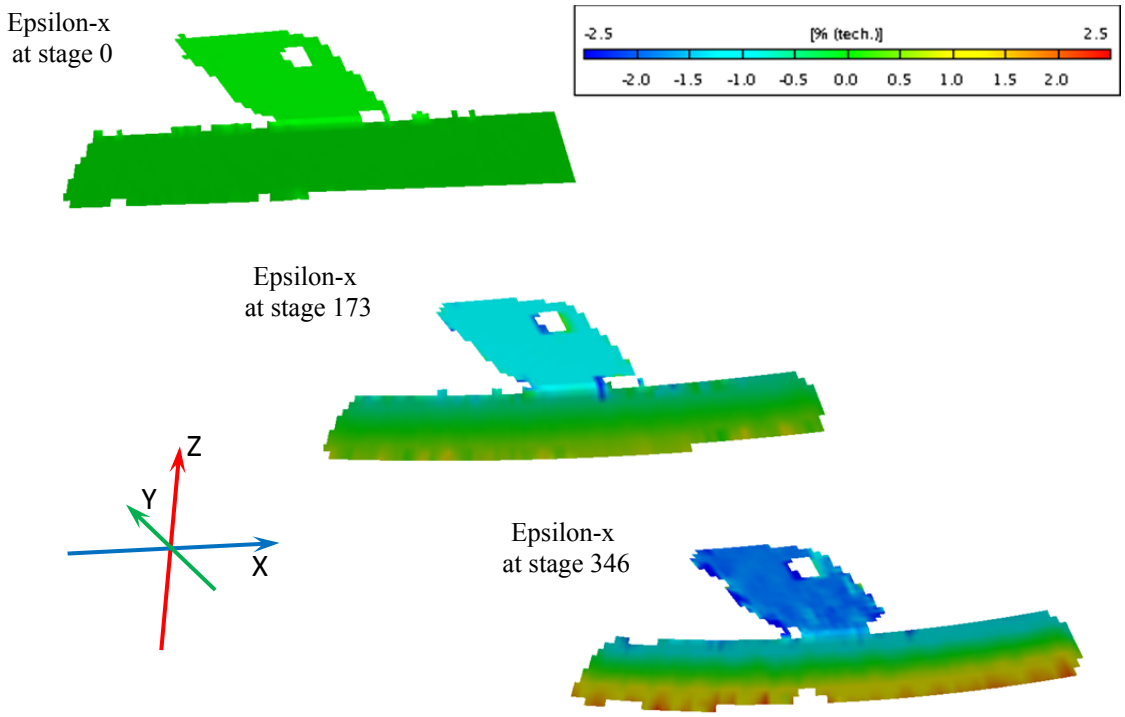

Figure 4.8. Flexural strain distribution progression for a flexural test specimen.

As in the prior study on marine grade laminates [1], the full-field strain produced by the system revealed high and low strain variations on the top surface of the specimen in accordance with the weave pattern of the fabric used. The high strain values developed on the tow regions of the fabric along the major strain direction of the specimen, perpendicular to the load-heads. The low strain values developed either at resin rich areas between tows, or on the tows perpendicular to the major strain direction, parallel to the load-heads. It is this strain gradient pattern that results in the larger variability when using conventional strain gages. Unlike the strain gage, which reports the strain in a small area of the specimen, the DIC system allows the experimenter to choose the location that presents a more representative strain result for the test specimen during failure.

4.9 Conclusions and Recommendations

The full-field strain measurements provided by the DIC system for the flexure tests demonstrated the benefits of using three-dimensional digital image correlation photogrammetry technology for flexural testing. The DIC system was successful at recording the mid-span deflections and photo documenting the flexure tests for further review. The system also gave a detailed visualization of, and quantified, the stress distribution on the top surface and through the thickness of the specimen.

The ability to obtain strain results in any orientation required, after the test is complete, reduces the variability inherent in applying a fixed conventional strain measuring device prior to testing. In addition to a reduction in experimental variability of the material properties obtained, the advantages of the DIC system over conventional strain measuring tools, include a reduction in specimen preparation time, fixture setup, and cost per specimen.

The DIC system's post processing capabilities allowed each individual test to be reviewed when desired. This review introduced not only a means to inspect the formation of the strain field, but also the ability to observe the nature of a progressive failure and a method of visually identifying test errors.

The DIC full-field strain measurement system has again demonstrated that it is an essential tool for determining material properties of marine composites reinforced with relatively heavy woven roving that exhibit localized strain variations. As the technology of photogrammetry and computer processing capabilities continues to improve, coupled with the advancement in the resolution of digital cameras, the accuracy and precision of

3-D DIC systems will follow suit leading to further reductions in the material property variability caused by data acquisition methods.

4.10 References

4.1 El-Chiti F, Lopez-Anido R A, Dagher H J, Thompson L, Muszynski L, and Hess P E (2005) Experimental Approach for Characterizing VARTM Composites Using a 3-D Digital Image Correlation System. Proceedings of the SEM XII Int. Congress and Exposition on Experimental and Applied Mechanics, Portland, OR, June 7-9, 2005, Society for Experimental Mechanics, Bethel, CT, 8p.

4.2 Bruck H A, McNeill S R, Sutton M A, and Peters W H I (1989) Digital Image Correlation Using Newton-Raphson Method of Partial Differential Correction. Experimental Mechanics, 29(3):261-267.

4.3 Ranson W F, Sutton M A, and Peters W H (1987) Holographic and Speckle Interferometry. In SEM Handbook of Experimental Mechanics, AS Kobayashi, Edito. Prentice-Hall, Inc, NJ, 388-429.

4.4 Mott L, Shaler S M, and Groom L H (1996) A Novel Technique to Measure Strain Distributions in Single Wood Fibers. Wood and Fiber Science, 28(4):429-437.

4.5 Muszynski L, Lagana R, and Shaler S M (2002) Optical Measurements of Wood Deformations in Changing Climate. In 2002 SEM IX International Congress on Experimental Mechanics, Milwaukee, WI.

4.6 Muszynski L, Wang F, and Shaler S M (2002) Short Term Creep Tests on Phenol Resorcinol Formaldehyde (PRF) Resin Undergoing Moisture Content Changes. Wood and Fiber Science, 34(4):612-624.

4.7 Muszynski L, Lopez-Anido R A, and Shaler S M (2000) Image Correlation Analysis Applied to Measurement of Shear Strains in Laminated Composites. In the SEM IX International Congress on Experimental Mechanics, Orlando, FL.

4.8 Melrose P, Lopez-Anido R A, and Muszynski L (2004) Elastic Properties of Sandwich Composite Panels Using 3-D Digital Image Correlation With the Hydromat Test System. In SEM XI International Congress and Exposition on Experimental and Applied Mechanics, Costa Mesa, CA.

4.9 Choi S and Shah S P (1997) Measurement of Deformations on Concrete Subjected to Compression Using Image Correlation. Experimental Mechanics, 37(3):307-313.

4.10 Souza B (2005) Fracture Mechanics Characterization of WPC-FRP Composite Materials Fabricated by the Composites Pressure Resin Infusion System (Compris) Process. MS Thesis in Civil Engineering, University of Maine, Orono, ME.

4.11 Durra M (2005) Behavior and Design of Reinforced Wood-Plastic Composite Sections for Use in Sustained Loading Structural Applications. MS Thesis in Civil Engineering, University of Maine, Orono, ME.

4.12 Schmidt T, Tyson J, and Galanulis K (2003) Full-Field Dynamic Displacement and Strain Measurement Using Advanced 3-D Image Correlation Photogrammetry-Part II. Experimental Techniques, 27(4):22-26.

4.13 Tyson J, Schmidt T, and Galanulis K (2002) Advanced Photogrammetry for Robust Deformation and Strain Measurement. In the SEM XI International Congress on Experimental Mechanics, Milwaukee, WI.

4.14 ASTM Standard D7264 (2007) Standard Test Method for Flexural Properties of Polymer Matrix Composite Materials. ASTM International, West Conshohocken, PA, www.astm.org.

4.15 Melrose P T (2004) Elastic Properties of Sandwich Composite Panels Using 3-D Digital Image Correlation With the Hydromat Test System, MS Thesis in Mechanical Engineering, University of Maine, Orono, ME.

CHAPTER 5

EFFECT OF PREFORM CONSOLIDATION ON FRACTURE TOUGHNESS OF MARINE GRADE POLYMER MATRIX COMPOSITE MATERIALS FABRICATED WITH A VARTM PROCESS

5.1 Abstract

The effect of fiber preform consolidation on Mode-I fracture toughness of composite laminates was investigated. Woven roving E-glass/vinyl-ester composite plates were fabricated with a pliable-bag VARTM process using consolidation pressures and consolidation times commonly incorporated when fabricating marine grade polymer composite parts. This study investigated the range of 0.85 to 0.98 bar (25 to 29 in-Hg) for consolidation pressure, and a consolidation time range of 1 to 5 hours. The general trend at the lower consolidation pressures was that shorter consolidation times produced larger onset fracture toughness values and smaller propagation fracture toughness values, while longer consolidation times produced smaller onset fracture toughness values and larger propagation fracture toughness values. There was not a consistent effect at the higher pressure. There was no correlation found between the global fiber volume fraction of the specimens and the fracture toughness properties.

5.2 Introduction

In recent years, the Navy has shown increased interest in ship construction using advanced fiber reinforced polymer (FRP) composites. This interest has been fueled by the Navy's continuing demand for vessels with reduced electronic and acoustic signatures and the initiative to reduce total-ownership-cost (TOC), which requires mitigating the

very high cost of maintenance on metallic ships. With an improved ability to affordably construct large composite parts over the past 25 years, assisted particularly by advances in resin-infusion processing [1], the promise of meeting the Navy's demands may become a reality in the near future.

While FRP manufacturing processes have advanced, questions remain regarding the consistency of material properties for large composite parts [2,3]. The Navy favors the vacuum assisted resin transfer molding process (VARTM) that incorporates a pliable vacuum-bag and permeable flow media. It is favored due to its ability to inexpensively fabricate large, quality, structural parts. The VARTM process has been investigated in several studies over the past 15 years [4-9]. The parameters that have been shown to have the greatest effect on composite mechanical properties include fiber preform consolidation, resin chemistry and curing, fiber sizing, interphase formation, and post-cure. A study to investigate the effects of fiber preform consolidation on the material properties of marine grade composites is presented here.

Fiber consolidation can affect the finished laminate properties through variations in laminate thickness [1,9], which directly affects the fiber volume fraction. This in turn affects the mechanical properties of the laminate. Pre-compaction of the fiber also influences the amount of consolidation pressure needed during infusion of the preform. Dimensional variations due to pressure gradients of the vacuum affect permeability and hence resin flow [9,11-13]. The main factors affecting fiber preform consolidation are fiber type, consolidation pressure, consolidation duration, consolidation speed, and the number of consolidation cycles [9,13-16]. While some studies have indicated that the number of consolidation cycles has the greatest effect on the volume fraction for plain

weave composites [13,17-19], the implementation of a repetitive multi-cycle consolidation routine can be impractical for large marine composite parts.

It has been shown that changes occur in the geometry of the textile structure and reorganization of the fiber network during preform consolidation [20-23]. The redistribution of the fiber network can have an effect on both the resin flow during the infusion [11,23-26] and the resulting material properties of the laminate [28-30], including variations in interlaminar fracture toughness [31-33]. Breiling [29] found that fiber nesting has the potential to create regions of stress concentration leading to reduced material properties without a significant change in the constituent volume fraction of the laminate. Compston [33] found that the global fiber volume fraction of the laminate was not a consistent predictor of the interlaminar fracture toughness, but that the localized fiber volume fraction in the region of the crack path and toughening mechanisms governed the fracture toughness. Kim observed that thicker fabrics yield greater fracture toughness due to fiber migration into the interply zones created by fabric nesting [34].

Cracks in the form of delaminations and disbonds are the most common defects found in composite structures [3,35-36] These types of defects can occur during manufacturing or during the operational life of the part, and are due to a lack of through-the-thickness fiber reinforcement which creates planes of weakness between the layers of the laminate. With the recent emphasis towards risk reduction when fabricating large composite parts [1], one of the Navy's areas of interest has been on fully understanding the effects of crack initiation and propagation in marine grade composite laminates [37].

The objective of the present study was to determine how preform consolidation routines commonly used during laminate fabrication affect the Mode-I fracture toughness

of marine grade polymer composites. This study is part of a larger project sponsored by the Office of Naval Research to investigate the causes of variability in material properties of E-glass/vinyl-ester marine grade composites. The sources of variability being investigated in the larger project include those due to manufacturing [38], post processing [39], and testing of composites [40-41].

5.3 Experimental

5.3.1 Panel Fabrication

A marine grade FRP composite reinforced with woven roving was used in this study. The FRP panels consisted of an E-glass/vinyl-ester system fabricated using a pliable-bag VARTM process. The fiber reinforcement used was a Saint Gobain Vetrotex E-324 woven roving with a weight per unit area of 814 g/m^2 (24 oz/yd^2). The fabric is a plain weave with a tow spacing of 5.1 mm (0.2 in.) in the warp direction, and 6.4 mm (0.25 in.) in the fill direction. This results in 55% of the fiber orientated in the warp direction and 45% in the fill direction. The polymer resin used was Ashland Derakane 8084, which is an elastomer-modified epoxy vinyl-ester resin.

The FRP panel dimensions were 610 mm x 965 mm (24 x 38 in.) and consisted of ten layers of fabric reinforcement in a warps-parallel configuration, for a nominal thickness of 6.4 mm (0.25 in.). The lay-up notation is $[0_{10}]_f$, where the orientation indicates the warp direction of the fabric. It is worth noting that the dimensions of the panel were chosen with two goals in mind: 1) Select a panel size such that a complete second set of specimens could be obtained from the panel if there were problems during specimen preparation or testing of the original set, and 2) Select a single panel size that could be fabricated during all phases of the larger study where additional material was

needed for other types of testing. The first of these measures reduces the variability that may occur during manufacturing by eliminating the need to re-fabricate panels. The second measure eliminates the variability that may occur when fabricating different panel sizes (i.e., thickness gradients), and allows the test results from one phase of the study to be compared to the other without having panel size as a manufacturing variable.

An 89 mm (3.5 in.) wide strip of 0.0127 mm (0.0005 in.) thick virgin PTFE film was placed at the mid-plane of the laminate along the edge of the panel where the vacuum line was placed, as shown in the panel schematic in Figure 5.1. The PTFE film provided the initial crack necessary for the Mode-I fracture specimens.

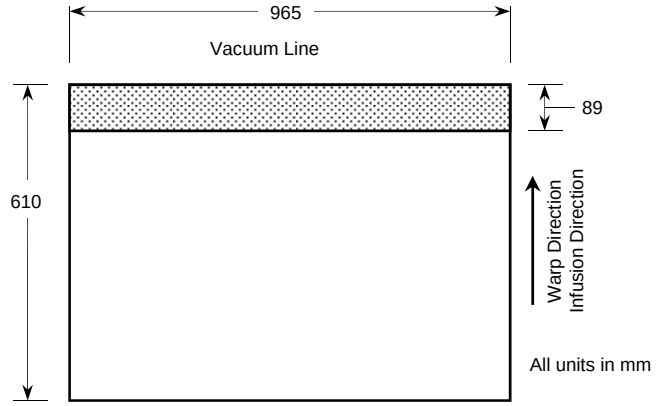

Figure 5.1. Composite panel dimensions.

Three different vacuum infusion pressures combined with three different consolidation times were investigated in the study. The three infusion pressures were 0.847, 0.914, and 0.982 bar (25.0, 27.0, and 29.0 in-Hg) and the three consolidation times were 1, 2, and 5 hours. Noting that ambient pressure varies from day-to-day, the value of 0.982 bar (29.0 in-Hg) was chosen as the maximum instead of a “full-vacuum condition” to ensure that the infusion pressure could be repeated for each of the infusions required at the maximum vacuum pressure.

The range of infusion pressures and consolidation times were chosen based on discussions with industry fabricators and personnel from the Naval Surface Warfare Center - Carderock Division (NSWC-CD), and were intended to encompass the range of pressures and times encountered when fabricating marine composite laminates of varying degrees of complexity.

The fabrication matrix is presented in Table 5.1. As seen in the table, three replicates were fabricated for each of the nine combinations of infusion pressure and consolidation time, resulting in a total of 27 panels fabricated during the study. As a means of reducing the total number of infusion cycles performed, it was decided to infuse three panels simultaneously, one at each of the three infusion pressures, but all at the same consolidation time. This also reduced the possibility of variations due to the other parameters like ambient conditions and resin recipe.

Table 5.1. Panel fabrication matrix.

Consolidation Pressure (gage)	**Panel Replicates for each Consolidation Time Period**		
bar (in-Hg)	***1 hour***	***2 hours***	***5 hours***
0.847 *(25.0)*	3	3	3
0.914 *(27.0)*	3	3	3
0.982 *(29.0)*	3	3	3

Preliminary panel infusion tests determined that a time of 45 min would be sufficient to entirely wet-out the panels in the configuration that was used for the infusions. The longer infusion time was required to properly wet-out around the PTFE film. A resin catalyzing recipe was chosen that would provide a gel time of approximately 1 hour 20 minutes. The catalyzing recipe consisted of 1.2% Trigonox 239 (Akzo Nobel) and 0.3% Cobalt 6% Naphthenate (Puritan Products). A single 55 gallon

drum of Ashland Derakane 8084 vinyl-ester resin was used for all of the infusions to eliminate resin batch as a variable.

An infusion pressure control system was implemented during the fabrication of the composite panels in the study. The system was comprised of three precision pressure transducers, three regulators, and a data acquisition system. This allowed the precise control and monitoring of the three infusion pressures used during the infusion process. During preform consolidation and infusion, the data acquisition system recorded data every 5 minutes for ambient temperature, resin temperature, and vacuum pressure for each panel.

The fabrication procedure that was used for all infusions was as follows.

- Lay up the fabric, and bag the three panels
- Pull vacuum on the 3 panels simultaneously
- Adjust regulators to stabilize pressures at desired magnitudes
- Hold vacuum for set time to consolidate fabric preform
- Add catalyzing recipe to resin 15 min before end of consolidation time
- At end of consolidation period, open resin lines to all three panels
- After the panels have wet-out, clamp off the resin and vacuum lines

The 27 panels were successfully infused during nine sets of infusions over a period of 12 days in an environmentally controlled composites fabrication laboratory at the AEWC Advanced Structures and Composites Laboratory at the University of Maine, Orono, Maine. The infusion configuration that was used during fabrication is presented in Figure 5.2. The results of the nine sets of panel infusions are presented in Table 5.2 in the

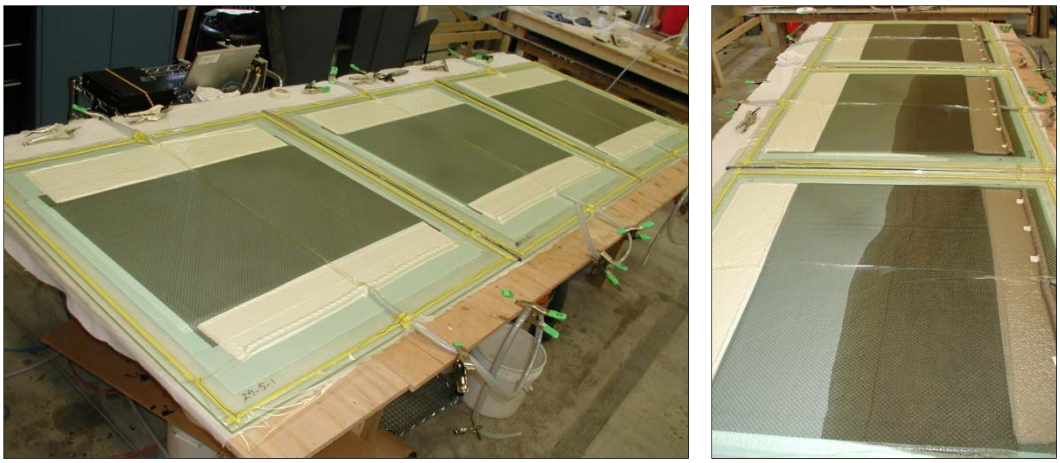

a) b)

Figure 5.2. Panel infusion setup: a) during consolidation and b) during infusion.

Table 5.2. Panel infusion summary.

Panel Set	Consolidation Time	Resin Gel Time	Ambient Temperature	Mean Gage Pressure During Consolidation & Infusion		
				Panel 1	***Panel 2***	***Panel 3***
ID	*h:min*	*h:min*	*°C (°F)*	*bar (in-Hg)*	*bar (in-Hg)*	*bar (in-Hg)*
IP-1-1	1:10	1:20	19.2 (66.6)	0.8467 (25.01)	0.9143 (27.00)	0.9818 (29.00)
IP-2-1	2:07	1:19	18.9 (66.0)	0.8490 (25.07)	0.9164 (27.07)	0.9830 (29.03)
IP-5-1	5:06	1:23	20.0 (68.0)	0.8476 (25.03)	0.9154 (27.04)	0.9839 (29.06)
IP-1-2	1:05	1:15	20.3 (68.5)	0.8471 (25.02)	0.9163 (27.06)	0.9798 (28.94)
IP-2-2	2:04	1:22	19.2 (66.6)	0.8480 (25.05)	0.9157 (27.05)	0.9820 (29.00)
IP-5-2	5:02	1:27	19.7 (67.5)	0.8471 (25.02)	0.9151 (27.03)	0.9827 (29.02)
IP-1-3	1:00	1:30	20.0 (68.0)	0.8476 (25.03)	0.9148 (27.02)	0.9816 (28.99)
IP-2-3	2:00	1:16	21.4 (70.5)	0.8474 (25.03)	0.9155 (27.04)	0.9831 (29.03)
IP-5-3	5:00	1:21	21.0 (69.8)	0.8467 (25.01)	0.9146 (27.01)	0.9818 (29.00)
Average		**1:21**	**20.0 (68.0)**	**0.8475 (25.03)**	**0.9153 (27.04)**	**0.9822 (29.01)**

order in which they were fabricated. In addition to the mean gage pressure applied to each of the three panels during the consolidation and infusion, the table includes the consolidation time, the resin gel time, and the mean ambient temperature for each of the nine infusions. The mean infusion pressure for each panel infused was within 0.26% of the target pressures presented in Table 5.1.

After curing at room temperature for 24 hours, each panel was post-cured at 82ºC (180ºF) for 4 hours. This temperature and duration for post-cure had been shown to be appropriate for this material system at this thickness in an earlier phase of the study [39].

5.3.2 Testing

The tests conducted during the study included Mode-I fracture and constituent volume fraction. The Mode-I fracture test was selected for this study since it was the material property of primary interest, and the constituent volume fraction test was selected since it is a good indicator of the effects of the consolidation of the preform. In addition, Barcol hardness measurements were made on resin samples prior to, and after, post-curing of the specimens as a means to verify the consistency of the post-cure process on the resin in the specimens.

ASTM test standard D5528 [42] was used as the guideline for conducting the Mode-I fracture tests. ASTM D5528 uses a double cantilever beam (DCB) configuration for the test specimens. The dimensions of the DCB specimens used in this study were 25.4 mm x 152.4 mm (1.0 in. x 6 in.) with a nominal initial crack length of 49 mm (1.9 in.). The edge of each specimen was marked in 1-mm increments over a 55 mm (2.2 in.) range which facilitated the identification of crack growth. A schematic of the specimen is presented in Figure 5.3. A total of 12 specimens were cut from each panel in the region indicated in Figure 5.4. As recommended in the standard, the Modified Beam Theory (MBT) method was used to calculate the fracture toughness values. The Mode-I fracture toughness properties computed in this study were the visual onset fracture toughness (G_{vis}), the nonlinear onset fracture toughness (G_{NL}), and the propagation fracture toughness (G_{prp}).

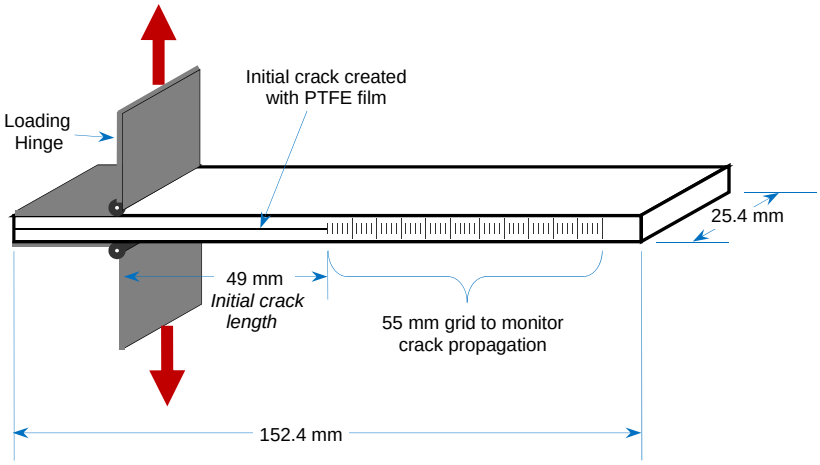

Figure 5.3. Mode-I DCB fracture specimen schematic.

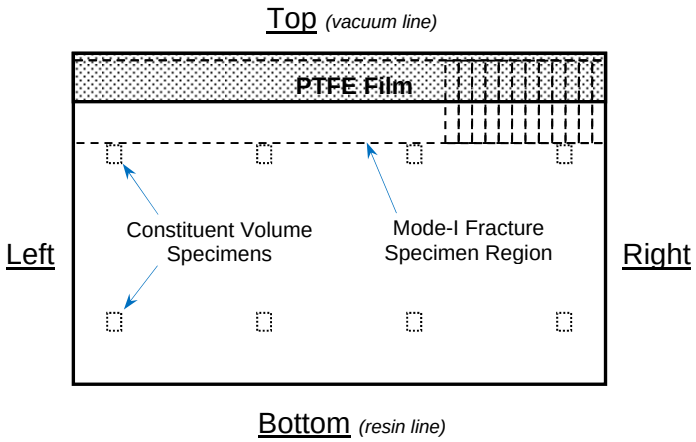

Figure 5.4. Panel schematic showing specimen locations and orientation.

The specimens were tested on an Instron 25 kN (5.6 kip) servo hydraulic test frame equipped with a 250 N (56.2 lb) load cell. The tests were conducted in displacement control at a rate of 2.5 mm/min (0.1 in/min) without pre-cracking the specimens. Crack onset was detected both visually (visual onset) and through the use of a numerical routine to determine the point of nonlinear onset (NL onset). Visual detection was performed using a digital image acquisition system, which collected data at a 1 Hz sampling rate. The digital images were post-processed and examined for visual onset and

crack growth increments of 1 mm or greater, and the load, displacement, and crack growth at each occurrence were recorded. The NL onset was determined by locating the point at which the load deflection (P-δ) curve became nonlinear. This was accomplished by comparing the initial stiffness in the linear region of the curve with the tangent stiffness of the curve as the test progressed. The initial stiffness of the P-δ curve was obtained over a range approximately equal to 20% of the mean NL onset load of each dataset. The initial 25% of the curve was not considered when determining the initial stiffness due to settling of the fixture and nonlinear behavior of the P-δ curve at small loads. The point at which the tangent stiffness differed from the initial stiffness by 5% was taken as the point of NL onset.

The method used by Dharmawan [43] was used to compute the Mode-I propagation fracture toughness values in this study. The method uses the region of the resistance curve (R-curve), where the fracture toughness has stabilized, to compute the mean propagation fracture toughness. The method produces a less conservative value for propagation fracture toughness, because it discards the lower values of fracture toughness computed prior to R-curve stabilization, but it is a repeatable method that leads to less variability in the results.

ASTM test standard D2584 [44] was used to determine the constituent volume fraction of the panel specimens. Eight specimens were cut from each of the panels as indicated in Figure 5.4. The specimens were distributed around the panel to capture spatial variations of the volume fraction resulting from the thickness gradients which occur along the infusion direction [1,9,45]. The nominal specimen dimensions were 25.4 mm x 35.0 mm (1.0 in. x 1.38 in.) with a nominal mass of 11.0 grams (0.39 oz). The

specimens were placed in a crucible in a muffle furnace at a temperature of 565ºC (1049ºF) for a period of 2.5 hours, which prior experience with this material system had shown to be sufficient for complete resin removal [38,40].

ASTM test standard D2583 [46] was used as a guide in conducting Barcol hardness tests on the resin samples. Residual resin from each of the nine infusions was retained for the purpose of hardness testing. This was used as a means to verify the consistency of the material properties of the resin from panel-to-panel. Five samples from each of the nine infusions were cut into 6.4 mm (0.25 in.) thick specimens. Fifteen Barcol hardness measurements were taken on each specimen prior to, and after, post-curing the specimens. The resin specimens were post-cured in an identical manner to that used on the composite test specimens (82ºC for 4 hours).

5.3.3 Data Analysis Procedure

The data from each of the three replicate panels were grouped and treated as a single dataset for the comparative analysis implemented for the constituent volume fraction and Mode-I fracture test results. After verifying the normality of the dataset distributions using the Anderson-Darling method, the mean and coefficient of variation (CV) were computed for each material property investigated. The datasets were then grouped by consolidation pressure and consolidation time to identify the effects on material properties. As a means of determining if the results from each material property dataset were statistically discernible for the different consolidation parameters investigated, the k-sample Anderson-Darling (ADK) method was employed [47]. The ADK test is a statistical procedure used to determine if the populations from which two or more datasets were sampled from are identical. If the calculated ADK value for the

dataset is less than the critical value, then one can conclude with a 2.5 percent risk of being in error, that the groups were drawn from the same population. The ratio of the computed value to critical value was calculated as a convenient means to determine the level to which the datasets were similar or not. This ratio (ADK ratio) is tabulated and presented with the mean and CV values for each dataset in the discussion of the results.

The Maximum Normed Residual (MNR) method was used to identify outliers. "A value is declared to be an outlier if it has an absolute deviation from the sample mean, which, when compared to the sample standard deviation, is too large to be due to chance." [47] Points identified as outliers were then examined to determine possible reasons not to include them in the dataset analysis. While a handful of data points were deemed to be outliers by the MNR method, valid reasons for excluding them from the datasets could not be determined.

5.4 Discussion of Results

5.4.1 Barcol Hardness Results

The results of the Barcol hardness tests are presented in Table 5.3 and Figure 5.5. The results indicate that the resin from each of the nine infusions equilibrated to a mean Barcol hardness value of 36.3 after being post-cured, regardless of their state of hardness prior to the post-curing process. In addition, there was a reduction in the CV for all of the datasets. This indicates that the state-of-cure of the resin was consistent in all of the specimens; therefore, the condition of the resin should not be a significant factor in the variability of the Mode-I fracture results, and no correlation between the two was found.

Table 5.3. Barcol hardness results.

Infusion Resin Set	As Gelled		Post-cured	
	mean	*CV*	*mean*	*CV*
IP-1-1	21.6	20%	36.1	5%
IP-2-1	25.8	14%	35.9	11%
IP-5-1	25.6	11%	36.1	7%
IP-1-2	35.9	14%	36.1	10%
IP-2-2	35.5	11%	36.3	6%
IP-5-2	28.3	20%	36.5	6%
IP-1-3	25.6	18%	36.5	7%
IP-2-3	26.9	8%	36.1	3%
IP-5-3	27.6	7%	36.7	3%
Total	**28.1**	**17%**	**36.3**	**0.7%**

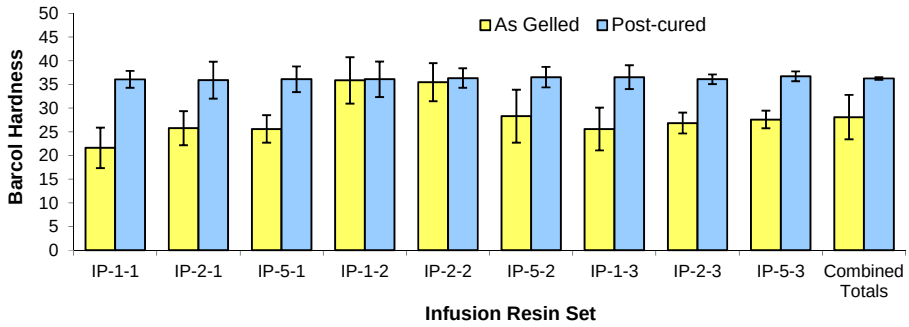

Figure 5.5. Barcol hardness results plot.

5.4.2 Constituent Volume Fraction Results

The datasets were grouped to identify the effects of consolidation pressure and consolidation time on the fiber volume fraction (FVF) results. Plots of the results, grouped by consolidation pressure and consolidation time, are presented in Figures 5.6a and 5.6b, respectively. It is worth noting that the FVFs were computed using a resin density of 1.13 g/cm^3 (0.653 oz/in^3) and a glass density of 2.54 g/cm^3 (1.47 oz/in^3), and that the data is plotted with a y-axis range of 40-60% for clarity. The FVF ranged from 52.9% to 54.6% while the CV ranged from 1.7% to 3.2%.

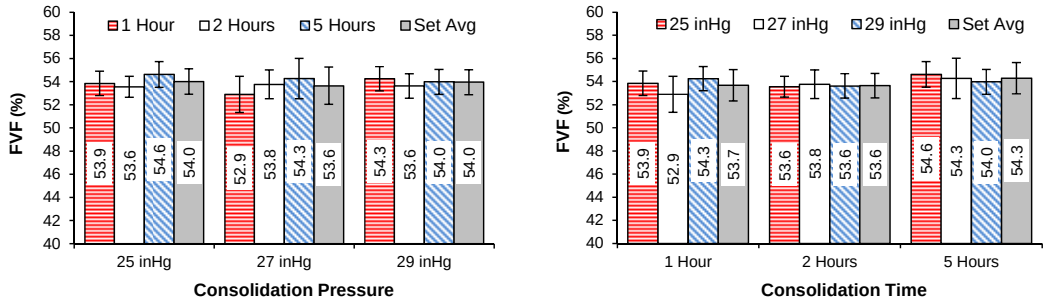

a) b)

Figure 5.6. Fiber volume fraction results comparison: a) consolidation pressure grouping and b) consolidation time grouping.

The ADK ratios for the FVF results are presented in Tables 5.4a and 5.4b for the consolidation pressure and consolidation time dataset groupings, respectively. In addition to the ADK ratios of the complete dataset comparison, the table includes ADK ratios for subset comparisons. This provides direct comparison of the individual datasets.

Table 5.4. ADK Ratios for fiber volume fraction datasets: a) consolidation pressure groupings and b) consolidation time groupings.

a)

Subsets Compared	Number of Specimens	ADK Ratios Pressure Datasets *25*	*27*	*29*
1, 2, 5	72	**1.27**	**1.15**	0.58
1 & 2	48	0.23	0.83	0.72
1 & 5	48	**1.05**	**1.34**	0.38
2 & 5	48	**1.62**	0.43	0.23

b)

Subsets Compared	Number of Specimens	ADK Ratios Hold Time Dataset *1*	*2*	*5*
25, 27, 29	72	**1.55**	0.37	0.62
25 & 27	48	**1.17**	0.39	0.35
25 & 29	48	0.36	0.13	0.65
27 & 29	48	**1.86**	0.31	0.46

ADK ratios greater than 1.0 indicate that the datasets in the comparison are statistically different.

As seen in Figure 5.6a and indicated by the ADK ratios greater than 1.0 in Table 5.4a for pressure dataset 25, the 5-hour consolidation time resulted in a statistically larger value of FVF when compared to both the 1-hour and 2-hour consolidation times. The 5-hour consolidation time resulted in FVFs that were 1.4% and 2.0% larger than the 1-hour and 2-hour dataset values, respectively. The only other statistically discernible difference

in FVF for the pressure datasets occurred between the 1-hour and 5-hour consolidation times for pressure dataset 27 where the 5-hour consolidation time was 2.6% larger.

As indicated in Figure 5.6b and Table 5.4b, the only statistically discernible difference in the FVF for the consolidation time dataset groupings occurred for the 1-hour dataset where subset 29 was larger than subset 27 by 2.6%, and subset 25 was larger than subset 27 by 1.8%.

The spatial distribution of the FVF in the panels was also investigated in this study. The spatial distribution results for the dataset groupings are presented visually in the plots of Figure 5.7 and numerically in Table 5.5. The orientation of the spatial locations listed in the figure and the table refer to the orientations presented in Figure 5.4. The FVF at each spatial location in the panel is the mean of the four FVF specimens in that spatial location. It is worth noting that the infusion direction was from the bottom to the top.

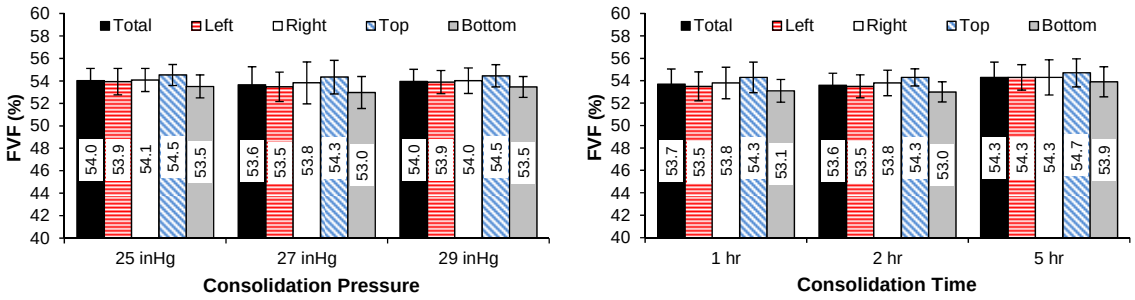

a) b)

Figure 5.7. Spatial distribution of fiber volume fraction: a) consolidation pressure grouping and b) consolidation time grouping.

Table 5.5. Spatial distribution of fiber volume fraction results.

Dataset Grouping		Fiber Volume Fraction (%)									
		Total		*Left*		*Right*		*Top*		*Bottom*	
type	*unit*	*mean*	*CV*	*mean*	*CV*	*mean*	*CV*	*mean*	*CV*	*mean*	*CV*
Consolidation	**25**	54.0	2.0%	53.9	2.2%	54.1	1.9%	54.5	1.7%	53.5	1.9%
Pressure	**27**	53.6	3.0%	53.5	2.5%	53.8	3.5%	54.3	2.8%	53.0	2.7%
(in-Hg)	**29**	54.0	2.0%	53.9	1.9%	54.0	2.1%	54.5	1.8%	53.5	1.7%
Consolidation	**1**	53.7	2.5%	53.5	2.4%	53.8	2.6%	54.3	2.5%	53.1	1.9%
Time	**2**	53.6	2.0%	53.5	1.9%	53.8	2.1%	54.3	1.4%	53.0	1.7%
(hr)	**5**	54.3	2.5%	54.3	2.1%	54.3	2.9%	54.7	2.3%	53.9	2.5%

NOTE: Each of the four spatial location results consist of 36 specimens and the "Total" result consists of 72 specimens.

As found in other studies, there was a noticeable difference in the FVF in the infusion direction [1,45]. This is due to a relaxation of the fiber preform that starts after the resin arrives at that location during the infusion and continues until fully relaxed, or until the resin starts to gel. The consolidation pressure dataset groupings exhibited differences of 1.0%, 1.3%, and 1.0% in FVF, between the top and bottom locations for consolidation pressure datasets 25, 29, and 27, respectively. The consolidation time dataset groupings exhibited differences of 0.8%, 1.2%, and 1.3% in FVF, between the top and bottom locations for the 5-hour, 1-hour, and 2-hour consolidation time datasets, respectively. Both of the consolidation dataset groupings also exhibited slightly larger FVFs (0.1% to 0.3%) for the right side of the panel compared to the left side of the panel. This was a result of the flow media used during the infusions, since the flow media had a cross hatch pattern that permitted the resin to flow more easily to the left than to the right resulting in a slight lag on the right side of the flow front, as seen in Figure 5.2a.

5.4.3 Mode-I Fracture Toughness Results

The Mode-I DCB specimens tested in this study typically produced P-δ curves in one of two forms, as exhibited by the P-δ curves presented in Figure 5.8. There was not a

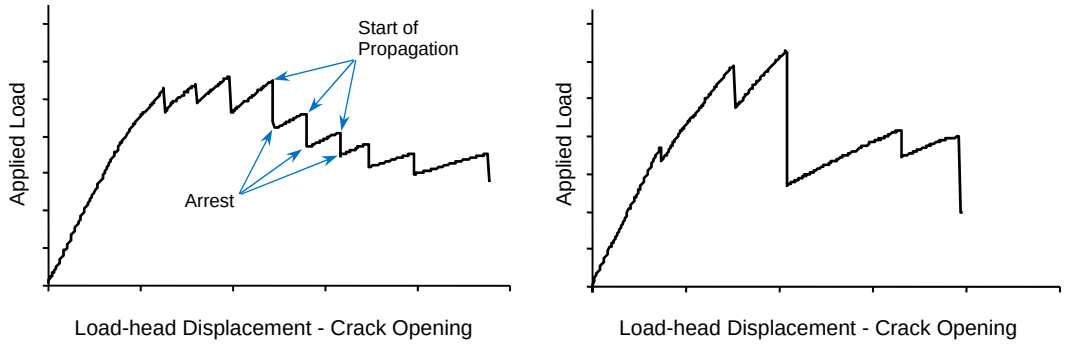

a) b)

Figure 5.8. Typical Mode-I fracture load-deflection curves: a) consistent load-drops and b) variable load-drops.

direct correlation between the type of P-δ curve produced and the consolidation procedure used during fabrication. Unlike unidirectional fiber composites, crack propagation in heavy woven fabric composites is typically unstable, with the resulting behavior described as run-arrest. As seen in Figure 5.8a, this is characterized by a monotonic increase in load with minimal crack growth, followed by a sudden drop in load when the crack propagates rapidly (runs) to a point where it stops (arrests). This process repeats for the duration of the test, sometimes with a significant drop in load, as displayed in Figure 5.8b. The run-arrest behavior has been attributed to the weave structure [31,48-49]. Unstable fracture initiation has been observed at the edge of the transverse tows, where the transverse tows act as a toughening mechanism [48]. In addition, fiber bridging has been observed in woven roving specimens at warp and fill intersections [31]. These points corresponded to the crack lengths at which unstable fracture occurred, indicating that failure of the bridged fibers contributed to the instability of the crack growth.

As the crack grew from the PTFE film insert, a resistance type fracture behavior developed, with the fracture toughness increasing monotonically and then stabilizing as

the crack propagated further. Resistance curves (R-curves) were generated to determine the propagation fracture toughness of each specimen in the dataset. An R-curve plot for a typical dataset is presented in Figure 5.9. The fracture toughness was computed for each instance where the crack length grew by 1 mm or more. The points in the plot represent the locations where the fracture toughness was computed for all 12 specimens in the dataset. The mean value of the stabilized R-curve data for the 12 specimens is indicated by the horizontal line in the middle of the data points. It is worth noting that the mean propagation fracture toughness value for each specimen was weighted equally when computing the mean value for the entire dataset, regardless of how many propagation points occurred in the stabilized region for each specimen. A crack length of 57 mm (2.25 in.) was used as the starting point for stabilized propagation in all of the datasets.

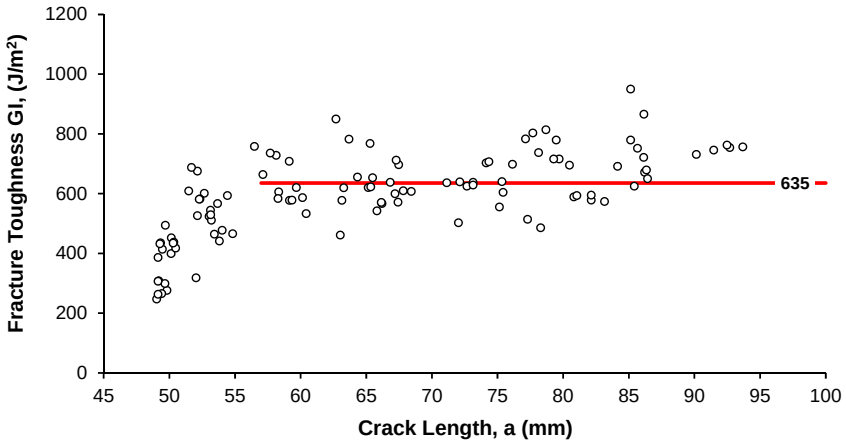

Figure 5.9. Typical Mode-I R-curve for a panel dataset.

A summary of the Mode-I fracture toughness test results is presented in Table 5.6. The table includes the Mode-I results for visual onset, nonlinear onset, and propagation fracture toughness. The mean visual onset fracture toughness ranged from 260 to 359 J/m^2, while the CV ranged from 20 to 34%. The nonlinear method produced more conservative onset fracture toughness results that ranged from 214 to 266 J/m^2, but with

Table 5.6. Mode-I test results for each dataset.

Dataset Designation	Fracture Toughness (J/m^2)						Peak Load (N)		Stiffness (N/mm)		Fiber Volume Fraction (%)	
	Onset				Propagation							
	Visual		Non-linear		Visual							
ID	mean	CV	mean	CV	mean	CV	mean	CV	mean	CV	mean	CV
25-1	297	34%	258	37%	724	17%	98	9.9%	14.5	8.0%	54.5	1.6%
25-2	264	28%	230	32%	730	17%	100	6.7%	14.5	3.7%	54.0	1.4%
25-5	264	31%	214	41%	841	14%	102	5.4%	13.7	3.7%	55.0	1.7%
27-1	296	24%	253	29%	720	16%	102	7.9%	14.1	4.3%	53.5	3.2%
27-2	280	28%	227	27%	733	19%	101	6.6%	14.1	3.6%	54.7	1.4%
27-5	260	26%	227	34%	736	14%	99	6.8%	14.2	3.6%	54.8	2.8%
29-1	347	27%	266	23%	738	20%	96	6.6%	13.8	4.3%	54.8	2.0%
29-2	359	20%	226	30%	822	15%	104	6.3%	14.1	5.3%	54.2	1.3%
29-5	325	30%	266	38%	796	13%	102	5.5%	14.3	4.1%	54.3	2.1%

NOTE: Each of the nine datasets consisted of 36 fracture specimens and 24 fiber volume fraction specimens.

more variability than the visual method, since the CV ranged from 23 to 41%. The propagation fracture toughness results ranged from 720 to 841 J/m^2, with a CV range of 13-20%. The propagation results are less conservative than either of the two onset results; however, the propagation values have much lower variability than the onset values, as the propagation had an average CV of 17% compared to 28 and 32% for the visual onset and nonlinear onset fracture toughness properties, respectively.

In addition to the three fracture properties, Table 5.6 includes the peak load attained during the Mode-I test, the stiffness from the linear portion of the P-δ curve, and the fiber volume fraction for each dataset. It is worth noting that the fiber volume fraction results presented in the table are from the top of the panel, since this is the region of the panel where the fracture specimens were located. There was no direct correlation displayed between any of the six properties in the table.

5.4.3.1 Consolidation Pressure Dataset Grouping of Fracture Data

The Mode-I dataset results, grouped by consolidation pressure, are presented visually in the plots of Figure 5.10. The error bars in the plots are ±1 standard deviation. It is worth noting that the scale of the y-axis for the propagation fracture toughness plot (Figure 5.10c) is twice as large as the y-axis of the two onset fracture toughness plots (Figures 5.10a and 5.10b). The mean and CV for the grouped datasets are presented in Table 5.7. In addition to the three fracture properties, the table contains the results for the peak load, the stiffness, and the fiber volume fraction of the grouped datasets. It is worth noting that the fiber volume fraction results presented in the table are from the top of the panel, since this is the region of the panel where the fracture specimens were located.

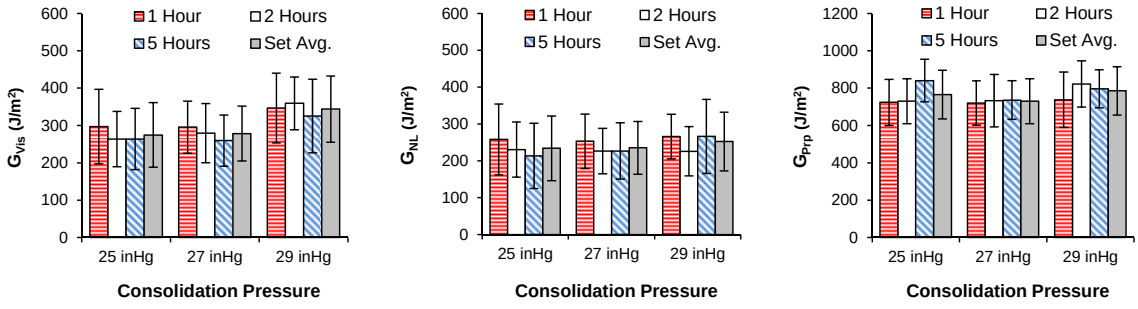

Figure 5.10. Mode-I fracture toughness results for the datasets grouped by consolidation pressure: a) visual onset (G_{vis}), b) nonlinear onset (G_{NL}), and c) propagation (G_{prp}).

Table 5.7. Test results for consolidation pressure dataset groupings.

Dataset Grouping	Fracture Toughness (J/m²)						Peak Load (N)		Stiffness (N/mm)		Fiber Volume Fraction (%)	
	Onset				Propagation							
	Visual		Non-linear		Visual							
in-Hg	*mean*	*CV*	*mean*	*CV*	*mean*	*CV*	*mean*	*CV*	*mean*	*CV*	*mean*	*CV*
25	275	32%	234	38%	765	17%	100	7.6%	14.2	6.0%	54.0	2.0%
27	278	26%	235	30%	730	17%	100	7.2%	14.1	3.8%	53.6	3.0%
29	344	26%	253	32%	786	17%	100	7.0%	14.1	4.7%	54.0	2.0%

NOTE: Each of the 3 consolidation pressure datasets consisted of 108 fracture specimens and 72 fiber volume fraction specimens

As seen in Figure 5.10a, the 5-hour consolidation time produced the smallest mean visual onset fracture toughness in all three of the consolidation pressure dataset groupings. The 1-hour consolidation time produced the largest mean nonlinear onset fracture toughness in each of the consolidation pressure dataset groupings, as seen in Figure 5.10b, while the 5-hour consolidation time produced the highest CV for the nonlinear onset fracture toughness in each of the three consolidation pressure dataset groupings. The general trend between groupings for the two onset fracture toughness properties was that the mean increased with increasing consolidation pressure. While there was not a definite trend in the mean propagation fracture toughness datasets, the 5-hour consolidation time produced the lowest CV for the propagation fracture toughness in all three consolidation pressure dataset groupings.

The results discussed above were strictly observed trends in the data and do not take into account the statistics of the comparisons, which is addressed through the ADK ratios. The ADK ratios for the Mode-I fracture toughness properties are presented in Table 5.8 for the consolidation pressure dataset groupings.

Table 5.8. ADK results for consolidation pressure dataset groupings.

		ADK Ratios								
		25 in-Hg			27 in-Hg			29 in-Hg		
Subsets Compared	Number of Specimens	Fracture Property			Fracture Property			Fracture Property		
		Vis	Nln	Prp	Vis	Nln	Prp	Vis	Nln	Prp
1, 2, 5	108	0.44	0.89	**2.13**	0.56	0.68	0.33	0.70	**1.40**	**1.55**
1 & 2	72	0.42	0.40	0.16	0.31	0.46	0.14	0.63	**1.67**	**1.62**
1 & 5	72	0.37	**1.03**	**2.39**	0.81	0.80	0.19	0.33	0.53	**1.57**
2 & 5	72	0.21	0.53	**2.32**	0.22	0.28	0.44	0.65	**1.21**	0.28

Vis - visual onset Nln - nonlinear onset Prp - propagation

ADK ratios greater than 1.0 indicate that the datasets in the comparison are statistically different.

As indicated by the ADK ratios greater than 1.0 in Table 5.8, statistically discernible differences were produced for consolidation pressure dataset 25 between the 1-hour and 5-hour data subsets for both the nonlinear onset and the propagation fracture toughness properties. The 5-hour subset value was 17% smaller than the 1-hour subset for the nonlinear onset, and 16% larger for the propagation fracture toughness. An additional statistically discernible result produced in pressure dataset 25 was between the 2-hour and 5-hour data subsets for the propagation fracture toughness, where the 5-hour subset value was 15% larger. Statistically relevant differences were not produced in consolidation pressure dataset 27 in any of the consolidation time subset comparisons for any of the fracture toughness properties.

Statistically discernible results were produced for consolidation pressure dataset 29 for both the nonlinear onset and the propagation fracture toughness properties. In the 1-hour and 2-hour subset comparisons, the 2-hour subset was 15% smaller for the nonlinear onset, and 11% larger for the propagation fracture toughness. In the 1-hour and 5-hour subset comparisons the 5-hour subset was 8% larger than the 1-hour for the propagation fracture toughness. In the 2-hour and 5-hour subset comparisons, the 5-hour subset was 18% larger for the nonlinear onset fracture toughness. The other result from the consolidation pressure dataset groupings worthy of noting is that the visual onset fracture toughness results did not produce any statistically discernible differences for any of the subset comparisons.

5.4.3.2 Consolidation Time Dataset Grouping of Fracture Data

The Mode-I fracture toughness results for the datasets grouped by consolidation time are presented visually in the plots of Figure 5.11. The error bars in the plots are ±1

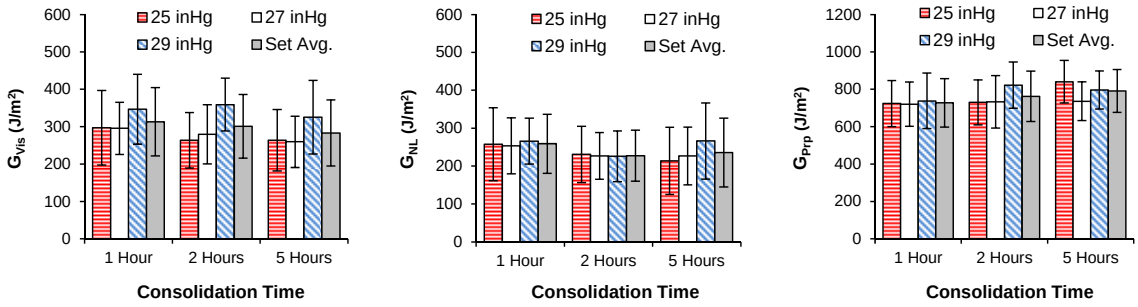

a) b) c)

Figure 5.11. Mode-I fracture toughness results for the datasets grouped by consolidation time: a) visual onset (G_{vis}), b) nonlinear onset (G_{NL}) and c) propagation (G_{prp}).

Table 5.9. Test results for consolidation time dataset groupings.

Dataset Grouping	Fracture Toughness (J/m²)						Peak Load (N)		Stiffness (N/mm)		Fiber Volume Fraction (%)	
	Onset				Propagation							
	Visual		Non-linear		Visual							
hours	*mean*	*CV*	*mean*	*CV*	*mean*	*CV*	*mean*	*CV*	*mean*	*CV*	*mean*	*CV*
1	313	29%	259	30%	728	18%	99	8.6%	14.2	6.1%	53.7	2.5%
2	301	28%	228	30%	762	18%	102	6.6%	14.2	4.4%	53.6	2.0%
5	283	31%	236	39%	791	14%	101	6.0%	14.1	4.1%	54.3	2.5%

NOTE: Each of the 3 consolidation time datasets consisted of 108 fracture specimens and 72 fiber volume fraction specimens.

standard deviation. It is worth noting that the scale of the y-axis for the propagation fracture toughness plot (Figure 5.11c) is twice as large as the y-axis of the two onset fracture toughness plots (Figures 5.11a and 5.11b). The mean and CV for the grouped datasets are presented in Table 5.9. In addition to the three fracture properties, the table contains the results for the peak load, the stiffness, and the fiber volume fraction of the grouped datasets. It is worth noting that the fiber volume fraction results presented in the table are from the top of the panel, since this is the region of the panel where the fracture specimens were located.

Consolidation pressure subset 25 produced the greatest variability in all three consolidation time dataset groupings for both of the onset fracture toughness properties,

with an average CV of 32 and 38% for the visual onset and the nonlinear onset, respectively. As seen in Figure 5.11a, consolidation pressure subset 29 produced the largest mean visual onset fracture toughness in each of the three consolidation time dataset groupings. The general trend between the groupings was that the onset fracture toughness properties decreased with increasing consolidation time while the propagation fracture toughness increased with increasing consolidation time.

The results discussed above for the consolidation time dataset groupings were strictly observed trends in the data and do not take into account the statistics of the comparisons, which is addressed through the ADK ratios. The ADK ratios for the Mode-I fracture toughness properties are presented in Table 5.10 for the consolidation time dataset groupings.

Table 5.10. ADK results for consolidation time dataset groupings.

		ADK Ratios								
		1 hour			2 hours			5 hours		
Subsets Compared	Number of Specimens	Fracture Property			Fracture Property			Fracture Property		
		Vis	Nln	Prp	Vis	Nln	Prp	Vis	Nln	Prp
25, 27, 29	108	**1.04**	0.43	0.25	**3.21**	0.26	**1.45**	**1.35**	**1.07**	**1.76**
25 & 27	72	0.30	0.16	0.08	0.19	0.20	0.40	0.23	0.50	**2.30**
25 & 29	72	**1.29**	0.54	0.25	**4.25**	0.23	**1.37**	**1.19**	**1.13**	0.58
27 & 29	72	0.90	0.33	0.22	**3.16**	0.21	**1.61**	**1.66**	0.81	**1.09**

Vis - visual onset Nln - nonlinear onset Prp - propagation

ADK ratios greater than 1.0 indicate that the datasets in the comparison are statistically different.

The only statistically discernible difference for the 1-hour consolidation time occurred between consolidation pressure data subsets 25 and 29 for the visual onset fracture toughness, where the subset 29 value was 17% larger than the subset 25 value. The 2-hour consolidation time produced statistically discernible results between consolidation pressure subsets 25 and 29, and subsets 27 and 29 for both the visual onset

and propagation fracture toughness properties. Subset 29 produced values that were 36% and 13% larger than the subset 25 values for the visual onset and propagation fracture toughness properties, respectively. Additionally, subset 29 produced values that were 28% and 12% larger than the subset 27 values for the visual onset and propagation fracture toughness properties, respectively.

The 5-hour consolidation time produced statistically discernible differences between consolidation pressure subsets 25 and 29 for both the visual onset and the nonlinear onset fracture properties. Subset 29 was 23% larger than subset 25 for the visual onset, and 25% larger than subset 25 for the nonlinear onset fracture toughness properties. The 5 hour consolidation time also produced discernible results between consolidation subsets 27 and 29 for the visual onset, where subset 29 was 25% larger, and the propagation fracture toughness, where subset 29 was 8% larger. The difference between consolidation pressure subsets 25 and 29 for the nonlinear onset fracture toughness was the only discernible difference for the nonlinear onset fracture toughness property among all of the consolidation time dataset grouping comparisons. The other statistically relevant comparison for the 5-hour consolidation time occurred between subsets 25 and 27 for the propagation fracture toughness, where subset 27 was 12% smaller than subset 25. This was the only statistically discernible difference between pressure subsets 25 and 27 for any of the consolidation time dataset grouping comparisons.

5.5 Conclusions and Recommendations

The effects of commonly employed fiber preform consolidation practices on Mode-I fracture toughness of composite laminates were investigated. Fiber volume

fraction was used as a means to discern the effects on preform consolidation. The longer consolidation times produced statistically discernible variations in the mean fiber volume fraction (1.4 to 2.6% higher) for the panels fabricated at the two lower consolidation pressures, but not for the panels fabricated at the higher consolidation pressure. Likewise, the variation in consolidation pressure produced discernible effects of 1.8 to 2.6% on the mean fiber volume fraction of the panels fabricated with the shortest consolidation time, but not on the panels fabricated with the two longer consolidation times.

There was no correlation found between the global fiber volume fraction of the panels and any of the three fracture properties computed in this study. This is similar to what other studies have found where fracture toughness was sensitive to the localized fiber volume fraction in the region of the crack tip and not to the global volume fraction of the specimen [32].

Barcol hardness of the resin from all of the datasets equilibrated to a similar value with a mean of 36.3 and a CV of 0.7% after post-curing, regardless of the state of hardness prior to post-curing. It is safe to conclude from this, that the material state of the resin should not have played a role in the variation of the fracture toughness properties, and no correlation between the two was observed.

Variation of consolidation pressure for a fixed consolidation time produced statistically discernible results for the visual onset fracture toughness property in each of the three consolidation times investigated; however, variations in the consolidation time for a fixed consolidation pressure did not produce any statistically discernible effects for any of the consolidation pressures investigated. The trend was such that the highest

pressure produced visual onset toughness values that were 17-36% larger than the lower pressures for a fixed consolidation time.

Statistically discernible results were produced for the nonlinear onset fracture toughness between the highest and lowest consolidation pressure data subsets, but only at the longest (5-hour) consolidation time, where the higher pressure produced a toughness value that was 25% larger. A few discernible results were produced for the nonlinear onset fracture toughness for consolidation time variations within a fixed consolidation pressure, but only within the upper and lower consolidation pressure groupings and with no consistent trend. The magnitude of these differences ranged from -17 to 18%.

The nonlinear onset fracture toughness results were more conservative than the visual onset fracture toughness results. In addition, the nonlinear onset had higher CV than the visual onset fracture toughness. The computed Mode-I onset fracture toughness produced results with CV in the range of 20-31% and 23-41% for the visual onset and nonlinear onset properties, respectively. The large scatter in the onset fracture toughness data is thought to result from the location of the initial crack front relative to the transverse tows and the interply regions, which create the toughening mechanisms discussed previously [50-51].

Variation of consolidation pressure for a fixed consolidation time produced statistically discernible results in propagation fracture toughness for the two longer consolidation time dataset groupings. While the longer consolidation times produced larger propagation fracture toughness values as a whole, there was not a consistent trend within each consolidation pressure grouping since the differences ranged from -12 to 13%. Variation in consolidation time for a fixed consolidation pressure produced

statistically discernible results in propagation fracture toughness at the upper and lower pressures, with the greatest difference occurring at the lower pressure; however, there was not a definite trend among the groups as a whole, or within each consolidation pressure subset where the differences ranged from 8 to 16%.

Overall, dataset grouping by consolidation time produced more statistically discernible results than grouping by consolidation pressure, 10-out-of-27 versus 7-out-of-27 comparisons, respectively. Additionally, the majority of those results, 5-out-of-10 and 4-out-of-7, were produced within the maximum consolidation time and maximum pressure dataset groupings, respectively. The number of statistically discernible results for the propagation, visual onset, and nonlinear onset fracture properties was 8, 5, and 4, respectively. While the onset properties produced a greater number of observable trends in the data than the propagation property, the larger coefficient of variation for the onset properties (20-41% compared to 13-20% for propagation) resulted in fewer statistically relevant results for the onset properties.

The general trend at the lower consolidation pressures was that shorter consolidation times produced the maximum onset fracture toughness values but minimum propagation toughness values, while longer consolidation times produced the minimum onset fracture toughness values but maximum propagation fracture toughness properties. Further study is recommended to investigate the inverse trend between the onset and propagation fracture toughness properties.

5.6 References

5.1 Tackitt K D, and Walsh S M (2005) Experimental Study of Thickness Gradient Formation in the VARTM Process. Materials and Manufacturing Processes, 20:607-627.

5.2 Govignon Q, Bickerton S, Morris J, and Kelly P A (2008) Full Field Monitoring of the Resin Flow and Laminate Properties during the Resin Infusion Process. Composites: Part A, 39:1412-1426.

5.3 Baley C, Davies P, Grohens Y, and Dolto G (2004) Application of Interlaminar Tests to Marine Composites: A Literature Review. Applied Composite Materials, 11:99-126.

5.4 Han K, Jiang S, Zhang C, and Wang B (2000) Flow Modeling and Simulation of SCRIMP for Composites Manufacturing. Composites: Part A, 31:79-86.

5.5 Hammami A and Gebart B R (2000) Analysis of Vacuum Infusion Molding Process. Polymer Composites, 21(1):28-40.

5.6 Hammami A (2001) Effect of Reinforcement Structure on Compaction Behavior in the Vacuum Infusion Process. Polymer Composites, 22(3):337-348.

5.7 Stadtfeld H C, Erninger M, Bickerton S, and Advani S G (2002) An Experimental Method to Continuously Measure Permeability of Fiber Preforms as a Function of Fiber Volume Fraction. Journal of Reinforced Plastics and Composites, 21:879-899.

5.8 Modi D, Johnson M, Long A, Rudd C (2009) Analysis of Pressure Profile and Flow Progression in the Vacuum Infusion Process. Composites Science and Technology, 69:1458-1464.

5.9 Yenilmez B and Sozer E M (2009) Variation of Part Thickness and Compaction Pressure in Vacuum Infusion Process. Composites Science and Technology, 69:1710-1719.

5.10 Yenilmez B and Sozer E M (2009) Compaction of E-Glass Fabric Preforms in the Vacuum Infusion Process, A - Characterization Experiments. Composites: Part A, 40:499-510.

5.11 Endruweit A, Gehrig S and Ermanni P (2003) Mechanisms of Hydrodynamically Induced In-Plane Deformation of Reinforcement Textiles in Resin Injection Processes. Journal of Composite Materials, 37:1675-1692.

5.12 Williams C D, Grove S M, Summerscales J (1998) The Compression Response of Fibre-Reinforced Plastic Plates During Manufacture by the Resin Infusion Under Flexible Tooling Method. Composites: Part A, 29A:111-114.

5.13 Hoes K, Dinescu D, Sol H, Parnas R S, Lomov S (2004) Study of Nesting Induced Scatter of Permeability Values in Layered Reinforcement Fabrics, Composites: Part A, 35:1407-1418.

5.14 Somashekar A A, Bickerton S, Bhattacharyya D (2006) An Experimental Investigation of Non-Elastic Deformation of Fibrous Reinforcements in Composites Manufacturing. Composites: Part A, 37:858-867.

5.15 Robitaille F and Gauvin R (1998) Compaction of Textile Reinforcements for Composites Manufacturing. II: Compaction and Relaxation of Dry and H2O-Saturated Woven Reinforcements. Polymer Composites, 19:543-557.

5.16 Bickerton S, Buntain M J, Somashekar A A (2003) The Viscoelastic Compression Behavior of Liquid Composite Molding Preforms. Composites: Part A, 34:431-444.

5.17 Robitaille F and Gauvin R (1998) Compaction of Textile Reinforcements for Composites Manufacturing. I: Review of Experimental Results. Polymer Composites, 19:198-216.

5.18 Pearce N and Summerscales J (1995) The Compressibility of a Reinforcement Fabric. Composites Manufacturing, 6:15-21.

5.19 Yuexin D, Zhaoyuan T, Yan Z, Jing S (2008) Compression Responses of Preform in Vacuum Infusion Process, Chinese Journal of Aeronautics, 21:370-377.

5.20 Saunders R A, Lekakou C, and Bader M G (1998) Compression and Microstructure of Fibre Plain Woven Cloths in the Processing of Polymer Composites. Composites: Part A, 29A:443-454.

5.21 Somashekar A A, Bickerton S, Bhattacharyya D (2007) Exploring the Non-Elastic Compression Deformation of Dry Glass Fibre Reinforcements. Composites Science and Technology, 67:183-200.

5.22 Robitaille F and Gauvin R (1999) Compaction of Textile Reinforcements for Composites Manufacturing. III: Reorganization of the Fiber Network. Polymer Composites, 20:48-61.

5.23 Saunders R A, Lekakou C, Bader M G (1999) Compression in the Processing of Polymer Composites - 1. A Mechanical and Microstructural Study for Different Glass Fabrics and Resins. Composites Science and Technology, 59:983-993.

5.24 Chen Z and Ye L (2006) A Micromechanical Compaction Model for Woven Fabric Preforms. Part II: Multilayer. Composites Science and Technology, 66(16):3263-3272.

5.25 Grujicic M, Chittajallu K M, Walsh S (2004) Effect of Shear, Compaction and Nesting on Permeability of the Orthogonal Plain-Weave Fabric Preforms (2004) Materials Chemistry and Physics, 86:358-369.

5.26 Bates P J, Taylor D, and Cunningham M F (2001) Compaction and Transverse Permeability of Glass Rovings. Applied Composite Materials, 8:163-178.

5.27 Bechtold G and Ye L (2003) Influence of Fibre Distribution on the Transverse Flow Permeability in Fibre Bundles. Composites Science and Technology, 63:2069-2079.

5.28 Potluri P, Sagar T V (2008) Compaction Modeling of Textile Preforms for Composite Structures. Composite Structures, 86:177-185.

5.29 Breiling K B and Adams D O (1996) Effects of Layer Nesting on Compression-Loaded 2-D Woven Textile Composites. Journal of Composite Materials, 30:1710-1728.

5.30 Alif N, Carlsson L A, and Boogh L (1998) The Effect of Weave Pattern and Crack Propagation Direction on Mode-I Delamination Resistance of Woven Glass and Carbon Composites. Composites: Part B, 29B:603-611.

5.31 Chen B and Chou T (2000) Compaction of Woven-Fabric Preforms: Nesting and Multi-Layer Deformation. Composites Science and Technology, 60:2223-2231.

5.32 Compston P and Jar P-Y B (1998) Comparison of Interlaminar Fracture Toughness in Unidirectional and Woven Roving Marine Composites. Applied Composite Materials, 5(3):189-206.

5.33 Compston P and Jar P-YB (1999) The Influence of Fibre Volume Fraction on the Mode I Interlaminar Fracture Toughness of a Glass-Fibre/Vinyl Ester Composite, Applied Composite Materials, 6:353-368.

5.34 Kim J K and Sham M L (2000) Impact and delamination failure of woven-fabric composites, Composites Science and Technology, 60:745-761.

5.35 Bolotin V V (2001) Mechanics of Delaminations in Laminate Composite Structures. Mechanics of Composite Materials, 37:367-380.

5.36 Sridharan S (2008) Delamination Behaviour of Composites. Woodhead Publishing Limited, Cambridge, England.

5.37 Blake S P (2010) Crack Propagation in Secondary Bonded FRP Composite Joints. MS Thesis in Civil Engineering, University of Maine, 141p.

5.38 Berube K A and Lopez-Anido R A (2010) Variability in the Material Properties of Polymer Matrix Composites for Marine Structures. Journal of ASTM International, 7(4):18p.

5.39 Cain J J, Post N L, Lesko J J, Case S W, Lin Y, Riffle J S, and Hess P E (2006) Post-Curing Effects on Marine VARTM FRP Composite Material Properties for Test and Implementation. Journal of Engineering Materials and Technology, Transactions of the ASME, 128:34-40.

5.40 El-Chiti F (2005) Experimental Variability of E-Glass Reinforced Vinyl Ester Composites Fabricated by VARTM/SCRIMP. MS Thesis in Mechanical Engineering, University of Maine, Orono, ME.

5.41 Berube K A and Lopez-Anido R A, Caccese V, and Hess P (2006) Variability in Flexural Response of E-Glass/Vinyl Ester Composites Fabricated Using the VARTM Process. Proceedings of the 51st International SAMPE Symposium and Exhibition, Creating New Opportunities for the World Economy, April 30-May 4, 2006, Long Beach, CA, 11p.

5.42 ASTM Standard D5528 (2001) Standard Test Method for Mode I Interlaminar Fracture Toughness of Unidirectional Fiber-Reinforced Polymer Matrix Composites. ASTM International, West Conshohocken, PA, www.astm.org.

5.43 Dharmawan F, Simpson G, Herszberg I, and John S (2006) Mixed Mode Fracture Toughness of GFRP Composites. Composite Structures, 75:328-338.

5.44 ASTM Standard D2584 (2002) Standard Test Method for Ignition Loss of Cured Reinforced Resins. ASTM International, West Conshohocken, PA, www.astm.org.

5.45 Li J, Zhang C, Liang R, Wang B, and Walsh S (2008) Modeling and Analysis of Thickness Gradient and Variations in Vacuum-Assisted Resin Transfer Molding Process. Polymer Composites, 29:473-482.

5.46 ASTM Standard D2583 (2004) Standard Test Method for Indentation Hardness of Rigid Plastics by Means of a Barcol Impressor. ASTM International, West Conshohocken, PA, www.astm.org.

5.47 MIL-HDBK-17F-1 (2002) Composite Materials Handbook Volume 1 - Polymer Matrix Composites Guidelines for Characterization of Structural Materials, ASTM International, West Conshohocken, PA, p8.1-110.

5.48 Kotaki M, and Hamada H, (1997) Effect of Interfacial Properties and Weave Structure on Mode I Interlaminar Fracture Behavior of Glass Satin Woven Fabric Composites. Composites Part A, 28A:257-266.

5.49 Suppakul P and Bandyopadhyay S (2002) The Effect of Weave Pattern on the Mode-I Interlaminar Fracture Energy of E-Glass/Vinyl Ester Composites. Composites Science and Technology, 62:709-717.

5.50 Naik N K, Reddy K S, Meduri S, Raju N B, Prasad PD, Azad SK N M, Ogde PA and Reddy B C K (2002) Interlaminar Fracture Characterization for Plain Weave Fabric Composites. Journal of Materials Science, 37:2983-2987.

5.51 Gill A F, Robinson P, and Pinho S (2009) Effect of Variation in Fibre Volume Fraction on Modes I and II Delamination Behaviour of 5HS Woven Composites Manufactured by RTM. Composites Science and Technology, 69:2368-2375.

CHAPTER 6

EFFECT OF RESIN CURE RECIPE AND AMBIENT PROCESSING TEMPERATURE ON THE MATERIAL PROPERTIES OF MARINE GRADE POLYMER MATRIX COMPOSITE MATERIALS

6.1 Abstract

The effects of resin curing recipe and ambient processing temperature on the mechanical properties of composite laminates were investigated. Woven roving E-glass/vinyl-ester composite plates were fabricated with a pliable-bag VARTM process over a range of ambient temperatures and resin gel times commonly encountered when fabricating polymer composite parts for the marine industry. Standardized tests for Mode-I interlaminar fracture toughness, compression, constituent volume fraction, and Barcol hardness were conducted. Interlaminar fracture toughness exhibited the most variability among the measured properties. While there were few direct correlations between the measured properties and the parameters in the study, there were several statistically significant differences that could not be discarded as random, since they were consistent among the replicate panels fabricated for each combination of parameters in the study.

6.2 Introduction

The recreational and commercial marine industry is an area where the vacuum assisted resin transfer molding (VARTM) process has been used extensively for many years to fabricate large composite structures. In recent years, the Navy has shown an increased interest in using fiber reinforced polymer (FRP) composites for various parts of ship construction. This interest is a result of the Navy's effort to minimize electronic and

acoustic signatures combined with a desire to reduce the high lifetime costs of metallic ships. The ability to affordably construct large composite structures has improved over the past 25 years, assisted by advances in resin-infusion processing [1-2], therefore, the promise of meeting the Navy's demands may become a reality in the near future.

Composite manufacturing methods continue to improve; however, questions still remain regarding the consistency of the material properties in large composite structures [3-6]. The Navy favors a VARTM process that incorporates a pliable vacuum-bag and permeable flow media [6]. It is favored due to its ability to inexpensively fabricate large, quality, structural parts [7]. The VARTM process has been investigated in several studies over the past 20 years [5-13]. The parameters that have been shown to have the greatest effect on composite material properties include fiber preform consolidation, resin chemistry and curing, fiber sizing, interphase formation, and post-cure. A study to investigate the effects of resin chemistry and gel time on the material properties of marine grade composites is presented here.

Resin catalyzing additives affect the curing reaction through variations in the magnitude of the peak exotherm and its duration [14-26], as well as degree of cure [14, 16, 18-19 21-23, 26-36]. The degree of cure directly affects the mechanical properties of the resin through a reduction in strength, stiffness, and an increase in creep [37-38]. The variations in catalyzing recipe and exotherm also produce variations in the microstructure of the polymerized resin [23, 29, 31, 35, 39-43], which again affects the properties.

Another factor complicating the prediction of the resin polymerization is the interaction of the resin with the fiber and the fiber sizing [44-55]. The resin/sizing interaction creates an interphase region such that there is a property gradient from the

surface of the glass fiber to the surrounding resin [49, 56-71]. The formation of this interphase region is itself affected by the same variations that affect the resin polymerization and is not completely understood [55, 70, 72-74]. Studies based solely on neat resin reactions simply can not capture the full scope of the polymerization process that occurs during composite material fabrication and its effect on the resulting material properties [51].

Post-curing of the resin or composite part has been shown to increase (or complete) the degree of cure of the part [75-77] and improve the material properties. This results in an increased modulus and reduced creep, which can aid the fatigue life. While it is generally agreed that some degree of post curing of the composite laminate is required, the effects due to variations of the resin recipe are unclear.

The fact that the curing of these resins (and thus the resulting mechanical properties) is affected in many different ways by the various interactions discussed, seems to get lost when selecting a composite material as a design solution. The resin manufacturers and the composite manufacturers themselves do not, and could not, have a complete grasp of the exact effects on the mechanical properties of a fabricated composite part when the exact nature and interaction of all the additives, sizings, and curing conditions is still unknown.

The objective of this study was to investigate the effects on composite material properties due to variations of resin recipe and ambient temperatures commonly encountered when infusing polymer composites for the marine industry. The proposed method is to evaluate relevant mechanical and physical properties to quantify the effects of the processing parameters investigated. While a complete investigation of all the

interactions that occur between the fiber and resin system during the infusion and curing of a composite part are beyond the scope of this study; the study was undertaken with the knowledge that these issues exist and with the intent of minimizing some of these effects in an attempt to capture the effects on some of the common material properties. This study is part of a larger project sponsored by the Office of Naval Research to investigate the causes of variability in material properties of E-glass/vinyl-ester marine grade polymer composites. The sources of variability being investigated in the larger project include those due to manufacturing [78-79], post processing [38], and testing of composites [80-81].

6.3 Experimental Methods

6.3.1 Panel Fabrication

A marine grade polymer composite reinforced with woven roving was used in this study. The FRP panels consisted of an E-glass/vinyl-ester system fabricated using a pliable-bag VARTM process. The fiber reinforcement used was a Saint-Gobain Vetrotex E-324 woven roving with a weight per unit area of 814 g/m^2 (24 oz/yd^2). The fabric is a plain weave with a tow spacing of 5.1 mm (0.2 in.) in the warp direction, and 6.4 mm (0.25 in.) in the fill direction. This results in 55% of the fiber orientated in the warp direction and 45% in the fill direction. The polymer resin used was Ashland Derakane 8084, which is an elastomer-modified epoxy vinyl-ester resin.

The FRP panel dimensions were 610 by 965 mm (24 by 38 in.) and consisted of ten layers of fabric reinforcement in a warps-parallel configuration, for a nominal thickness of 6.4 mm (0.25 in.). The lay-up notation is $[0_{10}]_f$, where the orientation indicates the warp direction of the fabric. It is worth noting that the dimensions of the

panel were chosen such that a complete second set of specimens could be obtained from the panel if there were problems during specimen preparation or testing. This reduces the variability that may occur during manufacturing by eliminating the need to re-fabricate panels. In addition, the same panel size was used throughout the entire larger study to eliminate the variability that may occur when fabricating different panel sizes. This allows a comparison of the results between all phases of the study without having panel size as a manufacturing variable.

An 89 mm (3.5 in.) wide strip of 0.0127 mm (0.0005 in.) thick virgin PTFE film was placed at the mid-plane of the laminate along the edge of the panel where the vacuum line was placed, as shown in the panel dimensions schematic in Figure 6.1 and the fabrication layup in Figure 6.2. The PTFE film provided the initial crack necessary for the Mode-I fracture specimens. The other materials used for the panel layup shown in Figure 6.2 were as follows:

- Peel Ply – 48 g (1.7 oz), 0.102 mm (0.004 in.) thick nylon (Northern Fiber Glass Sales)
- Flow Media - Vip Infusion Flow R750 (Richmond Aircraft Products)
- Bleeder – 113 g (4 oz), 3.18 mm (0.125 in.) thick , non-woven polyester (FibreGlast)
- Vacuum Bag – 0.051 mm (0.002 in.) thick nylon bagging film (FibreGlast)
- Exterior Tubing – 9.53 mm (0.375 in.) ID clear PVC tubing
- Interior Tubing – 12.7 mm (0.50 in.) OD Polyethylene spiral-cut cable wrap (M. M. Newman Corp.)

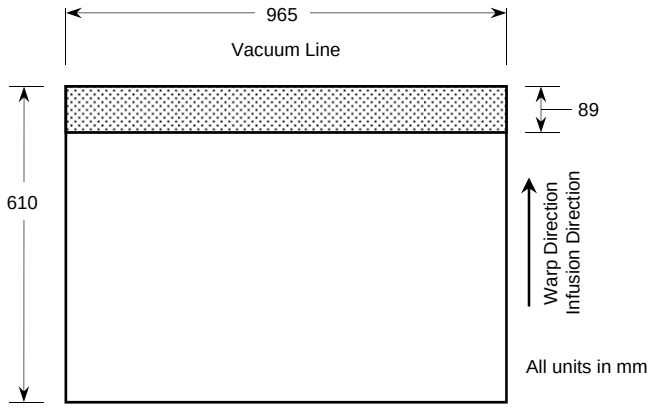

Figure 6.1. Composite panel dimensions.

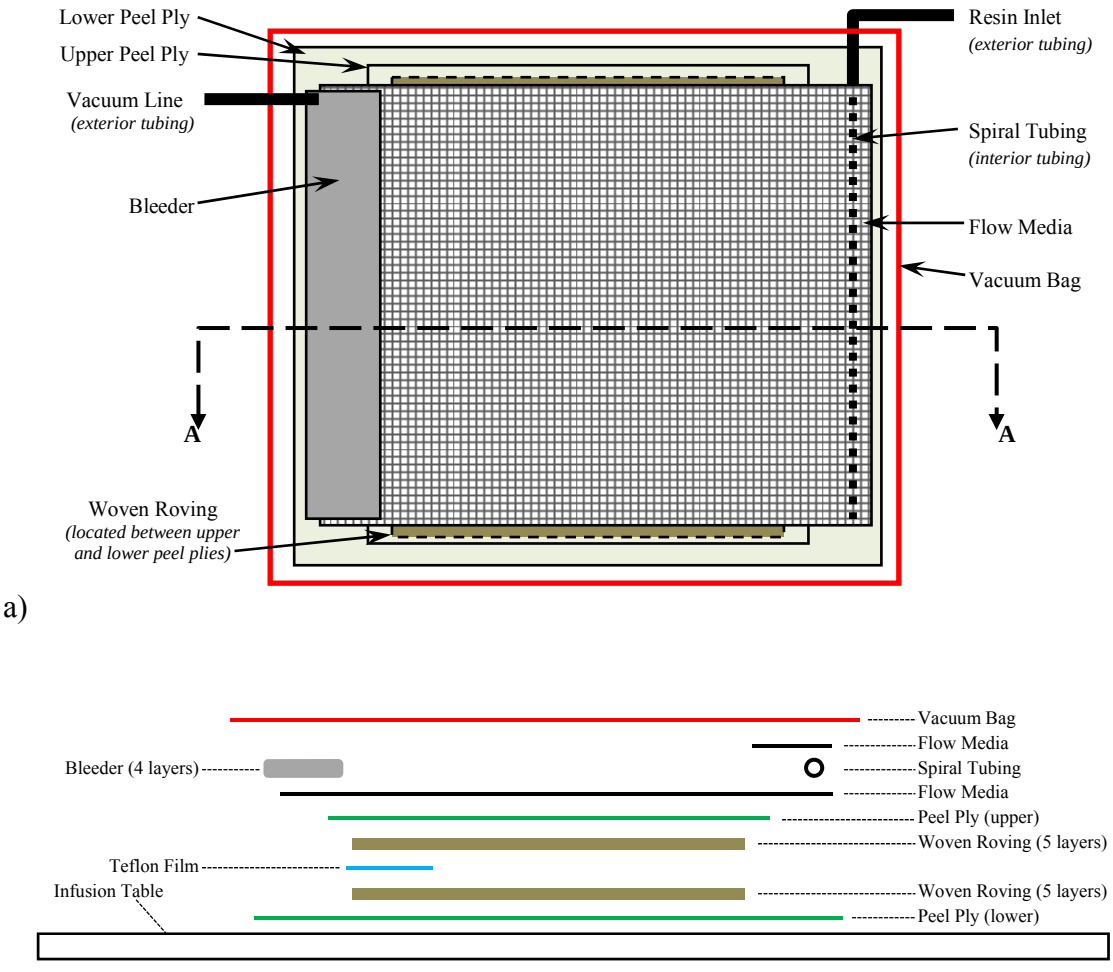

Figure 6.2. Panel layup: a) top view, and b) exploded view of section A-A.

Three different ambient temperatures combined with three different gel times were investigated in the study. The three target ambient temperatures were 15.6. 21.1, and 26.7ºC (60.0, 70.0 and 80.0 ºF), which will be referred to as Low (Lo), Standard (Sd), and High (Hi), respectively, in the tables, figures, and results discussions. The three target gel times were 1.0, 2.5, and 6.0 hours. The ambient relative humidity was held at 50±5% for each of the three temperatures investigated. Noting that ambient pressure varies from day-to-day, the value of 0.982 bar (29.0 in-Hg) was chosen as the infusion pressure instead of a "full-vacuum condition" to ensure that the infusion pressure could be repeated for each of the infusions. The range of ambient temperatures and gel times were chosen based on discussions with industry fabricators and personnel from the Naval Surface Warfare Center - Carderock Division (NSWC-CD). These ranges were intended to encompass the range of temperatures and gel times commonly encountered when fabricating marine composite laminates of varying degrees of complexity.

Three replicates were fabricated for each of the nine combinations of ambient temperature and gel time, resulting in a total of 27 panels fabricated during the study. As a means of reducing the total number of infusion cycles performed, it was decided to infuse three panels simultaneously, one at each of the three gel times, but all at the same ambient temperature. This also reduced the possibility of variations due to other parameters like infusion pressure and consolidation time, which had been shown to affect Mode-I fracture properties in a previous phase of the larger study [70].

The catalyzing recipes consisted of the following chemcials:

- Methyl Ethyl Ketone Peroxide, MEKP (Norox MEKP 925)
- Cobalt 6% Napthenate, *Cobalt* (Puritan Products)

- N,N-Dimethylaniline, DMA (Puritan Products)
- 2,4-Pentanedione, *2,4-P* (J.T. Baker).

The nine dataset designations along with their respective catalyzing recipes used in the study are presented in Table 6.1. The values listed in the table are based on the percent of the mass of resin used during the infusion. The recipes were determined based on consultation with Ashland, Inc. and verified with preliminary gel tests prior to panel fabrication. Specifically, Ashland provided the recommended amounts of Cobalt, DMA, and MEKP, while the exact amounts of 2,4-P were verified from gel tests, using 2 kg batches of resin, conducted at each gel time and temperature. The 2,4-P was adjusted until the gel times were within ±5, ±10, and ±20 minutes for the 1.0, 2.5 and 6.0 hour gel times, respectively, at each ambient temperature.

Table 6.1. Target parameters for each dataset.

Dataset Designation	Fabrication Parameters		Resin Catalyzing Recipe			
	Temperature	Gel Time	MEKP	Cobalt	DMA	2,4-P
ID	*°C (°F)*	*hr*	*%*	*%*	*%*	*%*
Lo10	15.6 (60.0)	1.0	1.65	0.400	0.100	0.025
Lo25	15.6 (60.0)	2.5	1.65	0.400	0.100	0.100
Lo60	15.6 (60.0)	6.0	1.65	0.400	0.100	0.200
Sd10	21.1 (70.0)	1.0	1.50	0.300	0.050	0.000
Sd25	21.1 (70.0)	2.5	1.50	0.300	0.050	0.100
Sd60	21.1 (70.0)	6.0	1.50	0.300	0.050	0.250
Hi10	23.3 (80.0)	1.0	1.50	0.300	0.050	0.075
Hi25	23.3 (80.0)	2.5	1.50	0.300	0.050	0.200
Hi60	23.3 (80.0)	6.0	1.50	0.300	0.050	0.325

Master batches of the resin were prepared in 14 kg amounts for each gel time two days in advance of manufacturing the three sets of panels at a given temperature. The master batches were “pre-promoted” with the Cobalt, DMA, and 2,4-P. The master batches were mixed by hand for 5 minutes after the addition of each chemical. Each master batch contained enough resin to fabricate the three replicate panels required for a

given gel-time at a given temperature. All of the resin, the glass fabric, and the chemicals used for the catalyzing recipes came from single lots to avoid possible variations in lot selection. It is worth noting that all items used during the infusion were allowed to equilibrate in the ambient conditions under study for a period of not less than 48 hours.

A prior phase of the study had shown that a time of 45 minutes would be sufficient to entirely wet-out the panels in the configuration that was used for the infusions [79]. The longer infusion time was required to properly wet-out around the PTFE film. An infusion pressure control system was implemented during the fabrication of the composite panels in the study. The system was comprised of a precision pressure transducer, a vacuum regulator, several thermocouples, humidity sensors, and a data acquisition system. The system allowed for the precise control and monitoring of the infusion pressure, the ambient conditions, and the resin temperature during the infusion process. During preform consolidation and infusion, the data acquisition system recorded data every five minutes for ambient temperature and humidity, resin temperature, and vacuum pressure for each panel.

The fabrication procedure that was used for all infusions was as follows.

- Lay up the fabric and bag the three panels (as shown in Figure 6.2)
- Pull vacuum on the three panels simultaneously
- Adjust regulator to stabilize pressure at 0.982 bar (29 in-Hg)
- Hold vacuum at pressure for 2.5 hours to consolidate fabric preform
- Add catalyzing recipe to resin 15 min before end of consolidation time
- At end of consolidation period, open resin lines to all three panels
- After the panels have wet-out, clamp off the resin and vacuum lines

The 27 panels were successfully infused during nine sets of infusions over a period of 24 days in an environmentally controlled composites fabrication chamber at the Advanced Manufacturing Center at the University of Maine, Orono, Maine. The three-panel configuration that was used during fabrication is presented in Figure 6.3. The results of the nine sets of panel infusions are presented in Table 6.2. In addition to the mean gage pressure applied to each of the three panels during the consolidation and infusion, the table includes the resin gel time, the mean ambient temperature, and the mean ambient relative humidity for each of the nine infusions. The mean infusion pressure for each panel infused was within 0.33% of the target pressure.

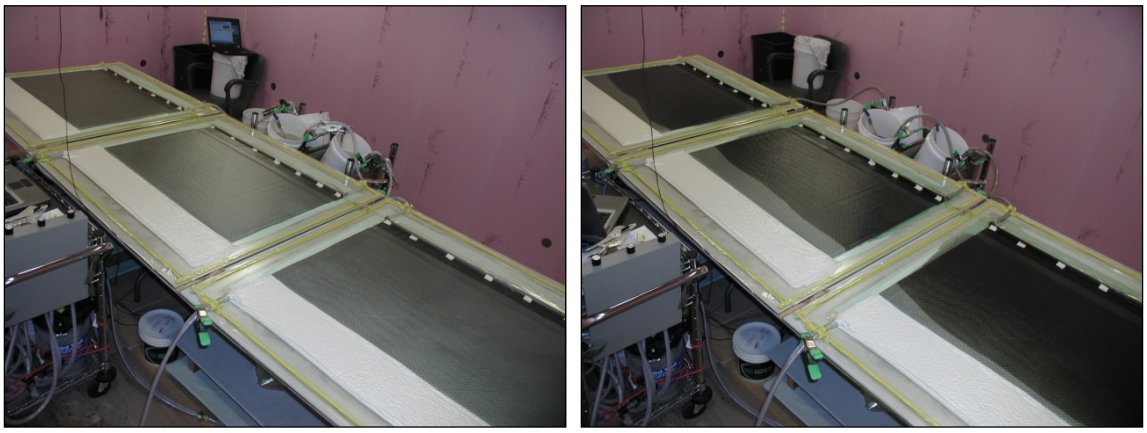

a) b)

Figure 6.3. Panel infusion setup: a) during consolidation, and b) during infusion.

Two issues are worth noting from the data in Table 6.2. The first is that the environmental chamber was unable to maintain the 15.6ºC (60.0ºF) target temperature due to the added thermal load from the presence of personnel during the infusion process; therefore, the minimum maintainable temperature of 17.8ºC (64.0ºF) was used. The second issue was that despite multiple successful gel tests for the 6-hour gel time at the 21.1ºC (70.0ºF) ambient temperature, the gel times varied from 7:45 to 9:00 hours during

Table 6.2. Panel infusion summary.

Panel Set	Infusion Pressure	Ambient Conditions		Resin Gel Time *(hr:min)*		
		Temperature	Humidity	*Dataset ID*		
ID	*in-Hg*	*°C (°F)*	*%RH*	***10***	***25***	***60***
Lo-1	0.9828 (29.02)	17.6 (63.6)	52.2	1:06	2:31	6:17
Lo-2	0.9836 (29.05)	17.5 (63.5)	51.6	1:14	2:45	6:41
Lo-3	0.9851 (29.09)	17.8 (64.1)	51.4	1:05	2:41	6:11
Sd-1	0.9831 (29.03)	21.1 (69.9)	51.6	1:07	2:47	9:01
Sd-2	0.9828 (29.03)	21.4 (70.6)	50.7	1:12	3:10	8:23
Sd-3	0.9818 (29.00)	21.6 (70.8)	49.8	1:15	3:05	7:47
Hi-1	0.9831 (29.03)	26.9 (80.4)	54.0	1:09	3:22	5:59
Hi-2	0.9835 (29.05)	27.1 (80.7)	51.4	1:06	3:18	5:38
Hi-3	0.9827 (29.02)	26.7 (80.1)	50.9	1:09	3:29	5:42

the actual panel infusions. The gel times for the other datasets were more consistent among replicates and closer to their intended target gel times.

The panels were post-cured at 82ºC (180ºF) for 4 hours. This post-cure cycle had been shown to be appropriate for this material system at this thickness and provided consistent results in earlier phases of the study. [38, 78-79] All specimens were examined prior to testing for visible defects due to manufacturing, or specimen preparation. In addition to inspecting the exterior of the specimens, the inspection included backlighting of the specimens. This would reveal macroscopic inclusions and voids produced during manufacturing, and delaminations produced during specimen preparation.

6.3.2 Test Methods

The experimental testing conducted for the study included Mode-I fracture, compression, and constituent volume fraction. The Mode-I fracture test was selected since it was the material property of primary interest, and an indicator of the fiber/resin interaction strength. The compression test was selected as a standard test that was performed throughout the larger study, and the constituent volume fraction test was

selected since it is a good indicator of the consistency of the consolidation of the preform, and a general predictor of fiber dominated material properties. In addition, Barcol hardness measurements were made on resin samples before and after post-curing of the specimens, as a means to verify the consistency of the post-cure process on the resin in the specimens [30, 82].

Mode-I fracture properties were obtained in accordance with ASTM test standard D5528 [83]. ASTM D5528 uses a double cantilever beam (DCB) configuration for the test specimens. The dimensions of the DCB specimens used in this study were 25.4 by 152.4 mm (1.0 by 6.0 in.) with a nominal initial crack length of 49 mm (1.9 in.). The edge of each specimen was marked in 1-mm increments over a 55 mm (2.2 in.) range to identify crack growth. A total of 12 specimens were cut from each panel in the region indicated in Figure 6.4, using computer numerical control (CNC) water-jet abrasive machining. As recommended in the standard, the corrected Modified Beam Theory (MBT) method was used to calculate the fracture toughness, $\boldsymbol{G_I}$, as given by the equation:

$$G_I = \frac{3P\delta}{2b\left(a + |\Delta|\right)} F \tag{1}$$

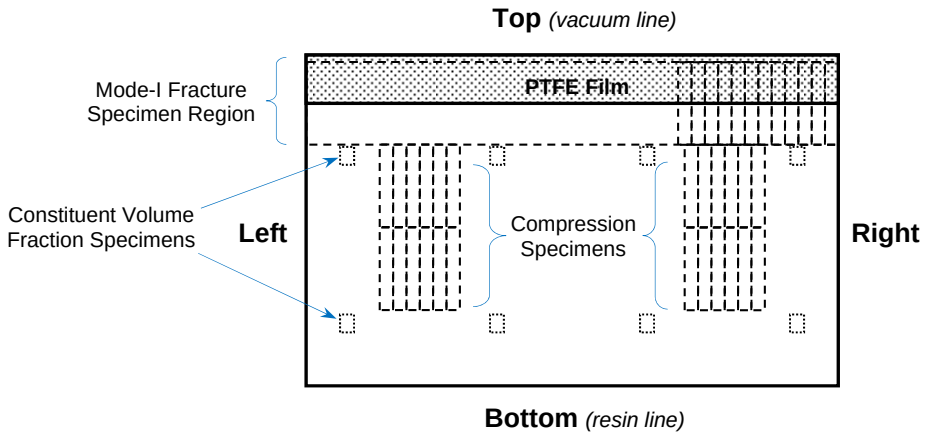

Figure 6.4. Panel schematic showing test specimen locations and panel orientation.

Where $\boldsymbol{P}$ is the applied load, $\boldsymbol{\delta}$ is the load point displacement, $\boldsymbol{b}$ is the specimen width, $\boldsymbol{a}$ is the crack length, $\boldsymbol{\Delta}$ is a correction factor to account for beam rotation at the crack front, and $\boldsymbol{F}$ is a correction factor to account for large deflections. The value of $\boldsymbol{\Delta}$ is determined empirically and is the x-axis intercept of a plot of the cube-root of the specimen compliance versus $\boldsymbol{a}$. The Mode-I fracture toughness properties computed in this study were the visual onset fracture toughness ($\mathbf{G_{vis}}$), the nonlinear onset fracture toughness ($\mathbf{G_{NL}}$), and the propagation fracture toughness ($\mathbf{G_{prp}}$).

The specimens were tested on a 25 kN (5.6 kip) Instron servo hydraulic test frame equipped with a 250 N (56.2 lb) load cell and hydraulic grips. The tests were conducted in displacement control at a rate of 2.5 mm/min (0.1 in/min) without pre-cracking the specimens. Crack onset was detected both visually and through the use of a numerical routine to determine the point of nonlinear onset (NL onset). The visual detection was performed using a digital image acquisition system, which collected data at a 1 Hz sampling rate. The digital images were post-processed and examined for visual onset and crack growth increments of 1 mm or greater. The load, displacement, and crack length at each of these occurrences was recorded. The NL onset was determined by locating the point at which the load-deflection (P-δ) curve became nonlinear. The details of this method were presented in a prior study [79, 84]. This method has been shown to produce repeatable and consistent results for similar material systems.

The Mode-I propagation fracture toughness values were computed in this study using the region of the resistance curve (R-curve) where the fracture toughness has stabilized to compute the mean propagation fracture toughness [85]. The method produces a less conservative value for propagation fracture toughness, because it discards

the lower values of fracture toughness computed prior to R-curve stabilization; However, it is a repeatable method and provides less variability in the results.

The compression properties of the composite specimens were obtained in accordance with ASTM test standard D6641 [86]. A three-dimensional digital image correlation (DIC) system was used to measure the strains on the test specimens during testing. The DIC system provides the means to monitor a larger area of the specimen during testing, as compared to conventional strain gages, which is advantageous when testing heavy woven fabric composites [78, 80]. Twelve specimens were cut from each of the panels in the region indicated in Figure 6.4, using CNC water-jet abrasive machining. The test specimen size was 25.4 by 152.4 mm (1.0 by 6.0 in.). The length of 152.4 mm is slightly longer than recommended in the standard and was chosen to allow more area of the specimen to be observed by the DIC system. This length was shown to allow the specimens to fail in compression while avoiding buckling failures [78, 80]. The specimens were tested on a 100 kN (22.5 kip) Instron servo hydraulic test frame equipped with a 100 kN (22.5 kip) load cell and hydraulic grips. The specimens were tested in displacement control at a crosshead rate of 0.01 mm/sec (0.0004 in/sec). This resulted in a test duration of approximately 5 minutes. Load and crosshead displacement data were recorded at a sampling rate of 10 Hz on the Instron control computer and at 1 Hz on the DIC system. This sampling rate has been shown to be sufficient in capturing the results at this rate of straining in the compression specimens [78-80].

The constituent volume fraction properties of the specimens were obtained in accordance with ASTM test standard D3171 [87]. Eight specimens were cut from each of the panels as indicated in Figure 6.4, using CNC water-jet abrasive machining. The

specimens were distributed around the panel to capture spatial variations of the volume fraction resulting from the thickness gradients, which occur along the infusion direction [1, 9, 88]. The nominal specimen dimensions were 25.4 by 35.0 mm (1.0 by 1.38 in.) with a nominal mass of 11.0 grams (0.39 oz). The resin burn-off method was performed in a muffle furnace at a temperature of 565ºC (1049ºF) for a period of 2.5 hours, which prior experience with this material system had shown to be sufficient for complete resin removal [78-81].

Barcol hardness properties of the resin samples were obtained in accordance with ASTM test standard D2583 [89]. Residual resin from each of the nine infusions was retained for this purpose. This was used as a means to quantify any variation of the material properties of the resin from each infusion. Five samples from each of the nine infusions were cut into 6.4 mm (0.25 in.) thick specimens. Fifteen Barcol hardness measurements were conducted on each of the specimens before and after post-curing. The post-cure procedure for the resin specimens was identical to that used on the composite test specimens.

6.3.3 Data Analysis Procedure

The data from each of the three replicate panels were grouped and treated as single datasets for the comparative analysis implemented for the constituent volume fraction, the compression, and the Mode-I fracture test results. After verifying the normality of the dataset distributions using the Anderson-Darling method, the mean and coefficient of variation (CV) were computed for each material property investigated. The datasets were then grouped by ambient temperature and gel time to identify the effects of these variables on material properties. The k-sample Anderson-Darling (ADK) method

[90] was used to determine if the results from each material property dataset were statistically discernible for the different parameters investigated. This method was chosen since it is the method recommended in the Composite Materials Handbook (MIL-17) to screen for pooling of datasets. If the calculated ADK value for the dataset is less than the standard critical value, then one can conclude with a 2.5 percent risk of being in error, that the groups were drawn from the same population. The ratio of the computed value to critical value was calculated as a means to determine the level to which the datasets were statistically discernible. This ADK ratio is tabulated and presented for each dataset comparison in the discussion of the results.

The Maximum Normed Residual (MNR) method was used to identify outliers [90]. A few data points were identified as outliers by the MNR method in portions of this study; however, valid reasons for excluding them from the data analyses were not identified.

6.4 Discussion of Results

6.4.1 Barcol Hardness Results

The results of the Barcol hardness tests are presented in Table 6.3. The mean Barcol hardness of the as-gelled resin ranged from 20.8 to 25.7. The post-cure results indicate that the resin from each of the nine infusions equilibrated to a mean Barcol hardness value between 33.5 and 36.1. There was a reduction in the CV for all of the datasets between the as-gelled (10 to 26%) to the post-cured state (3.9 to 6.3%). The variation in mean value of the Barcol hardness of the post-cured resin indicates that the state-of-cure of the resin was not consistent in all of the specimens; therefore, the condition of the resin could contribute to the variability of the material properties. While

Table 6.3. Barcol hardness results.

Resin Set	As Gelled		Post-cured	
	mean	*CV*	*mean*	*CV*
Lo10	25.5	10%	34.8	5.6%
Lo25	23.7	12%	33.5	4.9%
Lo60	25.4	10%	36.0	4.2%
Sd10	25.7	13%	36.1	4.3%
Sd25	23.9	18%	35.4	4.2%
Sd60	24.5	13%	35.3	6.1%
Hi10	21.1	26%	34.2	5.3%
Hi25	22.8	13%	34.2	6.3%
Hi60	20.8	18%	35.5	3.9%
Total	**23.7**	**7.7%**	**35.0**	**2.6%**

the difference between the maximum and minimum hardness of 7.2% may seem small, prior studies by the author on the same resin system without variations in resin chemistry produced variations of less than 2.5% [79].

6.4.2 Constituent Volume Fraction Results

The datasets were grouped to identify the effects of ambient temperature and gel time on the fiber volume fraction (FVF) results. The results for the ambient temperature and gel time dataset groupings are presented in the plots in Figure 6.5, and the ADK ratios in Table 6.4. The FVFs were computed using a resin density of 1.13 g/cm^3 (0.653 oz/in^3) and a glass density of 2.54 g/cm^3 (1.47 oz/in^3). It is worth noting that the data in Figure 6.5 is plotted with a y-axis range of 40-60% for clarity and that the error bars are ±1 standard deviation. The FVF ranged from 52.2% to 54.1% while the CV ranged from 1.5% to 3.0%. While the longer gel times tended to produce slightly larger FVFs for each ambient temperature, as seen in Figure 6.5a, the ADK ratios in Table 6.4a indicate that the subset comparisons for the high temperature dataset grouping, and the 1.0 hour and 6.0 hour subset comparison for the low temperature dataset grouping produced the

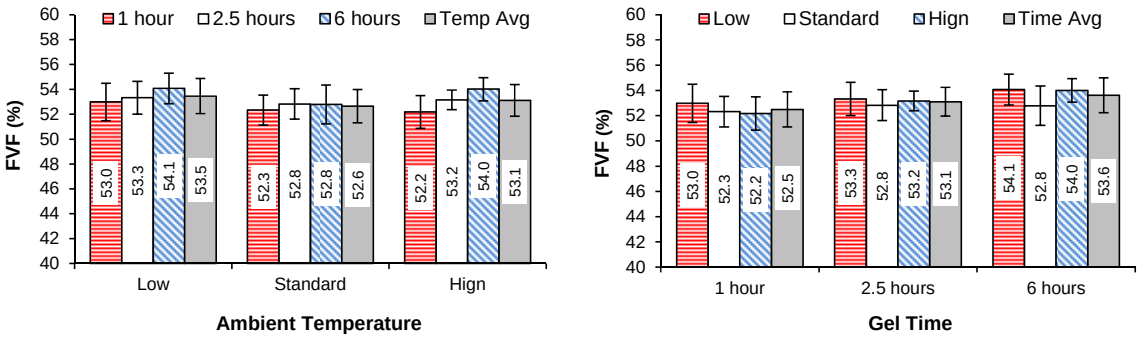

a) b)

Figure 6.5. Fiber volume fraction results comparison: a) ambient temperature dataset groupings, and b) gel-time dataset groupings.

Table 6.4. ADK ratios for fiber volume fraction: a) ambient temperature dataset groupings, and b) gel time dataset groupings.

a)

Subsets Compared	Number of Specimens	ADK Ratios Temperature Data Set Lo	Sd	Hi
1.0, 2.5, 6.0	216	0.89	0.42	**2.79**
1.0 & 2.5	144	0.21	0.37	**1.63**
1.0 & 6.0	144	**1.17**	0.47	**2.96**
2.5 & 6.0	144	0.70	0.19	**1.57**

b)

Subsets Compared	Number of Specimens	ADK Ratios Gel-Time Data Set 1.0	2.5	6.0
Lo, Sd, Hi	216	0.58	0.65	**1.56**
Lo & Sd	144	0.46	0.50	**1.55**
Lo & Hi	144	0.65	0.27	0.29
Sd & Hi	144	0.19	0.71	**1.57**

ADK ratios greater than 1.00 indicate that the datasets in the comparison are statistically different.

only statistically discernible results; however, they were not significant. The trend for the longer gel times can be explained since longer gel times provide more time for the resin to completely wet-out the fiber tows, and for gas bubbles from styrene boiling to rise out of the laminate and into the flow media.

As seen in Figure 6.5b, the low temperature dataset produced the largest mean FVF value within each of the gel time dataset groupings; however the ADK ratios in Table 6.4b indicate that the only low temperature subset comparison that produced discernible results was with the standard temperature subset at the 6 hour gel time. While there were a couple of trends in the FVF results, as discussed above, there was no direct

discernible correlation between the FVF and any of the parameters that were controlled or measured during the study.

The spatial distribution of the FVF in the panels was also investigated in this study. The spatial distribution results for the dataset groupings are presented in the plots of Figure 6.6. The orientation of the spatial locations listed in the figure refers to the orientation presented in Figure 6.4. The FVF at each spatial location in the panel is the mean of the four FVF specimens in that spatial location. It is worth noting that the infusion direction was from the bottom to the top; the data in Figure 6.6 is plotted with a y-axis range of 40-60% for clarity; and that the error bars are ±1 standard deviation.

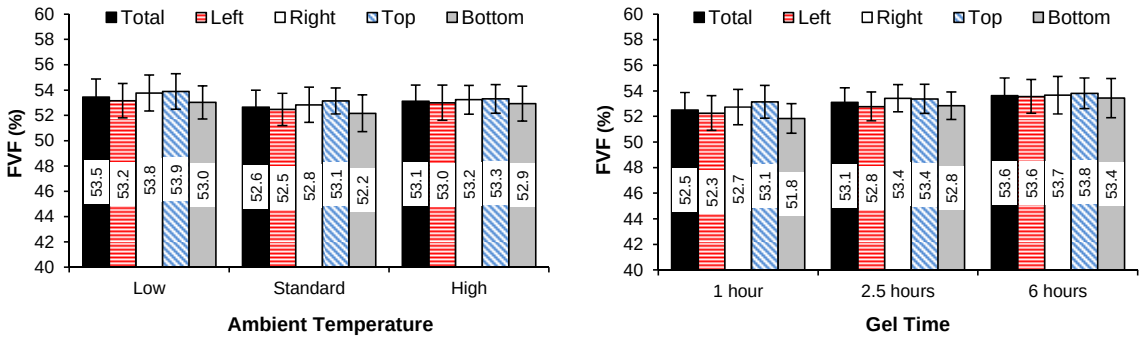

a) b)

Figure 6.6. Spatial distribution of fiber volume fraction: a) ambient temperature dataset groupings, and b) gel-time dataset groupings.

As found in other studies, there was a noticeable difference in the FVF in the infusion direction [1, 9, 78-79]. This is due to a relaxation of the fiber preform that starts after the resin front arrives at that position in the preform during the infusion and continues until fully relaxed, or until resin gelation. The ambient temperature dataset groupings exhibited differences of 1.6%, 1.8%, and 0.7% in FVF, between the top and bottom locations for temperature datasets 60, 70, and 80, respectively. The gel time dataset groupings exhibited differences of 2.4%, 1.0%, and 0.7% in FVF, between the top

and bottom locations for the 1-hour, 2.5-hour, and 6-hour gel time datasets, respectively. In both of the dataset groupings in Figure 6.6, longer gel times and higher temperatures resulted in less spatial variability in the panels. Longer gel times allow more time for the relaxation "gradient" of the preform to equilibrate, while the higher temperature reduces the viscosity of the resin which allows for a quicker wetting of the preform at all gel times, resulting in a smaller relaxation gradient across the length of the panel.

6.4.3 Compression Results

The compression strength test results for the ambient temperature and gel time dataset groupings are presented in the plots in Figure 6.7, and the ADK ratios in Table 6.5. The error bars in Figure 6.7 are ±1 standard deviation. The strengths ranged from 398 to 430 MPa (57.7 to 62.4 ksi), while the CV ranged from 5.6 to 8.9%. While there were general trends of either increasing or decreasing strength within individual ambient temperature or gel time dataset groupings, there was not a consistent trend across the datasets. In addition, there was not a direct correlation between compression strength and any of the parameters in the study.

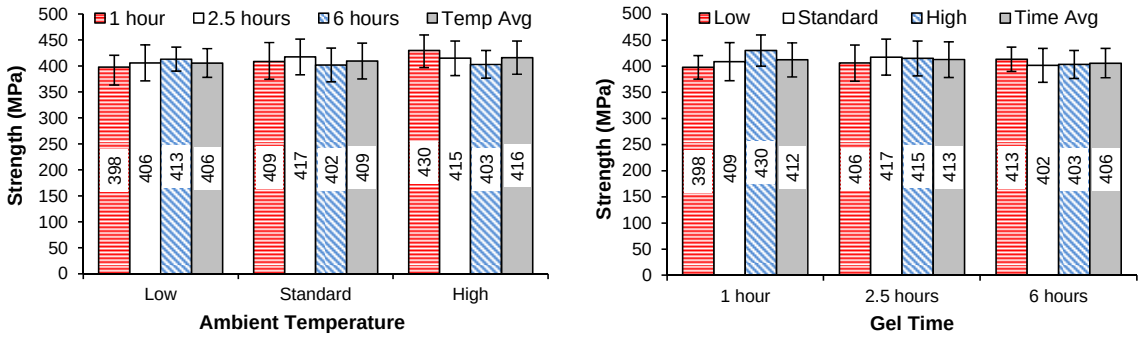

Figure 6.7. Compression strength results comparison: a) ambient temperature dataset groupings, and b) gel-time dataset groupings.

Table 6.5. ADK ratios for compression strength: a) ambient temperature dataset groupings, and b) gel-time dataset groupings.

a)

Subsets Compared	Number of Specimens	Strength ADK Ratios *Ambient Temperature Data Set Grouping* Lo	Sd	Hi
1.0, 2.5, 6.0	324	**1.05**	0.55	**1.52**
1.0 & 2.5	216	0.87	0.20	0.61
1.0 & 6.0	216	**1.37**	0.34	**2.16**
2.5 & 6.0	216	0.41	0.76	0.75

b)

Subsets Compared	Number of Specimens	Strength ADK Ratios *Gel Time Data Set Grouping* 1.0	2.5	6.0
Lo, Sd, Hi	324	**2.40**	0.43	0.59
Lo & Sd	216	0.84	0.40	0.72
Lo & Hi	216	**3.69**	0.34	0.56
Sd & Hi	216	**1.26**	0.21	0.14

ADK ratios greater than 1.00 indicate that the datasets in the comparison are statistically different

The compression modulus test results for the ambient temperature and gel time dataset groupings are presented in the plots in Figure 6.8, and the ADK ratios in Table 6.6. The error bars in Figure 6.8are ±1 standard deviation. The modulus values ranged from 28.2 to 29.7 GPa (4.09 to 4.31 Msi), while the CV ranged from 2.7 to 5.2%. There was a trend in the data where the standard temperature dataset produced the largest modulus value within each of the gel time dataset groupings; however, it was not statistically significant. While there was not a direct correlation between the compression modulus and any of the parameters that were measured or controlled in the study, the low temperature dataset did produce the highest mean Barcol hardness value, which could contribute to a higher modulus value for those datasets.

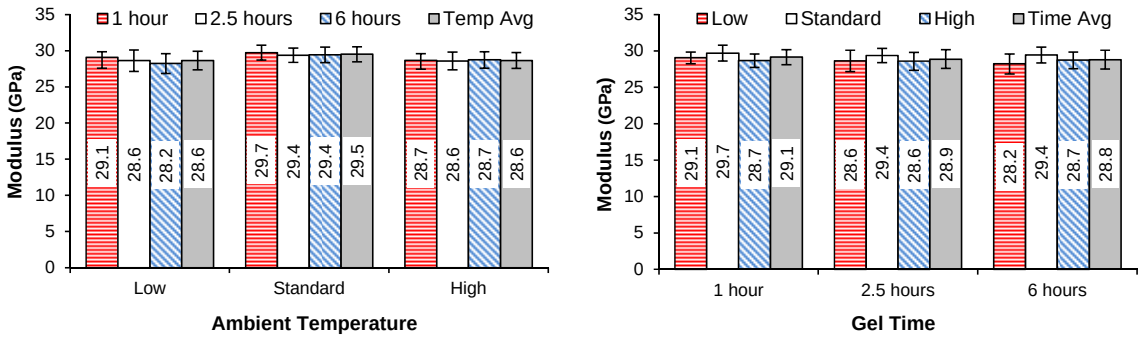

a) b)

Figure 6.8. Compression modulus results comparison: a) ambient temperature dataset groupings, and b) gel-time dataset groupings.

Table 6.6. ADK ratios for compression modulus: a) ambient temperature dataset groupings, and b) gel-time dataset groupings.

a)

Subsets Compared	Number of Specimens	Modulus ADK Ratios: *Ambient Temperature Data Set Grouping* Lo	Sd	Hi
1.0, 2.5, 6.0	324	**1.17**	0.41	0.18
1.0 & 2.5	216	0.86	0.44	0.21
1.0 & 6.0	216	**1.74**	0.32	0.15
2.5 & 6.0	216	0.27	0.18	0.07

b)

Subsets Compared	Number of Specimens	Modulus ADK Ratios: *Gel Time Data Set Grouping* 1.0	2.5	6.0
Lo, Sd, Hi	324	**2.25**	**1.08**	**2.03**
Lo & Sd	216	**1.49**	**1.07**	**2.75**
Lo & Hi	216	0.85	0.12	0.45
Sd & Hi	216	**2.57**	**1.43**	**1.41**

ADK ratios greater than 1.00 indicate that the datasets in the comparison are statistically different

6.4.4 Mode-I Fracture Toughness Results

Crack propagation in heavy woven fabric composites is typically referred to as unstable, with the resulting behavior described as run-arrest [91]. A typical P-δ curve for Mode-I DCB specimens tested in this study is presented in Figure 6.9. As seen in the figure, the curve is characterized by a monotonic increase in load with minimal crack growth, followed by a sudden drop in load when the crack propagates rapidly (runs) to a point where it stops (arrests). This process repeats for the duration of the test. The run-arrest behavior has been attributed to the weave structure [91-95]. Unstable fracture often initiates at the edge of the transverse tows, where the transverse tows act as a toughening mechanism. These intersection points correspond to crack lengths where unstable fracture occurs, which suggests that the failure of these bridged fibers and tows is the cause for the instability of the crack growth [91].

As the crack grew from its initial location, a resistance type fracture behavior developed, with the fracture toughness increasing monotonically before stabilizing as the crack propagated further. Resistance curves (R-curves) were generated to determine the propagation fracture toughness of each specimen in the dataset. An R-curve plot for a typical dataset is presented in Figure 6.10. The fracture toughness was computed at each

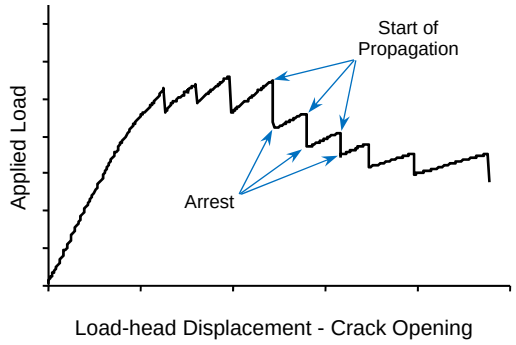

Figure 6.9. Typical Mode-I fracture load-deflection curve exhibiting run-arrest behavior.

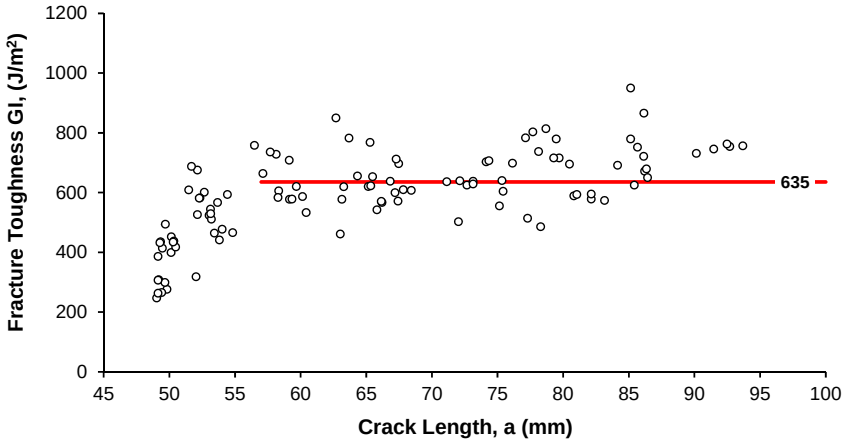

Figure 6.10. Typical Mode-I R-curve showing stabilized propagation.

instance where the crack length grew by 1 mm or more. The points in the plot are the locations where the fracture toughness was computed for each specimen in the dataset. The mean value of the stabilized R-curve data for the 12 specimens is indicated by the horizontal line in the middle of the data points. The propagation fracture toughness value for each specimen was weighted equally when computing the mean value for the entire dataset. A crack length of 57 mm (2.25 in.) was selected as the starting point for stabilized propagation in all of the datasets.

A summary of the Mode-I fracture toughness test results is presented in Table 6.7. The table includes the Mode-I results for visual onset, nonlinear onset, and propagation

Table 6.7. Mode-I fracture test results for each dataset.

Dataset Designation	Fracture Toughness (J/m^2)						Peak Load (N)		Stiffness (N/mm)		Fiber Volume Fraction (%)	
	Onset				Propagation							
	Visual		*Non-linear*		*Visual*							
ID	*mean*	*CV*	*mean*	*CV*	*mean*	*CV*	*mean*	*CV*	*mean*	*CV*	*mean*	*CV*
Lo10	345	40%	302	35%	995	14%	116	3.4%	15.0	0.9%	53.7	2.8%
Lo25	270	36%	281	35%	807	15%	113	5.2%	15.2	3.5%	53.7	2.6%
Lo60	346	47%	368	34%	1125	10%	118	4.5%	15.3	5.6%	54.3	2.5%
Sd10	305	25%	226	25%	860	14%	117	1.6%	15.3	3.0%	53.2	1.6%
Sd25	484	33%	335	43%	860	19%	114	5.4%	15.7	3.8%	53.1	2.3%
Sd60	404	34%	258	29%	872	22%	115	3.6%	15.1	2.5%	53.1	1.9%
Hi10	474	31%	374	33%	868	13%	108	2.6%	14.8	1.0%	52.6	2.3%
Hi25	400	27%	317	36%	836	16%	112	1.9%	14.2	3.3%	53.3	1.3%
Hi60	490	27%	307	31%	1016	17%	112	3.0%	13.8	4.4%	54.1	1.7%

fracture toughness. In addition to the three fracture toughness properties, Table 6.7 includes the peak load attained during the Mode-I test, the stiffness from the linear portion of the P-δ curve, and the fiber volume fraction for each dataset. The fiber volume fraction results presented in the table are from the top region of the panel, since this is the region of the panel where the fracture specimens were obtained from. There was no direct correlation displayed between any of the six properties in the table.

The mean visual onset fracture toughness ranged from 270 to 490 J/m^2, while the CV ranged from 25 to 47%. The nonlinear method produced more conservative onset fracture toughness results that ranged from 226 to 374 J/m^2, with a similar range in variability (25 to 43%). The propagation fracture toughness results ranged from 836 to 1125 J/m^2, with a CV range of 10-22%. The propagation results are less conservative than either of the two onset results; however, the propagation fracture has a much lower average variability (16%) compared to the visual onset (33%) or the NL onset (33%).

The Mode-I dataset results, grouped by ambient temperature, are presented in the plots in Figure 6.11. The error bars in the plots are ±1 standard deviation. It is worth

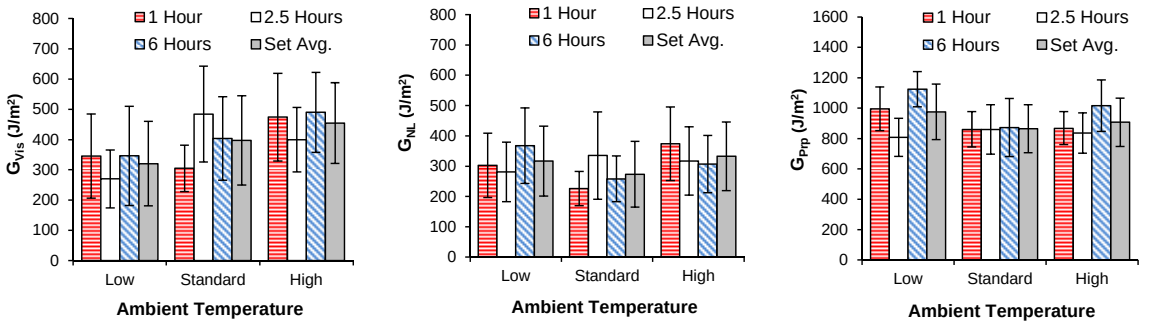

Figure 6.11. Mode-I fracture toughness results for the datasets grouped by ambient temperature: a) visual onset (G_{vis}), b) nonlinear onset (G_{NL}), and c) propagation (G_{prp}).

noting that the scale of the y-axis for the propagation fracture toughness plot (Figure 6.11c) is twice as large as the y-axis of the two onset fracture toughness plots (Figures 6.11a and 6.11b). The mean and CV for the grouped datasets are presented in Table 6.8. In addition to the three fracture properties, the table contains the results for the peak load, the stiffness, and the fiber volume fraction of the grouped datasets. The fiber volume fraction results presented in the table are from the top of the panel, since this is the region of the panel where the fracture specimens were located.

Table 6.8. Fracture results for ambient temperature dataset groupings.

Dataset Grouping	Fracture Toughness (J/m^2)						Peak Load (N)		Stiffness (N/mm)		Fiber Volume Fraction (%)	
	Onset				Propagation							
	Visual		*Non-linear*		*Visual*							
Temp.	*mean*	*CV*	*mean*	*CV*	*mean*	*CV*	*mean*	*CV*	*mean*	*CV*	*mean*	*CV*
Low	320	44%	317	36%	976	19%	115	7.6%	15.2	6.0%	53.9	2.6%
Standard	397	37%	273	40%	864	18%	115	7.2%	15.4	3.8%	53.1	1.9%
High	455	29%	333	34%	907	18%	111	7.0%	14.3	4.7%	53.3	2.1%

Each of the three ambient temperature dataset groupings consisted of 108 fracture specimens and 36 fiber volume fraction specimens

The very large CV exhibited by the onset properties are typical for heavy woven fabric composite specimens that have not been pre-cracked, and are a result of the variation in initial crack location and the unstable crack propagation issues discussed

previously [95]. The general trend in the visual onset fracture toughness was that laminates fabricated at higher ambient temperatures produced larger visual onset fracture values; however, this trend was not consistent across all gel times. There was not a consistent trend in NL onset or propagation fracture toughness properties with respect to ambient temperature.

The ADK ratios for the Mode-I fracture toughness properties are presented in Table 6.9 for the ambient temperature dataset groupings. In addition to the ADK ratios of the complete dataset comparison, the table includes ADK ratios for subset comparisons. This provides for direct comparison of the individual datasets. The visual onset and NL onset both produced statistically discernible differences within each of the ambient temperature dataset groupings; however, the complete dataset comparison at the low temperature dataset grouping for the visual onset and the comparison at the high temperature dataset grouping for the NL onset showed no statistical difference. This is a result of the large CV for both of the onset datasets.

Table 6.9. ADK ratios for ambient temperature dataset groupings of fracture results.

		ADK Ratios								
		Visual Onset			***Nonlinear Onset***			***Propagation***		
Subsets Compared	**Number of Specimens**	**Temperature Data Set**			**Temperature Data Set**			**Temperature Data Set**		
		Lo	Sd	Hi	Lo	Sd	Hi	Lo	Sd	Hi
1.0, 2.5, 6.0	324	0.93	**3.08**	**1.15**	**1.21**	**2.07**	0.90	**6.22**	0.58	**3.37**
1.0 & 2.5	216	**1.36**	**4.55**	**1.13**	0.19	**2.75**	0.88	**4.02**	0.59	0.32
1.0 & 6.0	216	0.15	**2.01**	0.18	0.97	0.65	**1.06**	**2.49**	0.52	**3.28**
2.5 & 6.0	216	0.75	0.81	**1.46**	**1.60**	**1.23**	0.12	**7.78**	0.24	**3.65**

ADK ratios greater than 1.00 indicate that the datasets in the comparison are statistically different.

The Mode-I fracture toughness results for the datasets grouped by gel time are presented in the plots of Figure 6.12. The error bars in the plots are ±1 standard deviation. As in the previous plots, the scale of the y-axis for the propagation fracture toughness

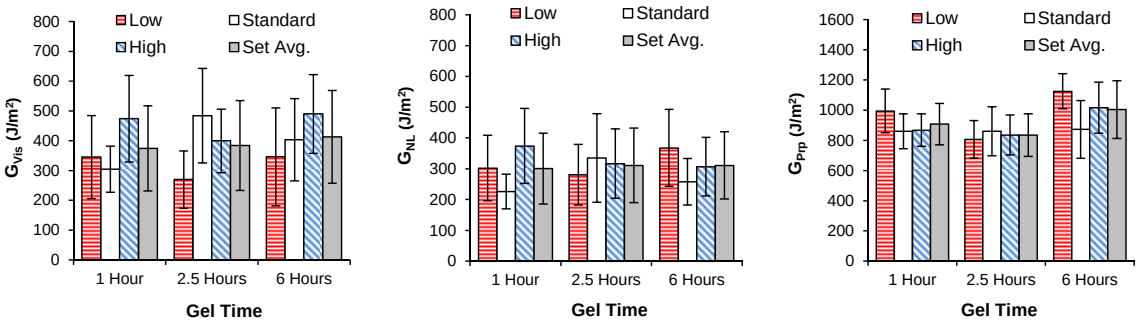

Figure 6.12. Mode-I fracture toughness results for the datasets grouped by gel time: a) visual onset (G_{vis}), b) nonlinear onset (G_{NL}), and c) propagation (G_{prp}).

plot (Figure 6.12c) is twice as large as the y-axis of the two onset fracture toughness plots (Figures 6.12a and 6.12b). The mean and CV for the grouped datasets are presented in Table 6.10. In addition to the three fracture properties, the table contains the results for the peak load, the stiffness, and the fiber volume fraction of the grouped datasets. As in the previous tables on fracture results, the FVF results presented are from the top of the panel, since this is the region where the fracture specimens were located.

Table 6.10. Fracture test results for gel time dataset groupings.

Dataset Grouping	Fracture Toughness (J/m²)						Peak Load (N)		Stiffness (N/mm)		Fiber Volume Fraction (%)	
	Onset				Propagation							
	Visual		Non-linear		Visual							
hours	mean	CV	mean	CV	mean	CV	mean	CV	mean	CV	mean	CV
1.0	375	38%	300	38%	907	15%	113	4.4%	15.0	2.2%	53.1	2.4%
2.5	385	39%	311	39%	834	17%	113	3.9%	15.1	5.3%	53.4	2.1%
6.0	413	38%	311	35%	1004	19%	115	3.9%	14.7	6.0%	53.8	2.2%

NOTE: Each of the three gel time dataset groupings consisted of 108 fracture specimens and 36 fiber volume fraction specimens

The overall trend for the two onset fracture toughness properties was that laminates fabricated with longer gel times produced larger onset fracture values; however, this trend was not consistent across all ambient temperatures. The correlation of FVF of the visual onset dataset groupings is most likely coincidental, since previous

studies have shown that the fracture properties are proportional to the FVF in the region of the crack tip and not the global FVF of the specimen [96, 97]. In addition, the visual onset property did not correlate to the FVF for the individual datasets.

There was not a consistent trend with respect to gel time for the propagation fracture toughness property, nor was there a correlation to the ambient temperature within the gel time dataset groupings. There was no correlation between the propagation fracture toughness and any of the other parameters in the study.

The ADK ratios for the Mode-I fracture toughness properties are presented in Table 6.11 for the gel time dataset groupings. Statistically discernible differences were produced within both of the onset fracture property dataset comparisons, with the 2.5 hour dataset grouping within the NL onset being the only exception. The ADK ratios for visual onset at the 1 and 6 hour dataset groupings support the observed trend that longer gel times produced larger visual onset fracture values. The ADK ratios indicated statistically discernible differences exists for the propagation fracture toughness within the 1 hour and 6 hour gel time dataset comparisons; however, as previously indicated, there was not a direct correlation to the parameters in the study.

Table 6.11. ADK ratios for gel time dataset groupings of fracture results.

		ADK Ratios								
		Visual Onset			***Nonlinear Onset***			***Propagation***		
Subsets Compared	**Number of Specimens**	**Gel Time Data Set**			**Gel Time Data Set**			**Gel Time Data Set**		
		1.0	2.5	6.0	1.0	2.5	6.0	1.0	2.5	6.0
Lo, Sd, Hi	324	**3.28**	**4.76**	**2.08**	**3.45**	0.40	**2.02**	**2.55**	0.73	**3.42**
Lo & Sd	216	0.78	**5.53**	0.74	**1.95**	0.46	**2.57**	**2.76**	0.94	**4.65**
Lo & Hi	216	**2.01**	**4.16**	**2.83**	**1.11**	0.38	0.83	**2.69**	0.36	**1.42**
Sd & Hi	216	**4.88**	**1.01**	**1.23**	**5.04**	0.11	**1.18**	0.08	0.41	**1.77**

ADK ratios greater than 1.00 indicate that the datasets in the comparison are statistically different.

6.5 Conclusions and Recommendations

The effects of resin cure recipe and ambient temperature on the mechanical properties of marine grade polymer composite laminates were investigated. Laminates were fabricated under three ambient temperature conditions, 15.6, 21.1, and 26.7ºC (60, 70, and 80ºF), and using three different gel times (1.0, 2.5 and 6.0 hours). Compression, Mode-I fracture, fiber volume fraction, and Barcol hardness tests were then conducted on specimens prepared from the laminates.

The Barcol hardness results showed a variation in mean hardness of 7.2% from maximum to minimum value, which is almost three times larger than previous values on the same base resin system [79]. This would indicate that some variation due to catalyzing recipe was present even after post curing of the specimens; however, a direct correlation to the parameters under study could not be identified. The datasets fabricated at 21.1ºC (70ºF) produced the largest mean value.

The compression tests produced statistically discernible strength results for a couple of the dataset comparisons, but no consistent trends in the data were identified that could be correlated to the parameters controlled, or measured, during the study. The compression modulus results showed a trend with the 21.1ºC (70ºF) datasets producing the highest values across all three gel times, which were corroborated by the ADK ratio results. While this trend could not be directly correlated to parameters in the study, it was similar to the trend in the Barcol hardness results.

The Mode-I fracture tests produced propagation toughness values (836-1125 J/m^2) that were less conservative than either the visual onset toughness (270-490 J/m^2) or the NL onset toughness (226-374 J/m^2); however, the propagation fracture toughness had

a much lower average coefficient of variation (16%) compared to either the visual onset (33%), or the NL onset (33%) fracture toughness properties.

The ambient temperature dataset groupings produced an overall trend where higher ambient temperatures resulted in larger visual onset fracture toughness values; however, this trend was not consistent across all gel times. There were no trends produced for the NL onset or propagation fracture toughness properties for the ambient temperature dataset groupings. The gel time dataset groupings produced an overall trend where longer gel times resulted in larger visual onset fracture toughness values, which was supported by the ADK ratio results for the 1 hour and 6 hour gel time dataset groupings.

The Mode-I results produced overall trends in the visual onset fracture property, with respect to gel time and ambient temperature, that were shown to be statistically discernible differences. Additionally, there were statistically discernible differences for both the NL onset and propagation fracture properties that could not be directly correlated with the parameters in the study.

While there were several statistically discernible differences in the measured properties investigated in this study, the magnitude of those changes were not as significant as the changes produced due to preform consolidation routine [79], or when using different manufacturers to produce the test panels [78]. This implies that the resin system used during the study has a wide range of acceptable catalyzing recipe formulations that will not greatly affect the overall performance of the final laminates. In addition, it shows that quality control of the vacuum infusion parameters is more

important to the final performance of the laminates than the catalyzing recipe or ambient temperature during the infusion of the laminates.

6.6 References

6.1 Tackitt K D, and Walsh S M (2005) Experimental Study of Thickness Gradient Formation in the VARTM Process. Materials and Manufacturing Processes, 20:607-627.

6.2 Hammami A (2001) Effect of Reinforcement Structure on Compaction Behavior in the Vacuum Infusion Process. Polymer Composites, 22(3):337-348.

6.3 Govignon Q, Bickerton S, Morris J, and Kelly P A (2008) Full Field Monitoring of the Resin Flow and Laminate Properties during the Resin Infusion Process. Composites: Part A, 39:1412-1426.

6.4 Baley C, Davies P, Grohens Y, and Dolto G (2004) Application of Interlaminar Tests to Marine Composites: A Literature Review. Applied Composite Materials, 11:99-126.

6.5 Rigas E J, Mulkern T J, Walsh S M, and Nguyen S P (2001) Effects of Processing Conditions on Vacuum Assisted Resin Transfer Molding Process (VARTM). Army Research Laboratory, Report # ARL-TR-2480, Aberdeen Proving Ground, MD, p.1-20.

6.6 Nguyen L B, Juska T and Mayes J S (1997) Evaluation of Low Cost Manufacturing Technologies for Large Scale Composite Ship Structures. Collection of Technical Papers - AIAA/ASME/ASCE/AHS/ASC Structures, Structural Dynamics and Materials Conference, 2:992-1001.

6.7 Hammami A and Gebart B R (2000) Analysis of Vacuum Infusion Molding Process. Polymer Composites, 21(1):28-40.

6.8 Han K, Jiang S, Zhang C, and Wang B (2000) Flow Modeling and Simulation of SCRIMP for Composites Manufacturing. Composites: Part A, 31:79-86.

6.9 Yenilmez B and Sozer E M (2009) Variation of Part Thickness and Compaction Pressure in Vacuum Infusion Process. Composites Science and Technology, 69:1710-1719.

6.10 Yenilmez B and Sozer E M (2009) Compaction of E-Glass Fabric Preforms in the Vacuum Infusion Process, A - Characterization Experiments. Composites: Part A, 40:499-510.

6.11 Chen B, Lang E J, and Chou TW (2001) Experimental and Theoretical Studies of Fabric Compaction Behavior in Resin Transfer Molding. Materials Science and Engineering, A317:188-196.

6.12 Babu B Z and Pillai K M (2004) Experimental Investigation of the Effect of Fiber-Mat Architecture on the Unsaturated Flow in Liquid Composite Molding. Journal of Composite Materials, 38:57-79.

6.13 Grimsley B W, Hubert P, Song X, Cano R J, Loos A C, and Pipes R B (2001) Flow and Compaction During the Vacuum Assisted Resin Transfer Molding Process. Proceedings of the 33nd International SAMPE Technical Conference - Advancing Affordable Materials Technology, Vol. 33, Seattle, WA, November 5-8, 2001, SAMPE, Covina, CA, 140 -153.

6.14 Abadie M J M, Mekhissi K, and Burchill P J (2002) Effects of Processing Conditions on the Curing of a Vinyl Ester Resin. Journal of Applied Polymer Science, 84(6):1146-1154.

6.15 Vaidya U K, Jadhav N C, Hosur M V, Gillespie Jr. J W, and Fink B K (2000) Assessment of Flow and Cure Monitoring Using Direct Current and Alternating Current Sensing in Vacuum-Assisted Resin Transfer Molding. Smart Materials and Structures, 9(6):727-736.

6.16 Cao X and Lee LJ (2003) Control of Shrinkage and Final Conversion of Vinyl Ester Resins Cured in Low-Temperature Molding Processes. Journal of Applied Polymer Science, 90(6):1486-1496.

6.17 Dua S, McCukkough R L, Palmese G R (1999) Copolymerization Kinetics of Styrene/Vinyl- Ester Systems: Low Temperature Reactions. Polymer Composites 20(3):379-391.

6.18 Cook W D, Simon G P, Burchill P J, Lau M, and Fitch T J (1997) Curing Kinetics and Thermal Properties of Vinyl Ester Resins. Journal of Applied Polymer Science, 64(4):769-781.

6.19 Aranguren M I, Elicabe G, Borrajo J, and Auad ML (1999) Curing Kinetics of Divinyl Ester Resins With Styrene. Journal of Applied Polymer Science, 74(5):1044-1053.

6.20 Karbhari VM (1998) Effect of Internal Mold Release Agent on the Cure and Property Variation in Resin Transfer Molding Composites. Journal of Materials Science Letters, 17(24):2061-2062.

6.21 Li L and Lee L J (2002) Effects of a Chelating Agent - 2,4-Pentanedione on Low Temperature Composite Molding of Vinyl Ester and Unsaturated Polyester Resins. Polymer Composites, 23(6):971-990.

6.22 Li L and Lee L J (2001) Effects of Inhibitors and Retarders on Low Temperature Free Radical Crosslinking Polymerization Between Styrene and Vinyl Ester Resin. Polymer Engineering and Science, 41(1):53-65.

6.23 Starr B C (2001) Inter-Relationships Between Chemistry, Network Structure and Properties of Chain Growth Dimethacrylate Thermosets. Ph.D Dissertation, Virginia Polytechnic Institute and State University, Blacksburg, VA, p.85-103.

6.24 Fink B K, Bogetti T A, Stone M A and Gillespie Jr. J W (2002) Thermochemical Response of Vinyl-Ester Resin. Army Research Laboratory, Report # ARL-TR-2653, Aberdeen Proving Ground, MD, p.1-25.

6.25 Zhao L, Cordovez M and Karbhari V M (2001) Exothermic Temperature History in the Processing of Resin Infused Composite Structural Components. Applied Composite Materials, 8:99-131.

6.26 Flores F, Gillespie Jr. J W, and Bogetti T A (2002) Experimental Investigation of the Cure-Dependent Response of Vinyl Ester Resin. Polymer Engineering and Science, 42(3):582-590.

6.27 Cummings L C (1983) Application of Differential Scanning Calorimetry to Cure Optimization and Quality Control of a Vinyl Ester Resin. Polymer Composites, 4(4):201-205.

6.28 Kim Y K and Daniel I M (2002) Cure Cycle Effect on Composite Structures Manufactured by Resin Transfer Molding. Journal of Composite Materials, 36:1725-1743.

6.29 Li P, Yang X, Yu Y, and Yu D (2004) Cure Kinetics, Microheterogeneity, and Mechanical Properties of the High-Temperature Cure of Vinyl Ester Resins. Journal of Applied Polymer Science, 92(2):1124-1133.

6.30 Kootsookos A and Burchill P J (2004) Effect of the Degree of Cure on the Corrosion Resistance of Vinyl Ester/Glass Fibre Composites. Composites Part A, 35(4):501-508.

6.31 Ziaee S and Palmese G R (1999) Effects of Temperature on Cure Kinetics and Mechanical Properties of Vinyl-Ester Resins. Journal of Polymer Science Part B: Polymer Physics, 37(7):725-744.

6.32 Brill R P and Palmese G R (2000) An Investigation of Vinyl-Ester/Styrene Bulk Copolymerization Cure Kinetics Using Fourier Transform Infrared Spectroscopy. Journal of Applied Polymer Science 76:1572-1582.

6.33 Li L, Sun X, and Lee L J (1999) Low Temperature Cure of Vinyl Ester Resins. Polymer Engineering and Science, 39(4):646-661.

6.34 Martin J S, Laza J M, Morras M L, Rodriguez M and Leon L M (2000) Study of the Curing Process of a Vinyl Ester Resin by Means of TSR and DMTA. Polymer, 41(11):4203-4211.

6.35 Ruiz, E and Trochu, F (2005) Thermomechanical Properties During Cure of Glass-Polyester RTM Composites: Elastic and Viscoelastic Modeling. Journal of Composite Materials, 39:881-916.

6.36 Fink B K, Dorairaj M B, and Gillespie Jr. J W (2001) Vinyl-Ester Cure Characterization Via Direct Current Sensors. Army Research Laboratory, Report # ARL-TR-2441, Aberdeen Proving Ground, MD, p.1-82.

6.37 Valea A, Martinez I, Gonzalez M L, Eceiza A, and Mondragon I (1998) Influence of Cure Schedule and Solvent Exposure on the Dynamic Mechanical Behavior of a Vinyl Ester Resin Containing Glass Fibers. Journal of Applied Polymer Science, 70(13):2595-2602.

6.38 Cain J J, Post N L, Lesko J J, Case S W, Lin Y, Riffle J S, and Hess P E (2006) Post-Curing Effects on Marine VARTM FRP Composite Material Properties for Test and Implementation. Journal of Engineering Materials and Technology, Transactions of the ASME, 128:34-40.

6.39 Michaud D J, Beris A N, and Dhurjati P S (1998) Curing Behavior of Thick-Sectioned RTM Composites. Journal of Composite Materials, 32:1273-1296.

6.40 Auad M L, Frontini P M, Borrajo J and Aranguren M I (2001) Liquid Rubber Modified Vinyl Ester Resins: Fracture and Mechanical Behavior. Polymer, 42(8):3723-3730.

6.41 Cardona S C, Ziaee S, and Advani S G (2002) Spatially Homogeneous Gelation in Liquid Composite Molding. Polymer Engineering and Science, 42(8):1667-1673.

6.42 Burts E (2000) Structure and Properties of Dimethacrylate-Styrene Resins and Networks. Ph.D Dissertation, Virginia Polytechnic Institute and State University, Blacksburg, VA, p.1-172.

6.43 Li H, (1998) Synthesis, Characterization and Properties of Vinyl Ester Matrix Resins. Ph.D Dissertation, Virginia Polytechnic Institute and State University, Blacksburg, VA, p.30-150.

6.44 Karbhari V M and Simacek P (1996) Notes on the Modeling of Preform Compaction: II-Effect of Sizing on Bundle Level Micromechanics. Journal of Reinforced Plastics and Composites, 15(8):837-861.

6.45 Marston C, Gabbitas B, and Adams J (1997) Effect of Fibre Sizing on Fibres and Bundle Strength in Hybrid Glass Carbon Fibre Composites. Journal of Materials Science, 32(6):1415-1423.

6.46 Kim J K, Sham M L, Sohn M S, and Hamada H (2001) Effect of Hybrid Layers With Different Silane Coupling Agents on Impact Response of Glass Fabric Reinforced Vinyl Ester Matrix Composites. Polymer, 4:7455-7460.

6.47 Tanoglu M, Mcknight S H, Palmese G R and Gillespie J W (2001) Effects of Glass-Fiber Sizings on the Strength and Energy Absorption of the Fiber/Matrix Interphase Under High Loading Rates. Composites Science Und Technology, 61(2):205-220.

6.48 Upadhyaya D and Tsakiropoulos P (1995) Evaluation of the Effect of Sizing Levels on Transverse Flexural and Shear Strengths of Carbon/Epoxy Composites. Journal of Materials Processing Technology, 54:17-20.

6.49 Jensen R E and Mcknight S H (2002) Strength and Durability of Glass Fiber Composites Treated With Multi-Component Sizing Formulations. Army Research Laboratory, Report # ARL-TR-2655, Aberdeen Proving Ground, MD, p.1-18.

6.50 Karbhari V M and Lee R (2002) On the Effect of E-Glass Fiber on the Cure Behavior of Vinylester Composites. Journal of Reinforced Plastics and Composites, 21:901-918.

6.51 Palmese G R, Andersen O A, and Karbhari V M (1999) Effect of Glass Fiber Sizing on the Cure Kinetics of Vinyl-Ester Resins. Composites Part A, 30(1):11-18.

6.52 Peters P W M and Springer G S (1987) Effects of Cure and Sizing on Fiber-Matrix Bond Strength. Journal of Composite Materials, 21(1):157-171.

6.53 Ikuta N, Yanagawa A, Suzuki Y, and Ochiai S (2001) Investigation on Resin Interphase Produced Near Silane-Treated Glass Fiber in Vinyl Ester Resin. Composite Interfaces, 8(2):121-125.

6.54 Karbhari V M and Palmese G R (1997) Sizing Related Kinetic and Flow Considerations in the Resin Infusion of Composites. Journal of Materials Science, 32:5761-5774 .

6.55 Karbhari V M and Kabalnova L (2001) Effect of Sizing and Loading Levels on the Cure Kinetics of Carbon Fiber Vinylester Composites. Journal of Reinforced Plastics and Composites, 20(2):90-104.

6.56 Saidpour S H and Richardson M W (1997) Glass Fibre Coating for Optimum Mechanical Properties of Vinyl Ester Composites. Composites Part A, 28A:971-975.

6.57 Hirai Y, Hamada H, and Kim J K (1998) Impact Response of Woven Glass-Fabric Composites - I Effect of Fibre Surface Treatment. Composites Science and Technology, 58:91-104.

6.58 Thomason J L (1995) Interface Region in Glass Fibre-Reinforced Epoxy Resin Composites: Characterization of Fibre Surface Coatings and the Interphase. Composites, 26(7):487-498.

6.59 Zinck P, Pay M F, Rezakhanlou R, and Gerard J F (1999) Mechanical Characterization of Glass Fibres as An Indirect Analysis of the Effect of Surface Treatment. Journal of Materials Science, 34(9):2121-2133.

6.60 Kessler A and Bledzki A (2000) Correlation Between Interphase-Relevant Tests and the Impact-Damage Resistance of Glass/Epoxy Laminates With Different Surface Treatments. Composites Science Und Technology, 60:125-130.

6.61 Robertson M A E, Bump M B, Verghese K E, Mccartney S R, Lesko J J, Riffle J S, Kim I C and Yoon T H (1999) Designed Interphase Regions in Carbon Fiber Reinforced Vinyl Ester Matrix Composites. Journal of Adhesion, 71(4):395-416.

6.62 Alvarez V A, Valdez M E, and Vazquez A (2003) Dynamic Mechanical Properties and Interphase Fiber/Matrix Evaluation of Unidirectional Glass Fiber/Epoxy Composites. Polymer Testing, 22(6):611-615.

6.63 Tanoglu, M, Mcknight S H, Palmese G R and Gillespie Jr. J W (2001) Dynamic Stress/Strain Response of the Interphase in Polymer Matrix Composites. Polymer Composites, 22(5):621-635.

6.64 Yang F and Pitchumani R (2004) Effects of Interphase Formation on the Modulus and Stress Concentration Factor of Fiber-Reinforced Thermosetting-Matrix Composites. Composites Science and Technology, 64:1437-1452.

6.65 Madhukar M S and Drzal L T (1992) Fiber-Matrix Adhesion and Its Effect on Composite Mechanical Properties. III Longitudinal (0°) Compressive Properties of Graphite/Epoxy Composites. Journal of Composite Materials, 26(3):310-333.

6.66 Madhukar M S and Drzal L T (1992) Fiber-Matrix Adhesion and Its Effect on Composite Mechanical Properties: IV Mode I and Mode II Fracture Toughness of Graphite/Epoxy Composites. Journal of Composite Materials, 26(7):936-968.

6.67 Zhang G and Latour Jr. RA (1993) FRP Composite Compressive Strength and Its Dependence Upon Interfacial Bond Strength, Fiber Misalignment, and Matrix Nonlinearity. Journal of Thermoplastic Composite Materials, 6(10):298-311.

6.68 Deng S and Ye L (1999) Influence of Fiber-Matrix Adhesion on Mechanical Properties of Graphite/Epoxy Composites: II Interlaminar Fracture and Inplane Shear Behavior. Journal of Reinforced Plastics and Composites, 18:1041-1057.

6.69 Mcdonough W G, Dunkers J P, Holmes G A, Feresenbet E, Kim Y H and Parnas R S (2002) Influence of Processing Rate and Formulation on the Interface Strength of Vinyl Ester/E-Glass Composites. Polymer Composites, 23(2):274-283.

6.70 Thomason J L (1995) Interface Region in Glass Fibre-Reinforced Epoxy Resin Composites: Sample Preparation, Void Content and Interfacial Strength. Composites 26:467-475.

6.71 Kim J K and Hodzic A (2003) Nanoscale Characterization of Thickness and Properties of Interphase in Polymer Matrix Composites. Journal of Adhesion, 79:383-414.

6.72 Wu H F, Dwight D W, and Huff N T (1997) Effects of Silane Coupling Agents on the Interphase and Performance of Glass-Fiber-Reinforced Polymer Composites. Composites Science and Technology, 57(8):975-983.

6.73 Broyles N S, Verghese K N E, Davis S V, Li H, Davis R M, Lesko J J, and Riffle J S (1998) Fatigue Performance of Carbon Fibre/Vinyl Ester Composites: The Effect of Two Dissimilar Polymeric Sizing Agents. Polymer, 39(15):3417-3424.

6.74 Tanoglu M, Ziaee S, Mcknight S H, Palmese G R, and Gillespie J W (2001) Investigation of Properties of Fiber/Matrix Interphase Formed Due to the Glass Fiber Sizings. Journal of Materials Science, 36(12):3041-3053.

6.75 Juska T and Mayes S (1995) Post-Cure Study of Glass/Vinyl Ester Laminates Fabricated by Vacuum Assisted Resin Transfer Molding. Naval Surface Warfare Center, Carderock Division, Report # CARDIVNSWC-SSM-64-94/18, Bethesda, MD, p.1-17.

6.76 Kumar C R, Radhakrishna K, and Rao, R M (2005) Postcuring Effects on Impact Behavior of Glass/Epoxy Composite Laminates. Journal of Reinforced Plastics and Composites, 24(6):949-960.

6.77 Tucker R, Compston P, and Jar P-YB (2001) The Effect of Post-Cure Duration on the Mode I Interlaminar Fracture Toughness of Glass-Fibre Reinforced Vinylester. Composites: Part A, 32:129-134.

6.78 Berube K A and Lopez-Anido R A (2010) Variability in the Material Properties of Polymer Matrix Composites for Marine Structures. Journal of ASTM International 7(4):18p.

6.79 Berube K A and Lopez-Anido R A (2011) Effect of Preform Consolidation on the Fracture Toughness of Marine Grade Polymer Matrix Composite Materials Fabricated With a VARTM Process. Journal of Advanced Materials 43(1):30-48.

6.80 El-Chiti F (2005) Experimental Variability of E-Glass Reinforced Vinyl Ester Composites Fabricated by VARTM/SCRIMP. MS Thesis in Mechanical Engineering, University of Maine, Orono, ME.

6.81 Berube K A and Lopez-Anido R A, Caccese V, and Hess P (2006) Variability in Flexural Response of E-Glass/Vinyl Ester Composites Fabricated Using the VARTM Process. Proceedings of the 51st International SAMPE Symposium and Exhibition, Creating New Opportunities for the World Economy, April 30-May 4, 2006, Long Beach, CA, p.1-11.

6.82 Al-Assafi S, (2004) Thermal Analysis of Initiator Systems for High-Temperature-Cure Composites. Composites Part A, 5:1027-1031.

6.83 ASTM Standard D5528 (2001) Standard Test Method for Mode I Interlaminar Fracture Toughness of Unidirectional Fiber-Reinforced Polymer Matrix Composites. ASTM International, West Conshohocken, PA, www.astm.org.

6.84 Blake S P (2010) Crack Propagation in Secondary Bonded FRP Composite Joints. MS Thesis in Civil Engineering, University of Maine, 141p.

6.85 Dharmawan F, Simpson G, Herszberg I, and John S (2006) Mixed Mode Fracture Toughness of GFRP Composites. Composite Structures, 75:328-338.

6.86 ASTM Standard D6641 (2009) Standard Test Method for Determining the Compressive Properties of Polymer Matrix Composite Laminates Using a Combined Loading Compression (CLC) Test Fixture. ASTM International, West Conshohocken, PA, www.astm.org.

6.87 ASTM Standard D3171 (2006) Standard Test Methods for Constituent Content of Composite Materials. ASTM International, West Conshohocken, PA, www.astm.org.

6.88 Li J, Zhang C, Liang R, Wang B, and Walsh S (2008) Modeling and Analysis of Thickness Gradient and Variations in Vacuum-Assisted Resin Transfer Molding Process. Polymer Composites, 29:473-482.

6.89 ASTM Standard D2583 (2004) Standard Test Method for Indentation Hardness of Rigid Plastics by Means of a Barcol Impressor. ASTM International, West Conshohocken, PA, www.astm.org.

6.90 MIL-HDBK-17F-1 (2002) Composite Materials Handbook Volume 1 - Polymer Matrix Composites Guidelines for Characterization of Structural Materials, ASTM International, West Conshohocken, PA, p.8.29-31.

6.91 Compston P and Jar P-Y B (1998) Comparison of Interlaminar Fracture Toughness in Unidirectional and Woven Roving Marine Composites. Applied Composite Materials, 5(3):189-206.

6.92 Chen B and Chou T (2000) Compaction of Woven-Fabric Preforms: Nesting and Multi-Layer Deformation. Composites Science and Technology, 60:2223-2231.

6.93 Kotaki M, and Hamada H, (1997) Effect of Interfacial Properties and Weave Structure on Mode I Interlaminar Fracture Behavior of Glass Satin Woven Fabric Composites. Composites Part A, 28A:257-266.

6.94 Suppakul P and Bandyopadhyay S (2002) The Effect of Weave Pattern on the Mode-I Interlaminar Fracture Energy of E-Glass/Vinyl Ester Composites. Composites Science and Technology, 62:709-717.

6.95 Naik N K, Reddy K S, Meduri S, Raju N B, Prasad PD, Azad SK N M, Ogde PA and Reddy B C K (2002) Interlaminar Fracture Characterization for Plain Weave Fabric Composites. Journal of Materials Science, 37:2983-2987.

6.96 Gill A F, Robinson P, and Pinho S (2009) Effect of Variation in Fibre Volume Fraction on Modes I and II Delamination Behaviour of 5HS Woven Composites Manufactured by RTM. Composites Science and Technology, 69:2368-2375.

6.97 Compston P and Jar P-YB (1999) The Influence of Fibre Volume Fraction on the Mode I Interlaminar Fracture Toughness of a Glass-Fibre/Vinyl Ester Composite, Applied Composite Materials, 6:353-368.

CHAPTER 7

EFFECT OF FIBER PREFORM CONDITIONING ON THE PROPERTIES OF MARINE GRADE POLYMER COMPOSITES

7.1 Abstract

Woven roving E-glass fabric was conditioned at two different environments prior to fabricating e-glass/vinyl-ester composite laminates to investigate mechanical property variations due to fabric sizing degradation. The first environment was a control at 21°C (70°F) and 50% relative humidity and the second was at 32°C (90°F) and 80% relative humidity. The elevated temperature and humidity conditioning was meant to simulate what could occur to fabric during the lay-up of a large part where the fabric could be exposed to the ambient environment for an extended period of time prior to infusion.

Standardized testing for fiber volume fraction, compression, Mode-I fracture, and Barcol hardness were performed on test specimens from each composite panel fabricated for both of the environmental conditions. Barcol hardness exhibited the most variability both within and between the conditioning datasets; however, this is typical for thermoset polymers. Fiber volume fraction results were consistent with prior studies for this material system with minor variations attributed to infusion variations and not related to conditioning. Compression and Mode-I fracture properties were consistent with previous studies and indicated no statistical variation between fabric conditioning. The results of the testing indicate that the elevated conditioning had negligible effect on the material properties investigated in this study.

7.2 Introduction

E-glass fiber sizings are multipurpose coatings usually containing silane. The intent of the coatings is aimed at protecting the fiber from damage during processing and handling and increasing the quality of fiber-matrix adhesion [1], but they have also been shown to produce gradients in material properties and affect processing conditions and resin cure [2-5]. The chemical composition of the sizing can also influence the failure properties and hygrothermal stability [6]. The composition of the sizings varies and has been investigated by several authors [7], but most of the formulations are proprietary, making repeated investigations difficult. Therefore, there is a lack of information regarding mechanical properties and morphology of the sizing layer produced during industrial processing. In addition, little has been established regarding the exact corrosion mechanisms of sizings in various environmental conditions [8].

During the fabrication of large composite parts, fabric reinforcements can be placed in the mold days or weeks prior to the actual infusion of the part, making them susceptible to whatever the ambient conditions may be. Information on the effects of moisture absorbed from the environment by glass fibers is hardly available in the literature [9]. While it is known that fabric environmental storage conditions as well as age, can affect sizings [10], degradation of the sizing layer due to environmental exposure of the fabrics prior to composite fabrication has not been thoroughly investigated.

In this study woven roving E-glass fabric was environmentally conditioned prior to fabricating e-glass/vinyl-ester composite laminate panels to investigate possible variations in composite mechanical properties due to degradation of the fabric sizing.

7.3 Experimental Methods

7.3.1 Fabric Conditioning

The woven roving fabric was conditioned in an environmentally controlled chamber at the Advanced Manufacturing Center at the University of Maine, Orono, Maine. Conditioning a roll of E-glass fabric would have required a long period of time, since the moisture diffusion rate through the tightly rolled layers of fabric would have been very slow [11] and would not have resulted in uniform conditioning of the entire lot of material required to fabricate the panels for each condition. To accelerate the exposure rate and provide uniform conditioning [12], the fabric was cut from the roll and hung in the chamber where it was constantly exposed to the chamber environment, as shown in Figure 7.1. As seen in the figure, a layer of polyethylene vacuum bag material was placed over the fabric. This minimized the exposure to dust and debris without preventing exposure to the surrounding conditioned environment. The E-glass sheets were conditioned in the chamber for ten days at the selected environment followed by three days at 70°F and 50% RH. The conditioning matrix is presented in Table 7.1.

Figure 7.1. Fabric hanging in conditioning chamber.

Table 7.1. Environmental conditioning matrix.

Dataset *Id*	Conditioning °C - °F (RH)	Duration *Days*
7050	21 - 70 (50%)	10
	21 - 70 (50%)	3
9080	32 - 90 (80%)	10
	21 - 70 (50%)	3

The first environment was a control at 21°C (70°F) and 50% relative humidity and the second was at 32°C (90°F) and 80% relative humidity. The elevated temperature and humidity conditioning was meant to simulate what could occur to fabric during the lay-up of a large part where the fabric could be exposed to the ambient environment for an extended period of time prior to infusion.

7.3.2 Panel Fabrication

The FRP panels consisted of an E-glass/vinyl-ester system. The reinforcement was a Saint-Gobain Vetrotex E-324 woven roving with a weight per unit area of 814 g/m^2 (24 oz/yd^2). It is a plain weave fabric with a tow spacing of 5.1 mm (0.2 in.) in the warp direction, and 6.4 mm (0.25 in.) in the fill direction. The polymer resin used was Ashland Derakane 8084, which is an elastomer-modified epoxy vinyl-ester resin.

The FRP panel dimensions were 610 by 965 mm (24 by 38 in.) with a nominal thickness of 6.4 mm (0.25 in.). The lay-up notation is $[0_{10}]_f$, where the orientation indicates the warp direction of the E-glass fabric. The dimensions of the panel were selected such that a second set of specimens could be obtained from the panel if issues arose with the original set of specimens during specimen preparation or testing. This reduced the possibility of increased variability resulting from fabricating a 2nd set of panels at a later date. Additionally, the same panel size was used throughout the entire

larger study to allow a comparison of the results between all phases of the study without having panel size as a manufacturing variable.

An 89 mm (3.5 in.) wide strip of 0.0127 mm (0.0005 in.) thick virgin polytetrafluoroethylene (PTFE) film was placed at the mid-plane of the laminate along the edge of the panel, as shown in Figure 7.2. The PTFE film provided the initial crack length required for the Mode-I fracture test specimens.

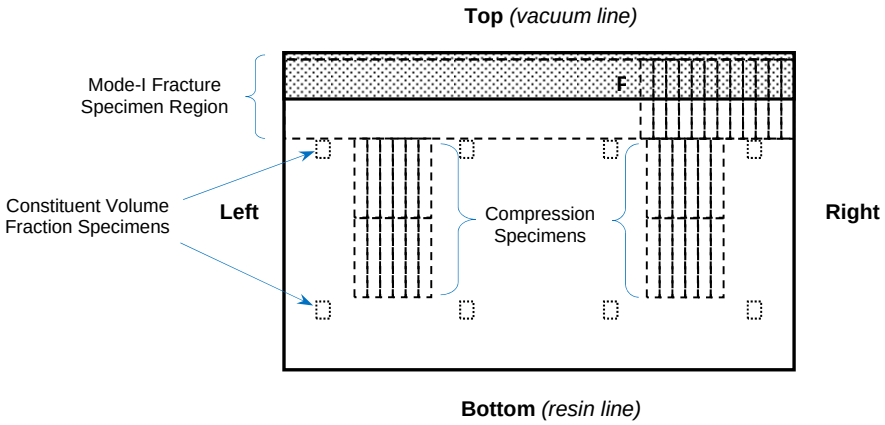

Figure 7.2. Schematic of panel indicating panel orientation and specimen locations.

Prior phases of the larger study indicated that a time of 45 minutes was sufficient to entirely wet-out the panels; however, a gel time of 2.5 hours had been shown to produce the most consistent results in properties and better dimensional uniformity [13]. The catalyzing recipe that provided a 2.5 hour gel time consisted of 1.5% MEKP 925 (Norox), 0.3% Cobalt 6% Naphthenate (Puritan Products), 0.5% DMA (Puritan Products), and 0.1% 2,4-Pentanedione (J.T. Baker).

An infusion control system was implemented during the fabrication of the composite panels which allowed for the precise control and monitoring of the infusion pressure, the ambient conditions, and the resin temperature during the infusion process.

The fabrication procedure that was used for all infusions was as follows.

- Lay up the fabric and place the PTFE film
- Bag the panel and pull vacuum
- Adjust regulator to stabilize pressure at 0.982 bar (29 in-Hg)
- Hold vacuum at target pressure for 2.5 hours to consolidate fabric preform [14]
- Add catalyzing recipe to resin 15 min before end of consolidation time
- At end of consolidation period, open resin line
- After the panel has wet-out, clamp off the resin and vacuum lines

Three replicates were fabricated for each of the two combinations of temperature and relative humidity, for a total of six panels fabricated during the study. The panels were fabricated over a period of eight days. All of the resin, the glass fabric, and the chemicals used for the catalyzing recipes came from single lots. The panels were post-cured at 82ºC (180ºF) for 4 hours, which had been shown to be appropriate for this material system at this thickness in an earlier phases of the study [13-15].

7.3.3 Test Methods

The experimental testing conducted during the study included Mode-I fracture, compression, constituent volume fraction, and Barcol hardness. The Mode-I fracture test was selected as an indicator of the fiber/resin interaction strength [16-20]. The compression test was a standard test that was performed throughout the larger study [13-14] and has also been shown to indicate fiber matrix adhesion properties [21]. Constituent volume fraction is a good indicator of the consistency of the consolidation of the preform, and a general predictor of fiber dominated material properties [22]. Barcol hardness was

used as a means to verify the consistency of the resin gelation after room temperature curing and after the post-cure process [23-25].

Mode-I fracture properties were obtained in accordance with ASTM test standard D5528 [26]. ASTM D5528 uses a double cantilever beam (DCB) configuration for the test specimens. The specimen dimensions were 25.4 by 152.4 mm (1.0 by 6.0 in.) with an initial crack length of 49 mm (1.9 in.). The edge of each specimen was marked in 1-mm increments over a span of 55 mm (2.2 in.) to identify crack growth. Twelve specimens were cut from each panel in the region indicated in Figure 7.2, using CNC water-jet abrasive machining. The corrected Modified Beam Theory (MBT) was used to calculate the fracture toughness, G_I, as given by the Equation 1.

$$G_I = \frac{3P\delta}{2b(a+|\Delta|)}F \tag{1}$$

where:

P is the applied load,

δ is the load point displacement,

b is the specimen width,

a is the crack length,

Δ is a correction factor to account for beam rotation at the crack front, and

F is a correction factor to account for large deflections.

The Mode-I fracture toughness properties computed in the study were the visual onset fracture toughness (G_{vis}), the nonlinear onset fracture toughness (G_{NL}), and the propagation fracture toughness (G_{prp}).

The specimens were tested on a 25 kN (5.6 kip) Instron servo hydraulic test frame equipped with a 250 N (56.2 lb) load cell and hydraulic grips. The tests were conducted

in displacement control at a rate of 2.5 mm/min (0.1 in/min) without pre-cracking the specimens. Crack onset was detected both visually and through the use of a numerical routine to determine the point of nonlinear (NL) onset. The visual detection was performed using a digital image acquisition system, which collected data at a sampling rate of 1 Hz. The digital images were post-processed to identify visual onset and crack growth increments of 1 mm or greater. The load, displacement, and crack length at each occurrence was recorded. The NL onset was determined by locating the point at which the load-deflection (P-δ) curve became nonlinear. When implemented correctly this method produces repeatable and consistent results [13, 14, 27].

The Mode-I propagation fracture toughness values were computed using the region of the resistance curve (R-curve) where the fracture toughness had stabilized to compute the mean propagation fracture toughness [28]. Using this method produces a less conservative propagation fracture toughness value, because it discards the lower values computed prior to R-curve stabilization; however, it produces less variability in the results.

The compression properties were obtained in accordance with ASTM D6641 [29]. A three-dimensional digital image correlation (DIC) system was used to measure strain during testing. The DIC system provides an advantage over conventional foil gages, since it is able to monitor a larger area of the specimen during testing. This is advantageous when testing heavy woven fabric composites [30, 31]. Twelve compression specimens were cut from each of the panels in the region indicated in Figure 7.2, using CNC water-jet abrasive machining. The test specimen size was 25.4 by 152.4 mm (1.0 by 6.0 in.). This length allows the specimens to fail in compression and provides a larger specimen

viewing area for the DIC system [30, 31]. The specimens were tested on a 100 kN (22.5 kip) Instron servo hydraulic test frame equipped with a 100 kN (22.5 kip) load cell and hydraulic grips. The specimens were tested in displacement control at a crosshead rate of 0.01 mm/sec (0.0004 in/sec). This produced a test duration of approximately 5 minutes. Load and crosshead displacement data were recorded at a sampling rate of 10 Hz on the Instron control computer and at 1 Hz on the DIC system. This sampling rate is sufficient to capture the strain results in the compression specimens [14, 30, 31].

The constituent volume fraction properties of the specimens were obtained in accordance with ASTM test standard D3171 [32]. Eight specimens were cut from each of the panels, as indicated in Figure 7.2, using CNC water-jet abrasive machining. The specimens were distributed around the panel to capture spatial variations of the volume fraction resulting from thickness gradients, which can occur in the infusion direction [33-35]. The nominal specimen dimensions were 25.4 by 35.0 mm (1.0 by 1.38 in.) with a nominal mass of 11.0 grams (0.39 oz). The resin burn-off method was performed in a muffle furnace at a temperature of 565ºC (1049ºF) for a period of 2.5 hours, which had shown to be sufficient for complete resin removal [13, 14, 30, 31].

Barcol hardness properties of the resin samples were obtained in accordance with ASTM test standard D2583 [36]. This was used as a means to quantify any variation of the material properties of the resin from each infusion. Five samples from each of the six infusions were cut into 6.4 mm (0.25 in.) thick specimens. Fifteen Barcol hardness measurements were performed on each of the specimens before and after post-curing. The post-cure procedure for the resin specimens was identical to that used on the composite test specimens.

7.3.4 Data Analysis Procedure

The data from each of the three replicate panels were grouped and treated as a single dataset for the comparative analysis implemented. After verifying normality of the dataset distributions using the Anderson-Darling method, the mean and coefficient of variation (CV) were computed for each material property investigated. The k-sample Anderson-Darling (ADK) method was used to determine if the results from each material property dataset were statistically discernible for the two environmental conditions [22]. The ADK method is the method recommended in the Composite Materials Handbook (MIL-17) to screen for pooling of datasets and was implemented throughout the different phases of the larger study [14, 30]. If the calculated ADK value for the dataset is less than the standard critical value, then one can conclude with a 2.5 percent risk of being in error, that the groups were drawn from the same population. The ratio of the computed value to critical value was calculated as a means to determine the level to which the datasets were statistically discernible. This ADK ratio is tabulated and presented for each dataset comparison in the discussion of the results.

The Maximum Normed Residual (MNR) method was used to identify outliers [22]; however, there were no outliers identified in any of the datasets.

7.4 Results

7.4.1 Barcol Hardness Results

The results of the Barcol hardness tests are presented in the plot in Figure 7.3. The plot includes the mean hardness value for each of the datasets, both before and after post-curing the specimens. The error bars are ±1 standard deviation. The statistical results for the post-cured specimens are presented in Table 7.2. The table includes the mean, CV,

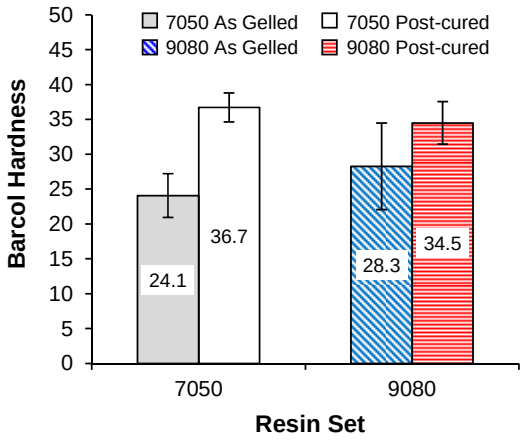

Figure 7.3. Barcol hardness results.

Table 7.2. Barcol hardness statistical results.

Dataset *Id*	mean *#*	CV *%*	ADK Ratio
7050	36.7	5.7	***2.09***
9080	34.5	8.9	***4.13***
Total	35.8	7.7	***2.87***

Note: ADK ratios < 1 indicate no statistically discernible difference between datasets

and ADK ratio for each of the datasets as well as the combined results. The post-cured hardness results were in the range of 34-37 with a CV of 5-9%, which is typical for this resin system [13, 14]. The ADK ratios less than 1.0 indicate that the data is not from the same population; however, the scatter in the data is typical for Barcol hardness testing of thermoset polymers, due to the heterogeneity of the polymerized structure.

7.4.2 Constituent Volume Fraction Results

The results of the fiber volume fraction (FVF) tests are presented in the plot in Figure 7.4, and the statistical results are presented in Table 7.3. The FVFs were computed using a resin density of 1.13 g/cm^3 (0.653 oz/in^3) and a glass density of 2.54 g/cm^3 (1.47 oz/in^3). It is worth noting that the results in Figure 7.4 are plotted with a y-axis range of 40-60% for clarity, and that the error bars are ±1 standard deviation.

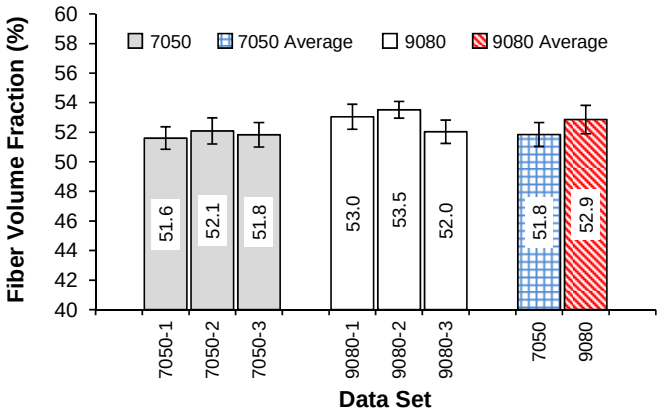

Figure 7.4. Fiber volume fraction results.

Table 7.3. Fiber volume fraction statistical results.

Dataset *Id*	mean *%*	CV *%*	ADK Ratio
7050	51.8	1.6	0.30
9080	52.9	1.8	***1.35***
Total	52.4	1.9	***2.10***

Note: ADK ratios < 1 indicate no statistically discernible difference between datasets

As seen in the figure and table, the specimens in dataset 9080 had higher fiber volume fractions than dataset 7050 (1.1 percentage-points on average), with both datasets producing CV less than 2%. Dataset 9080-3 took 20% longer to wet-out the fabric preform during infusion which is the most likely cause of the noticeably lower FVF for that dataset as compared to the other two in that series. It also resulted in an ADK ratio greater than 1.0 for the 9080 dataset grouping.

The spatial distribution of the FVF in the panels was also investigated in this study. The spatial distribution results for the dataset groupings are presented in the plots of Figure 7.5. The orientation of the spatial locations listed in the figure refers to the orientation presented in Figure 7.2. The FVF at each spatial location in the panel is the mean of the four FVF specimens in that spatial location. As in the previous figure, the data is plotted with a y-axis range of 40-60% and the error bars are ±1 standard deviation.

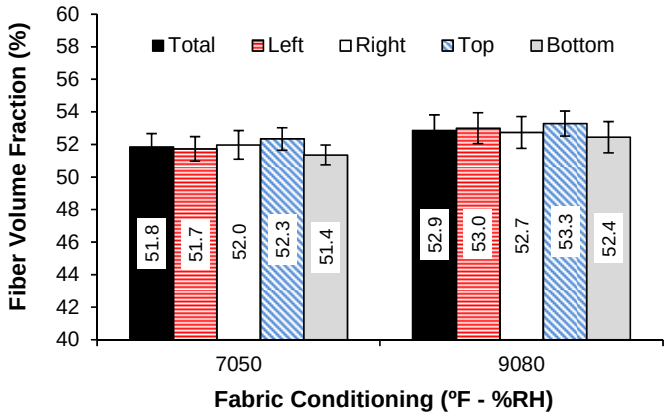

Figure 7.5. Spatial distribution of FVF results.

There was a noticeable, yet minor difference (0.9 percentage-points) in the FVF in the infusion direction, which is of the same magnitude as found in previous studies [13, 14, 30]. This is a result of a relaxation of the fiber preform after the resin front arrives at that position in the preform during the infusion and continues until fully relaxed, or until resin gelation [34, 35]. It has been shown that shorter gel times produce larger variations , and longer gel times produce smaller differences for a fixed infusion length [13].

7.4.3 Compression Results

The strength and modulus results for the compression tests were normalized with respect to panel thickness as recommended in MIL-HDBK-17F-1 for warps-parallel laminates. This procedure accounts for variations in fiber volume fraction, due to thickness variations, for fiber dominated material properties when the same fiber reinforcement has been used for fabrication of the test laminates. A nominal thickness of 6.1 mm (0.24 in.) was used to normalize the results in this study.

The results of the compression tests are presented in Figures 7.6 and 7.7 for the compression strength and modulus, respectively. The magnitude of the results were similar with the results from prior phases of the study [13, 14], and there was not a

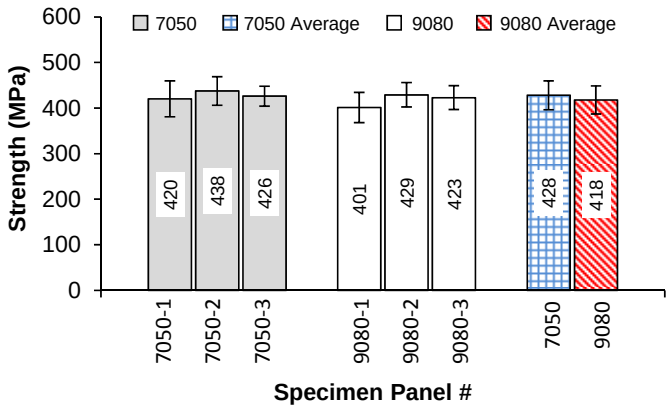

Figure 7.6. Compression strength results.

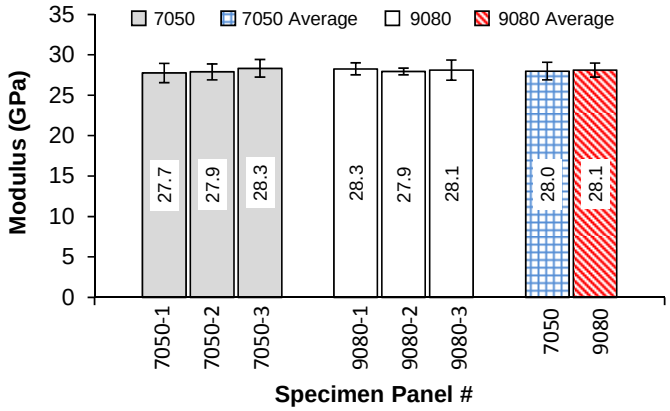

Figure 7.7. Compression modulus results.

statistically significant difference in the mean strength or modulus values between the two datasets, as indicated by the ADK ratios less than 1.0 in Table 7.4. It is worth noting that the lower FVF for dataset 9080-3 did not manifest itself in the compression results, due to the thickness normalization procedure.

Table 7.4. Compression statistical results.

	Strength			Modulus		
Dataset	**mean**	**CV**	**ADK**	**mean**	**CV**	**ADK**
Id	*MPa*	*%*	**Ratio**	*GPa*	*%*	**Ratio**
7050	428	7.4	0.51	28.0	3.9	0.35
9080	418	7.3	0.63	28.1	3.1	0.54
Total	423	7.4	0.40	28.0	3.5	0.15

Note: ADK ratios < 1 indicate no statistically discernible difference between datasets

7.4.4 Mode-I Fracture Toughness Results

Crack propagation in woven fabric composites is typically referred to as unstable, with the resulting behavior described as run-arrest [37]. A typical P-δ curve for Mode-I DCB specimens tested in this study is presented in Figure 7.8. As seen in the figure, the curve is characterized by a monotonic increase in load with minimal crack growth, followed by a sudden drop in load when the crack propagates rapidly (runs) to a point where it stops (arrests). This process repeats for the duration of the test. The run-arrest behavior has been attributed to the weave structure [37-40]. Unstable fracture often initiates at the edge of the transverse tows, since the transverse tows act as a toughening mechanism. These intersection points correspond to crack lengths where unstable fracture occurs, which suggests that the failure of these bridged fibers and tows is the cause for the instability of the crack growth [37].

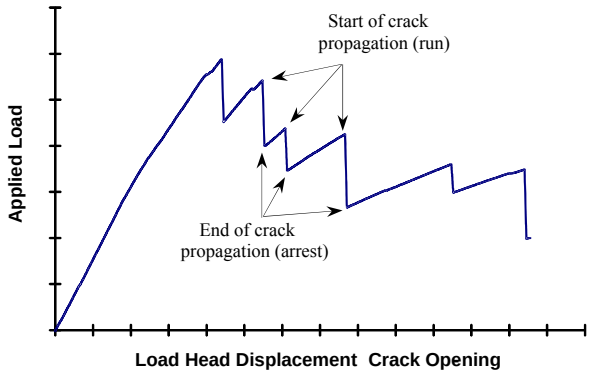

Figure 7.8. Typical Mode-I fracture load-deflection curve exhibiting run-arrest behavior.

As the crack grew from its initial location, a resistance type fracture behavior developed, with the fracture toughness increasing monotonically before stabilizing as the crack propagated further. Resistance curves (R-curves) were generated to determine the propagation fracture toughness of each specimen in the dataset. An R-curve plot for a

typical dataset is presented in Figure 7.9. The fracture toughness was computed at each instance where the crack length propagated by 1 mm or more. The points in the plot are the locations where the fracture toughness was computed for each specimen in the dataset. A crack length of 57.0 mm (2.25 in.) was selected as the starting point for stabilized propagation for each of the test specimens. The mean value of the stabilized R-curve data for the twelve specimens is indicated by the horizontal line in the plot. The propagation fracture toughness value for each of the twelve specimens received equal weighting when computing the mean value for the dataset.

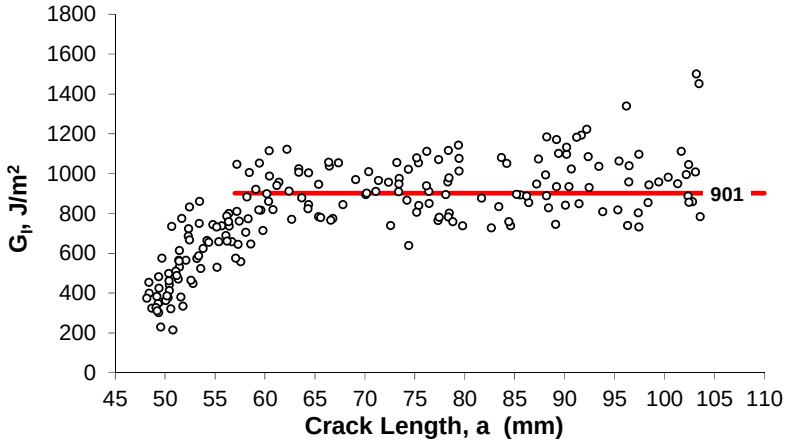

Figure 7.9. Typical Mode-I R-curve showing stabilized propagation.

A summary of the Mode-I fracture toughness test results is presented in Figure 7.10 and Table 7.5. The figure and table include the Mode-I mean results for visual onset, nonlinear onset, and propagation fracture toughness. In addition to the mean and CV for the three fracture toughness properties the table includes the ADK ratios for each dataset and the combined results.

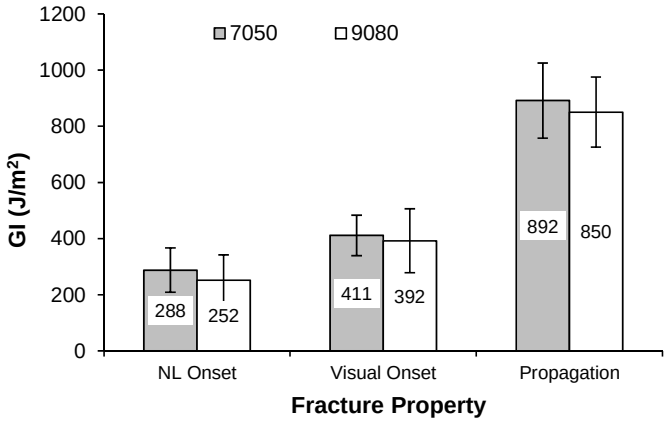

Figure 7.10. Mode-I fracture toughness results.

Table 7.5. Mode-I fracture toughness statistical results.

	Visual Onset Toughness			NL Onset Toughness			Propagation Toughness		
Dataset	**mean**	**CV**	**ADK**	**mean**	**CV**	**ADK**	**mean**	**CV**	**ADK**
Id	*J/m²*	*%*	**Ratio**	*J/m²*	*%*	**Ratio**	*J/m²*	*%*	**Ratio**
7050	411	17	0.62	288	27	0.33	892	15	***1.98***
9080	392	29	***1.01***	252	36	0.62	850	15	***1.00***
Total	402	24	0.48	270	32	0.74	871	15	0.29

Note: ADK ratios > 1 indicate no statistically discernible difference between datasets

As seen in the table, and as in the previous phases of the study, the propagation toughness produced the largest mean value and the lowest CV, while the NL onset produced the most conservative toughness values and a relatively large CV. The large CV exhibited by the onset properties are typical for specimens fabricated with heavy woven fabrics that have not been pre-cracked, and are a result of the variation in initial crack location and the unstable crack propagation issues discussed previously [38].

The large scatter in the data resulted in a statistical difference within dataset 7050 for the propagation toughness, as indicated by the ADK ratio of 1.98, and a couple of ADK ratio values near 1.0 for the visual onset (1.01) and propagation toughness (1.00) for dataset 9080.

Dataset 9080 produced lower mean values than dataset 7050 for all three fracture properties, but there was not a statistically distinguishable difference between the datasets for the three fracture toughness properties and the values were within the same range as what had been produced in previous studies for specimens fabricated with the same material system under similar conditions [13]. In addition, there was not a visually distinguishable difference in the degree of run-arrest response of the P-δ curves for the two datasets which could indicate degradation in the sizing of the fibers [25].

7.5 Conclusions

Woven roving E-glass fabric was condition at two different environments for a period of ten days prior to fabricating e-glass/vinyl-ester composite laminates (using a vacuum assisted resin transfer molding process) to investigate possible mechanical property variations due to fabric sizing degradation. The first environment was a control at 21°C (70°F) and 50% relative humidity and the second was at 32°C (90°F) and 80% relative humidity. The elevated temperature and humidity conditioning was meant to simulate what could occur to fabric during the lay-up of a large part where the fabric could be exposed to the ambient environment for an extended period of time prior to infusion.

Standardized testing for fiber volume fraction, compression, Mode-I fracture, and Barcol hardness were performed on test specimens from each of the three replicate composite panels fabricated for both of the environmental conditions.

Barcol hardness exhibited the most variability both within and between the conditioning datasets; however, this is typical for this type of test on thermoset polymers. Fiber volume fraction magnitudes and spatial distributions were consistent with prior

studies for this material system. Minor variations in fiber volume fraction were attributed to infusion duration and not related to conditioning.

Compression strength and modulus values were consistent with previous studies and indicated no statistical variation between fabric conditioning. The magnitudes of the visual onset, non-linear onset and propagation fracture toughness properties from the Mode-I fracture tests were also consistent with previous studies and showed no statistical difference between fabric conditioning. There was however, a statistical difference between individual panels within the 7050 conditioning dataset for the Mode-I propagation fracture toughness property. The exact cause of this variability could not be identified.

The results of the testing indicate that the elevated conditioning had a negligible effect on the material properties investigated in this study. Since research by other investigators has shown a degradation of fiber sizing due to environmental conditioning, longer durations of conditioning should be investigated in the future.

7.6 References

7.1 Thomason J L and Adzima L J (2001) Sizing Up the Interphase: An Insider's Guide to the Science of Sizing. Composites Part A, 32:313-321.

7.2 Karbhari V M and Palmese G R (1997) Sizing Related Kinetic and Flow Considerations in the Resin Infusion of Composites. Journal of Materials Science, 32:5761-5774 .

7.3 Palmese G R and Karbhari V M, (1995) Effects of Sizings on Microscopic Flow in Resin Transfer Molding. Polymer Composites, 16(4):313-318.

7.4 Karbhari V M and Kabalnova L (2001) Effect of Sizing and Loading Levels on the Cure Kinetics of Carbon Fiber Vinylester Composites. Journal of Reinforced Plastics and Composites, 20(2):90-104.

7.5 Larson B K, Drzal L T, and Van Antwerp J (1995) Swelling and Dissolution Rates of Glass Fiber Sizings in Matrix Resin Via Micro-Dielectrometry. Polymer Composites 16(5):415-420.

7.6 Sjogren A, Joffe R, Berglund L, and Mader E (1999) Effects of Fibre Coating (Size) on Properties of Glass Fibre/Vinyl-Ester Composites. Composites Part A, 30:1009-1015.

7.7 DiBenedetto A T (2001) Tailoring of Interfaces in Glass Fiber Reinforced Polymer Composites: A Review. Materials Science and Engineering, A302:74-82.

7.8 Gao S L, Mader E, Abdkader A, and Offermann P (2003) Sizings on Alkali-Resistant Glass Fibers: Environmental Effects on Mechanical Properties. Langmuir, 19:2496-2506.

7.9 Plonka R, Mader E, Gao S L, Bellmann C, Dutschk V, and Zhandarov S (2004) Adhesion of Epoxy/Glass Fibre Composites Influenced by Aging Effects on Sizings. Composites Part A, 35:1207-1216.

7.10 Ramos G, Gomez A, and Guardiola J (1996) Influence of Stability of Raw Materials Used in Sizings for E and AR Fiberglass Manufacture. Polymer Degradation and Stability, 51:316-365.

7.11 Pan N and Gibson P, Editors (2006) Thermal and Moisture Transport in Fibrous Materials. Woodhead Publishing Limited, Cambridge, England.

7.12 ASTM Standard D1776 (2004) Standard Practice for Conditioning and Testing Textiles. ASTM International, West Conshohocken, PA, www.astm.org.

7.13 Berube K A and Lopez-Anido R A (2012) Effect of Resin Cure Recipe and Ambient Processing Temperature on the Material Properties of Marine Grade

Polymer Matrix Composite Materials. Submitted for Publication to Materials Performance and Characterization.

7.14 Berube K A and Lopez-Anido R A (2011) Effect of Preform Consolidation on the Fracture Toughness of Marine Grade Polymer Matrix Composite Materials Fabricated With a VARTM Process. Journal of Advanced Materials 43(1):30-48.

7.15 Cain J J, Post N L, Lesko J J, Case S W, Lin Y, Riffle J S, and Hess P E (2006) Post-Curing Effects on Marine VARTM FRP Composite Material Properties for Test and Implementation. Journal of Engineering Materials and Technology, Transactions of the ASME, 128:34-40.

7.16 Kotaki M, and Hamada H, (1997) Effect of Interfacial Properties and Weave Structure on Mode I Interlaminar Fracture Behavior of Glass Satin Woven Fabric Composites. Composites Part A, 28A:257-266.

7.17 Kotaki M, Kuriyama T, Hamada H, Maekawa Z, and Narisawa I (2002) Mode I and Mode II Interlaminar Fracture Behavior of Glass Woven Fabric Composites. Science and Engineering of Composite Materials, 10(5):333-343.

7.18 Feih S, Wei J, Kingshott P, Sorensen B F (2005) The Influence of Fibre Sizing on the Strength and Fracture Toughness of Glass Fibre Composites. Composites Part A, 36:245-255.

7.19 Compston P, Jar Y B, Burchill P J, and Takahashi K (2002) Transfer of Matrix Toughness to Composite Mode I Interlaminar Fracture Toughness in Glass-Fibre/Vinyl Ester Composites. Applied Composite Materials, 9:291-314.

7.20 Madhukar M S and Drzal L T (1992) Fiber-Matrix Adhesion and Its Effect on Composite Mechanical Properties: IV Mode I and Mode II Fracture Toughness of Graphite/Epoxy Composites. Journal of Composite Materials, 26(7):936-968.

7.21 Madhukar M S and Drzal L T (1992) Fiber-Matrix Adhesion and Its Effect on Composite Mechanical Properties. III Longitudinal (0°) Compressive Properties of Graphite/Epoxy Composites. Journal of Composite Materials, 26(3):310-333.

7.22 MIL-HDBK-17F-1 (2002) Composite Materials Handbook Volume 1 - Polymer Matrix Composites Guidelines for Characterization of Structural Materials, ASTM International, West Conshohocken, PA, p8.1-110.

7.23 Kootsookos A and Burchill P J (2004) Effect of the Degree of Cure on the Corrosion Resistance of Vinyl Ester/Glass Fibre Composites. Composites Part A, 35(4):501-508.

7.24 Al-Assafi S, (2004) Thermal Analysis of Initiator Systems for High-Temperature-Cure Composites. Composites Part A, 5:1027-1031.

7.25 Di Pietro A, Compston P (2009) Resin Hardness and Interlaminar Shear Strength of a Glass-Fibre/Vinylester Composite Cured With High Intensity Ultraviolet (UV) Light. Journal of Materials Science, 44:4188-4190.

7.26 ASTM Standard D5528 (2001) Standard Test Method for Mode I Interlaminar Fracture Toughness of Unidirectional Fiber-Reinforced Polymer Matrix Composites. ASTM International, West Conshohocken, PA, www.astm.org.

7.27 Blake S P, Berube K A, and Lopez-Anido R A (2011) Interlaminar Fracture Toughness of Woven E-Glass Fabric Composites. Journal of Composite Materials, 46(13):1583-1592.

7.28 Dharmawan F, Simpson G, Herszberg I, and John S (2006) Mixed Mode Fracture Toughness of GFRP Composites. Composite Structures, 75:328-338.

7.29 ASTM Standard D6641 (2009) Standard Test Method for Determining the Compressive Properties of Polymer Matrix Composite Laminates Using a Combined Loading Compression (CLC) Test Fixture. ASTM International, West Conshohocken, PA, www.astm.org.

7.30 Berube K A and Lopez-Anido R A (2010) Variability in the Material Properties of Polymer Matrix Composites for Marine Structures. Journal of ASTM International 7(4):18p.

7.31 El-Chiti F (2005) Experimental Variability of E-Glass Reinforced Vinyl Ester Composites Fabricated by VARTM/SCRIMP. MS Thesis in Mechanical Engineering, University of Maine, Orono, ME.

7.32 ASTM Standard D3171 (2006) Standard Test Methods for Constituent Content of Composite Materials. ASTM International, West Conshohocken, PA, www.astm.org.

7.33 Li J, Zhang C, Liang R, Wang B, and Walsh S (2008) Modeling and Analysis of Thickness Gradient and Variations in Vacuum-Assisted Resin Transfer Molding Process. Polymer Composites, 29:473-482.

7.34 Yenilmez B and Sozer E M (2009) Variation of Part Thickness and Compaction Pressure in Vacuum Infusion Process. Composites Science and Technology, 69:1710-1719.

7.35 Tackitt K D, and Walsh S M (2005) Experimental Study of Thickness Gradient Formation in the VARTM Process. Materials and Manufacturing Processes, 20:607-627.

7.36 ASTM Standard D2583 (2004) Standard Test Method for Indentation Hardness of Rigid Plastics by Means of a Barcol Impressor. ASTM International, West Conshohocken, PA, www.astm.org.

7.37 Compston P and Jar P-Y B (1998) Comparison of Interlaminar Fracture Toughness in Unidirectional and Woven Roving Marine Composites. Applied Composite Materials, 5(3):189-206.

7.38 Naik N K, Reddy K S, Meduri S, Raju N B, Prasad PD, Azad SK N M, Ogde PA and Reddy B C K (2002) Interlaminar Fracture Characterization for Plain Weave Fabric Composites. Journal of Materials Science, 37:2983-2987.

7.39 Chen B and Chou T (2000) Compaction of Woven-Fabric Preforms: Nesting and Multi-Layer Deformation. Composites Science and Technology, 60:2223-2231.

7.40 Suppakul P and Bandyopadhyay S (2002) The Effect of Weave Pattern on the Mode-I Interlaminar Fracture Energy of E-Glass/Vinyl Ester Composites. Composites Science and Technology, 62:709-717.

CHAPTER 8

VARIABILITY IN FLEXURAL RESPONSE OF E-GLASS/VINYL-ESTER COMPOSITES FABRICATED USING THE VARTM PROCESS

8.1 Abstract

Despite advances in the Vacuum Assisted Resin Transfer Molding (VARTM) manufacturing process, questions remain regarding the consistency of material properties in large, fiber-reinforced polymer composite parts. In this paper, a parametric study designed to examine the variability in flexural response of marine grade composites, fabricated via a VARTM process, is presented and a method of data analysis is discussed. The objectives of the study were: 1) to determine the specimen geometry and test configuration for 25.4 mm (1.0 in.) thick woven fabric reinforced composite flexural members, which result in a repeatable test method; and 2) to characterize the variability in flexural strength and modulus. A three-dimensional digital image correlation (DIC) system was used to record full-field strain measurements during the tests. The DIC system allowed for through-the-thickness strain measurements to be recorded during testing. The effects of load-head size, and shear deformations, on the stress distribution, flexural strength, flexural modulus, and failure type were investigated.

8.2 Introduction

Despite advances in the Vacuum-Assisted Resin Transfer Molding (VARTM) manufacturing process, questions remain regarding the consistency of material properties in large, fiber-reinforced polymer composite parts. The study reported here is part of a

larger project to investigate the variability in material properties of thick E-glass vinyl-ester composites used for marine applications.

The sources of variability being investigated in the larger project include those due to manufacturing, post processing [1], and testing of composites [2]. The prior study on testing investigated the variability in tension, compression, and in-plane shear testing of E-glass vinyl-ester composites. The parametric flexure study, currently underway, will investigate the effects of span-to-thickness, width-to-thickness, and load-head size on the variability in flexural strength, flexural modulus, and failure location of 12.7 mm (0.5 in.) and 25.4 mm (1.0 in.) thick E-glass vinyl-ester composites. The use of a three-dimensional digital image correlation (DIC) system to record full-field strain measurements should allow the effects of shear deformations, on beam displacement, and stress concentrations, at the load-head contact points, to be investigated.

The work reported here is the first phase of the flexure study and is intended to investigate the variability in flexural strength, flexural modulus, stress distribution, failure type, and failure location due to selection of load-head size. The use of a tabbing material, between the specimen and the load/support points of the flexure fixture, was also investigated. The results of this phase will be used to examine the effects of span-to-thickness and width-to-thickness ratios in the next phase of the study.

8.3 Composite Material System Evaluated

The fiber-reinforced polymer (FRP) composite panels were made of E-glass/vinyl-ester. They were fabricated using a VARTM process with the proprietary Seemann Composites Resin Infusion Molding Process (SCRIMP) technology.

The fiber reinforcement used was Saint Gobain Vetrotex 324, which is a plain weave woven roving with a weight per unit area of 814 g/m^2 (24 oz/yd^2). The warp and fill directions have 55% and 45%, respectively, of the total fiber weight. The tow spacing is 5.1 mm (5 tows per inch) in the warp direction, and 6.4 mm (4 tows per inch) in the fill direction.

The test panels consisted of 40 layers of fabric reinforcement with the warp direction alternating (from 0 to 90 degrees) from layer to layer, for a nominal thickness of 25.4 mm (1.0 in.). The lay-up notation is $[0/90]_{10sf}$, where the warp direction corresponds to the principal material direction-1, and the fill direction to the principal material direction-2, as shown in Figure 8.1. The polymer resin used was Ashland Derakane 8084, which is an elastomer-modified epoxy vinyl-ester resin.

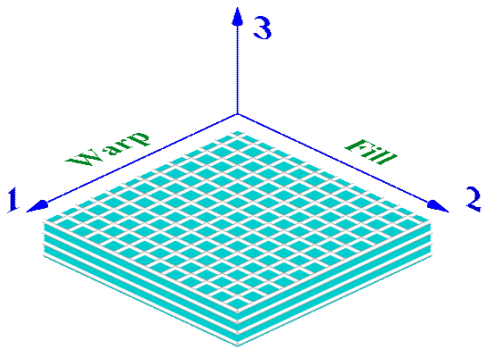

Figure 8.1. Woven roving coordinate reference system.

8.4 Specimen Preparation

The test specimens were cut from the panels to a nominal dimension of 38.1 mm (1.5 in.) wide by 610 mm (24 in.) long, using a wet saw with a diamond coated blade. The dimensions of each specimen were measured and recorded as per ASTM D5947 [3].

The specimens were then prepared for the Digital Image Correlation (DIC) measurement system by applying a speckled grayscale pattern of paint to the side of the

specimen as shown in Figure 8.2. In addition to providing the mid-span deflection measurement this allows full-field strain measurements to be recorded through-the-thickness of the beam during testing. Prior to testing, all specimens were conditioned at 23 ± 2°C and 50 ± 5% relative humidity, as outlined in ASTM D5229 [4].

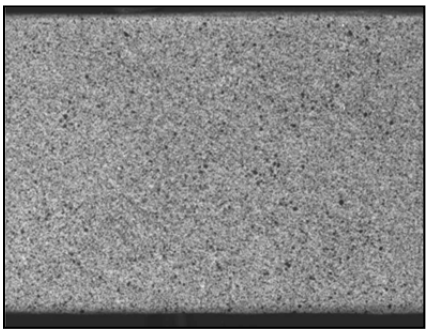

Figure 8.2. Speckled grayscale pattern on face of specimen.

8.5 Experimental Setup

A 4-point flexural test configuration, with quarter-point loading, was used for this investigation, as shown in Figure 8.3. A span-to-thickness ratio of 22-to-1 was used for all of the tests. While the ASTM D6272 flexural standard [5] recommends ratios of 16, 32 or 40-to-1, the ratio of 22-to-1 was selected for two reasons. 1) The span ratio of 16-to-1 was deemed to be too short for the material system and specimen thickness under investigation, and 2) a size limitation of 610 mm (24 in.) existed, because the panels had been fabricated before the flexural testing had been incorporated into the variability study.

Six different load-head configurations were investigated during this study. Specifically, 12.7 mm (0.5 in.), 25.4 mm (1.0 in.), and 50.8 mm (2.0 in.) diameter load-heads, with and without tabbing material, were investigated. The test specimen configurations are presented in Table 8.1. These three diameters correspond to diameter-

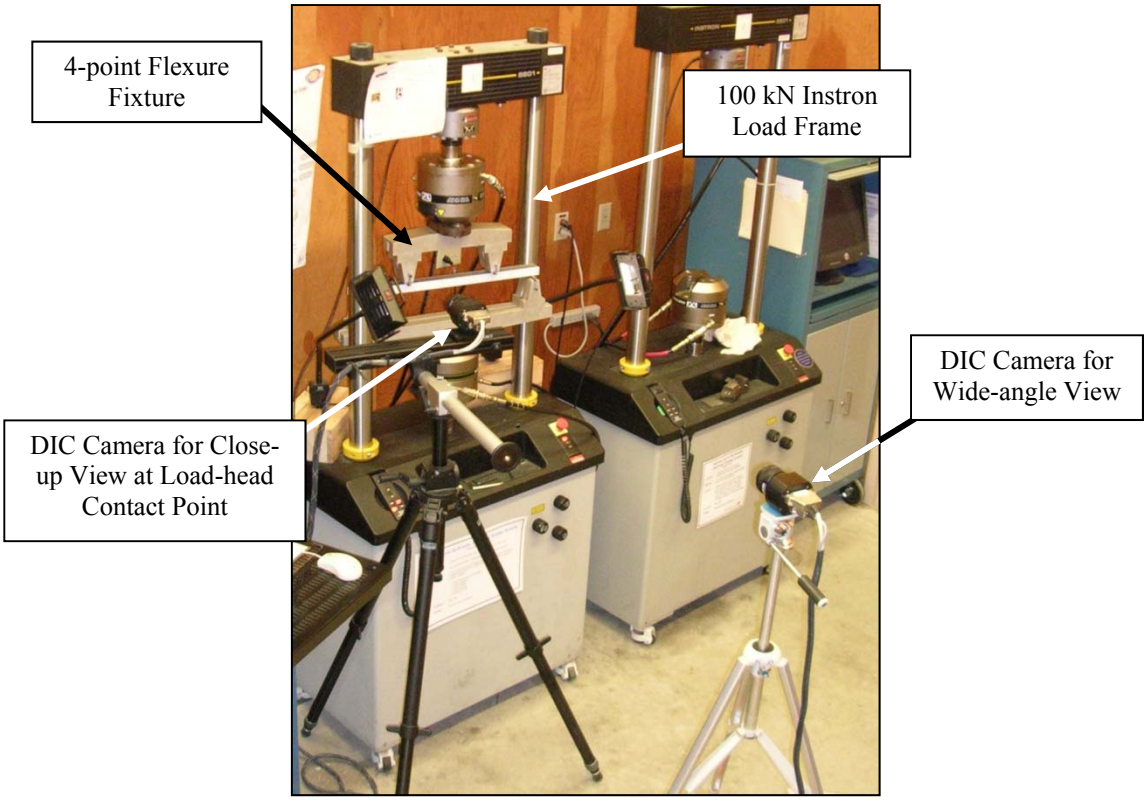

Figure 8.3. Four-point flexure experimental setup.

Table 8.1. Flexural test matrix.

Specimen Configuration *Id*	Load-head Diameter *mm (in)*	Load-head Tabbing Material	Number of Specimens *#*
05LH	12.7 (0.5)	None	8
05TM	12.7 (0.5)	Tabbing	8
10LH	25.4 (1.0)	None	8
10TM	25.4 (1.0)	Tabbing	8
20LH	50.8 (2.0)	None	8
20TM	50.8 (2.0)	Tabbing	8

to-thickness ratios of 0.5, 1.0, and 2.0 for the 25.4 mm (1.0 in.) thick composite specimens used in this study. Eight specimens were tested for each of the six configurations. The material used for tabs between the load-head and the specimen was 25.4 mm (1.0 in.) wide by 1.6 mm (0.0625 in.) thick FRP tabbing material.

The testing was performed on a 100 kN (22.5 Kip) servo-hydraulic Instron load frame equipped with hydraulic grips, in an environmentally controlled test lab, at the Advanced Structures and Composites Center, at the University of Maine, Orono, Maine. The rate of crosshead loading was constant at 0.10 in/min. This rate was calculated based on the rate equation given in section 10.1.4 of the ASTM D 6272 flexural standard.

A 3-D Digital Image Correlation (DIC) system was used to record the mid-span deflection and the full-field strain distribution during each test. The system was used in a 2-D mode, with each of the two cameras observing a different location. The information being sought, during this testing, was restricted to in-plane movements and strains of the test specimen. The test configuration used in this study allowed for simultaneous 2-D monitoring of two locations without the loss of critical data. A wide angle view recorded the mid-span deflection and strain distributions throughout the viewing area, while the close-up view allowed for a more detailed investigation of the stress distribution under the load-head.

In addition to the load and displacement data, recorded during the tests, the load at which the first audible sound, or the "crack load", was recorded through operator observation. Future testing will incorporate acoustic emission sensors to properly quantify the crack load.

8.6 Data Analysis

The statistical analysis methods outlined in the Composite Materials Handbook (MIL-HDBK-17F-1) for single point data were used to analyze the material property test results in this study [6]. After verifying the normality of the dataset distributions using the Anderson-Darling method, the mean and coefficient of variation (CV) were computed

for each material property. As a means of determining if the results from each material property dataset were statistically discernible for the load-head parameters investigated, the k-sample Anderson-Darling (ADK) method was employed. If the calculated ADK value for the dataset is less than the critical ADK value, then one can conclude (with a 2.5 percent risk of being in error) that the groups were drawn from the same population. The ratio of the computed value to critical value was calculated as a means to determine the level to which the datasets were statistically different. This ADK ratio is tabulated and presented for each dataset comparison in the results that follow.

8.7 Discussion of Results

The test results for the six test configurations investigated in this study are presented in Table 8.2. The table includes the mean and CV for the flexural strength and flexural modulus of the six configurations. All of the datasets produced results with a normal distribution. The results of the statistical analyses are presented in Table 8.3. Table 8.3 includes the mean, CV, and ADK ratios for the datasets grouped by load-head diameter, tabbing material, and all total datasets combined.

Table 8.2. Flexural strength and modulus results.

Specimen Configuration	Strength		Modulus	
	Mean	CV	Mean	CV
ID	*MPa (ksi)*	*%*	*GPa (Msi)*	*%*
05LH	379 (54.9)	4.1	25.6 (3.72)	2.4
05TM	356 (51.7)	3.7	25.1 (3.65)	1.4
10LH	379 (54.9)	3.1	25.4 (3.69)	1.1
10TM	396 (57.4)	2.7	25.4 (3.68)	0.8
20LH	401 (58.1)	2.2	26.4 (3.83)	1.1
20TM	391 (56.7)	3.7	26.0 (3.77)	1.0

Table 8.3. Statistical results for dataset groupings.

Grouping type	Dataset ID	Strength Mean MPa (ksi)	Strength CV %	Strength ADK Ratio	Modulus Mean GPa (Msi)	Modulus CV %	Modulus ADK Ratio
Load-Head Diameter	05	368 (53.3)	4.9	***1.37***	25.4 (3.68)	2.1	0.81
	10	387 (56.2)	3.6	***1.25***	25.4 (3.69)	0.9	0.16
	20	396 (57.4)	3.2	0.43	26.2 (3.80)	1.3	***1.09***
Tabbing	LH	386 (56.0)	4.1	***1.26***	25.9 (3.75)	2.2	***1.62***
	TM	381 (55.2)	5.7	***1.77***	25.5 (3.70)	1.8	***1.63***
Total	Total	384 (55.6)	4.9	***1.95***	25.7 (3.73)	2.2	***1.94***

Note: ADK ratios < 1 indicate no statistically discernible difference between datasets

The flexural strength and modulus results were grouped by load-head diameter and are plotted in Figures 8.4 and 8.5, respectively. The use of the 25.4 mm (1.0 in.), versus the 12.7 mm (0.5 in.), load-heads had virtually no effect on the mean flexural strength for the tests without tabbing material, but showed an 11% increase for the tests with tabbing material. The CV had a 25% reduction both with and without the tabbing material for the 25.4 mm (1.0 in.) load-heads compared to the 12.7 mm (0.5 in.) diameter load-heads. The use of the 50.8 mm (2.0 in.), versus the 25.4 mm (1.0 in.), load-heads had a 5.7% increase in the mean flexural strength for the tests without tabbing material, but showed a 1.3% reduction for the tests with tabbing material.

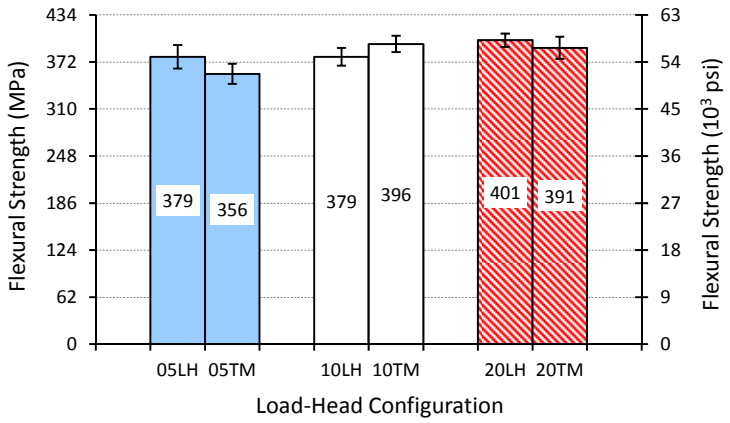

Figure 8.4. Flexural strength results.

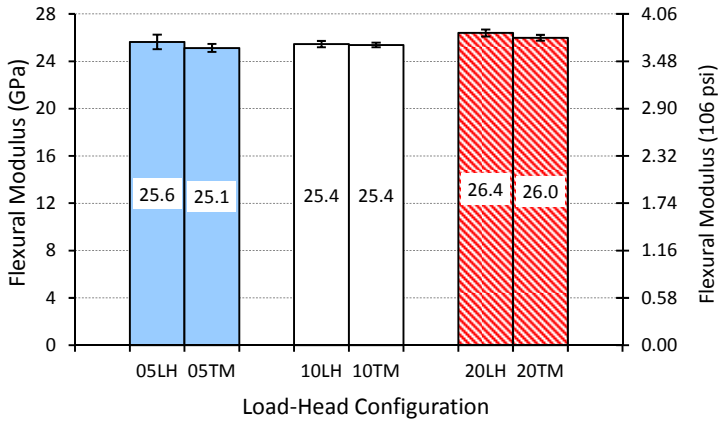

Figure 8.5. Flexural modulus results.

The use of the tabbing material under the load-heads and supports resulted in statistically discernible differences in strength, but not modulus, for the two smaller load-head diameters. There was a 5.9% decrease in the mean flexural strength for the 12.7 mm (0.5 in.) load-head and a 4.5% increase for the 25.4 mm (1.0 in.) load-head. The opposite was true for the 50.8 mm (2.0 in.) load-head where the use of tabbing material resulted in a statistically discernible difference in modulus (-1.5%), but not in strength.

As seen by the ADK ratios in Table 8.3, all other dataset groupings produced statistically discernible results, indicating that the change in load-head diameter and use of tabbing material did affect the results. In general, the use of the tabbing material led to less surface damage occurring under the load-heads, as presented in Figures 8.6-8.8. The use of the tabbing material to help prevent failures near the load-head (within one load-head diameter), was inconclusive. While the percentage of failures in the gage area increased from 25 to 87.5% for the 12.7 mm (0.5 in.) load-heads, it remained unchanged at 62.5% for the 50.8 mm (2.0 in.) and decreased from 50 to 25% for the 25.4 mm (1.0 in.) load-heads.

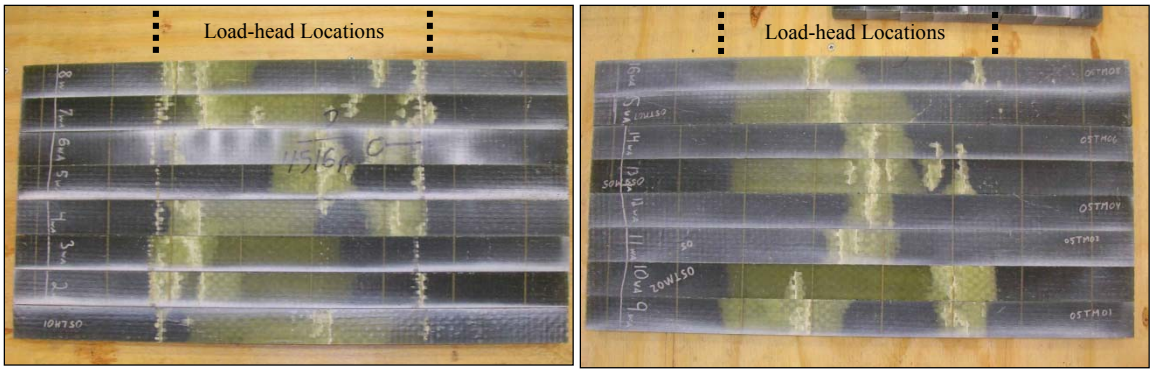

Figure 8.6. Failed specimens - 05LH (left) and 05TM (right).

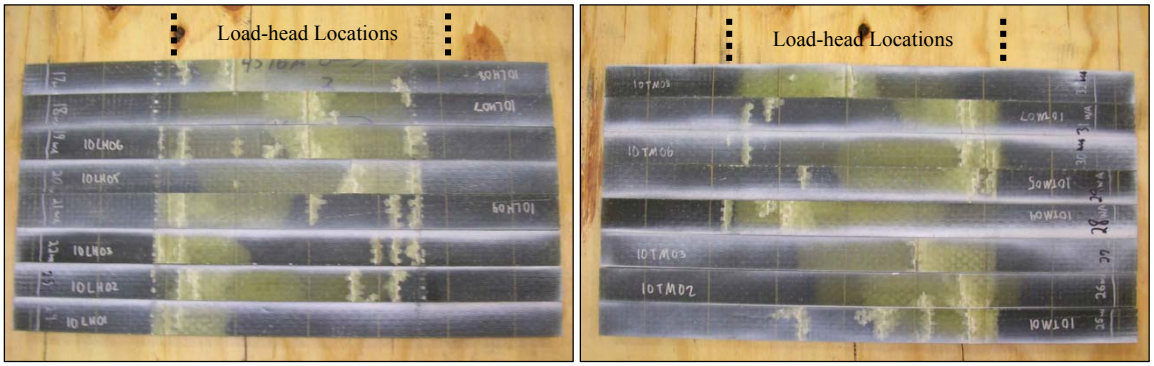

Figure 8.7. Failed specimens - 10LH (left) and 10TM (right).

Figure 8.8. Failed specimens. - 20LH (left) and 20TM (right).

The mean and CV for the crack loads and failure loads are given in Table 8.4 and plotted in Figure 8.9. The ratio of crack load to failure load increased with increasing load-head size, from 85% to 89%, for the tests without tabbing material. The same ratio for the tests with tabbing material was larger, but showed slightly less variation at 94% to

Table 8.4. Crack and failure load results.

Specimen Configuration	Crack Load		Failure Load	
	Mean	CV	Mean	CV
Id	*kN (lb)*	*%*	*kN (lb)*	*%*
05LH	18.2 (4084)	5.3	21.4 (4807)	4.4
05TM	19.0 (4280)	2.7	19.8 (4447)	4.1
10LH	18.9 (4256)	5.4	21.5 (4839)	2.5
10TM	21.1 (4750)	6.4	22.5 (5064)	3.7
20LH	19.5 (4378)	3.8	21.8 (4896)	2.5
20TM	20.9 (4701)	6.0	21.6 (4863)	4.1

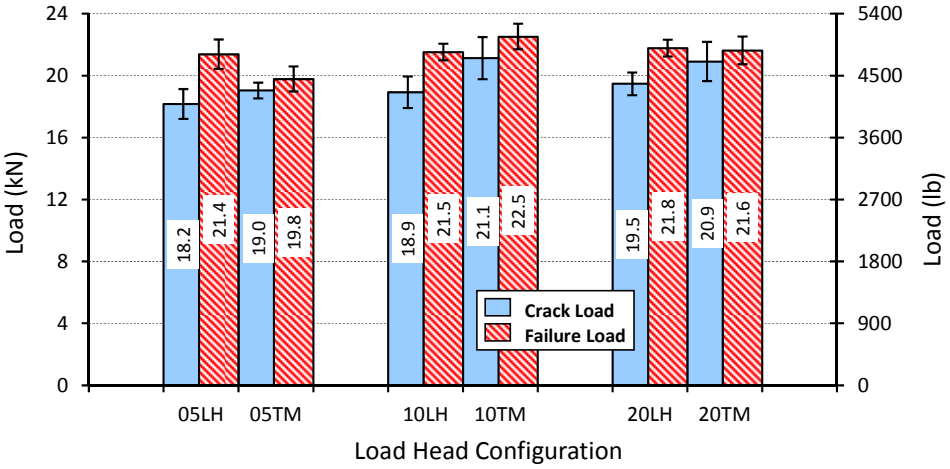

Figure 8.9. Plot of crack and failure loads.

96%. The increase in ratio both with and without tabbing material is another indication that damage at the load application points decreased with increasing load-head diameter.

Figures 8.10-8.12 show close up views of specimen failures, with the specimens placed in the orientation that they were cut from the original panels. As seen in these photos, cracks and failures occurred at the same locations in adjacent specimens indicating a possible flaw location in the original panels at these locations. Without pretest nondestructive evaluation data it is not possible to say with certainty that the common failure locations were a result of panel flaws, but it is the author's opinion that failures occurring at the same location through three specimens (as seen in Figures 8.10

and 8.11) greatly reduces the possibility of the damage occurring as a result of specimen preparation.

Figure 8.10. Possible specimen flaw in 05LH series.

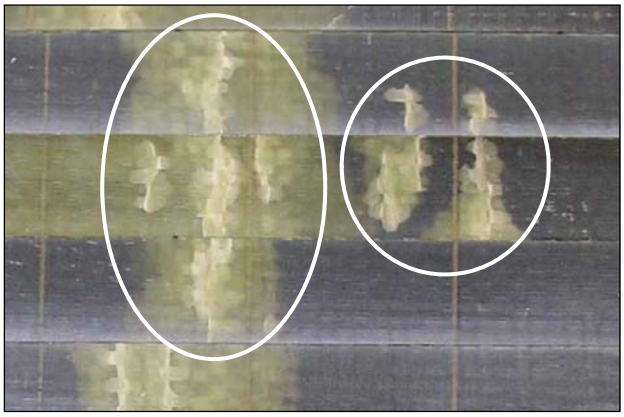

Figure 8.11. Possible specimen flaw in 05TM series.

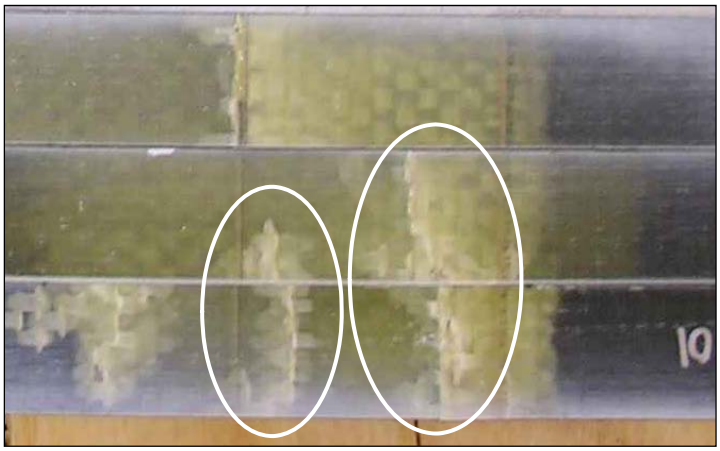

Figure 8.12. Possible specimen flaw in 10TM series.

The majority of the specimens failed in compression of the top surface followed by a delamination, as shown in Figure 8.13. The remainder of the specimens failed in compression either near the center of the beam, or at the load-head. 90% of the ultimate failures were preceded by localized failures without a drop in the applied load leading to an eventual progressive failure with a drop in load. The remaining 10% were of a more catastrophic nature not preceded by a drop in load.

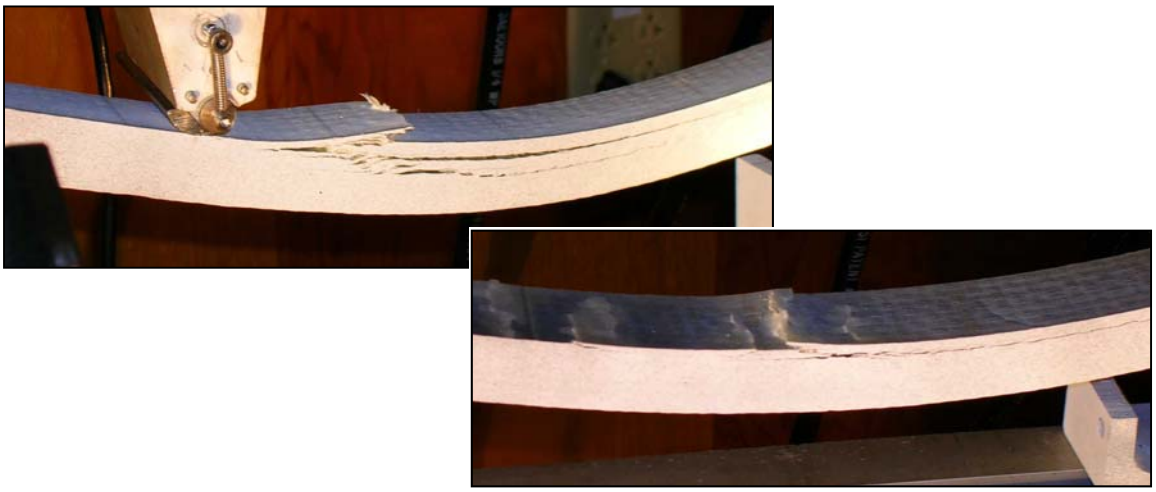

Figure 8.13. Typical failures of the flexure test specimens.

The stress distribution through-the-thickness of a typical beam can be seen in Figure 8.14. As shown in the series of pictures, the top of the beam goes into compression while the bottom of the beam experiences a tensile strain equal in magnitude, but opposite in sign, to the compressive strain on the top of the beam.

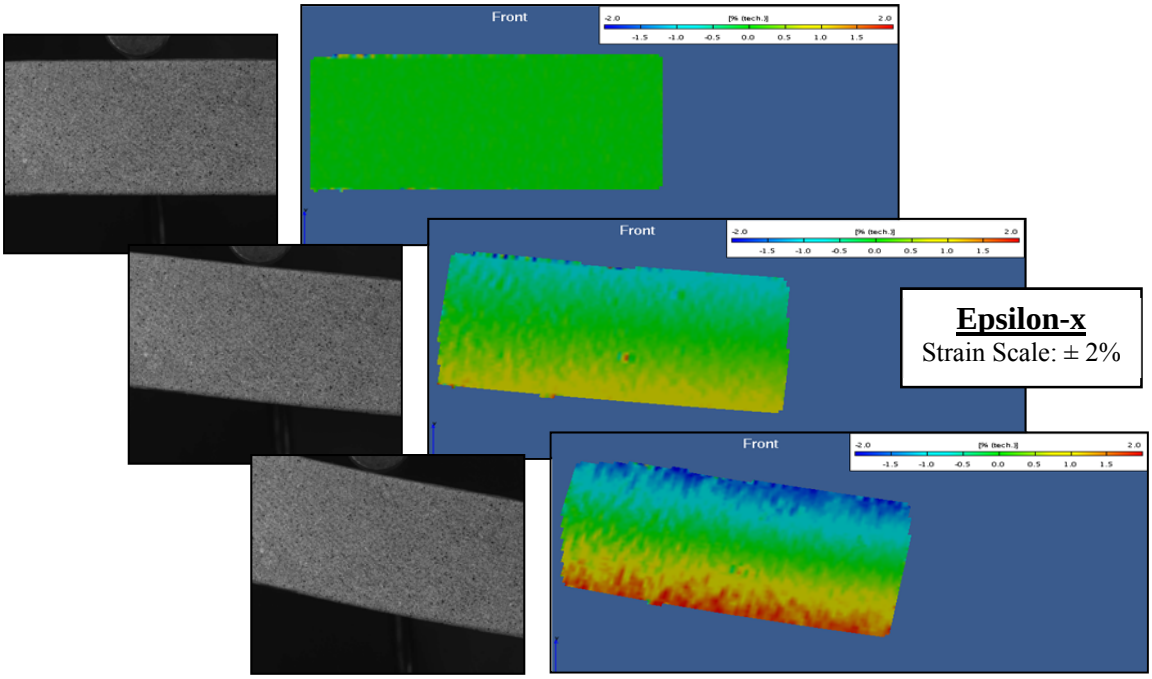

Figure 8.14. Flexural strain distribution progression during testing.

8.8 Conclusions and Recommendations

A load-head diameter of 50.8 mm (2.0 in.), without tabbing material, resulted in the highest mean and lowest CV for the flexural strength, for the six test configurations investigated. This configuration also resulted in 62.5% of the failures occurring near the load-heads. The tabbing material helped reduce the surface damage to the specimens but showed less benefit at reducing failures near the load-heads for larger diameter load-heads.

The DIC system was successful at recording the mid-span deflections and photo documenting the tests. The system also gave a detailed visualization of, and quantified, the stress distribution through the thickness of the specimen. Further processing and analysis of the data is necessary to distinguish the stress concentrations at the load-head contact point. This is an area of ongoing work on the project.

Based on the results of this study, a load-head diameter of 50.8 mm (2.0 in.), without tabbing material, will be used in the next phase of the study to examine the effects of different span-to-thickness ratios and width-to-thickness ratios, on the flexural response of 25.4 mm (1.0 in.) thick E-glass vinyl-ester specimens.

8.9 References

8.1 Cain J J, Post N L, Lesko J J, Case S W, Lin Y, Riffle J S, and Hess P E (2006) Post-Curing Effects on Marine VARTM FRP Composite Material Properties for Test and Implementation. Journal of Engineering Materials and Technology, Transactions of the ASME, 128:34-40.

8.2 El-Chiti F (2005) Experimental Variability of E-Glass Reinforced Vinyl Ester Composites Fabricated by VARTM/SCRIMP. MS Thesis in Mechanical Engineering, University of Maine, Orono, ME.

8.3 ASTM Standard D5947 (2003) Standard Test Methods for Physical Dimensions of Solid Plastics Specimens. ASTM International, West Conshohocken, PA, www.astm.org.

8.4 ASTM Standard D5229/D5229M (2004) Standard Test Method for Moisture Absorption Properties and Equilibrium Conditioning of Polymer Matrix Composite Materials. ASTM International, West Conshohocken, PA, www.astm.org.

8.5 ASTM Standard D6272 (2010) Standard Test Method for Flexural Properties of Unreinforced and Reinforced Plastics and Electrical Insulating Materials by Four-Point Bending. ASTM International, West Conshohocken, PA, www.astm.org.

8.6 MIL-HDBK-17F-1 (2002) Composite Materials Handbook Volume 1 - Polymer Matrix Composites Guidelines for Characterization of Structural Materials, ASTM International, West Conshohocken, PA, p8.1-110.

CHAPTER 9

DETERMINING THE FLEXURAL AND SHEAR MODULI OF FIBER REINFORCED POLYMER COMPOSITES USING THREE-DIMENSIONAL DIGITAL IMAGE CORRELATION

9.1 Abstract

A three-dimensional digital image correlation system was implemented into the flexural tests of fiber reinforced polymer composite beams to characterize the shear deformation. An optimization routine that minimized the error between the analytic and experimental data was implemented with first-order shear deformation beam theory to compute the flexural and shear moduli using the deflection and slope of the neutral axis of the beam. A relatively coarse 814 g/m^2 (24 oz/yd^2) woven roving E-glass fabric and a rubber-toughened vinyl-ester resin system were used to fabricate the 10.0 mm (0.38 in.) thick laminates in a quasi-isotropic laminate configuration. Span-to-thickness ratios of 8, 12, 16, and 24-to-1 were adopted for the laminate beams at a width-to-thickness ratio of 1.5-to-1. The full-field displacement- and slope-optimization fitting methods were compared with conventional discrete point methods to determine flexural and shear moduli. The slope-optimization produced consistent and reasonable values for the flexural modulus at all span-to-thickness ratios, but produced higher than expected values for the shear modulus at shorter spans. The deflection-optimization produced more variability in the flexural and shear moduli than the slope-optimization, and lower than expected values of shear modulus at larger span-to-thickness ratios. Tests where higher resolution images were used produced slightly larger values for shear modulus. Overall,

the slope-optimization produced the least amount of variability in the results for the flexural and shear moduli.

9.2 Introduction

Flexural and shear moduli of composite beams can be obtained by discrete-point conventional methods during four-point flexure. Typically, these methods rely on measuring beam deflections at two points (e.g., mid-span and under the applied loads) and assuming first-order shear deformation theory (FSDT) to determine the flexural and shear moduli. However, these methods are not sensitive enough to determine the shear moduli. To overcome this limitation, full-field strain and position data collected with non-contact digital image correlation (DIC) were acquired and utilized with optimization routines to solve the inverse problem assuming FSDT to compute flexural (E) and shear (G) moduli. This paper provides an insight to the potential, challenges, and limitations of using full-field experimental data as part of a test method to determine elastic properties.

When computing material properties from flexural tests, the Euler-Bernoulli beam theory is usually implemented. An assumption of this theory is that plane sections normal to the neutral axis of the beam remain plane and normal to the neutral axis after flexure of the beam. This assumption amounts to neglecting both transverse shear and transverse normal strains, which implies that the deflection is entirely due to flexure. For most materials this assumption does not pose an issue when computing flexural properties, as long as a sufficiently large span-to-thickness ratio is incorporated into the test. Materials such as laminated composites where G is significantly smaller than E, require longer spans to avoid introducing significant deflections due to shear.

In the FSDT theory for laminated composites, the transverse shear strain is assumed to be constant through the thickness of the part. The inclusion of this basic form of shear deformation removes the assumption of transverse normals remaining normal after flexure of the beam. A more complete discussion of beam theories can be found in Wang [1].

Four-point flexure of composite laminate beams was investigated in this study. The general equations for transverse beam deflection, *w*, of an FSDT simply-supported beam for the four-point loading condition as a function of longitudinal position, *x*, along the beam are:

for $0 < x < a$ or $(L\text{-}a) < x < L$ $$w_1(x) = \frac{Px}{6EI}\left(3La - 3a^2 - x^2\right) + \frac{Px}{kGA} \quad (1)$$

for $a < x < (L\text{-}a)$ $$w_2(x) = \frac{Pa}{6EI}\left(3Lx - 3x^2 - a^2\right) + \frac{Pa}{kGA} \quad (2)$$

where:

P is the force applied to the beam

x is the position along the beam

L is the span between the support-heads

a is the distance between the load-head and support-head

E is the flexural modulus

G is shear modulus

I is moment of inertia of the beam

A is the cross-sectional area of the beam

k is the shear correction factor

The equations for the slope, θ, of the neutral axis at any position, x, along the beam are:

for $0 < x < a$ or $(L\text{-}a) < x < L$ $\quad \theta_1(x) = \frac{dw_1(x)}{dx} = \frac{P}{6EI}\left(3La - 3a^2 - 3x^2\right) + \frac{P}{kGA}$ (3)

for $a < x < (L\text{-}a)$ $\quad \theta_2(x) = \frac{dw_2(x)}{dx} = \frac{Pa}{6EI}\left(3L - 6x\right)$ (4)

Included in the FSDT formulation of the beam equations is the shear correction factor, k. This factor is necessary to account for the difference between the assumed linear response of the transverse shear stress through the thickness and the actual transverse shear stress distributions. Several investigators have proposed methods for obtaining the value of k, which normally range from 0.8 to 0.9; however, such an investigation is not within the scope of the current work and a brief discussion of the various investigations is included in Madabhusi-Raman's work [2]. The lack of a known value for k was dealt with in this study by using a value of 1.0 in the optimization routine and presenting all results for shear modulus as kG.

For the study presented in this paper, equations 1-4 were implemented in the optimization routine for the case of ¼-point loading ($a = L/4$). A schematic of the load configuration is presented in Figure 9.1, and representative plots of the FSDT analytical equations for the deflection, slope, moment, and shear for this loading configuration are presented in Figure 9.2.

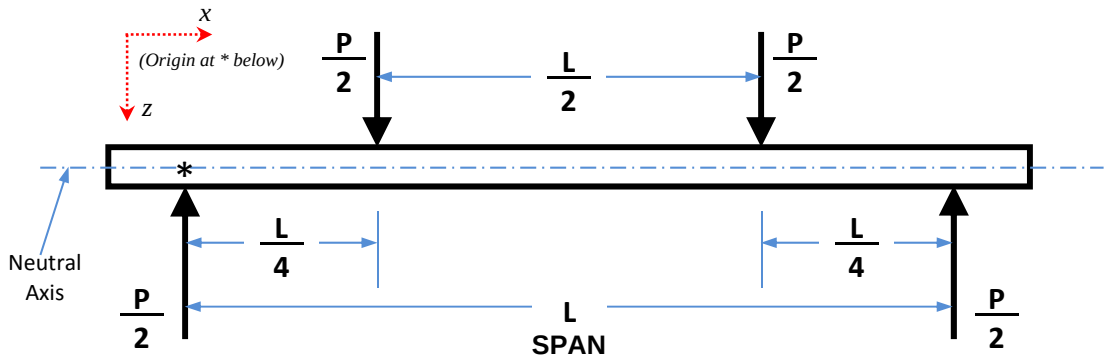

Figure 9.1. Four-point flexure with ¼-point load configuration.

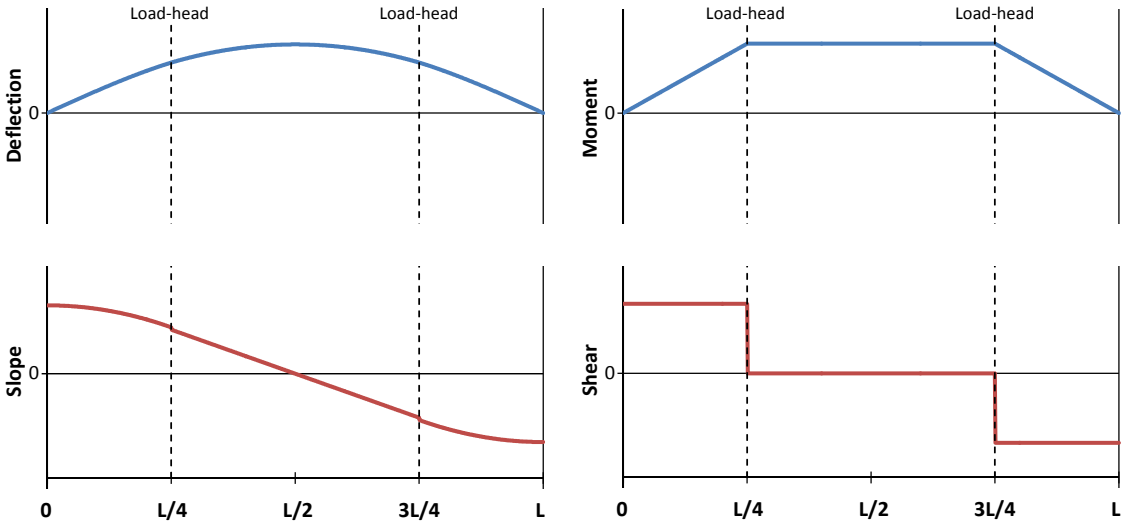

Figure 9.2. FSDT analytical plots for four-point flexure with ¼-point loading.

As seen in Equations 1 and 2, the terms on the far right, which are proportional to *P/kGA*, are the deflection of the beam due to shear, while the remainder of the equation is the deflection due to flexure. For metals, the shear deflection terms are usually negligible even for shorter spans, but for materials where *G* is small compared to *E* (like polymer composites), these terms takes on greater meaning, especially at shorter spans. It can be shown by solving Equations 1 and 2 for a material with *E* = 22.5 GPa and *G* = 3.2 GPa, that the deflection at the mid-span due to shear is 7.4, 3.4, 2.0, and 0.9% of the total deflection for span-to-thickness ratios of 8, 12, 16, and 24-to-1, respectively. Test

standards for composite materials recommend using specimens with span-to-thickness ratios of at least 32-to-1 for this loading configuration to avoid deflections due to shear and permit the use of the simpler Euler-Bernoulli beam equations, which neglect the shear terms in Equations 1-3.

Previous studies have been conducted to investigate the effect of shear deflections and simultaneously measure the flexural and shear moduli; however, they have usually employed discrete-point methods on a three-point flexure configuration [3-6]. Fischer [3] computed *E* and *G* from the beam deflection equation by obtaining load deflection data from a single beam tested at two different spans using three-point flexure. Bank [4] also used three-point flexure with multiple spans, but he used a graphical approach by plotting the linearized deflection equation and equating *E* and *G* to the slope and intercept, respectively, of the plotted data. Browne [5] used three-point flexure and the deflection equation in an investigation to determine alternative methods of measuring the shear modulus. In addition to varying the span in his tests, he varied the beam thickness as a means of changing the span-to-thickness ratio, and varied the moment of inertia (*I*) by rotating the beam 90°. Other investigators have looked at the effects of transverse compressibility and cross-section warping on the shear deflections in both three-point [6] and four-point flexure [7-8].

The DIC method provides full-field strain and position data over the visible imaging area during testing. It has been used for determining material properties in many studies [9-13] and has shown that it is a useful method for measuring properties at multiple scales [12] and under conditions that preclude more conventional techniques [13]. As a non-contact technique, it allows for simplified experiment test setup and

provides reduced specimen preparation time and reduced time between tests. Additionally, the image acquisition process permits test review and post-processing long after the time of testing which enables additional analysis to be conducted on the same test specimens at a later date in time.

The DIC technique was implemented into this study with the objective of simultaneously measuring the flexural and shear moduli of polymer matrix composite beams during flexural testing. The ability to provide full-field position data was the motive for its implementation. It is theorized that the incorporation of a continuum of experimental data points for use in curve-fitting the FSDT equations through an optimization routine can improve upon the more conventional discrete-point methods for computing E and G.

9.3 Experimental Methods

A marine grade fiber-reinforced polymer (FRP) composite reinforced with woven roving E-glass fabric was tested in this study. The FRP panels consisted of E-glass/vinyl-ester constituents and were fabricated using a vacuum assisted resin transfer molding (VARTM) process. The fiber reinforcement used was a Saint Gobain Vetrotex 324 woven roving with a weight per unit area of 814 g/m^2 (24 oz/yd^2), which is a plain weave fabric with a tow spacing of 5.1 mm (5 tows per inch) in the warp direction, and 6.4 mm (4 tows per inch) in the fill direction. The polymer resin used was Ashland Derakane 8084, which is an elastomer-modified epoxy vinyl-ester resin. This FRP system was chosen since it was the material system under investigation in a larger study being conducted by the authors on variability of material properties in marine grade composite materials [14].

The test panels consisted of 16 layers of the woven roving in a quasi-isotropic configuration $[0/\pm45/0]_{2S}$ for a nominal thickness of 9.65 mm (0.380 in.). The test specimens were cut from the panels to a nominal width of 38.1 mm (1.5 in.) and various lengths using a wet-saw with a diamond coated blade. Prior to testing, all specimens were conditioned at 23 ± 2°C and 50 ± 5% relative humidity for a minimum of one week. The specimens were then prepared for the 3-D DIC measurement system by applying a speckled grayscale pattern of paint to the side of the specimen as shown in Figure 9.3. This allows full-field strain and displacement measurements to be recorded for the entire observed area of the beam during testing.

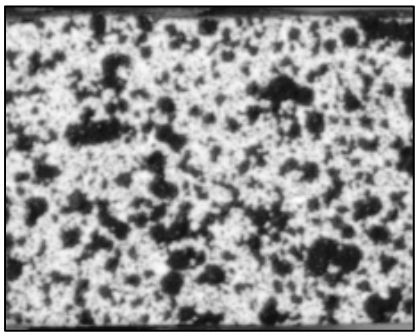

Figure 9.3. Typical speckle pattern on the face of a test specimen.

An ARAMIS™ 3-D DIC system was used to record the full-field strains and displacements on the test specimens during testing. The DIC system provides an advantage over conventional strain and displacement sensors as it allows a larger area of the specimen to be monitored during testing without the need to make physical contact with the specimen. This is especially advantageous when testing composites fabricated with heavy woven fabrics where strain gage size and placement can influence test results [15], or when testing small specimens where space availability for instrumentation is an issue.

ASTM test standard D7264 [16] was used to conduct the flexural tests. The specimens were tested in four-point flexure with a ¼-point load configuration, as shown in the schematic in Figure 9.1, at span-to-thickness ratios of 8, 12, 16, and 24-to-1. The flexure tests were performed on a 25 kN (5.6 kip) Instron load frame equipped with side-loading hydraulic grips at a temperature of 23 ± 2°C and 50 ± 5% relative humidity in an environmentally controlled test lab at the Advanced Structures and Composites Center, at the University of Maine in Orono, Maine. The specimens were tested in displacement control at a cross-head rate such that a strain of 0.75% was achieved at the outer fibers at the mid-span of the specimen in 60 seconds. After the 0.75% strain rate was reached, the specimens were unloaded. The 0.75% outer-fiber strain was selected since it provided deflection data in the linear elastic range of the material without producing any damage to the specimens. This allowed the specimens to be retested if necessary.

Each span-to-thickness ratio required a different cross-head rate to achieve the 0.75%/min strain rate. The cross-head rate was computed using Equation 5, as recommended in ASTM D6272 [17]. The experimental test matrix that includes the cross-head rate is presented in Table 9.1.

$$R = \frac{ZL^2}{6h} \tag{5}$$

where:

R is the rate of cross-head displacement

Z is the strain rate (0.75%)

h is the beam thickness

L is the support span

Table 9.1. Experimental test matrix.

Dataset *Id*	**Span-Ratio** *L/h*	**Span (*L*)** *mm (in)*	**Load-Rate(*R*)** *mm/min (in/min)*	**Number of Specimens**
8-1	8	77 (3.0)	0.771 (0.0304)	8
[a]**50-8-1**	8	77 (3.0)	0.771 (0.0304)	8
12-1	12	116 (4.57)	1.75 (0.0689)	8
[a]**50-12-1**	12	116 (4.57)	1.75 (0.0689)	8
16-1	16	156 (6.14)	3.13 (0.123)	8
24-1	24	232 (9.13)	6.99 (0.275)	6

[a] A 50 mm focal length camera lens was used for these datasets.

The 3-D DIC system was used to record the neutral axis deflections over the visible span of the specimen. A photo of the 3-D DIC observation areas for each span-to-thickness ratio is presented in Figure 9.4. As seen in the figure, two different camera configurations were used during the testing. A 12 mm focal length lens was used to capture each of the span-to-thickness ratios (Figures 9.4a-9.4d) and a 50 mm focal length lens was used to capture close-up views of span-to-thickness ratios 8 and 12 (Figures 9.4e and 9.4f). Digital cameras with a 1.3 mega-pixel (1280 x 1024 pixels) resolution were used for all of the testing.

Load and cross-head displacement data were recorded at a sampling rate of 10 Hz on the Instron control computer and at 2.0 Hz on the DIC system. This produced a total of 120 data-stages to be analyzed by the DIC system for each test.

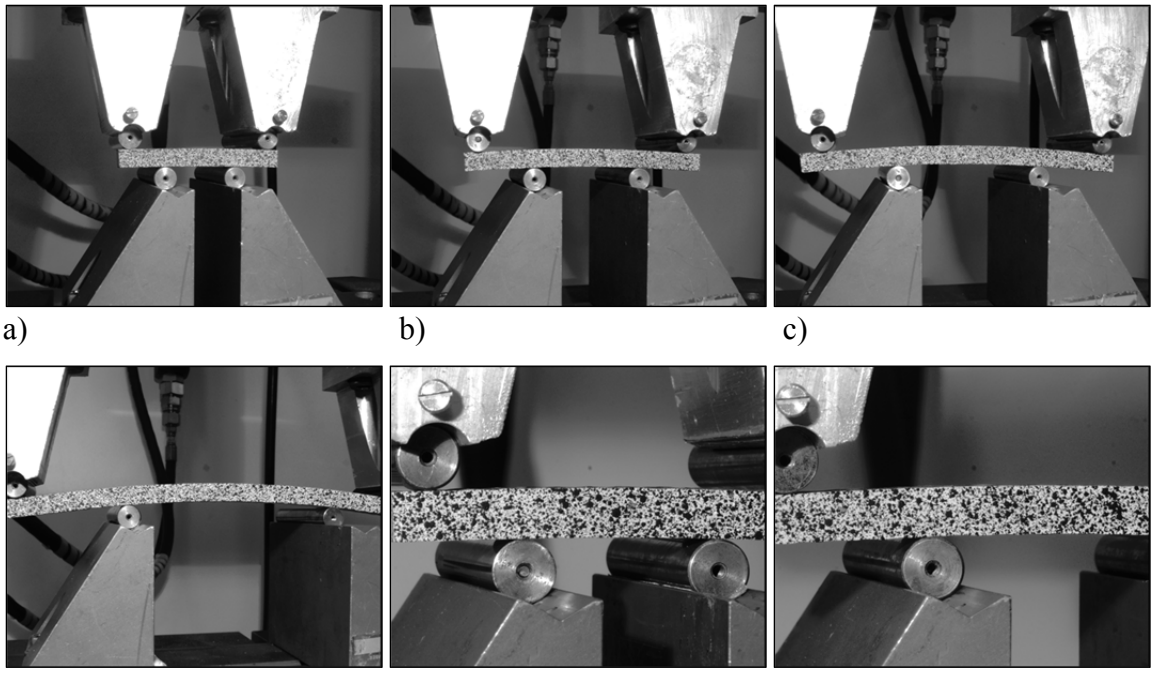

Figure 9.4. Field of view for the flexural tests at different span-to-thickness ratios: a) 8:1 ratio, b) 12:1 ratio, c) 16:1 ratio, d) 24:1 ratio, e) 8:1 ratio w/50 mm lens, and f) 12:1 ratio w/50 mm lens.

9.4 Analysis and Results

9.4.1 Analysis Procedure

The DIC results were post-processed to obtain the neutral axis deflections at each data-stage. The DIC post-processing required the selection of a pixel grid size (facet size) and grid overlap (point spacing) to produce a grid of points on the surface of the specimens. A facet size of 35 x 35 pixels was selected since it produced the least amount of noise in the data (±0.004 mm). The point spacing for the 12 mm and 50 mm focal length lens images was 0.81 mm and 0.29 mm, respectively. Once the grid was produced on the surface of each specimen, a section line was created along the neutral axis of the beam. The *y*-coordinates of the section line provided the deflected shape of the beam for each of the 120 data-stages. The *y*-coordinates and corresponding *x*-coordinates and load

at each data-stage comprised the experimental data that were used to fit the FSDT beam equations (Equations 1-4). The slope data were produced from the evenly spaced deflection data using a five-point smooth noise-robust differentiator.

$$\theta_i = \frac{w_{i+1} - w_{i-1}}{2(u_{i+1} - u_{i-1})} + \frac{w_{i+2} - w_{i-2}}{2(u_{i+2} - u_{i-2})} \tag{6}$$

where:

θ_t is the slope at point *i* of the neutral axis

w_i is the *y*-position at point *i* of the neutral axis

u_i is the *x*-position at point *i* of the neutral axis

This method was chosen as a means of suppressing the noise in the experimental data, since smoothing to eliminate noise prior to differentiating load-deflection data has been shown to improve the results without skewing the data [18].

An optimization routine was implemented to fit the analytical equations to the experimental data and compute the flexural and shear moduli. MatLab's *fminsearch* function was used for the optimization. The *fminsearch* function finds the minimum of an unconstrained multivariable function using a derivative-free method (Nelder-Mead simplex method). The error was computed by taking the 2-norm (square root of the sum of the squares) of the normalized difference between the experimental data and analytical solution. The difference was normalized with respect to the maximum value in the experimental dataset. The default convergence criterion of $1x10^{-6}$ was used with a 1000 iteration maximum during optimization. The optimization routine was used on both the deflection data (using Equations 1 and 2) and the slope data (using Equations 3 and 4).

Guess values for *E* and *G* were provided to the *fminsearch* function. Guess value pairs for (*E*,*G*) of (30,0), (30,10), (20,0) and (20,10) were used with the optimization

routine, and it was found that the routine converged to within 0.15% of the same values of *E* and *G* for each pair. The guess-value pair of (30,0) was used in the optimization results presented in this paper.

One of the assumptions with the analytical solution is that the deflected shape is symmetric about the mid-point; therefore, only one half of the beam was required to compute *E* and *G*. Since actual specimen behavior is seldom perfect during an experiment, especially when testing composites fabricated from heavy woven fabrics, it was decided to analyze both sides (left and right) of the beam independently for the load cases where the full span was visible. The full span of the beam was visible for span-to-thickness ratios of 8, 12, and 16-to-1, as seen in Figures 9.4a-9.4c, respectively.

As seen in the slope plot in Figure 9.2, there exists a discontinuity at the load-heads ($x=L/4$ and $x=3L/4$) in the analytical solution for the slope (Equations 3 and 4) that is proportional to P/kGA. The magnitude of the discontinuity is governed by the ratio E/G. The actual experimental data does not possess such an abrupt change in slope, but displays a more gradual transition. To account for this discrepancy during the curve-fitting of the data, the experimental data points in the vicinity of the load-heads were removed within the MatLab program and not used during the optimization. The magnitude of this data offset from the load-heads was selected to be ½ the specimen thickness (~5 mm). This value was sufficient to account for the discrepancy without compromising the curve-fit at the shorter span-to-thickness ratios.

As a means of comparing the optimization results for the flexural modulus, *E*, the experimental flexural chord-modulus (E_C) was calculated using the single-point method as recommended in ASTM D7264 for four-point flexure with ¼-point loading. To

compute E_C using Equation 7, the stress (σ) and strain (ε) were first calculated on the outer surface of the beam at the mid-span for each data-stage using Equations 8 and 9, respectively. At small span-to-thickness ratios this method results in an apparent value of E, which is lower than the actual value, because it fails to account for the effect of shear deformation.

$$E_C = \frac{\Delta\sigma}{\Delta\varepsilon} \tag{7}$$

$$\sigma = \frac{3PL}{4bh^2} \tag{8}$$

$$\varepsilon = \frac{48\delta h}{11L^2} \tag{9}$$

where:

σ is the flexural stress at the outer surface of the beam between the load-heads

ε is the strain at the outer surface of the beam between the load-heads

$\Delta\sigma$ is the difference in flexural stress between the two selected strain points

$\Delta\varepsilon$ is the difference between the two selected strain points

P is the force on the beam

L is the support span

b is the width of the beam

h is the thickness of the beam

δ is the mid-span deflection

Additionally, E and kG were computed at each data-stage with a two-point method, which used Equations 1 and 2 with the deflections at the mid-span and the load-head, $x = L/2$ and $L/4$, respectively. This method is commonly employed when testing

larger span beams in four-point bending by using displacement transducers placed at these two locations. The data analysis matrix is presented in Table 9.2.

Table 9.2. Dataset analysis matrix.

Dataset *Id*	Span-Ratio *L/h*	Beam Section	Number of Datasets	Method of Computing Flexural Modulus (E)[b]	Method of Computing Shear Modulus (G)[b]
8-1	8	Left & Right	16	1, 2, 3	1, 3
50-8-1[a]	8	Left	8	1, 2, 3	1, 3
12-1	12	Left & Right	16	1, 2, 3	1, 3
50-12-1[a]	12	Left	8	1, 2, 3	1, 3
16-1	16	Left & Right	16	1, 2, 3	1, 3
24-1	24	Left	6	1, 2, 3	1, 3

[a] A 50 mm focal length camera lens was used for these datasets.

[b] **1** = Optimization (Slope and Deflection), **2** = ASTM D7264 Chord Modulus, and **3** = Two-Point Method.

9.4.2 Results

Typical curve-fits for the slope- and deflection-optimizations, over the half-span of the beam, for each of the span-to-thickness ratios are presented in Figures 9.5 and 9.6, respectively. The discontinuity in the analytical equation for the slope is clearly visible in the plots in Figure 9.5.

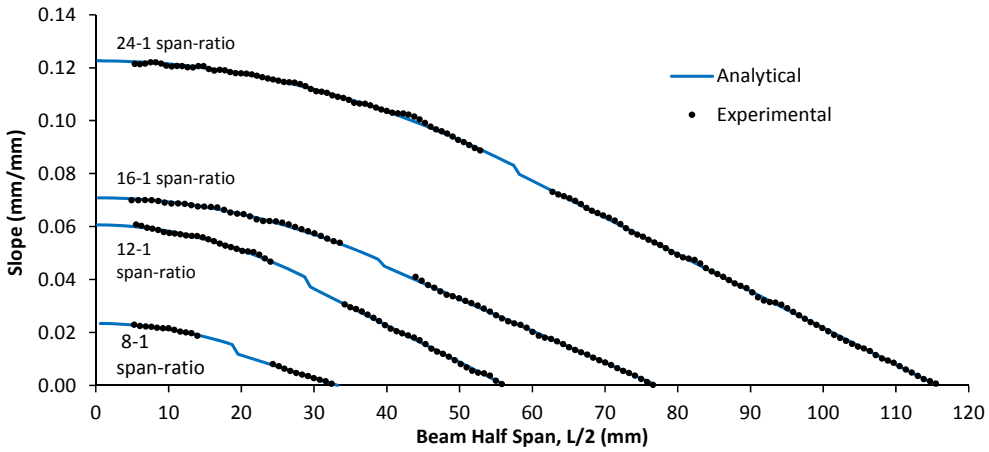

Figure 9.5. Typical slope curve-fits for the different span-ratios.

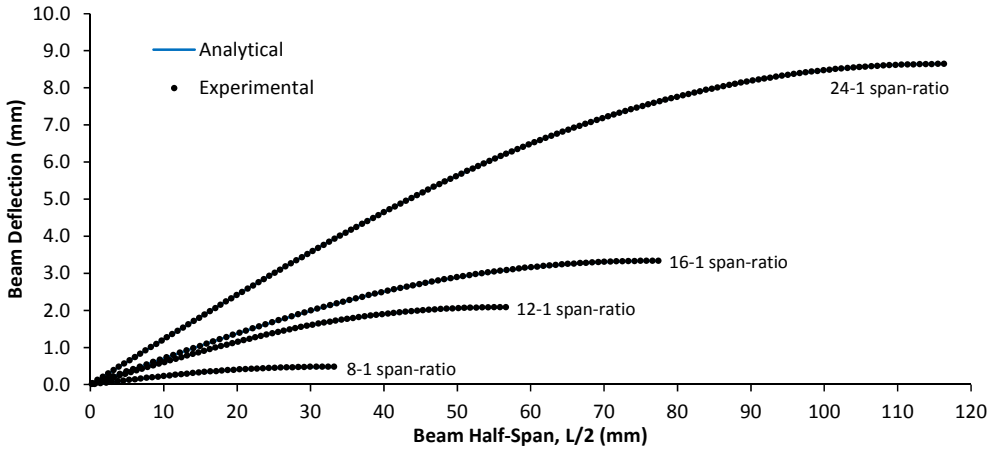

Figure 9.6. Typical deflection curve-fits for the different span-ratios.

As a means of comparing the results between span-to-thickness ratios, the mean results for E and kG were computed over three different strain ranges using Equation 9; 0.1-0.3%, 0.3-0.5%, and 0.5-0.7% strain. Not all of the datasets produced reasonable values for the shear modulus. In several instances the optimization routine produced very large values for kG ($kG > 10^{10}$ GPa), and in a few instances values between 10 and 100 GPa. Very large values of kG reduce the FSDT equations to Euler-Bernoulli equations and indicate that shear deflections were not detected by the optimization routine. Previous studies by the authors [19] with similar materials produced values in the range of 3.5-4.5 GPa for G_{xz}. Therefore, a threshold of 7.0 GPa was used to indicate specimens that produced reasonable results for kG. Since different span-to-thickness ratios consisted of different numbers of datasets (as indicated in Table 9.2), the datasets that produced reasonable values for kG are presented on a percentage basis in Figure 9.7 for each analysis method, span-to-thickness ratio, and strain range. Only the datasets that produced values where $0 < kG < 7$ are included in the results for E and kG that follow.

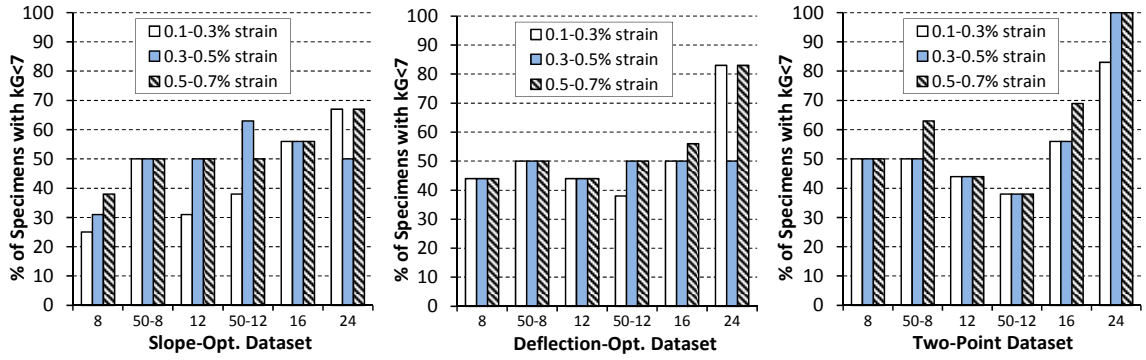

Figure 9.7. Percent of specimens that resulted in $0 < kG < 7$.

As seen in Figure 9.7, there is a general trend where the larger spans produced a higher percentage of reasonable values for *kG* for the slope-optimization routine, and to a lesser degree for the deflection-optimization. There is not a consistent trend for the percentage results in the two-point dataset plot of Figure 9.7.

The majority of the datasets that used the 50 mm focal length lenses (50-8-1 and 50-12-1) produced a higher percentage of results than their corresponding 12 mm focal length lens datasets (8-1 and 12-1) for both the slope- and deflection-optimization results. The two-point method showed an improvement in percentage of results for only the 0.5-0.7% strain range for the 8-to-1 span ratio, while the majority of the results either remained the same or declined in percentage.

The results for *E* and *kG* computed from the slope-optimization, the deflection-optimization, and the two-point method are presented in Figures 9.8-9.10, respectively. The plots in these figures present the mean values of *E* and *kG* for each span-to-thickness dataset over each of the three strain ranges. The number of datasets used to compute the mean is indicated in the *x*-axis of the plot. Error-bars are included on the plots and are equal to ±1standard deviation. It is worth noting that a larger *y*-axis scale was used for

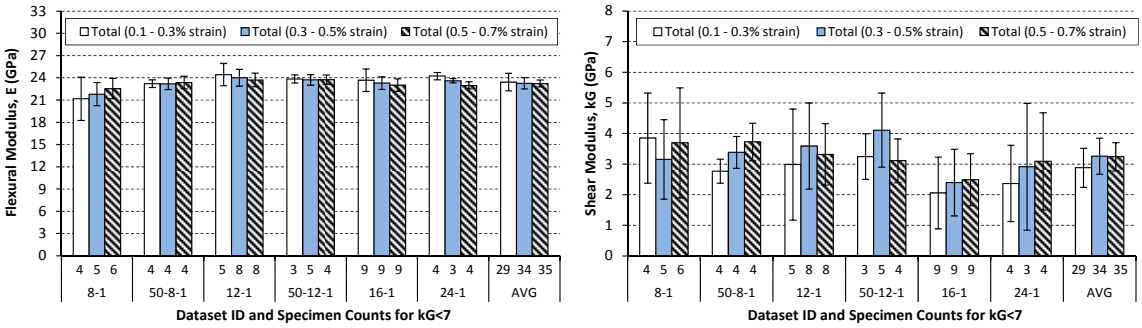

Figure 9.8. *E* and *kG* results for each strain range using slope-optimization.

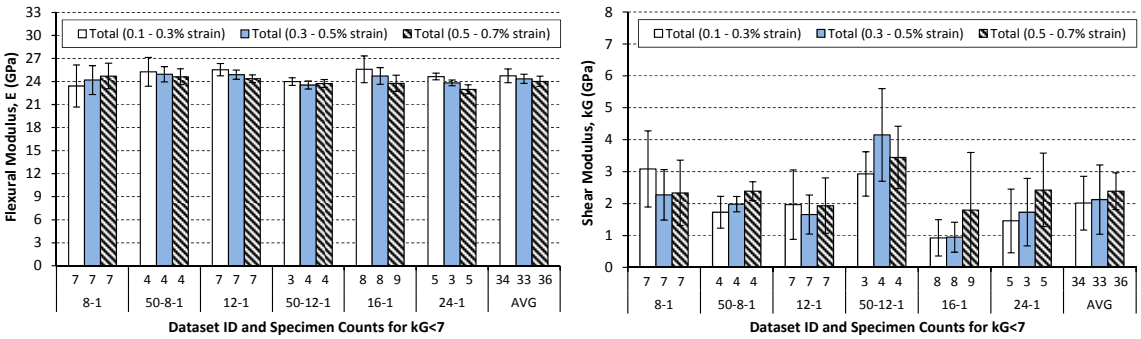

Figure 9.9. *E* and *kG* results for each strain range using deflection-optimization.

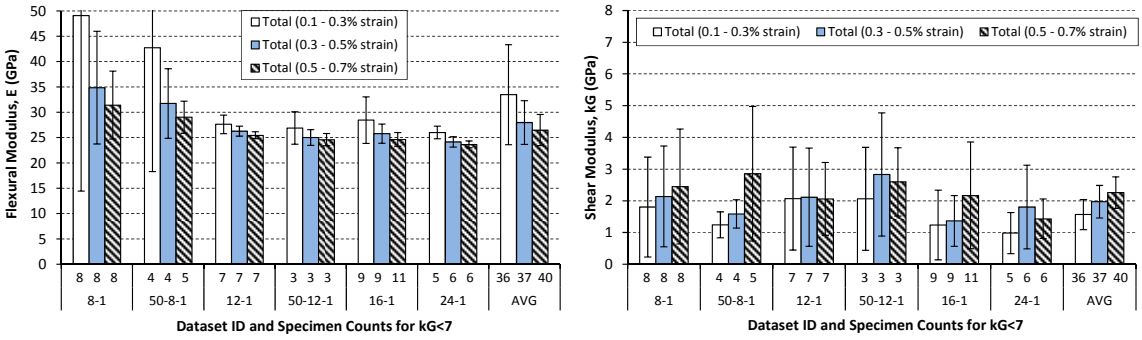

Figure 9.10. *E* and *kG* results for each strain range using the two-point method.

the plot of *E* in Figure 9.10 to account for the large values at lower span-to-thickness ratios computed using the two-point method.

Previous studies by the authors with the same material system produced a value of $E = 23.5$ GPa for flexural testing at a larger span-to-thickness ratio (40-to-1), which

minimized the effect of shear deflections. The slope-optimization method produced values of E very similar to the previous study and also showed less variability than the deflection-optimization or two-point methods.

The noise in the DIC analysis was measured at ±0.004 mm in the direction of beam deflection. Since the smaller span-ratios produce smaller deflections than the larger span-ratios for the same strain level, the effect of the noise should be more pronounced on the smaller span-to-thickness ratios and at the lower strain levels. The noise-to-signal ratio at the peak deflection of the test specimens is 1.0, 0.25, 0.15, and 0.05% for the 8-, 12-, 16-, and 24-to-1 span-to-thickness ratios, respectively, and would be significantly larger at the earlier data stages. This should manifest itself as higher variability in the results and fewer specimens that result in reasonable values for E and kG at the lower span-to-thickness ratios and strain levels. The majority of the results for E show this trend, but there is not a consistent trend of this nature for kG. As was previously discussed the shear deflection relative to the overall deflection at the mid-span of the beam for this material system is 7.4, 3.4, 2.0, and 0.9% for span-ratios of 8-, 12-, 16-, and 24-to-1, respectively. It is most likely this reduced contribution of the shear deflection at larger spans that dominates the computation of kG.

The results for E and E_c (Equation 7) over the strain range of 0.1-0.3% strain are presented in Figure 9.11 for the slope- and deflection-optimizations. E_c is computed from the Euler-Bernoulli beam equations which means that it should be smaller than E, since it assumes that all of the deflection is due to flexure and not from shear. As seen in Figure 9.11, the majority of the results indicate that $E > E_c$ except for the 8-1, and 50-8-1 ratio datasets in the slope-optimization, and the 8-1 ratio dataset in the deflection-optimization.

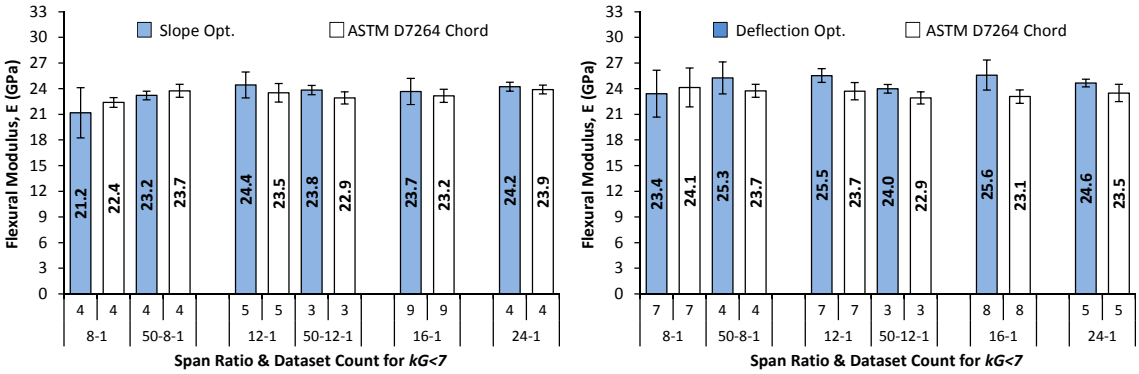

Figure 9.11. E and E_c for 0.1-0.3% strain slope and deflection-optimization, $0 < kG < 7$.

The large variability in results for the shorter spans are thought to be the main contributing factor of this discrepancy and are attributed to the noise-to-signal ratio, as previously discussed.

It was found that only three specimens (one at 12:1 and two at 16:1) produced comparable shear modulus results for both the left and right halves of the beam for the slope-optimization, while the deflection-optimization produced only one specimen (at 16:1) with comparable shear results for both halves. Additionally, the optimization routine was not able to discern a shear modulus on either side of the beam for two (25%) of the specimens from the 8-to-1 dataset during slope-optimization, and for one (12.5%) of the specimens from each of the 8-to-1 and 12-to-1 datasets during deflection-optimization. While the assumption of symmetry is convenient for analytical solutions, the realities of experimental work can override this assumption. The possible reasons for the non-symmetry of the deflected shapes in this experiment were the geometry of the test fixture, specimen dimensional variation, and specimen material non-homogeneity.

The dimensions of the flexural test fixture and alignment of the load and support heads were confirmed to within 0.3 mm for each span-to-thickness ratio, which was within 1.0% of the ¼-span dimensions except for the 8-to-1 dataset where it was 1.6%.

Fabricating FRP panels with a VARTM process that incorporates a flexible membrane opposite the mold side, produced specimens with a standard deviation in the range of 0.1 mm for the specimen thickness. Additionally, the laminate consisted of only 16 layers of woven roving fabric, which results in relatively large areas of non-homogeneity when compared with the geometry of the beam. While the magnitude of these values seems small, they can produce adverse effects when considering the magnitude of the deflections of the beam at shorter spans and the small contribution of the shear to the overall deflection of the beam.

9.5 Conclusions

A 3-D DIC system was implemented with an analytical optimization routine to measure the flexural and shear moduli during flexure testing of FRP composite laminate beams. The 3-D DIC system recorded the deflected shape at the neutral axis of beams during four-point flexural testing with a ¼-point loading configuration, at span-to-thickness ratios of 8, 12, 16, and 24-to-1. A MatLab optimization routine was used to curve-fit the FSDT analytical equations, over the half-span of the beam, to the experimental deflection and slope data from the neutral axis of the beam.

The majority of the span-to-thickness ratios investigated produced reasonable results for G for 50% of the specimens in the dataset. The slope-optimization produced less variability and more realistic results for E and G when compared to the deflection-optimization for the range of span-to-thickness ratios investigated in this study. The deflection-optimization produced values of G that were lower than the slope-optimization routine. The slope-optimization is thought to be more sensitive at discerning the

magnitude of the shear modulus due to the sharp discontinuity in the analytical equation at the load points.

The optimization results were compared to the conventional single-point method (ASTM D7264) and two-point methods for computing *E* and *G*. The values of *E* over the strain range of 0.1-0.3% strain were consistently larger than the single-point method of ASTM D7264 for computing chord modulus, which is what would be expected when computing *E* for shorter spans where shear deflection contributes to the overall deflection of the beam. This was not the case at the shortest span-to-thickness ratio (8-to-1) where the noise-to-signal ratio was thought to affect the results. The two-point method produced results similar to the deflection-optimization, which are considered to be low for values of *G*, and high for *E*, as compared to previous studies with the same material system.

The asymmetry of the deflected shape of the neutral axis about the mid-span of the beam is thought to be the main reason for the variability in the results and the inability of the optimization routine to detect shear deflection in approximately 50% of the datasets analyzed.

9.6 References

9.1 Wang C M, Reddy J N, Lee K H (2000) Shear Deformable Beams and Plates - Relationships With Classical Solutions. Elsevier Science Ltd. Oxford, England.

9.2 Madabhusi-Raman P, Davalos J F (1996) Static Shear Correction Factor for Laminated Rectangular Beams. Composites Part B 27B:285-293.

9.3 Fischer S, Roman I, Harel H, Marom G, and Wagner H D (1981) Simultaneous Determination of Shear and Young's Moduli in Composites. Journal of Testing and Evaluation. 9(5):303-307.

9.4 Bank L C (1989) Flexural and Shear Modulus of Full-Section Fiber Reinforced Plas-Tic (FRP) Pultruded Beams. Journal of Testing and Evaluation, 17(1):40-45.

9.5 Browne C M (1988) Alternative Methods for the Determination of Shear Modulus in a Composite Material. Testing Technology of Metal Matrix Composites, ASTM STP 964, American Society for Testing and Materials, Philadelphia. 259-274.

9.6 Dufort L, Grediac M, and Surrel Y (2001) Experimental Evidence of the Cross-Section Warping in Short Composite Beams Under Three Point Bending. Composite Structures 51:37-47.

9.7 Hayes M D and Lesko J J (2007) Measurement of the Timoshenko Shear Stiffness. I: Effect of Warping. Journal of Composites for Construction, 11(3):336-342.

9.8 Hayes M D and Lesko J J (2007) Measurement of the Timoshenko Shear Stiffness. II: Effect of Transverse Compressibility. Journal of Composites for Construction, 11(3):343-349.

9.9 Lopez-Anido R A, El-Chiti F W, Muszynski L, Dagher H J, Thompson L, and Hess P E (2004) Composite Material Testing Using a 3-D Digital Image Correlation System. Proceedings of the ACMA Composites 2004 Convention and Trade Show, Tampa, FL, October 6-8, 2004, American Composites Manufacturers Association, Arlington, VA.

9.10 El-Chiti F, Lopez-Anido R A, Dagher H J, Thompson L, Muszynski L, and Hess P E (2005) Experimental Approach for Characterizing VARTM Composites Using a 3-D Digital Image Correlation System. Proceedings of the SEM XII Int. Congress and Exposition on Experimental and Applied Mechanics, Portland, OR, June 7-9, 2005, Society for Experimental Mechanics, Bethel, CT, 8p.

9.11 Berube K A and Lopez-Anido R A (2008) Full-Field Strain Measurements for DeterminIng Mechanical Properties of Marine Composite Laminates. Experimental Mechanics Applied to Damage: Detection, Analysis and Mitigation, SEM XI International Congress Exposition on Experimental and Applied Mechanics, Orlando, FL, June 2-5, 2008, Society for Experimental Mechanics, Bethel, CT, 8p.

9.12 Nicoletto G, Marin T, Anzelotti G, and Roncella R (2011) Application of High Mag-Nification Digital Image Correlation Technique to Micromechanical Strain Analysis. Strain 47:E66-E73.

9.13 Khennouf D, Dulieu-Barton J M, Chambers A R, Lennard F J, and Eastop D D (2010) Assessing the Feasibility of Monitoring Strain in Historical Tapestries Using Digital Image Correlation. Strain, 46:19-32.

9.14 Berube K A and Lopez-Anido R A (2010) Variability in the Material Properties of Polymer Matrix Composites for Marine Structures. Journal of ASTM International 7(4):18p.

9.15 Masters J (1996) Strain Gage Selection Criteria for Textile Composite Materials. NASA Contractor Report 198286, National Aeronautics and Space Administration, Langley Research Center, VA.

9.16 ASTM Standard D7264 (2007) Standard Test Method for Flexural Properties of Polymer Matrix Composite Materials. ASTM International, West Conshohocken, PA, www.astm.org.

9.17 ASTM Standard D6272 (2010) Standard Test Method for Flexural Properties of Unreinforced and Reinforced Plastics and Electrical Insulating Materials by Four-Point Bending. ASTM International, West Conshohocken, PA, www.astm.org.

9.18 Daniewicz S R (1999) Smoothing and Differentiating Load-Displacement Data Using a Low-Pass Filter for Improved Crack Opening Load Estimates. Fatigue & Fracture of Engineering Materials & Structures, 22(4):273-279.

9.19 Kittridge M, Lopez-Anido R A, Marquis J, Williams D, Snape T, Eary S, Duncan C J, and Berube K A (2012) Advanced Design and Optimization of High Performance Combatant Craft: Material Testing and Computational Tools. AEWC Report 12-46.780, AEWC Advanced Structures and Composites Center, University of Maine, Orono, ME, 687p.

BIBLIOGRAPHY

Abadie M J M, Mekhissi K, and Burchill P J (2002) Effects of Processing Conditions on the Curing of a Vinyl Ester Resin. Journal of Applied Polymer Science, 84(6):1146-1154.

Abdelwahab M, Agag T, Akelah A, Takeichi T (2012) Synthesis and Characterization of Styrene Modified Vinylester Resin-Clay Nanocomposites. Polymer Engineering and Science, 52(1):125-132.

Agarwal N, Singh A, Varma I K, Choudhary V (2008) Effect of Structure on Mechanical Properties of Vinyl Ester Resins and Their Glass Fiber-Reinforced Composites. Journal of Applied Polymer Science, 108:1942-1948.

Al-Assafi S, (2004) Thermal Analysis of Initiator Systems for High-Temperature-Cure Composites. Composites Part A, 5:1027-1031.

Alif N, Carlsson L A, and Boogh L (1998) The Effect of Weave Pattern and Crack Propagation Direction on Mode-I Delamination Resistance of Woven Glass and Carbon Composites. Composites: Part B, 29B:603-611.

Alvarez V A, Valdez M E, and Vazquez A (2003) Dynamic Mechanical Properties and Interphase Fiber/Matrix Evaluation of Unidirectional Glass Fiber/Epoxy Composites. Polymer Testing, 22(6):611-615.

Aranguren M I, Elicabe G, Borrajo J, and Auad ML (1999) Curing Kinetics of Divinyl Ester Resins With Styrene. Journal of Applied Polymer Science, 74(5):1044-1053.

Ashland Chemical (2011) Technical Datasheet, Document 1820 V3 F2, Revised: 2011-8-30, 4p.

ASTM Standard D1776 (2004) Standard Practice for Conditioning and Testing Textiles. ASTM International, West Conshohocken, PA, www.astm.org.

ASTM Standard D2583 (2004) Standard Test Method for Indentation Hardness of Rigid Plastics by Means of a Barcol Impressor. ASTM International, West Conshohocken, PA, www.astm.org.

ASTM Standard D2584 (2002) Standard Test Method for Ignition Loss of Cured Reinforced Resins. ASTM International, West Conshohocken, PA, www.astm.org.

ASTM Standard D3039 (2007) Standard Test Method for Tensile Properties of Polymer Matrix Composite Materials. ASTM International, West Conshohocken, PA, www.astm.org.

ASTM Standard D3171 (2006) Standard Test Methods for Constituent Content of Composite Materials. ASTM International, West Conshohocken, PA, www.astm.org.

ASTM Standard D4255 (2001) Standard Test Method for In-Plane Shear Properties of Polymer Matrix Composite Materials by the Rail Shear Method. ASTM International, West Conshohocken, PA, www.astm.org.

ASTM Standard D5229/D5229M (2004) Standard Test Method for Moisture Absorption Properties and Equilibrium Conditioning of Polymer Matrix Composite Materials. ASTM International, West Conshohocken, PA, www.astm.org.

ASTM Standard D5528 (2001) Standard Test Method for Mode I Interlaminar Fracture Toughness of Unidirectional Fiber-Reinforced Polymer Matrix Composites. ASTM International, West Conshohocken, PA, www.astm.org.

ASTM Standard D5947 (2003) Standard Test Methods for Physical Dimensions of Solid Plastics Specimens. ASTM International, West Conshohocken, PA, www.astm.org.

ASTM Standard D6272 (2010) Standard Test Method for Flexural Properties of Unreinforced and Reinforced Plastics and Electrical Insulating Materials by Four-Point Bending. ASTM International, West Conshohocken, PA, www.astm.org.

ASTM Standard D6641 (2009) Standard Test Method for Determining the Compressive Properties of Polymer Matrix Composite Laminates Using a Combined Loading Compression (CLC) Test Fixture. ASTM International, West Conshohocken, PA, www.astm.org.

ASTM Standard D7264 (2007) Standard Test Method for Flexural Properties of Polymer Matrix Composite Materials. ASTM International, West Conshohocken, PA, www.astm.org.

Auad M L, Frontini P M, Borrajo J and Aranguren M I (2001) Liquid Rubber Modified Vinyl Ester Resins: Fracture and Mechanical Behavior. Polymer, 42(8):3723-3730.

Babu B Z and Pillai K M (2004) Experimental Investigation of the Effect of Fiber-Mat Architecture on the Unsaturated Flow in Liquid Composite Molding. Journal of Composite Materials, 38:57-79.

Baley C, Davies P, Grohens Y, and Dolto G (2004) Application of Interlaminar Tests to Marine Composites: A Literature Review. Applied Composite Materials, 11:99-126.

Bank L C (1989) Flexural and Shear Modulus of Full-Section Fiber Reinforced Plas-Tic (FRP) Pultruded Beams. Journal of Testing and Evaluation, 17(1):40-45.

Bates P J, Taylor D, and Cunningham M F (2001) Compaction and Transverse Permeability of Glass Rovings. Applied Composite Materials, 8:163-178.

Bechtold G and Ye L (2003) Influence of Fibre Distribution on the Transverse Flow Permeability in Fibre Bundles. Composites Science and Technology, 63:2069-2079.

Berube K A and Lopez-Anido R A (2008) Full-Field Strain Measurements for DeterminIng Mechanical Properties of Marine Composite Laminates. Experimental Mechanics Applied to Damage: Detection, Analysis and Mitigation, SEM XI International Congress Exposition on Experimental and Applied Mechanics, Orlando, FL, June 2-5, 2008, Society for Experimental Mechanics, Bethel, CT, 8p.

Berube K A and Lopez-Anido R A (2010) Variability in the Material Properties of Polymer Matrix Composites for Marine Structures. Journal of ASTM International 7(4):18p.

Berube K A and Lopez-Anido R A (2011) Effect of Preform Consolidation on the Fracture Toughness of Marine Grade Polymer Matrix Composite Materials Fabricated With a VARTM Process. Journal of Advanced Materials 43(1):30-48.

Berube K A and Lopez-Anido R A (2012) Effect of Resin Cure Recipe and Ambient Processing Temperature on the Material Properties of Marine Grade Polymer Matrix Composite Materials. Submitted for Publication to Materials Performance and Characterization.

Berube K A and Lopez-Anido R A, Caccese V, and Hess P (2006) Variability in Flexural Response of E-Glass/Vinyl Ester Composites Fabricated Using the VARTM Process. Proceedings of the 51st International SAMPE Symposium and Exhibition, Creating New Opportunities for the World Economy, April 30-May 4, 2006, Long Beach, CA, 11p.

Bickerton S, Buntain M J, Somashekar A A (2003) The Viscoelastic Compression Behavior of Liquid Composite Molding Preforms. Composites: Part A, 34:431-444.

Blake S P (2010) Crack Propagation in Secondary Bonded FRP Composite Joints. MS Thesis in Civil Engineering, University of Maine, 141p.

Blake S P, Berube K A, and Lopez-Anido R A (2011) Interlaminar Fracture Toughness of Woven E-Glass Fabric Composites. Journal of Composite Materials, 46(13):1583-1592.

Bolotin V V (2001) Mechanics of Delaminations in Laminate Composite Structures. Mechanics of Composite Materials, 37:367-380.

Breiling K B and Adams D O (1996) Effects of Layer Nesting on Compression-Loaded 2-D Woven Textile Composites. Journal of Composite Materials, 30:1710-1728.

Brill R P and Palmese G R (2000) An Investigation of Vinyl-Ester/Styrene Bulk Copolymerization Cure Kinetics Using Fourier Transform Infrared Spectroscopy. Journal of Applied Polymer Science 76:1572-1582.

Browne C M (1988) Alternative Methods for the Determination of Shear Modulus in a Composite Material. Testing Technology of Metal Matrix Composites, ASTM STP 964, American Society for Testing and Materials, Philadelphia. 259-274.

Broyles N S, Verghese K N E, Davis S V, Li H, Davis R M, Lesko J J, and Riffle J S (1998) Fatigue Performance of Carbon Fibre/Vinyl Ester Composites: The Effect of Two Dissimilar Polymeric Sizing Agents. Polymer, 39(15):3417-3424.

Bruck H A, McNeill S R, Sutton M A, and Peters W H I (1989) Digital Image Correlation Using Newton-Raphson Method of Partial Differential Correction. Experimental Mechanics, 29(3):261-267.

Burts E (2000) Structure and Properties of Dimethacrylate-Styrene Resins and Networks. Ph.D Dissertation, Virginia Polytechnic Institute and State University, Blacksburg, VA, 208p.

Cain J J, Post N L, Lesko J J, Case S W, Lin Y, Riffle J S, and Hess P E (2006) Post-Curing Effects on Marine VARTM FRP Composite Material Properties for Test and Implementation. Journal of Engineering Materials and Technology, Transactions of the ASME, 128:34-40.

Cain J J, Post N L, Lesko J J, Case S W, Lin Y, Riffle J S, and Hess P E (2006) Post-Curing Effects on Marine VARTM FRP Composite Material Properties for Test and Implementation. Journal of Engineering Materials and Technology, Transactions of the ASME, 128:34-40.

Cao X and Lee LJ (2003) Control of Shrinkage and Final Conversion of Vinyl Ester Resins Cured in Low-Temperature Molding Processes. Journal of Applied Polymer Science, 90(6):1486-1496.

Cardona F, Rogers D, Davey S, Van Erp G (2007) Investigation of the Effect of Styrene Content on the Ultimate Curing of Vinylester Resins by TGA-FTIR. Journal of Composite Materials, 41(2):137-152.

Cardona S C, Ziaee S, and Advani S G (2002) Spatially Homogeneous Gelation in Liquid Composite Molding. Polymer Engineering and Science, 42(8):1667-1673.

Chen B and Chou T (2000) Compaction of Woven-Fabric Preforms: Nesting and Multi-Layer Deformation. Composites Science and Technology, 60:2223-2231.

Chen B, Lang E J, and Chou TW (2001) Experimental and Theoretical Studies of Fabric Compaction Behavior in Resin Transfer Molding. Materials Science and Engineering, A317:188-196.

Chen Z and Ye L (2006) A Micromechanical Compaction Model for Woven Fabric Preforms. Part II: Multilayer. Composites Science and Technology, 66(16):3263-3272.

Choi S and Shah S P (1997) Measurement of Deformations on Concrete Subjected to Compression Using Image Correlation. Experimental Mechanics, 37(3):307-313.

Compston P and Jar P-Y B (1998) Comparison of Interlaminar Fracture Toughness in Unidirectional and Woven Roving Marine Composites. Applied Composite Materials, 5(3):189-206.

Compston P and Jar P-YB (1999) The Influence of Fibre Volume Fraction on the Mode I Interlaminar Fracture Toughness of a Glass-Fibre/Vinyl Ester Composite, Applied Composite Materials, 6:353-368.

Compston P, Jar Y B, Burchill P J, and Takahashi K (2002) Transfer of Matrix Toughness to Composite Mode I Interlaminar Fracture Toughness in Glass-Fibre/Vinyl Ester Composites. Applied Composite Materials, 9:291-314.

Cook W D, Simon G P, Burchill P J, Lau M, and Fitch T J (1997) Curing Kinetics and Thermal Properties of Vinyl Ester Resins. Journal of Applied Polymer Science, 64(4):769-781.

Crawford S and Lungu C T (2011) Influence of Temperature on Styrene Emission from a Vinyl Ester Resin Thermoset Composite Material, Science of the Total Environment 409:3403-3408.

Cummings L C (1983) Application of Differential Scanning Calorimetry to Cure Optimization and Quality Control of a Vinyl Ester Resin. Polymer Composites, 4(4):201-205.

Daniewicz S R (1999) Smoothing and Differentiating Load-Displacement Data Using a Low-Pass Filter for Improved Crack Opening Load Estimates. Fatigue & Fracture of Engineering Materials & Structures, 22(4):273-279.

Deng S and Ye L (1999) Influence of Fiber-Matrix Adhesion on Mechanical Properties of Graphite/Epoxy Composites: II Interlaminar Fracture and Inplane Shear Behavior. Journal of Reinforced Plastics and Composites, 18:1041-1057.

Dharmawan F, Simpson G, Herszberg I, and John S (2006) Mixed Mode Fracture Toughness of GFRP Composites. Composite Structures, 75:328-338.

Di Pietro A, Compston P (2009) Resin Hardness and Interlaminar Shear Strength of a Glass-Fibre/Vinylester Composite Cured With High Intensity Ultraviolet (UV) Light. Journal of Materials Science, 44:4188-4190.

DiBenedetto A T (2001) Tailoring of Interfaces in Glass Fiber Reinforced Polymer Composites: A Review. Materials Science and Engineering, A302:74-82.

Dua S, McCukkough R L, Palmese G R (1999) Copolymerization Kinetics of Styrene/Vinyl- Ester Systems: Low Temperature Reactions. Polymer Composites 20(3):379-391.

Dufort L, Grediac M, and Surrel Y (2001) Experimental Evidence of the Cross-Section Warping in Short Composite Beams Under Three Point Bending. Composite Structures 51:37-47.

Durra M (2005) Behavior and Design of Reinforced Wood-Plastic Composite Sections for Use in Sustained Loading Structural Applications. MS Thesis in Civil Engineering, University of Maine, Orono, ME.

El-Chiti F (2005) Experimental Variability of E-Glass Reinforced Vinyl Ester Composites Fabricated by VARTM/SCRIMP. MS Thesis in Mechanical Engineering, University of Maine, Orono, ME.

El-Chiti F (2005) Experimental Variability of E-Glass Reinforced Vinyl Ester Composites Fabricated by VARTM/SCRIMP. MS Thesis in Mechanical Engineering, University of Maine, Orono, ME.

El-Chiti F, Lopez-Anido R A, Dagher H J, Thompson L, Muszynski L, and Hess P E (2005) Experimental Approach for Characterizing VARTM Composites Using a 3-D Digital Image Correlation System. Proceedings of the SEM XII Int. Congress and Exposition on Experimental and Applied Mechanics, Portland, OR, June 7-9, 2005, Society for Experimental Mechanics, Bethel, CT, 8p.

Endruweit A, Gehrig S and Ermanni P (2003) Mechanisms of Hydrodynamically Induced In-Plane Deformation of Reinforcement Textiles in Resin Injection Processes. Journal of Composite Materials, 37:1675-1692.

Feih S, Wei J, Kingshott P, Sorensen B F (2005) The Influence of Fibre Sizing on the Strength and Fracture Toughness of Glass Fibre Composites. Composites Part A, 36:245-255.

Fink B K, Bogetti T A, Stone M A and Gillespie Jr. J W (2002) Thermochemical Response of Vinyl-Ester Resin. Army Research Laboratory, Report # ARL-TR-2653, Aberdeen Proving Ground, MD, 56p.

Fink B K, Dorairaj M B, and Gillespie Jr. J W (2001) Vinyl-Ester Cure Characterization Via Direct Current Sensors. Army Research Laboratory, Report # ARL-TR-2441, Aberdeen Proving Ground, MD, 184p.

Fischer S, Roman I, Harel H, Marom G, and Wagner H D (1981) Simultaneous Determination of Shear and Young's Moduli in Composites. Journal of Testing and Evaluation. 9(5):303-307.

Flores F, Gillespie Jr. J W, and Bogetti T A (2002) Experimental Investigation of the Cure-Dependent Response of Vinyl Ester Resin. Polymer Engineering and Science, 42(3):582-590.

Gao S L, Mader E, Abdkader A, and Offermann P (2003) Sizings on Alkali-Resistant Glass Fibers: Environmental Effects on Mechanical Properties. Langmuir, 19:2496-2506.

Gill A F, Robinson P, and Pinho S (2009) Effect of Variation in Fibre Volume Fraction on Modes I and II Delamination Behaviour of 5HS Woven Composites Manufactured by RTM. Composites Science and Technology, 69:2368-2375.

Govignon Q, Bickerton S, Morris J, and Kelly P A (2008) Full Field Monitoring of the Resin Flow and Laminate Properties during the Resin Infusion Process. Composites: Part A, 39:1412-1426.

Grimsley B W, Hubert P, Song X, Cano R J, Loos A C, and Pipes R B (2001) Flow and Compaction During the Vacuum Assisted Resin Transfer Molding Process. Proceedings of the 33nd International SAMPE Technical Conference - Advancing Affordable Materials Technology, Vol. 33, Seattle, WA, November 5-8, 2001, SAMPE, Covina, CA, 140 -153.

Grujicic M, Chittajallu K M, Walsh S (2004) Effect of Shear, Compaction and Nesting on Permeability of the Orthogonal Plain-Weave Fabric Preforms (2004) Materials Chemistry and Physics, 86:358-369.

Hammami A (2001) Effect of Reinforcement Structure on Compaction Behavior in the Vacuum Infusion Process. Polymer Composites, 22(3):337-348.

Hammami A and Al-Ghuilani N (2004) Durability and Environmental Degradation of Glass-Vinylester Composites. Polymer Composites, 25(6):609-616.

Hammami A and Gebart B R (2000) Analysis of Vacuum Infusion Molding Process. Polymer Composites, 21(1):28-40.

Han K, Jiang S, Zhang C, and Wang B (2000) Flow Modeling and Simulation of SCRIMP for Composites Manufacturing. Composites: Part A, 31:79-86.

Hayes M D and Lesko J J (2007) Measurement of the Timoshenko Shear Stiffness. I: Effect of Warping. Journal of Composites for Construction, 11(3):336-342

Hayes M D and Lesko J J (2007) Measurement of the Timoshenko Shear Stiffness. II: Effect of Transverse Compressibility. Journal of Composites for Construction, 11(3):343-349.

Hirai Y, Hamada H, and Kim J K (1998) Impact Response of Woven Glass-Fabric Composites - I Effect of Fibre Surface Treatment. Composites Science and Technology, 58:91-104.

Hoes K, Dinescu D, Sol H, Parnas R S, Lomov S (2004) Study of Nesting Induced Scatter of Permeability Values in Layered Reinforcement Fabrics, Composites: Part A, 35:1407-1418.

Ikuta N, Yanagawa A, Suzuki Y, and Ochiai S (2001) Investigation on Resin Interphase Produced Near Silane-Treated Glass Fiber in Vinyl Ester Resin. Composite Interfaces, 8(2):121-125.

Jensen R E and Mcknight S H (2002) Strength and Durability of Glass Fiber Composites Treated With Multi-Component Sizing Formulations. Army Research Laboratory, Report # ARL-TR-2655, Aberdeen Proving Ground, MD, 38 pp.

Juska T and Mayes S (1995) Post-Cure Study of Glass/Vinyl Ester Laminates Fabricated by Vacuum Assisted Resin Transfer Molding. Naval Surface Warfare Center, Carderock Division, Report # CARDIVNSWC-SSM-64-94/18, Bethesda, MD, 22p.

Karbhari V M and Kabalnova L (2001) Effect of Sizing and Loading Levels on the Cure Kinetics of Carbon Fiber Vinylester Composites. Journal of Reinforced Plastics and Composites, 20(2):90-104.

Karbhari V M and Lee R (2002) On the Effect of E-Glass Fiber on the Cure Behavior of Vinylester Composites. Journal of Reinforced Plastics and Composites, 21:901-918.

Karbhari V M and Palmese G R (1997) Sizing Related Kinetic and Flow Considerations in the Resin Infusion of Composites. Journal of Materials Science, 32:5761-5774.

Karbhari V M and Simacek P (1996) Notes on the Modeling of Preform Compaction: II-Effect of Sizing on Bundle Level Micromechanics. Journal of Reinforced Plastics and Composites, 15(8):837-861.

Karbhari V M and Zhang S (2003) E-Glass/Vinyl Ester Composites in Aqueous Environments - I: Experimental Results. Applied Composite Materials 10:19-48.

Karbhari VM (1998) Effect of Internal Mold Release Agent on the Cure and Property Variation in Resin Transfer Molding Composites. Journal of Materials Science Letters, 17(24):2061-2062.

Kessler A and Bledzki A (2000) Correlation Between Interphase-Relevant Tests and the Impact-Damage Resistance of Glass/Epoxy Laminates With Different Surface Treatments. Composites Science Und Technology, 60:125-130.

Khennouf D, Dulieu-Barton J M, Chambers A R, Lennard F J, and Eastop D D (2010) Assessing the Feasibility of Monitoring Strain in Historical Tapestries Using Digital Image Correlation. Strain, 46:19-32.

Kim J K and Hodzic A (2003) Nanoscale Characterization of Thickness and Properties of Interphase in Polymer Matrix Composites. Journal of Adhesion, 79:383-414.

Kim J K and Sham M L (2000) Impact and delamination failure of woven-fabric composites, Composites Science and Technology, 60:745-761.

Kim J K, Sham M L, Sohn M S, and Hamada H (2001) Effect of Hybrid Layers With Different Silane Coupling Agents on Impact Response of Glass Fabric Reinforced Vinyl Ester Matrix Composites. Polymer, 4:7455-7460.

Kim J, Shioya M, Kobayashi H, Junichi Kaneko J, and Kido M (2004) Mechanical Properties of Woven Laminates and Felt Composites Using Carbon Fibers. Part 1: In-Plane Properties. Composites Science and Technology 64:2221-2229.

Kim Y K and Daniel I M (2002) Cure Cycle Effect on Composite Structures Manufactured by Resin Transfer Molding. Journal of Composite Materials, 36:1725-1743.

Kittridge M, Lopez-Anido R A, Marquis J, Williams D, Snape T, Eary S, Duncan C J, and Berube K A (2012) Advanced Design and Optimization of High Performance Combatant Craft: Material Testing and Computational Tools. AEWC Report 12-46.780, AEWC Advanced Structures and Composites Center, University of Maine, Orono, ME, 687p.

Kootsookos A and Burchill P J (2004) Effect of the Degree of Cure on the Corrosion Resistance of Vinyl Ester/Glass Fibre Composites. Composites Part A, 35(4):501-508.

Kotaki M, and Hamada H, (1997) Effect of Interfacial Properties and Weave Structure on Mode I Interlaminar Fracture Behavior of Glass Satin Woven Fabric Composites. Composites Part A, 28A:257-266.

Kotaki M, Kuriyama T, Hamada H, Maekawa Z, and Narisawa I (2002) Mode I and Mode II Interlaminar Fracture Behavior of Glass Woven Fabric Composites. Science and Engineering of Composite Materials, 10(5):333-343.

Kumar C R, Radhakrishna K, and Rao, R M (2005) Postcuring Effects on Impact Behavior of Glass/Epoxy Composite Laminates. Journal of Reinforced Plastics and Composites, 24(6):949-960.

Larson B K, Drzal L T, and Van Antwerp J (1995) Swelling and Dissolution Rates of Glass Fiber Sizings in Matrix Resin Via Micro-Dielectrometry. Polymer Composites 16(5):415-420.

Lavoie J A, Soutis C, and Morton J (2000) Apparent Strength Scaling in Continuous Fiber Composite Laminates. Composites Science and Technology, 60(2):283-299.

Lee J and Soutis C A (2007) Study on the Compressive Strength of Thick Carbon Fi-Bre/Epoxy Laminates. Composites Science and Technology, 67(10):2015-2026.

Li H, (1998) Synthesis, Characterization and Properties of Vinyl Ester Matrix Resins. Ph.D Dissertation, Virginia Polytechnic Institute and State University, Blacksburg, VA, 169p.

Li J, Zhang C, Liang R, Wang B, and Walsh S (2008) Modeling and Analysis of Thickness Gradient and Variations in Vacuum-Assisted Resin Transfer Molding Process. Polymer Composites, 29:473-482.

Li L and Lee L J (2001) Effects of Inhibitors and Retarders on Low Temperature Free Radical Crosslinking Polymerization Between Styrene and Vinyl Ester Resin. Polymer Engineering and Science, 41(1):53-65.

Li L and Lee L J (2002) Effects of a Chelating Agent - 2,4-Pentanedione on Low Temperature Composite Molding of Vinyl Ester and Unsaturated Polyester Resins. Polymer Composites, 23(6):971-990.

Li L, Sun X, and Lee L J (1999) Low Temperature Cure of Vinyl Ester Resins. Polymer Engineering and Science, 39(4):646-661.

Li P, Yang X, Yu Y, and Yu D (2004) Cure Kinetics, Microheterogeneity, and Mechanical Properties of the High-Temperature Cure of Vinyl Ester Resins. Journal of Applied Polymer Science, 92(2):1124-1133.

Li P, Yu Y, Yang X (2008) Effects of Initiators on the Cure Kinetics and Mechanical Properties of Vinyl Ester Resins. Journal of Applied Polymer Science 109(4):2539-2545.

Lopez-Anido R A, El-Chiti F W, Muszynski L, Dagher H J, Thompson L, and Hess P E (2004) Composite Material Testing Using a 3-D Digital Image Correlation System. Proceedings of the ACMA Composites 2004 Convention and Trade Show, Tampa, FL, October 6-8, 2004, American Composites Manufacturers Association, Arlington, VA.

Madabhusi-Raman P, Davalos J F (1996) Static Shear Correction Factor for Laminated Rectangular Beams. Composites Part B 27B:285-293.

Madhukar M S and Drzal L T (1992) Fiber-Matrix Adhesion and Its Effect on Composite Mechanical Properties. III Longitudinal (0°) Compressive Properties of Graphite/Epoxy Composites. Journal of Composite Materials, 26(3):310-333.

Madhukar M S and Drzal L T (1992) Fiber-Matrix Adhesion and Its Effect on Composite Mechanical Properties: IV Mode I and Mode II Fracture Toughness of Graphite/Epoxy Composites. Journal of Composite Materials, 26(7):936-968.

Marston C, Gabbitas B, and Adams J (1997) Effect of Fibre Sizing on Fibres and Bundle Strength in Hybrid Glass Carbon Fibre Composites. Journal of Materials Science, 32(6):1415-1423.

Martin J S, Laza J M, Morras M L, Rodriguez M and Leon L M (2000) Study of the Curing Process of a Vinyl Ester Resin by Means of TSR and DMTA. Polymer, 41(11):4203-4211.

Masters J (1996) Strain Gage Selection Criteria for Textile Composite Materials. NASA Contractor Report 198286, National Aeronautics and Space Administration, Langley Research Center, VA.

Mcdonough W G, Dunkers J P, Holmes G A, Feresenbet E, Kim Y H and Parnas R S (2002) Influence of Processing Rate and Formulation on the Interface Strength of Vinyl Ester/E-Glass Composites. Polymer Composites, 23(2):274-283.

Melrose P T (2004) Elastic Properties of Sandwich Composite Panels Using 3-D Digital Image Correlation With the Hydromat Test System, MS Thesis in Mechanical Engineering, University of Maine, Orono, ME.

Melrose P, Lopez-Anido R A, and Muszynski L (2004) Elastic Properties of Sandwich Composite Panels Using 3-D Digital Image Correlation With the Hydromat Test System. In SEM XI International Congress and Exposition on Experimental and Applied Mechanics, Costa Mesa, CA.

Michaud D J, Beris A N, and Dhurjati P S (1998) Curing Behavior of Thick-Sectioned RTM Composites. Journal of Composite Materials, 32:1273-1296.

MIL-HDBK-17F-1 (2002) Composite Materials Handbook Volume 1 - Polymer Matrix Composites Guidelines for Characterization of Structural Materials, ASTM International, West Conshohocken, PA, p8.1-110.

MIL-HDBK-17F-1 (2002) Composite Materials Handbook Volume 1 - Polymer Matrix Composites Guidelines for Characterization of Structural Materials, ASTM International, West Conshohocken, PA, p8.1-110.

Modi D, Johnson M, Long A, Rudd C (2009) Analysis of Pressure Profile and Flow Progression in the Vacuum Infusion Process. Composites Science and Technology, 69:1458-1464.

Mott L, Shaler S M, and Groom L H (1996) A Novel Technique to Measure Strain Distributions in Single Wood Fibers. Wood and Fiber Science, 28(4):429-437.

Muszynski L, Lagana R, and Shaler S M (2002) Optical Measurements of Wood Deformations in Changing Climate. In 2002 SEM IX International Congress on Experimental Mechanics, Milwaukee, WI.

Muszynski L, Lopez-Anido R A, and Shaler S M (2000) Image Correlation Analysis Applied to Measurement of Shear Strains in Laminated Composites. In the SEM IX International Congress on Experimental Mechanics, Orlando, FL.

Muszynski L, Wang F, and Shaler S M (2002) Short Term Creep Tests on Phenol Resorcinol Formaldehyde (PRF) Resin Undergoing Moisture Content Changes. Wood and Fiber Science, 34(4):612-624.

Naik N K, Reddy K S, Meduri S, Raju N B, Prasad PD, Azad SK N M, Ogde PA and Reddy B C K (2002) Interlaminar Fracture Characterization for Plain Weave Fabric Composites. Journal of Materials Science, 37:2983-2987.

Nguyen L B, Juska T and Mayes J S (1997) Evaluation of Low Cost Manufacturing Technologies for Large Scale Composite Ship Structures. Collection of Technical Papers - AIAA/ASME/ASCE/AHS/ASC Structures, Structural Dynamics and Materials Conference, 2:992-1001.

Nicoletto G, Marin T, Anzelotti G, and Roncella R (2011) Application of High Mag-Nification Digital Image Correlation Technique to Micromechanical Strain Analysis. Strain 47:E66-E73.

Palmese G R and Karbhari V M, (1995) Effects of Sizings on Microscopic Flow in Resin Transfer Molding. Polymer Composites, 16(4):313-318.

Palmese G R, Andersen O A, and Karbhari V M (1999) Effect of Glass Fiber Sizing on the Cure Kinetics of Vinyl-Ester Resins. Composites Part A, 30(1):11-18.

Pan N and Gibson P, Editors (2006) Thermal and Moisture Transport in Fibrous Materials. Woodhead Publishing Limited, Cambridge, England.

Pearce N and Summerscales J (1995) The Compressibility of a Reinforcement Fabric. Composites Manufacturing, 6:15-21.

Peters P W M and Springer G S (1987) Effects of Cure and Sizing on Fiber-Matrix Bond Strength. Journal of Composite Materials, 21(1):157-171.

Plonka R, Mader E, Gao S L, Bellmann C, Dutschk V, and Zhandarov S (2004) Adhesion of Epoxy/Glass Fibre Composites Influenced by Aging Effects on Sizings. Composites Part A, 35:1207-1216.

Potluri P, Sagar T V (2008) Compaction Modeling of Textile Preforms for Composite Structures. Composite Structures, 86:177-185.

Puccini G (1993) Environmental Aspects, In Composite Materials in Maritime Structures: Vol. 1, Shenoi R A (Editor), Cambridge University Press, Cambridge, UK.

Ramos G, Gomez A, and Guardiola J (1996) Influence of Stability of Raw Materials Used in Sizings for E and AR Fiberglass Manufacture. Polymer Degradation and Stability, 51:316-365.

Ranson W F, Sutton M A, and Peters W H (1987) Holographic and Speckle Interferometry. In SEM Handbook of Experimental Mechanics, AS Kobayashi, Edito. Prentice-Hall, Inc, NJ, 388-429.

Rigas E J, Mulkern T J, Walsh S M, and Nguyen S P (2001) Effects of Processing Conditions on Vacuum Assisted Resin Transfer Molding Process (VARTM). Army Research Laboratory, Report # ARL-TR-2480, Aberdeen Proving Ground, MD, 54p.

Robertson M A E, Bump M B, Verghese K E, Mccartney S R, Lesko J J, Riffle J S, Kim I C and Yoon T H (1999) Designed Interphase Regions in Carbon Fiber Reinforced Vinyl Ester Matrix Composites. Journal of Adhesion, 71(4):395-416.

Robitaille F and Gauvin R (1998) Compaction of Textile Reinforcements for Composites Manufacturing. I: Review of Experimental Results. Polymer Composites, 19:198-216.

Robitaille F and Gauvin R (1998) Compaction of Textile Reinforcements for Composites Manufacturing. II: Compaction and Relaxation of Dry and H2O-Saturated Woven Reinforcements. Polymer Composites, 19:543-557.

Robitaille F and Gauvin R (1999) Compaction of Textile Reinforcements for Composites Manufacturing. III: Reorganization of the Fiber Network. Polymer Composites, 20:48-61.

Rodriguez E, Larranaga M, Mondragon I, Vazquez A (2006) Relationship Between the Network Morphology and Properties of Commercial Vinyl Ester Resins. Journal of Applied Polymer Science 100:3895-3903.

Rosario A C, Burts-Cooper E, Riffle J S (2007) Copolymerization Behavior and Properties of Dimethacrylate-Styrene Networks. Polymer 48:1203-1211

Ruiz, E and Trochu, F (2005) Thermomechanical Properties During Cure of Glass-Polyester RTM Composites: Elastic and Viscoelastic Modeling. Journal of Composite Materials, 39:881-916.

Saidpour S H and Richardson M W (1997) Glass Fibre Coating for Optimum Mechanical Properties of Vinyl Ester Composites. Composites Part A, 28A:971-975.

Saunders R A, Lekakou C, and Bader M G (1998) Compression and Microstructure of Fibre Plain Woven Cloths in the Processing of Polymer Composites. Composites: Part A, 29A:443-454.

Saunders R A, Lekakou C, Bader M G (1999) Compression in the Processing of Polymer Composites - 1. A Mechanical and Microstructural Study for Different Glass Fabrics and Resins. Composites Science and Technology, 59:983-993.

Schmidt T, Tyson J, and Galanulis K (2003) Full-Field Dynamic Displacement and Strain Measurement Using Advanced 3-D Image Correlation Photogrammetry-Part II. Experimental Techniques, 27(4):22-26.

Scott T F, Cook W D, Forsythe J S (2003) Photo-DSC Cure Kinetics of Vinyl Ester Resins II: Influence of Diluent Concentration. Polymer 44:671-680

Scott T F, Cook W D, Forsythe J S (2008) Effect of the Degree of Cure on the Viscoelastic Properties of Vinyl Ester Resins. European Polymer Journal 44:3200-3212

Shan L, Robertson C G, Verghese K N E, Burts E, Riffle J S, Ward T C, Reifsnider K L (2001) Influence of Vinyl Ester/Styrene Network Structure on Thermal and Mechanical Behavior. Journal of Applied Polymer Science 80:917-927

Sjogren A, Joffe R, Berglund L, and Mader E (1999) Effects of Fibre Coating (Size) on Properties of Glass Fibre/Vinyl-Ester Composites. Composites Part A, 30:1009-1015

Somashekar A A, Bickerton S, Bhattacharyya D (2006) An Experimental Investigation of Non-Elastic Deformation of Fibrous Reinforcements in Composites Manufacturing. Composites: Part A, 37:858-867.

Somashekar A A, Bickerton S, Bhattacharyya D (2007) Exploring the Non-Elastic Compression Deformation of Dry Glass Fibre Reinforcements. Composites Science and Technology, 67:183-200.

Souza B (2005) Fracture Mechanics Characterization of WPC-FRP Composite Materials Fabricated by the Composites Pressure Resin Infusion System (Compris) Process. MS Thesis in Civil Engineering, University of Maine, Orono, ME

Sridharan S (2008) Delamination Behaviour of Composites. Woodhead Publishing Limited, Cambridge, England

Stadtfeld H C, Erninger M, Bickerton S, and Advani S G (2002) An Experimental Method to Continuously Measure Permeability of Fiber Preforms as a Function of Fiber Volume Fraction. Journal of Reinforced Plastics and Composites, 21:879-899

Starr B C (2001) Inter-Relationships Between Chemistry, Network Structure and Properties of Chain Growth Dimethacrylate Thermosets. Ph.D Dissertation, Virginia Polytechnic Institute and State University, Blacksburg, VA, 187p

Sultania M, Yadaw S B, Rai J S P, Srivastava D (2010) Laminates Based on Vinyl Ester Resin and Glass Fabric: A Study on the Thermal, Mechanical and Morphological Characteristics. Materials Science and Engineering A 527:4560-4570

Suppakul P and Bandyopadhyay S (2002) The Effect of Weave Pattern on the Mode-I Interlaminar Fracture Energy of E-Glass/Vinyl Ester Composites. Composites Science and Technology, 62:709-717

Tackitt K D, and Walsh S M (2005) Experimental Study of Thickness Gradient Formation in the VARTM Process. Materials and Manufacturing Processes, 20:607-627

Tanoglu M, Mcknight S H, Palmese G R and Gillespie J W (2001) Effects of Glass-Fiber Sizings on the Strength and Energy Absorption of the Fiber/Matrix Interphase Under High Loading Rates. Composites Science Und Technology, 61(2):205-220.

Tanoglu M, Ziaee S, Mcknight S H, Palmese G R, and Gillespie J W (2001) Investigation of Properties of Fiber/Matrix Interphase Formed Due to the Glass Fiber Sizings. Journal of Materials Science, 36(12):3041-3053.

Tanoglu, M, Mcknight S H, Palmese G R and Gillespie Jr. J W (2001) Dynamic Stress/Strain Response of the Interphase in Polymer Matrix Composites. Polymer Composites, 22(5):621-635.

Tarnopol'skii Y M and Kulakov V L (2001) Tests Methods for Composites, Mechanics of Composite Materials, 37(5/6):431-448

Thomason J L (1995) Interface Region in Glass Fibre-Reinforced Epoxy Resin Composites: Characterization of Fibre Surface Coatings and the Interphase. Composites, 26(7): 487-498.

Thomason J L (1995) Interface Region in Glass Fibre-Reinforced Epoxy Resin Composites: Sample Preparation, Void Content and Interfacial Strength. Composites 26:467-475.

Thomason J L and Adzima L J (2001) Sizing Up the Interphase: An Insider's Guide to the Science of Sizing. Composites Part A, 32:313-321

Tucker R, Compston P, and Jar P-YB (2001) The Effect of Post-Cure Duration on the Mode I Interlaminar Fracture Toughness of Glass-Fibre Reinforced Vinylester. Composites: Part A, 32:129-134.

Tyson J, Schmidt T, and Galanulis K (2002) Advanced Photogrammetry for Robust Deformation and Strain Measurement. In the SEM XI International Congress on Experimental Mechanics, Milwaukee, WI

Upadhyaya D and Tsakiropoulos P (1995) Evaluation of the Effect of Sizing Levels on Transverse Flexural and Shear Strengths of Carbon/Epoxy Composites. Journal of Materials Processing Technology, 54:17-20.

Vaidya U K, Jadhav N C, Hosur M V, Gillespie Jr. J W, and Fink B K (2000) Assessment of Flow and Cure Monitoring Using Direct Current and Alternating Current Sensing in Vacuum-Assisted Resin Transfer Molding. Smart Materials and Structures, 9(6):727-736.

Valea A, Martinez I, Gonzalez M L, Eceiza A, and Mondragon I (1998) Influence of Cure Schedule and Solvent Exposure on the Dynamic Mechanical Behavior of a Vinyl Ester Resin Containing Glass Fibers. Journal of Applied Polymer Science, 70(13):2595-2602.

Walls J and Thompson L (2005) Parametric Shape Optimization of Tensile Coupons for Marine Grade Glass Fiber Reinforced Plastics. Report# ATS-RELY/2-2005-02, Applied Thermal Sciences, Orono, ME

Wang C M, Reddy J N, Lee K H (2000) Shear Deformable Beams and Plates - Relationships With Classical Solutions. Elsevier Science Ltd. Oxford, England

Williams C D, Grove S M, Summerscales J (1998) The Compression Response of Fibre-Reinforced Plastic Plates During Manufacture by the Resin Infusion Under Flexible Tooling Method. Composites: Part A, 29A:111-114.

Wu H F, Dwight D W, and Huff N T (1997) Effects of Silane Coupling Agents on the Interphase and Performance of Glass-Fiber-Reinforced Polymer Composites. Composites Science and Technology, 57(8):975-983.

Yang B, Kozeya V, Adanurb S, and Kumara S (2000) Bending, Compression, and Shear Behavior of Woven Glass Fiber-Epoxy Composites. Composites Part B 31:715-721

Yang F and Pitchumani R (2004) Effects of Interphase Formation on the Modulus and Stress Concentration Factor of Fiber-Reinforced Thermosetting-Matrix Composites. Composites Science and Technology, 64:1437-1452.

Yang H and Lee J (2001) A Kinetic Model for Free-Radical Crosslinking Co-Polymerization of Styrene/Vinylester Resin. Polymer Composites 22(5):668-679

Yenilmez B and Sozer E M (2009) Compaction of E-Glass Fabric Preforms in the Vacuum Infusion Process, A - Characterization Experiments. Composites: Part A, 40:499-510.

Yenilmez B and Sozer E M (2009) Variation of Part Thickness and Compaction Pressure in Vacuum Infusion Process. Composites Science and Technology, 69:1710-1719

Yuexin D, Zhaoyuan T, Yan Z, Jing S (2008) Compression Responses of Preform in Vacuum Infusion Process, Chinese Journal of Aeronautics, 21:370-377.

Zhang G and Latour Jr. RA (1993) FRP Composite Compressive Strength and Its Dependence Upon Interfacial Bond Strength, Fiber Misalignment, and Matrix Nonlinearity. Journal of Thermoplastic Composite Materials, 6(10):298-311.

Zhao L, Cordovez M and Karbhari V M (2001) Exothermic Temperature History in the Processing of Resin Infused Composite Structural Components. Applied Composite Materials, 8:99-131.

Ziaee S and Palmese G R (1999) Effects of Temperature on Cure Kinetics and Mechanical Properties of Vinyl-Ester Resins. Journal of Polymer Science Part B: Polymer Physics, 37(7):725-744.

Zinck P, Pay M F, Rezakhanlou R, and Gerard J F (1999) Mechanical Characterization of Glass Fibres as An Indirect Analysis of the Effect of Surface Treatment. Journal of Materials Science, 34(9):2121-2133

BIOGRAPHY OF THE AUTHOR

Keith Andrew Berube was born in Lewiston, Maine on March 21, 1964. He was the third of six children born to Raynald G. Berube and Elaine A. (Cyr) Berube. He was educated in the Auburn, Maine school system and graduated from Edward Little High School in 1982. After high school, Keith worked for several years in the printing and newspaper industries before attending the University of Maine in Orono. He received his Bachelor of Science in Mechanical Engineering at the University of Maine in 1997 and continued on to obtain a Master of Science in Mechanical Engineering in 1999. Following his graduation, Keith worked as a Research Engineer for the Department of Mechanical Engineering at the University of Maine. In 2004, he returned to the graduate program at the University of Maine to work toward his doctorate. He is a candidate for the Doctor of Philosophy degree in Mechanical Engineering from The University of Maine in December, 2012.